DTIC FILE COPY

DOT/FAA/CT-87/13

FAA TECHNICAL CENTER
Atlantic City Airport
N.J. 08405

KRASH Parametric Sensitivity Study — Transport Category Airplanes

AD-A189 962

Gil Wittlin
Bill LaBarge

Prepared by
Lockheed-California Company
Burbank, California

DTIC
ELECTE
FEB 05 1988
S D
H

December 1987

This document is available to the U.S. public through the National Technical Information Service, Springfield, Virginia 22161

U.S. Department of Transportation
Federal Aviation Administration

DISTRIBUTION STATEMENT A
Approved for public release;
Distribution Unlimited

88 2 2 079

NOTICE

This document is disseminated under the sponsorship of the Department of Transportation in the interest of information exchange. The United States Government assumes no liability for the contents or use thereof.

The United States Government does not endorse products or manufacturers. Trade or manufacturer's names appear herein solely because they are considered essential to the object of this report.

1. Report No.	2. Government Accession No.	3. Recipient's Catalog No.
DOT/FAA/CT-87/13		

4. Title and Subtitle	5. Report Date
KRASH PARAMETRIC SENSITIVITY STUDY- TRANSPORT CATEGORY AIRPLANES	December 1987
	6. Performing Organization Code

7. Author(s)	8. Performing Organization Report No.
G. Wittlin, W. L. LaBarge	LR-31114
	10. Work Unit No.

9. Performing Organization Name and Address	11. Contract or Grant No.
Lockheed-California Company Burbank, CA. 91520	DTFA03-84-C-00004

12. Sponsoring Agency Name and Address	13. Type of Report and Period Covered
U.S. Department of Transportation Federal Aviation Administration, Technical Center Atlantic City International Airport, NJ 08405	FINAL Oct. 1985 - June 1986
	14. Sponsoring Agency Code ACT-330

15. Supplementary Notes

fr. p. 1-1

16. Abstract

This report describes a study subsequent to the CID pre-test and CID correlation presented previously in DOT/FAA/CT-85/9 and DOT/FAA/CT-86/13, respectively. KRASH models are used to perform parameter sensitivity studies. Analyses are performed for air-to-ground, ground-to-ground, and longitudinal-only impacts. The results are presented in the form of triangular pulses with definitions of the peak amplitude, base time duration and pulse change of velocity. The analytically obtained data are integrated with the full-scale aircraft and section test data to formulate crash design velocity envelopes. The results of the study are used to suggest seat dynamic test conditions. Keywords:

The study results are summarized and major data areas are reviewed. Additional requirements are defined.

17. Key Words (Suggested by Author(s))	18. Distribution Statement
~~KRASH~~, crash dynamics, ~~CID~~, ~~velocity envelope~~, dynamic pulse, design criteria, transport category airplanes, analysis, correlation.	This document is available to the U.S. public through the National Technical Information Services, Springfield, Va. 22161

19. Security Classif. (of this report)	20. Security Classif. (of this page)	21. No. of Pages	22. Price*
UNCLASSIFIED	UNCLASSIFIED	155	

* For sale by the National Technical Information Service, Springfield, Virginia 22161

ii

FOREWORD

This report was prepared by the Lockheed-California Company under Contract DTFA03-84-C-00004. This report contains a description of the effort performed as part of Task Order No. 6 and covers the period from October 1985 to June 1986. The work was administered under the direction of L. Neri, Technical Monitor, Federal Aviation Administration.

The program leader and principal investigator was Gil Wittlin of the Lockheed-California Company. Bill LaBarge provided KRASH analysis support. The Lockheed effort was performed in the Flutter and Dynamics Department.

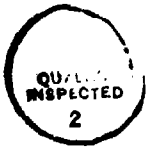

Accession For
NTIS GRA&I ☑
DTIC TAB ☐
Unannounced ☐
Justificati...
By
Distribution/
Availability Codes
Dist | Avail and/or Special
A-1

TABLE OF CONTENTS

LIST OF FIGURES

LIST OF FIGURES (continued)

LIST OF FIGURES (continued)

LIST OF FIGURES (continued)

LIST OF FIGURES (continued)

LIST OF TABLES

LIST OF TABLES (continued)

EXECUTIVE SUMMARY

This document describes the effort performed under Contract DTFA03-84-00004, Task Order No. 6. The study described in this report is subsequent to the CID pre-test and CID correlation presented in references 1 and 2, respectively.

The KRASH model refined in the aforementioned efforts was used to perform parameteric sensitivity studies for severe, but survivable, crash scenarios. The previous KRASH correlation and model refinements are briefly discussed in this report. Analyses were performed for air-to-ground, ground-to-ground, and longitudinal impacts and the results are presented in the form of triangular pulses with definitions of the peak amplitude, base time duration and pulse change of velocity. The analytically obtained data are integrated with the full-scale aircraft and section test data to formulate crash design velocity envelopes. The results of the parameter study suggest the following dynamic test conditions for seats:

1. Combined Vertical-Longitudinal pulse with seat oriented 30 degrees from the vertical; the resultant floor pulse parameters are: $\Delta V \cong 32$ ft/sec, $\Delta t \cong .15$ sec., Amplitude $\cong$ 13g.

2. Longitudinal pulse; the floor pulse parameters are: $\Delta V \cong 33$ ft/sec, $\Delta t \cong .20$ sec.; Amplitude $\cong$ 10g

The pulses presented are higher than the indicated airframe fuselage bending and shear strengths to account for rebound and rotational effects.

The study results are summarized with regard to the impact that the test and analyses data have had on formulating crash design criteria. In the process of discussing the major data areas, the progress achieved as well as associated limitations are discussed suggested additional efforts are defined.

SECTION 1

INTRODUCTION

On December 1, 1984, the FAA/NASA jointly sponsored ~~(reference 1)~~ Controlled Impact Demonstation (CID) test was conducted. The CID test was a major milestone in a series of inter-related analyses and tests prescribed in the FAA Crash Dynamics program ~~which is depicted in figure 1-1.~~ Prior to the CID test, several section and impact tests including analyses were performed. The results of these experiments are described in reference 2. Subsequent to the CID test, correlation between KRASH pretest analyses and actual test data was evaluated. The actual CID test resulted in an unsymmetrical impact which was modeled and the results compared with the recorded test data (reference 3). The results of this effort (described in reference 3) showed generally good agreement between the pretest analyses and the actual test data for both a stick (figure 1-2) and an expanded model (figure 1-3). The stick model responses were more representative of the floor pulses measured during the CID test than were the expanded model results. The measured responses indicated that the fuselage fundamental bending frequency was evident and contributed significantly to the CID test floor pulse. The CID test impact level was not sufficiently high enough to verify the additional beam responses obtained from the expanded model. Thus, with emphasis on establishing floor pulses based on fuselage structural integrity limits (ultimate shear and bending moment), the use of the stick model provides the most feasible and direct approach and as such was used in the initial parameter studies. The overall program from pre-CID to parametric sensitivity studies is depicted in figure 1-4. Prior to the CID test, fuselage sections and a full airplane were drop tested. The data obtained from these tests were used to refine KRASH simulations to obtain structure acceleration responses and moment/shear distributions. The KRASH output was used in the assessment of a planned impact condition which called for a severe, but survivable impact.

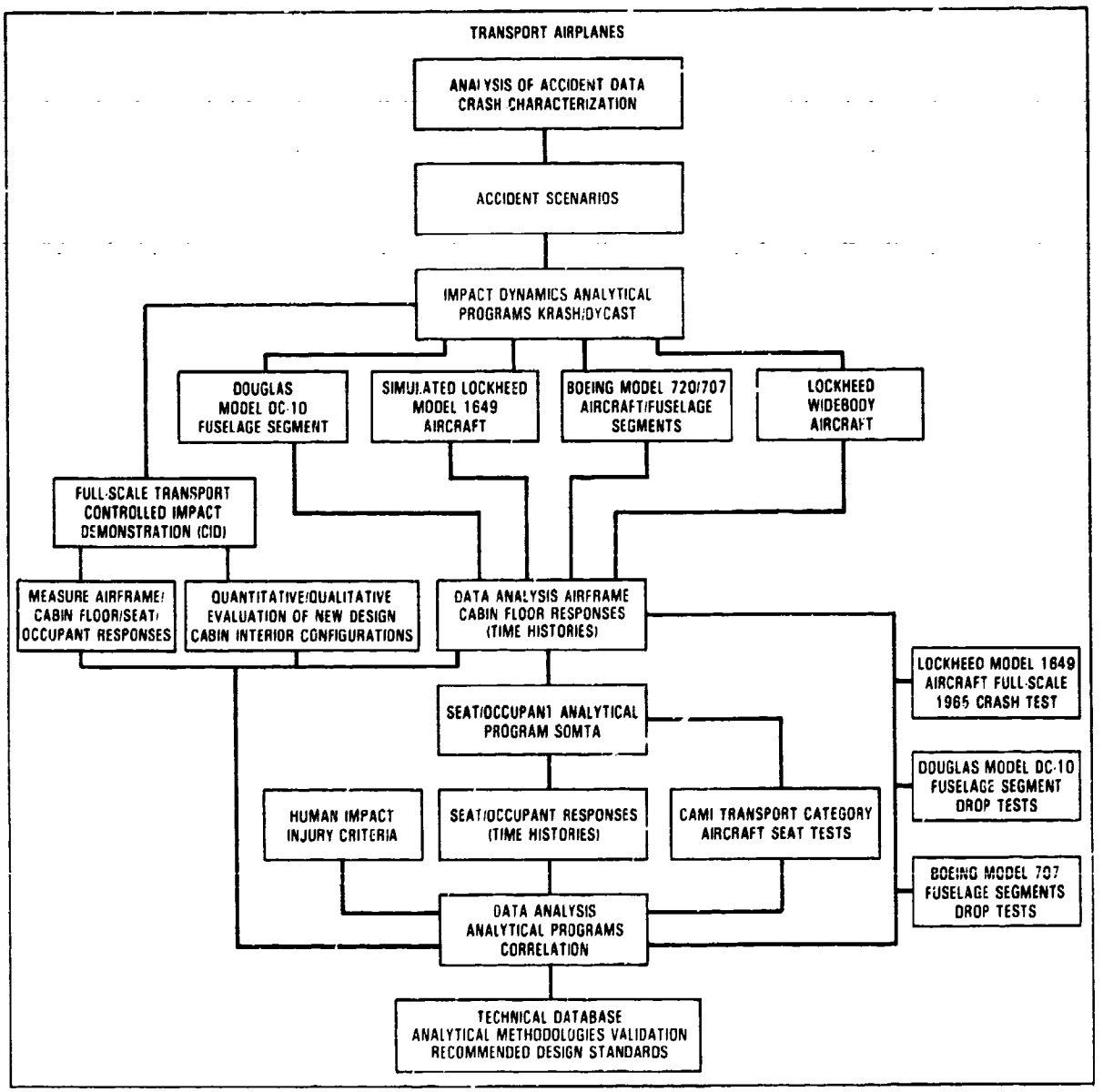

Figure 1-1. FAA Crash Dynamics Engineering and Development Program

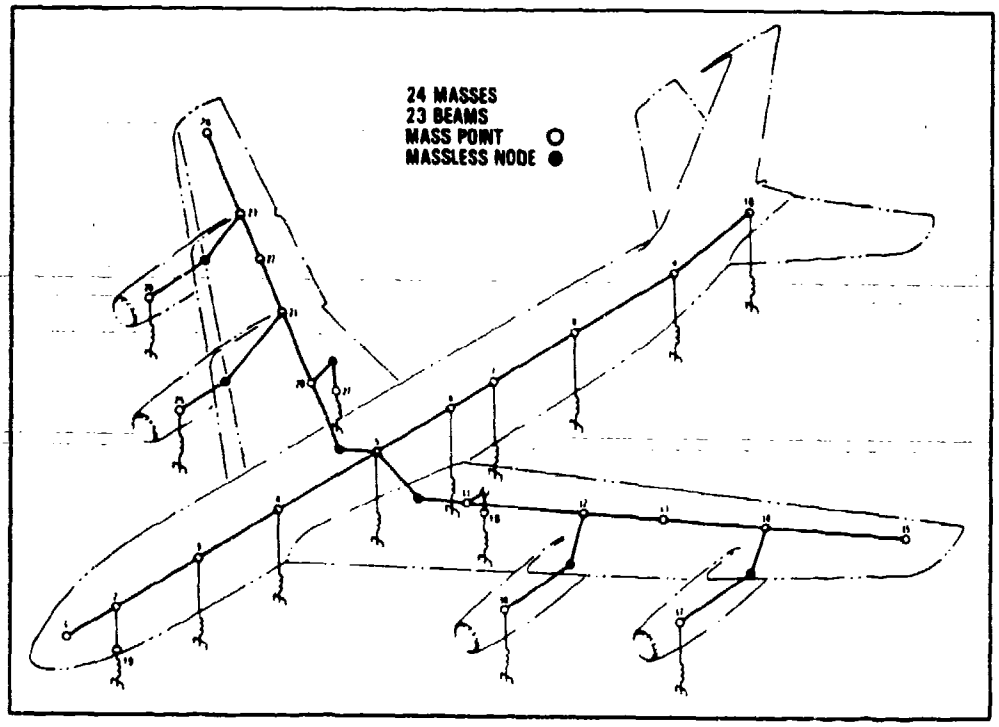

Figure i-2. CID KRASH Stick Model

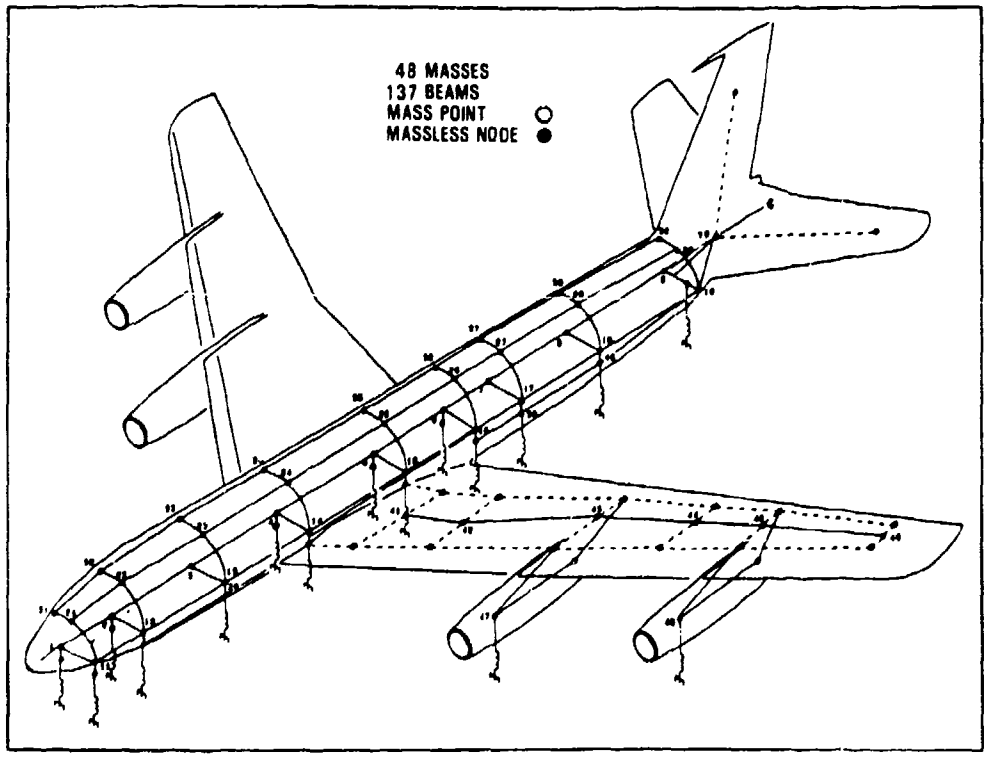

Figure 1-3. Expanded CID KRASH Model

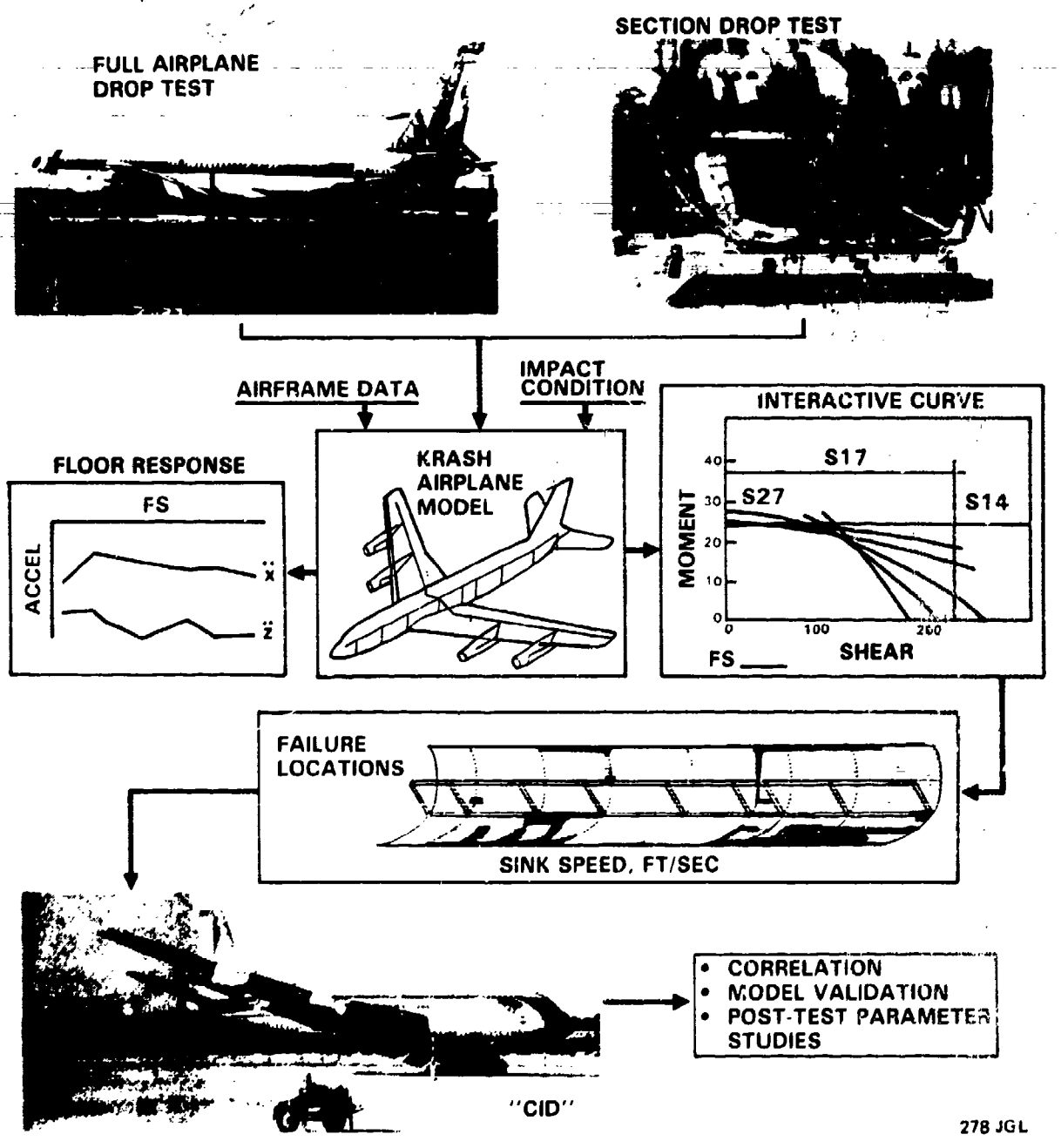

Figure 1-4. Outline Of Methodology Approach

The validated KRASH simulation model provides the basis for the post-CID effort. This report briefly summarizes the correlation results and then describes some initial modifications to the KRASH model subsequent to the correlation and prior to the parameter sensitivity analyses. During the course of the parameter variation investigation the following crash scenarios were analyzed:

- Air-to-Ground impact (gears retracted)
- Air-to-Ground impact (gears extended)
- Ground-to-Ground impact (gears retracted)

The program flow chart, shown in figure 1-5, depicts the sequence of analyses events leading to the development of crash design velocity envelopes. This phase of the effort involved several interactions as a result of the input of additional data during the course of the investigation. As noted earlier, prior to the parametric sensitivity analyses the KRASH model's capabilities were refined to (a) improve the expanded model's flexibility to be in better agreement with available data, and (b) correct the stick model's geometry. The initial analyses were then performed for the air-to-ground (gears retracted) scenario, followed by the ground-to-ground scenario, also with gears retracted. The results from the ground-to-ground analyses indicated a need to update the nose-gear bulkhead representation. This refinement was made using existing available test data (reference 4). KRASH's modeling capabilities were revised and a new set of results was obtained. In addition to the two scenarios initially investigated, air-to-ground (gears extended) and longitudinal impacts were also analyzed. The latter analysis was aided by the use of existing available cylinder axial crush test data, also obtained from reference 4. The analytical results yielded vertical, longitudinal, and combined vertical-longitudinal pulses. The analyses results, along with the full-scale test data (L-1649, CID) and fuselage section test data, were then used to formulate crash design velocity envelopes.

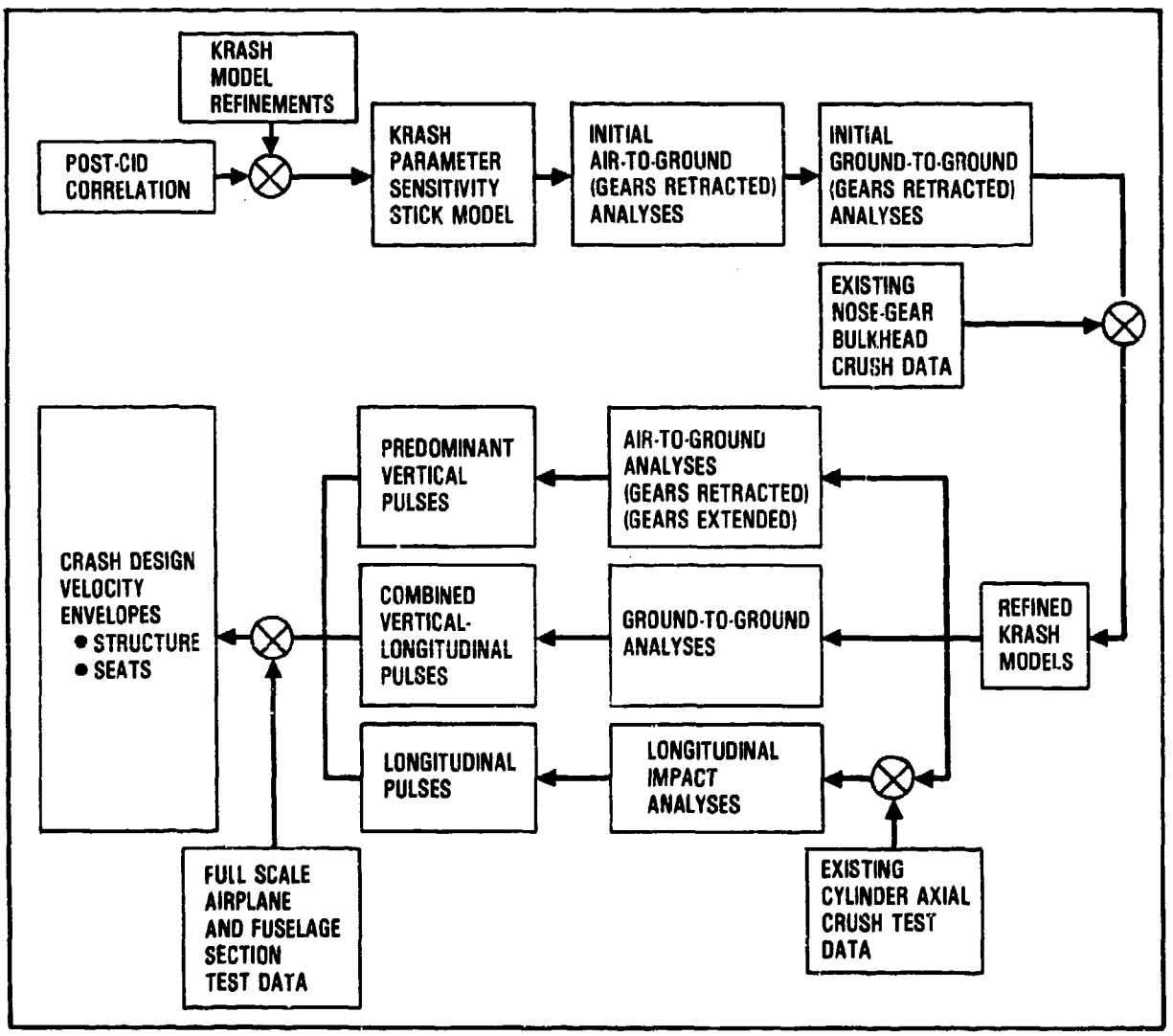

Figure 1-5. Parametric Sensitivity Analyses Program Flow Diagram

SECTION 2

POST-CORRELATION STUDIES

2.1 SUMMARY OF CID CORRELATION RESULTS

The CID correlation effort is described in detail in reference 3. A synopsis of the findings of this study follow below:

The initial fuselage impact with the ground occurred at a sink speed of approximately 14 feet/second (ft/sec), nose down (-2 degrees). This condition, modeled as a symmetrical impact with the KRASH stick model, showed agreement with the test data with regard to peak vertical acceleration and fuselage underside crush distance. The analysis indicated higher shear and moment load interaction curve (LIC) values than were estimated from the measured bending moments. However, the analytically determined LIC values indicated that the airframe strength had not been exceeded, which was consistent with the results from the CID test.

The KRASH stick model results depicting the CID unsymmetrical air-to-ground impact from the time of engine No. 1 contact through to fuselage contact shows agreement with the sequence and time of occurrence of siginificant events such as engine No. 1, engine No. 2 and fuselage ground contact. The airplane cg velocity is reduced from an initial 17.3 ft/sec to approximately 14 ft/sec when the fuselage hits the ground which is consistent with the test data. The crush magnitudes and distritution, as well as the LIC values which indicate fuselage airframe strength margins exist at that impact level, are also consistent with the test results. However, the fuselage vertical accelerations from the mid-fuselage (FS820) through to the aft fuselage (FS1400) are higher than the levels recorded during the CID test. The actual test data also differs from the results obtained from the abbreviated 14 ft/sec fuselage impact analysis results. The analyses showed that the responses are somewhat sensitive to the initial loading (aerodynamics) conditions and the manner in which those loads change. The difference in acceleration responses noted may be due to the manner in which these external forces are represented in the KRASH model.

The fuselage vertical acceleration responses obtained from the post-CID analyses, both the symmetrical impact on the fuselage at 14 ft/sec, and the unsymmetrical impact on the No. 1 engine at 17.3 ft/sec are shown in figure 2-1, along with the measured CID test data range. The acceleration values represent peak g's for a triangular pulse with a base duration between 0.100 and 0.150 second. The longitudinal pulses are approximately 3 to 4 g's along the fuselage.

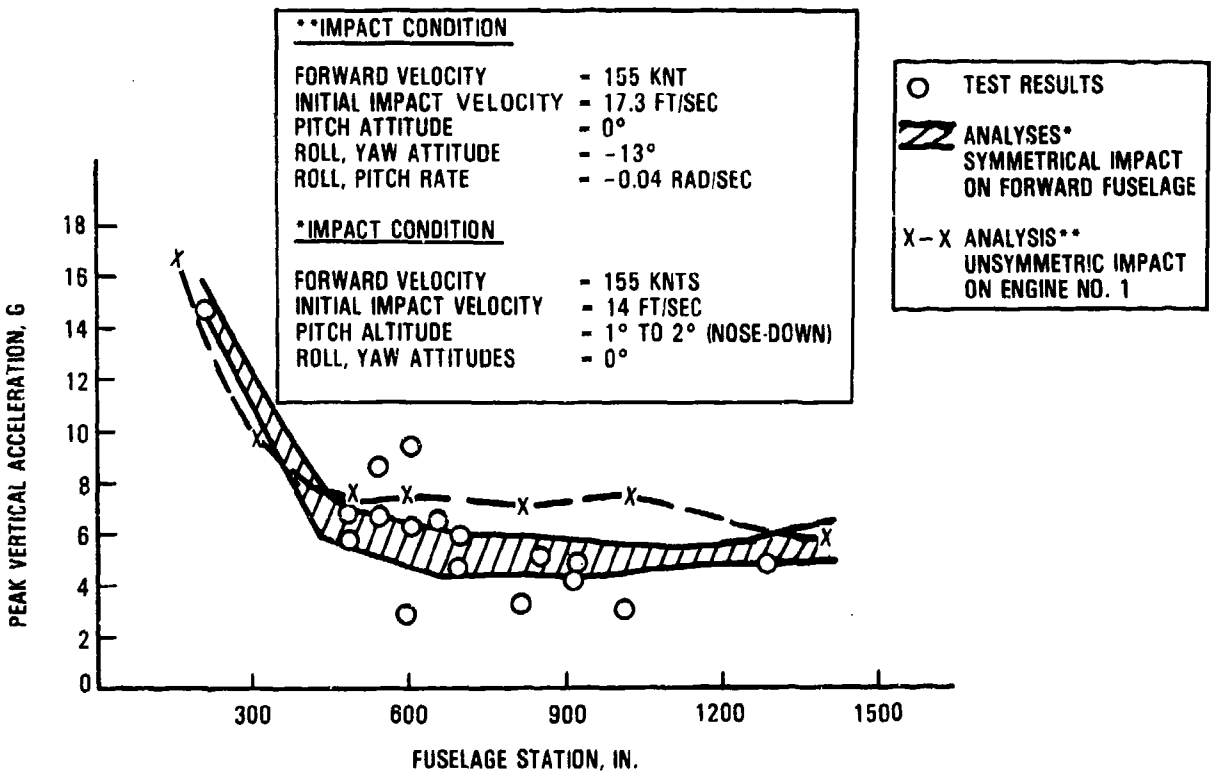

Figure 2-1. Comparison of Post-test CID KRASH Analysis and Test Results for Fuselage Impact

An analyses of the results for the planned CID symmetrical (0-degree roll, yaw) and the actual CID unsymmetrical (-13 degree roll, yaw) condition for the one-degree nose-up and 17.3 ft./sec sink rate impact are shown in figure 2-2. The fuselage crush distribution is similar to that experienced during the full-scale airplane drop test, commonly referred to as the "Laurinburg" test, which was a symmetrical, 17 ft/sec sink speed impact. The 17.3 ft/sec symmetrical impact shows a peak LIC of 0.78. By linear extrapolation, this data indicates the LIC ratio of 1.0 (limit of airframe strength) would be reached at a sink speed of 20 ft/sec. However, the responses are most likely not a linear relationship with impact velocity, but more a function of available crush distance.

Comparisons of the stick model versus the expanded model fuselage results for a symmetrical 17 ft/sec impact with a 1 degree nose-up attitude engines-on are shown in figure 2-3. The LIC values generally range between 0.60 and 0.70. The peak vertical accelerations, also shown in figure 2-3 are reasonably close for fuselage station 199 through to fuselage station 960. Aft of this location station the expanded model responses are approximately 2/3 the values of the stick model. The crush distributions for both the stick and the expanded models follow the same trend. They are both within the crush distances observed for the "Laurinburg" test, which was performed for the same impact condition as the CID. The "Laurinburg" test differed from the CID test in that the former did not have aerodynamic loading and forward velocity. As noted in reference 3, the differences between the stick and expanded model representations need further investigation to ascertain their influence on the respective results.

The fuselage peak vertical acceleration versus base duration for the triangular pulses associated with the analyses and test results is shown in figure 2-4. The acceleration responses are shown for the passenger region only (FS460-FS1400). As expected there is substantial scatter. For the most part the test and analyses results fall in the shaded area which is between 4g to 10g peak and 0.100 to 0.170 second base duration.

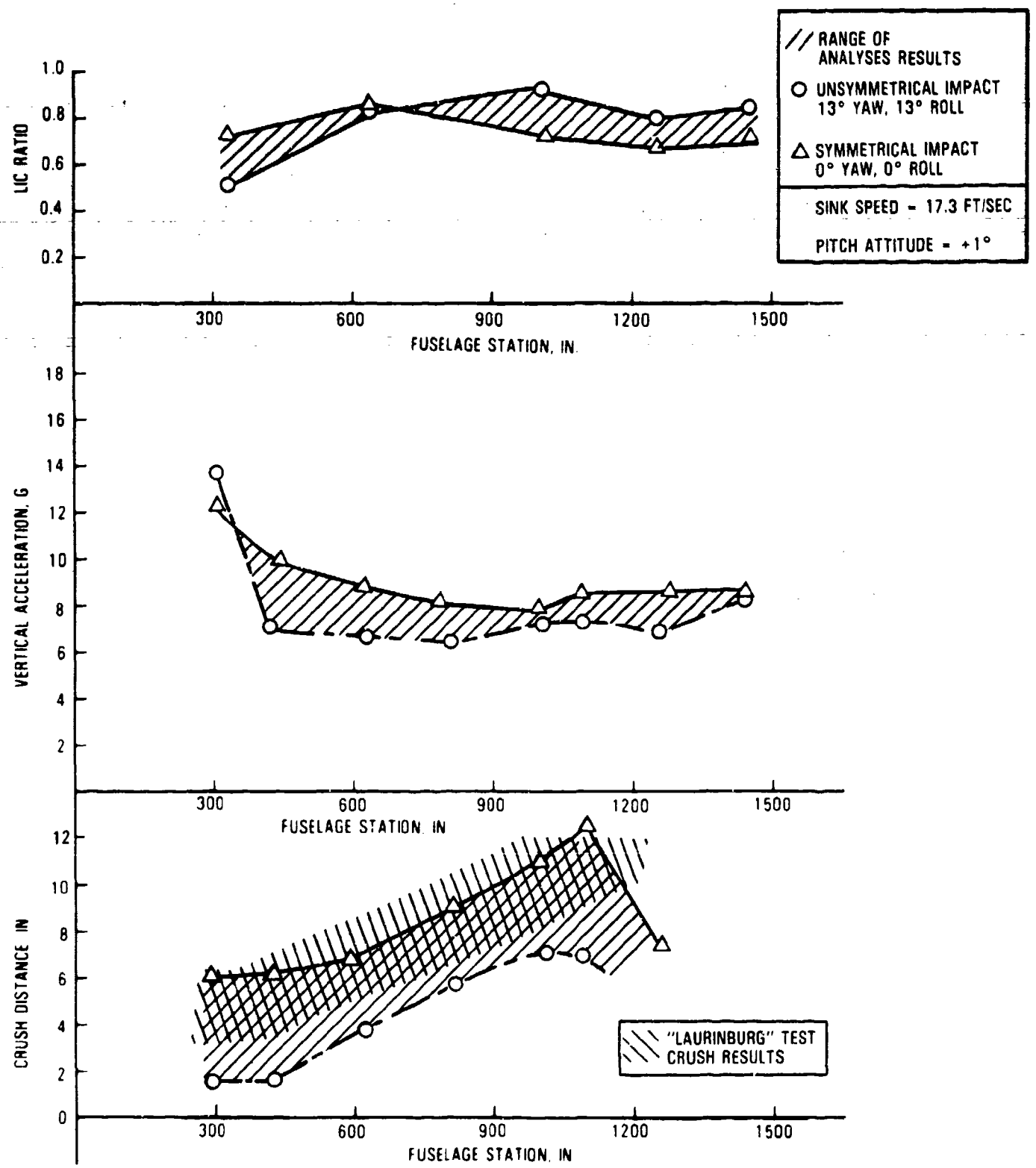

Figure 2-2. Symmetrical Versus Unsymmetrical Impact at 17.3 Ft/Sec Sink Speed, 1 Degree Nose-Up Attitude With Engines On

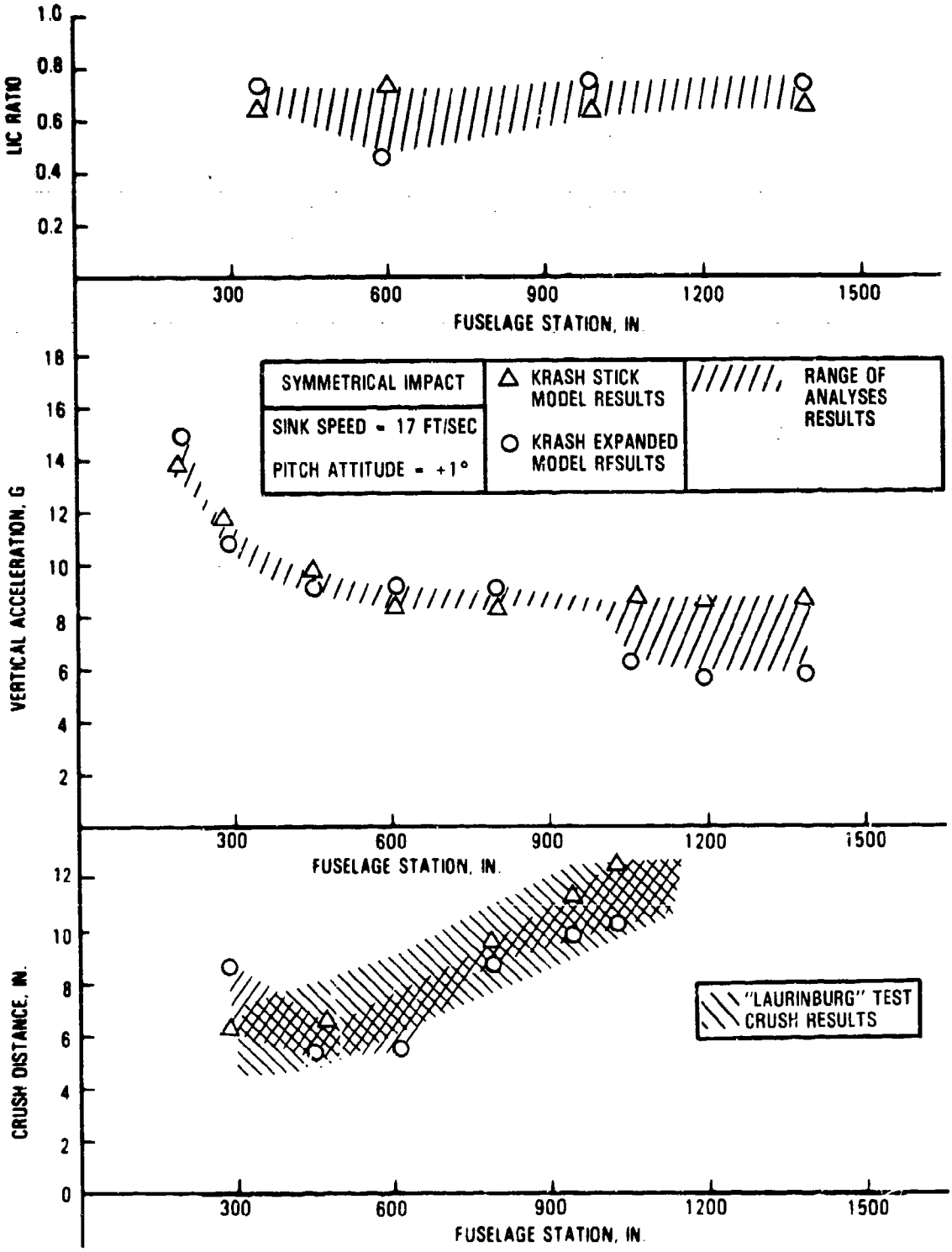

Figure 2-3. Stick Model Versus Expanded Model Results for a Symmetrical Impact at 17 Ft/Sec, 1 Degree Nose-Up Attitude

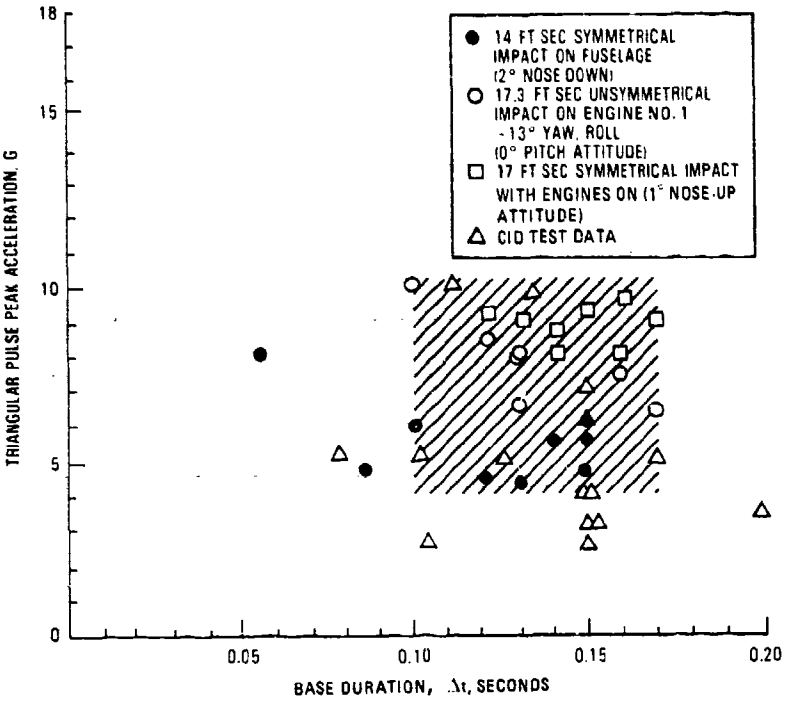

Figure 2-4. Triangular Shaped Vertical Acceleration Responses From Analyses and Test; Peak Magnitude Versus Base Duration, Passenger Region FS460-1400

From figure 2-1, shown earlier, there are differences between the peak vertical accelerations obtained from the full unsymmetrical analysis, the analysis of the symmetrical impact on the forward fuselage and the test data. Several areas in the model and impact condition representation may contribute to such a difference. These include:

- The effect of both the initial and time varying aerodynamic loading - For example, the moment response data as shown in figure 2-5 shows the No. 1 engine impacting first and then followed by impact of the fuselage while, the symmetrical model analysis starts at the point designated "nose-impact," with an aerodynamic loading applied so as to develop the moment distribution measured. The unsymmetrical model analysis starts at the point noted "initial engine impact." For the analyses to be identical, the moments would have to be developed from "initial engine impact" through "initial fuselage impact" as shown in figure 2-5. This does not occur in the model. Model revisions to allow more detail in engine/wing attachment and application of aerodynamic loading may be needed to evaluate this effect.

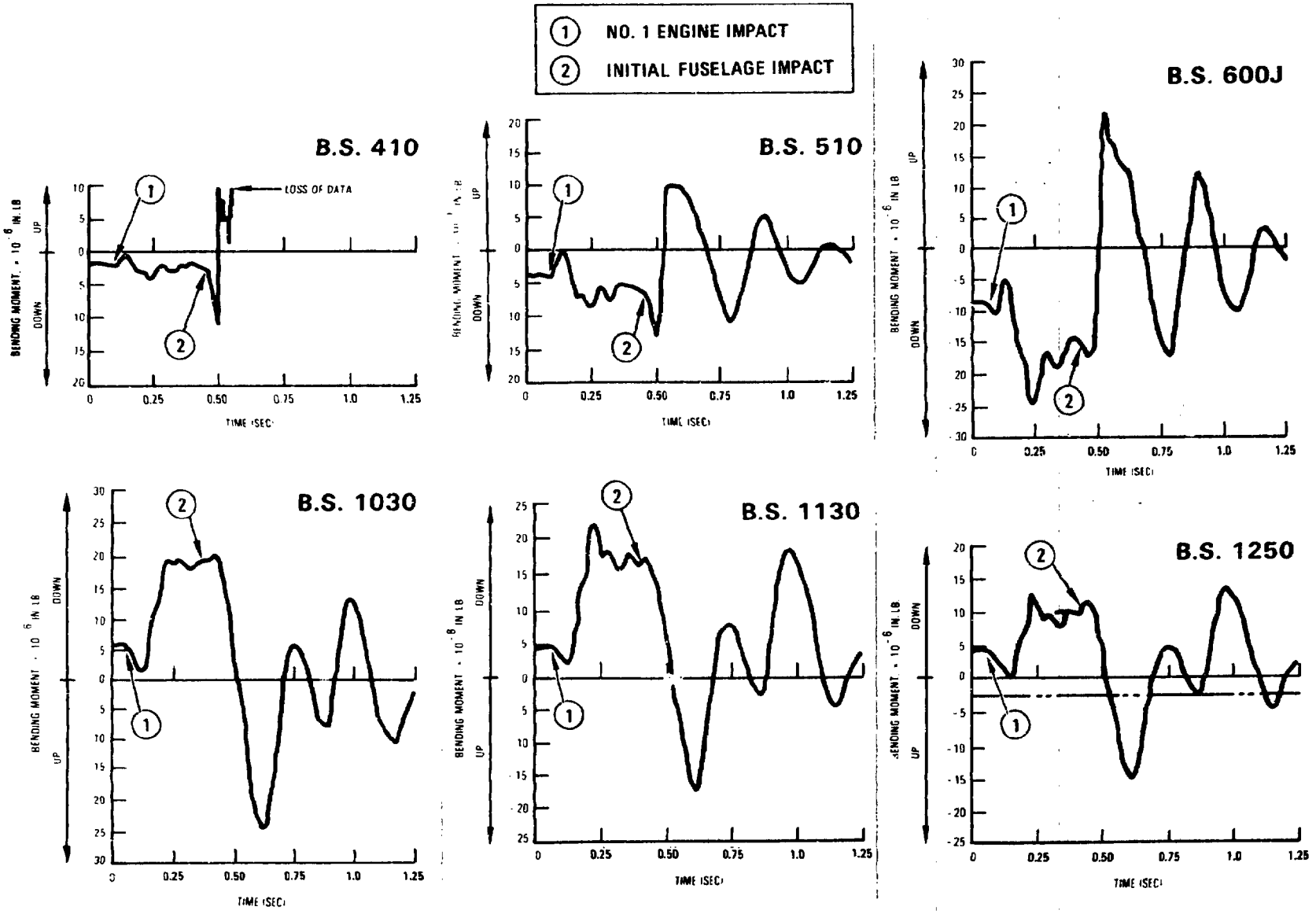

Figure 2-5. CID Test Results, Engine and Fuselage Impacts

- Representation of engine/wing/fuselage attachments - For example, the unsymmetrical model results indicate that a pitch rotational velocity develops at the time the fuselage impacts; it is approximately 0.05 to 0.010 rad/sec. The actual contact velocity of the fuselage mass at time of ground contact, in some cases, is noted to be higher than the cg velocity, resulting in higher peak acceleration values. When initial pitch and roll rotational velocities were included such that the resultant 17.3 ft/sec vertical contact velocity consisted of both translational and rotational components, the results were in better agreement with the test data.

The analytical wing response results are of interest in light of the measured and observed (photographic) CID test results. The analytically obtained moment and shear distributions, along with estimated strength levels and available test data, are shown in figures 2-6 and 2-7, respectively. The curves suggest that for the 13 degree roll, 17.3 ft/sec. sink speed condition the wing structural integrity is at or near its limit. For this impact condition, the left outboard wing section has the highest potential for failure. Failure initiated at the left wing tip would progressively work its way inboard. Since there was no fuel tank rupture, nor significant fuel spill as a result of this failure, it is presumed that the wing fuel containment requirements are met for this crash scenario. Analytical studies, described in reference 17, were performed for a gears-up airplane contacting the ground with one wing low. The pitch attitude was level, or slightly nose-up. These conditions are similar to the CID test. The report goes on to state that crushing and wearing-off the tip and outer wing will begin when contact is made with the ground and will progress along the wing until either a fuel tank is opened, the wing is broken off, or the airplane is righted by the loads which are crumbling the outer wing. The study concluded that for an airplane carrying fuel in the entire span of the structural box, the fuel can be contained at roll attitudes up to 12 degrees, independent of descent angle. With no fuel carried outboard of the 80 percent semi-span location, the fuel

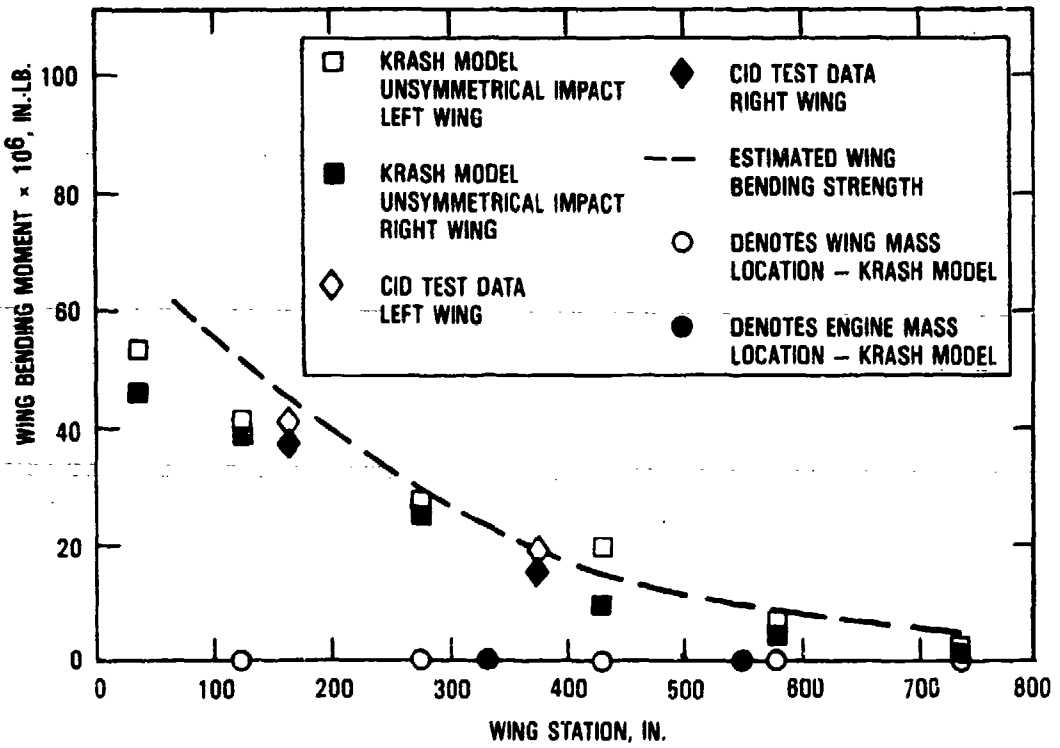

Figure 2-6. Comparison of KRASH Analysis and CID Airplane Test Wing Berding

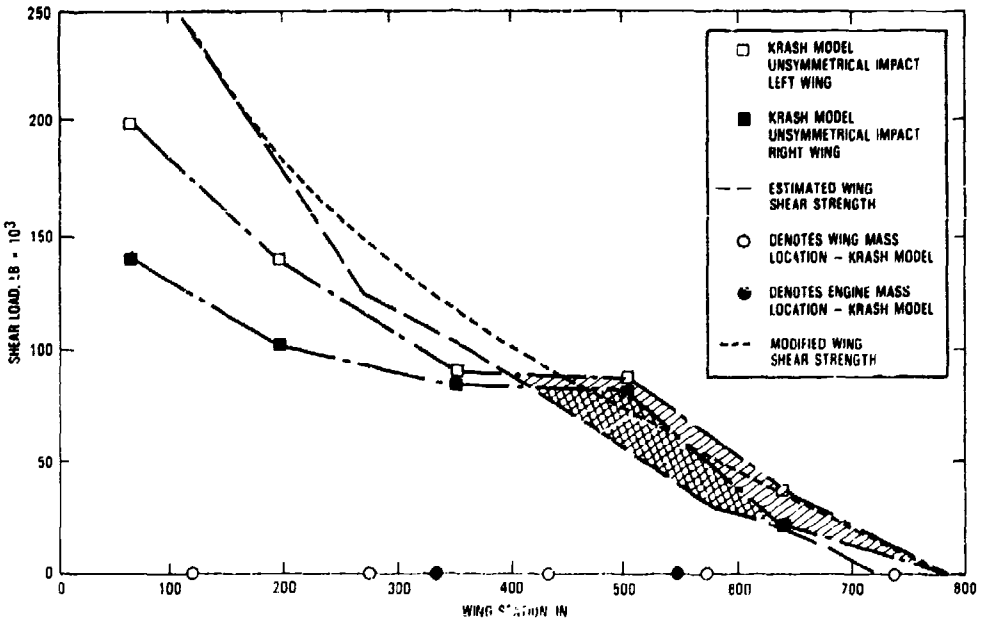

Figure 2-7. KRASH Analysis Wing Shear Distribution

can be contained up to a roll attitude of 15 ±1 degrees. The CID test, with a roll attitude of 13 degrees and considering the extent of wing damage experienced at impact tend to confirm these earlier findings.

The analyses results showed that for symmetrical impact at 17.3 ft/sec impact and a +1 degree pitch attitude, the moment and shear distribution along the wing will be substantially below its estimated strength as is depicted in figures 2-8 and 2-9, respectively.

The correlation results suggested several concerns that need to be addressed with additional analyses and/or tests. The following is a brief discussion of these items:

- How sensitive are the responses to assumed external loading (aerodynamics) and initial rotational velocities (pitch, roll, yaw) within the range of survivable impact speeds and attitudes? Analysis, as opposed to testing, is a more practical attempt to clarify this item.

- What is the trend of the response of the airframe as a function of pitch attitude? For example, do the fuselage extremities respond in the manner indicated by the results of the limited range of analyses performed during the correlation study? Additional analysis supported by limited testing appears necessary.

- What is the appropriate representation of the engine/wing and wing/fuselage attachments and can a refined model provide better agreement with test data, both during initial engine-ground contact and subsequent fuselage-ground contact? While the effort (described in reference 3) did not dwell on the engine or wing representation, the results indicate that this is an area that could be further explored.

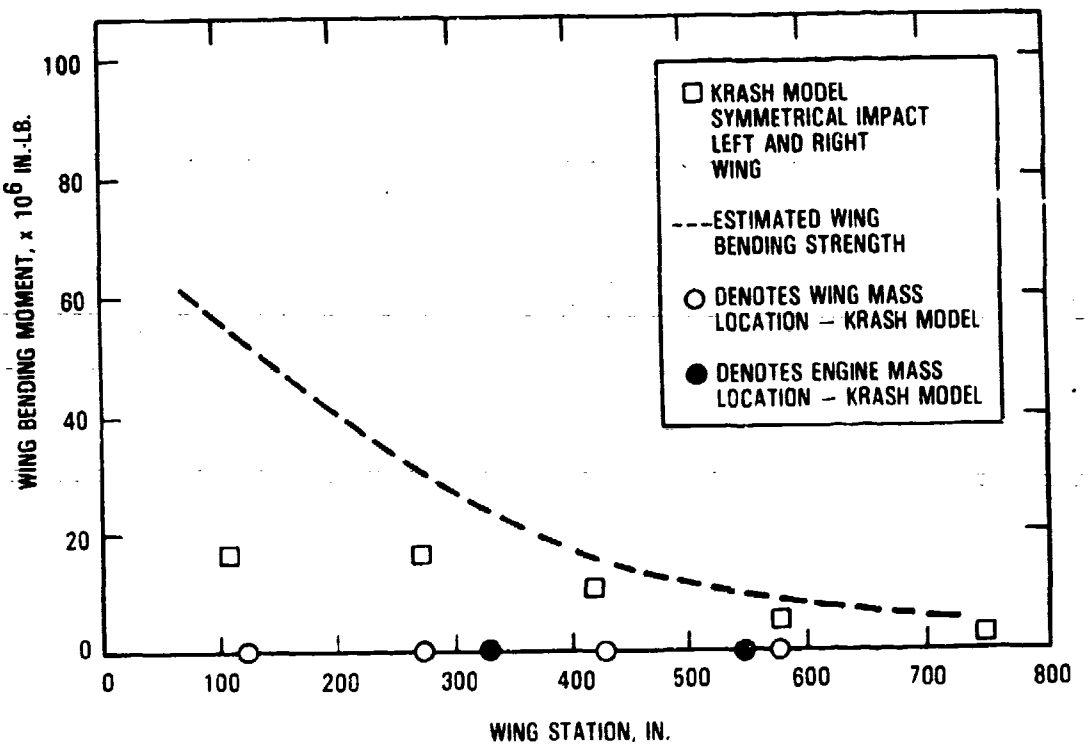

Figure 2-8. KRASH Analysis Wing Bending Distribution for Symmetrical Impact; 17.3 Ft/Sec Sink Speed, +1 Degree Pitch Attitude

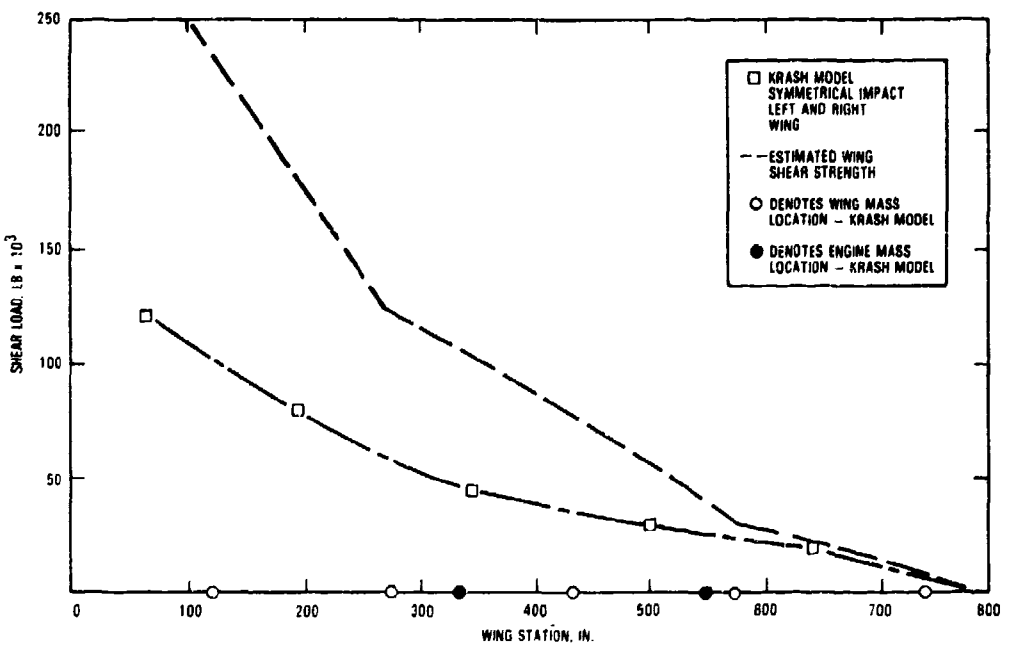

Figure 2-9. KRASH Analysis Wing Shear Distribution for Symmetrical Impact; 17.3 Ft/Sec Sink Speed, +1 Degree Pitch Attitude

2.2 POST-CID CORRELATION MODEL REFINEMENTS

Subsequent to the KRASH correlation with test data, additional analyses have been performed to determine the effect of model refinements. As noted in Section 6 (reference 2), the comparison of the stick model's versus the expanded model's initial static deflections and LIC ratios were improved as a result of model refinements. The refinements discussed in this section were not included in the pre-CID analyses results reported in reference 2 nor in the correlation analyses reported in reference 3. Specifically, the changes are:

- Stick Model

  (a) Correct wing waterline locations. The original stick model was formulated prior to the NASTRAN-LC code change to KRASH85 and contained wing stations for a deflected position due to an initial aerodynamic loading distribution.

  (b) Provide an additional wing-to-fuselage beam attachment at the wing leading edge location (FS620). This change increases the number of beams to 17 and 25, for the symmetric and unsymmetric models, respectively. The number of masses remains 17 and 24, respectively.

- Expanded Model

  (a) Provide the lower fuselage longitudinal beams with additional compressive area to be in agreement with the cross-sectional area distribution as shown in the data.

  (b) Eliminate one mass and beam from each wing. This change reduces a symmetrical model from 48 masses and 137 beams to 47 masses and 136 beams. This change makes the wing representation alike for both the stick and expanded models.

A comparison of stick and expanded model initial static deflections and LIC ratios is shown in tables 2-1 and 2-2, respectively. Results prior to and after the aforementioned changes are noted. In general, the model changes resulted in an improved comparison between the stick and expanded models.

The results from several impact conditions were compared to determine the effect the model changes would have on overall response. Table 2-3 shows stick model generated data of LIC, fuselage crush and peak impulse for both symmetrical and unsymmetrical impacts. Representation A compares favorably with Representation B, and Representation C compares favorably with Representation D. The latter comparison shows a relatively large discrepancy in the LIC value at FS300. A closer review of the response data shows that the LICs at FS300, for Representations C and D, are equal to 0.15 at about 0.45 second after impact. At that time, the downward shear is between 18,200 and 18,600 lb. and the downward moment is between 2.44×10^6 and 2.64×10^6 in-lb. Thereafter, both analyses show extremely low LICs except for the latter analysis, Representation D, which exhibits a short duration upward shear of 49,000 lb. accompanied by a low (1×10^6 in-lb) upward moment. This combination of loading results in a sharp rise in the LIC value to 0.30 which quickly reduces to less than 0.10. This situation occurs at the time the forward spring (FS199) reaches its peak deflection and starts to unload. For Representation C, wnen the forward-most spring (FS199) starts to unload at 0.531 sec, the shear reverses but is only 8,400 lb. While the exact cause of the discrepancy is not known, the phasing of external spring loading and unloading at FS199 and FS300 most likely contributed to this situation.

Table 2-4 shows the comparison of results generated by the expanded model changes. The results for a symmetrical impact condition with a 17.3 ft/sec sink speed and +1 degree pitch show that while some differences may exist, the overall assessment of LIC, crush and impulse data is unaltered by the model changes. The model changes described do not alter the correlation results.

TABLE 2-1. COMPARISON OF STATIC DEFLECTIONS

LOCATION	DEFLECTION, INCHES		DIFFERENCE, INCHES
	STICK MODEL FIGURE 1-2	EXPANDED MODEL FIGURE 1-3	
FUSELAGE			
FS 199	-1.07 (-1.30)	-3.42 (-1.90)	2.35 (0.60)
FS 300	-0.83 (-1.01)	-2.99 (-1.71)	2.09 (0.70)
FS 460	-0.45 (-1.35)	-2.25 (-1.35)	1.80 (0.77)
FS 620	-0.16 (-0.23)	-1.32 (-0.80)	1.16 (0.57)
FS 820	0 (0)	0 (0)	0 (0)
FS 960	-0.21 (-0.21)	-0.03 (-0.09)	0.18 (0.12)
FS 1040	-0.49 (-0.49)	-0.16 (-0.09)	0.33 (0.26)
FS 1200	-1.25 (-1.25)	-0.94 (-0.99)	0.31 (0.26)
FS 1400	-2.65 (-2.65)	-2.54 (-2.57)	0.11 (0.08)
FS 1570	-4.07 (-4.07)	-4.03 (-4.10)	0.40 (0.03)
WING			
ROOT	+0.81 (+0.84)	+0.61 (+0.63)	0.20 (0.21)
TIP	+40.5 (+39.6)	+41.2 (+39.9)	0.70 (0.30)

(XXX) REVISED MODEL RESULTS

TABLE 2-2. COMPARISON OF BEAM INITIAL LOAD INTERACTION CURVE (LIC) RATIOS

CURVE NO.	FUSELAGE STATION	LOAD INTERACTION CURVE RATIO	
		STICK MODEL	EXPANDED MODEL
1	300	0.011 (0.011)	0.009 (0.009)
2	350	0.061 (0.061)	0.062 (0.062)
3	450	0.058 (0.057)	0.052 (0.052)
4	480	0.122 (0.123)	0.120 (0.118)
5	540	0.122 (0.123)	0.120 (0.118)
6	600	0.124 (0.124)	0.121 (0.121)
7	620	0.151 (0.332)	0.258 (0.233)
8	820	0.209 (0.344)	0.360 (0.326)
9	820	0.426 (0.427)	0.431 (0.429)
10	960	0.203 (0.203)	0.205 (0.204)
11	960	0.203 (0.203)	0.205 (0.204)
12	1000	0.249 (0.249)	0.251 (0.250)
13	1080	0.245 (0.245)	0.248 (0.247)
14	1160	0.273 (0.273)	0.276 (0.275)
15	1210	0.190 (0.190)	0.192 (0.191)
16	1320	0.158 (0.158)	0.163 (0.162)
17	1400	0.199 (0.199)	0.203 (0.202)
18	1400	0.177 (0.177)	0.181 (0.181)

(XXX) REVISED MODEL RESULTS

TABLE 2-3. COMPARISON OF STICK MODEL REVISIONS

	-2° PITCH, 14 FT/SEC SINK SPEED, SYMMETRICAL IMPACT		0° PITCH, -13° ROLL AND YAW, 17.3 FT/SEC SINK SPEED, UNSYMMETRICAL IMPACT	
	(A) 17 MASSES 16 BEAMS	(B) 17 MASSES 17 BEAMS	(C) 24 MASSES 23 BEAMS	(D) 24 MASSES 25 BEAMS
LIC @ FS				
300	0.50	0.52	0.15	0.30
350	0.49	0.49	0.57	0.55
450	0.40	0.40	0.51	0.49
600	0.45	0.48	0.44	0.38
990	0.59	0.47	0.78	0.80
1090	0.63	0.64	0.77	0.78
1210	0.46	0.44	0.75	0.75
CRUSH (INCHES) @ FS				
300	7.6	8.0	7.8	8.4
460	4.6	4.5	5.5	6.0
620	4.0	3.8	4.5	4.7
820	2.8	2.9	3.5	3.5
960	5.9	6.9	3.0	3.0
1040	8.0	9.4	1.9	1.8
1200	2.3	4.8	–	–
PEAK IMPUSE G-SEC @ FS				
199	0.93	1.00	1.06	1.04
300	0.85	0.91	0.94	0.93
460	0.72	0.75	0.77	0.77
620	0.62	0.63	0.72	0.71
820	0.51	0.50	0.66	0.64
960	0.46	0.45	0.58	0.61
1040	0.44	0.42	0.55	0.54
1200	0.41	0.39	0.57	0.56
1400	0.39	0.38	0.57	0.55

TABLE 2-4. COMPARISON OF RESULTS DUE TO EXPANDED MODEL REVISIONS

	+1° PITCH, 17.3 FT/SEC SINK SPEED, SYMMETRICAL [a]		
	CORRELATION MODEL 48 MASSES 137 BEAMS	STIFFER MODEL 48 MASSES 137 BEAMS	STIFFER MODEL REVISED WING 47 MASSES 136 BEAMS
LIC @ FS			
300	0.25	0.28	0.29
350	0.78	0.77	0.66
450	0.64	0.66	0.57
600	0.60	0.70	0.68
990	0.82	0.79	0.68
1090	0.82	0.79	0.82
1210	0.58	0.68	0.57
CRUSH (IN.) @ FS [b]			
300	7.8/7.6	8.0/8.0	7.9/7.6
460	5.0	5.7	5.1
620	4.8/5.1	5.3/5.4	4.7/4.7
820	7.7/8.2	7.2/8.0	6.5/7.4
960	9.0/9.8	6.3/9.2	6.0/8.7
1080	9.1	8.5	8.1
1240	3.4	3.4	3.1
PEAK IMPULSE G-SEC @ FS [b]			
199	0.97/0.95	0.95/0.90	0.94/1.00
300	0.91/0.87	0.87/0.83	0.77/0.90
450	0.73/0.74	0.73/0.72	0.63/0.73
620	0.61/0.63	0.63/0.63	0.63/0.64
820	0.64/0.61	0.64/0.62	0.63/0.61
960	0.60/0.62	0.58/0.61	0.60/0.60
1080	0.64/0.63	0.61/0.62	0.60/0.61
1240	0.77/0.66	0.69/0.66	0.68/0.64
1400	0.71/0.73	0.77/0.74	0.76/0.73

(a) MODELS INCLUDE PRE-CID ENGINE LOAD-DEFLECTION CURVE AND AERODYANMIC LOADING DISTRIBUTION

(b) TWO VALUES REPRESENT CENTERLINE AND FLOOR/FRAME INTERSECTION LOCATIONS, RESPECTIVELY

SECTION 3

PARAMETRIC SENSITIVITY INVESTIGATION

3.1 VERTICAL PULSE

The floor vertical pulse magnitudes and distribution are affected by the vertical descent rate or effective normal velocity (ENV), airplane pitch attitude, aerodynamic loads, initial impact location, and engine configuration and involvement. However, if criteria is established for a tolerable floor pulse based on an acceptable level of fuselage shell structural integrity, then an entire crash sequence may not be necessary. Knowing the cause of the fuselage impact conditions may not be as important as knowing the actual fuselage impact levels. For example, the CID test impact condition is noted as 17.3 ft/sec sink speed, 0-degree pitch, 13-degree yaw, 13-degree roll. For this particular attitude the left wing engines are involved prior to fuselage impact. The engine involvement is such that the fuselage impacts at a reduced sink speed (14 ft/sec) and different attitude (2 degrees nose-down). For a 17.3 ft/sec symmetrical impact at a level pitch attitude, the engine involvement is less and the initial fuselage impact speed is at, or near, the original impact velocity. In reality then, for purposes of evaluating floor pulses, the 17.3 ft/sec symmetrical impact is the condition which directly affects the fuselage, while the 17.3 ft/sec unsymmetrical impact is, in reality, a 14 ft/sec, -2-degree pitch fuselage impact. The aerodynamic loading distribution and/or the subsequent loading consequence of earlier sequential events (i.e., engine-wing failures) can alter the fuselage responses. While the monitoring of the complete sequence of events is of interest, a more direct approach would be to develop an envelope of airframe loads and floor accelerations for a range of fuselage impact velocities and attitudes. Either a no-external-loading (aerodynamic) condition or a predetermined aerodynamic distribution should be applied throughout the range investigated. Probably the most difficult decision is determining the appropriate level of airframe structural integrity to be established as criteria. For the purpose of this study it was decided that breakup of the

airframe is initiated when the fuselage strength, bending moment and/or shear is exceeded. The initiation of fuselage breakup represents the limit of structural integrity because the events that occur beyond this point are difficult to project.

3.1.1 Air-to-Ground, Gears Retracted

3.1.1.1 Initial Analyses

The initial parametric sensitivity analyses were performed with the KRASH stick model. The following assumptions were made.

- Impact directly on fuselage, no engine crush involved
- Symmetrical impact, no roll or yaw
- No initial external loading, i.e., aerodynamic forces
- No rupture of beams
- Load interaction curve (LIC) > 1.0 indicates limit of airframe integrity.
- Maximum crush before restiffening occurs is:

  10-inch wing center section, FS620-820

  18-inch wing MLG aft bulkhead FS960

  24-inch fuselage frame sections, FS300, 460, 1040, 1240

Figures 3-1 through 3-5 contain plots of the peak acceleration for a triangular pulse, time duration of the pulse and associated change in velocity for fuselage impacts with pitch attitudes of +6 degrees, +3 degrees, 0 degree, -3 degrees and -6 degrees, respectively. Included on each plot is a tabulation of the fuselage underside crush and LIC ratios. These data are cross-plotted on figures 3-6 and 3-7 for the forward fuselage locations (460, 820) and aft fuselage locations (960, 1200), respectively. Figure 3-8 shows the crush at the respective fuselage locations in relation to the respective

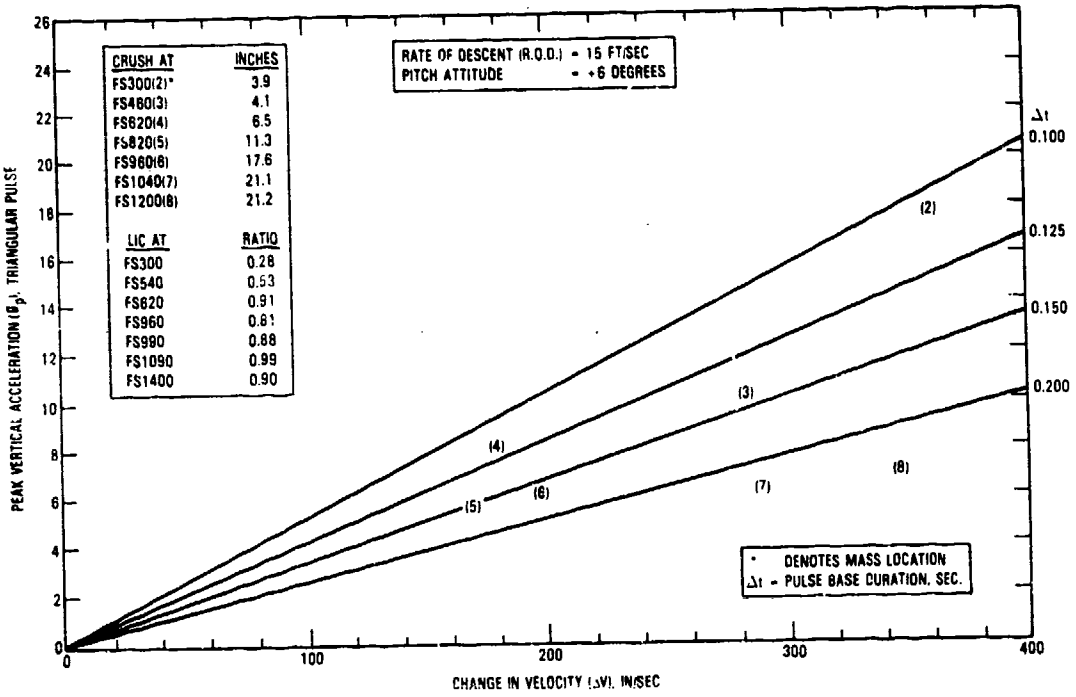

Figure 3-1. Floor Pulses for +6 Degree Pitch Attitude and 15 Ft/Sec Airplane Rate of Descent

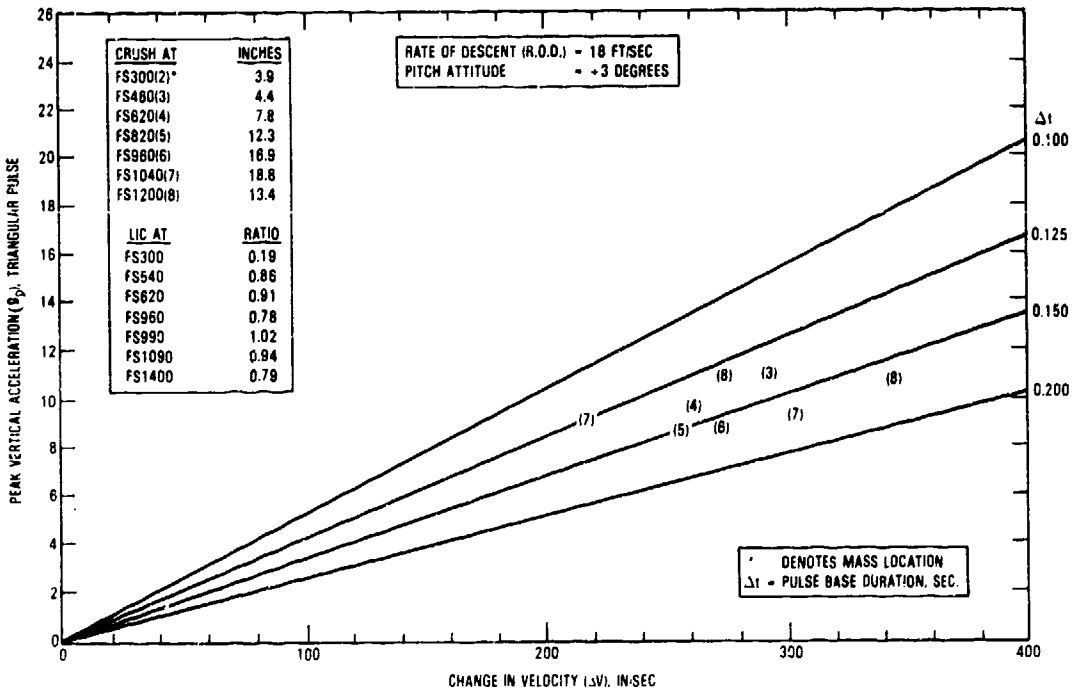

Figure 3-2. Floor Pulses for +3 Degree Pitch Attitude and 18 Ft/Sec Airplane Rate of Descent

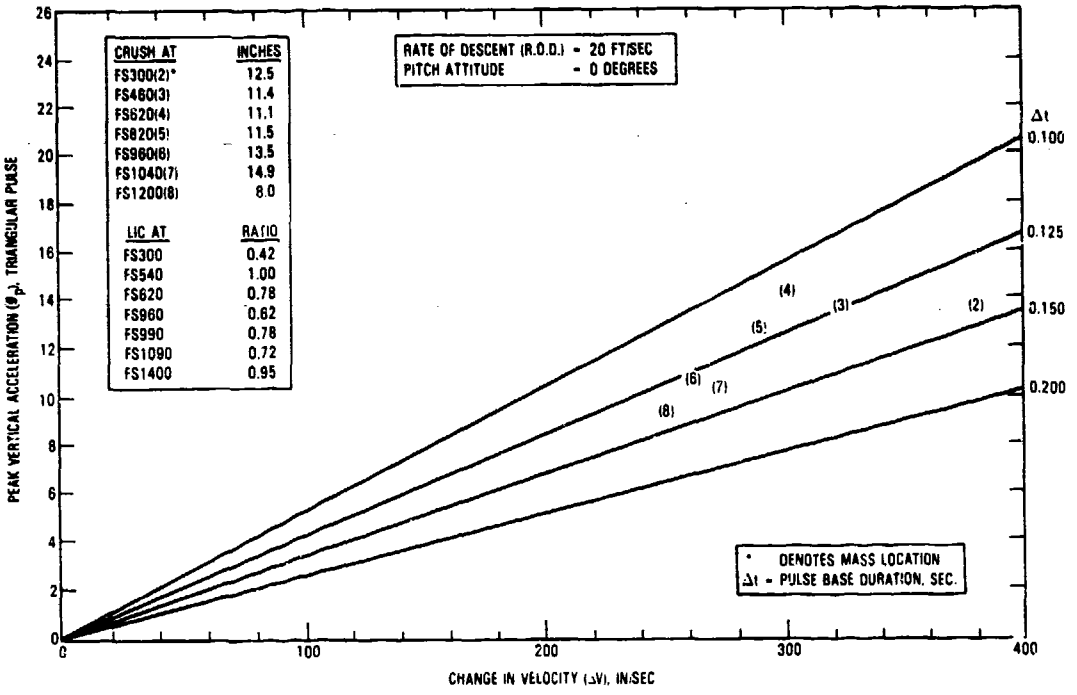

Figure 3-3. Floor Pulses for 0 Degree Pitch Attitude and 20 Ft/Sec Airplane Rate of Descent

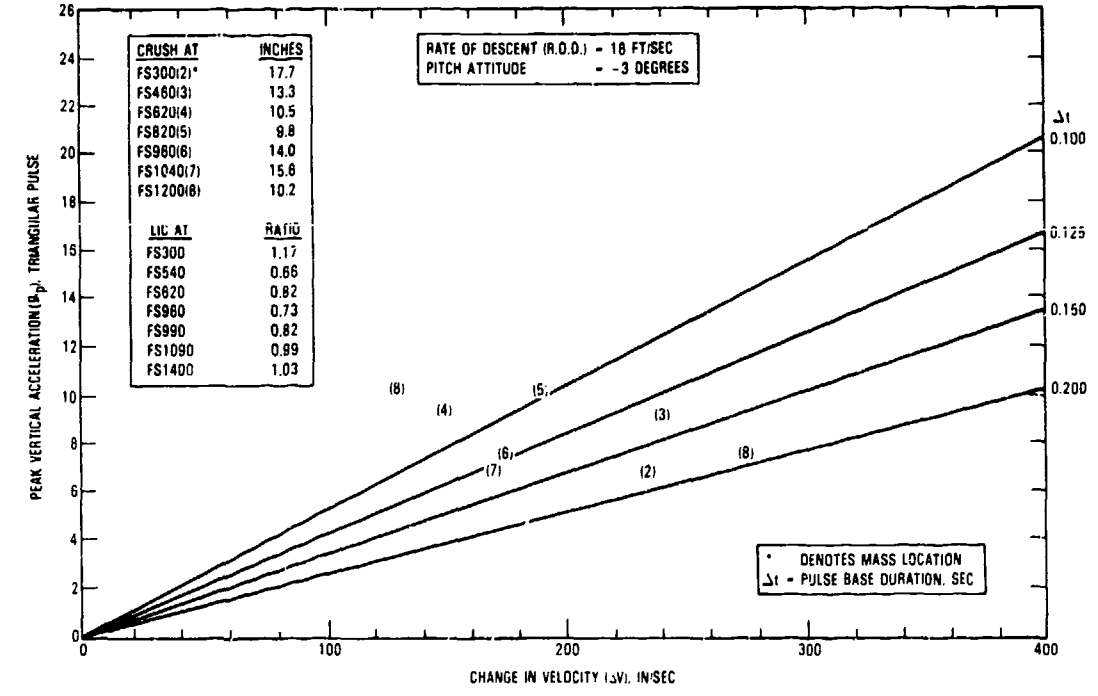

Figure 3-4. Floor Pulses for -3 Degree Pitch Attitude and 18 Ft/Sec Airplane Rate of Descent

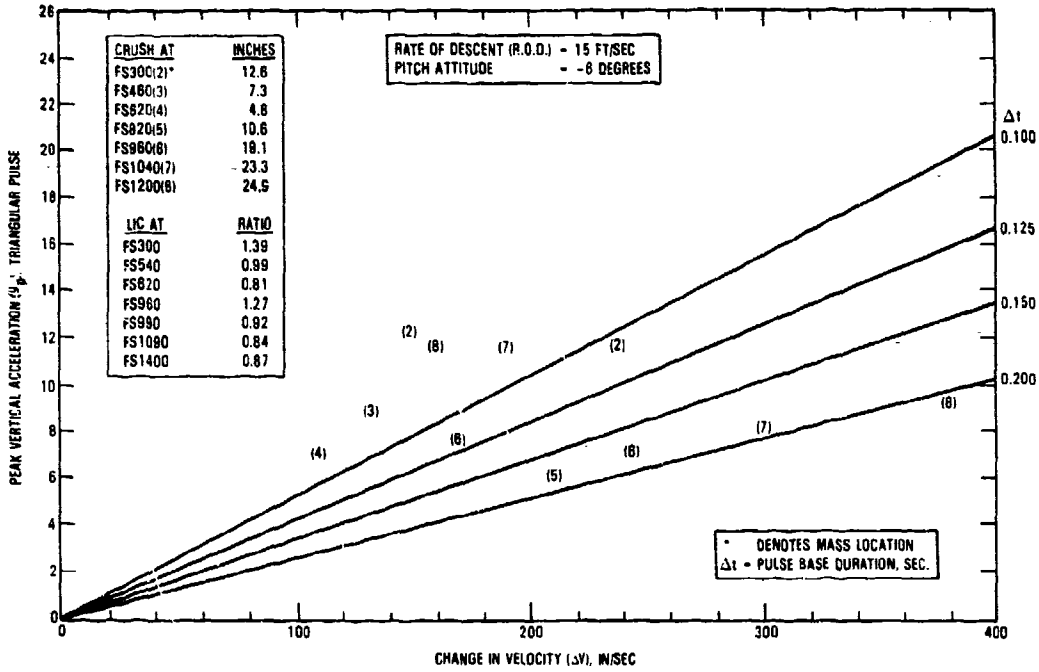

Figure 3-5. Floor Pulses for -6 Degree Pitch Attitude and 15 Ft/Sec Airplane Rate of Descent

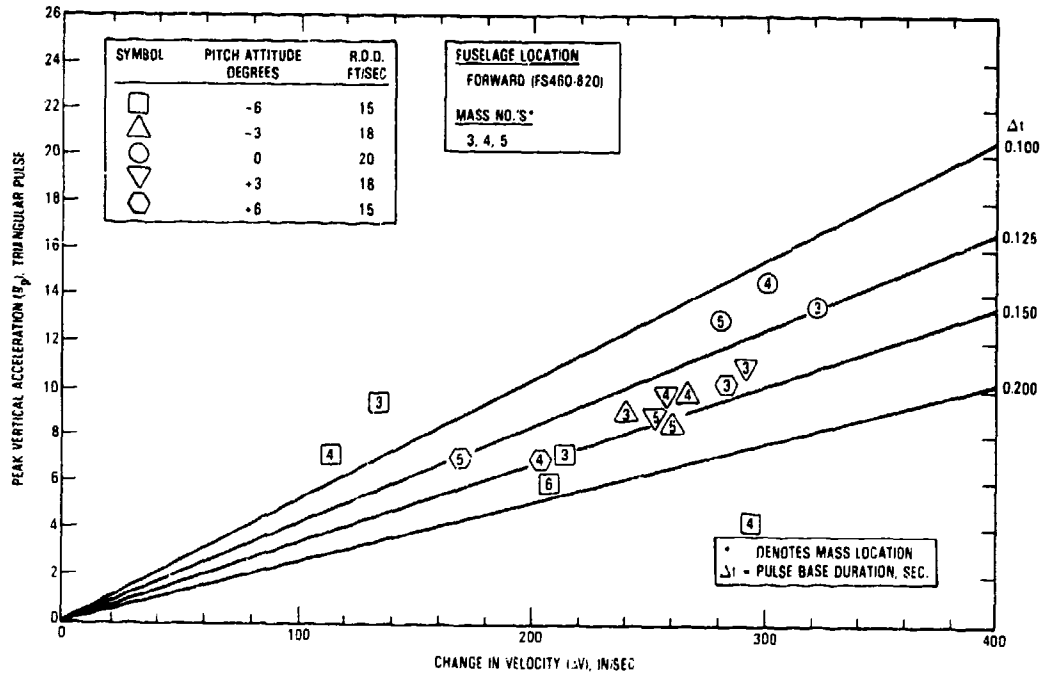

Figure 3-6. Floor Pulses at FS460-820

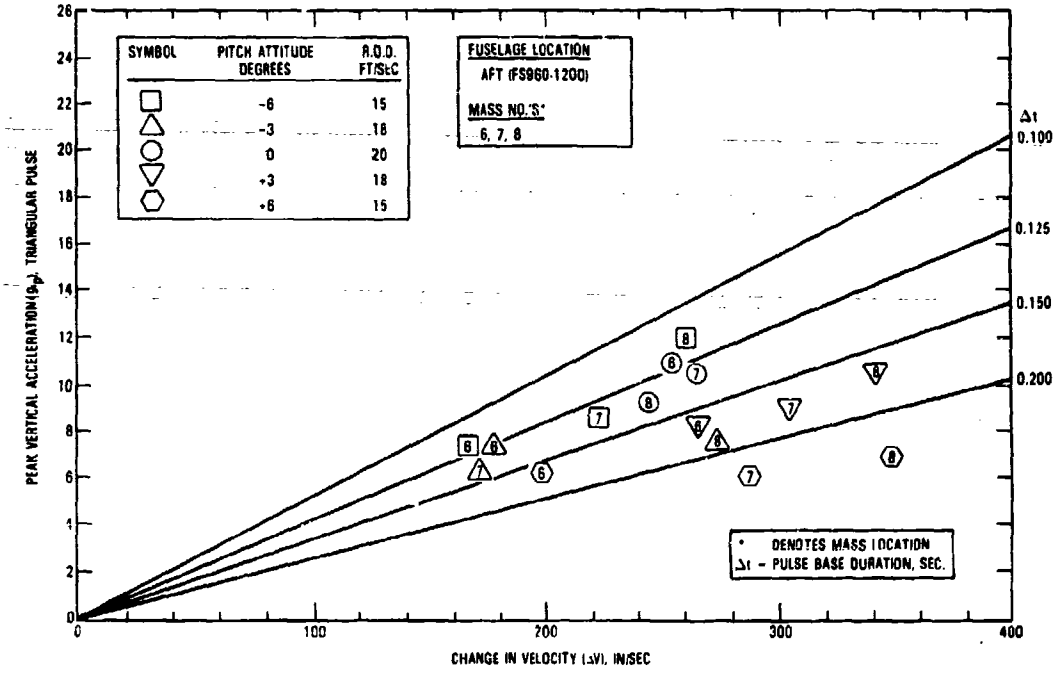

Figure 3-7. Floor Pulses at FS960-1200

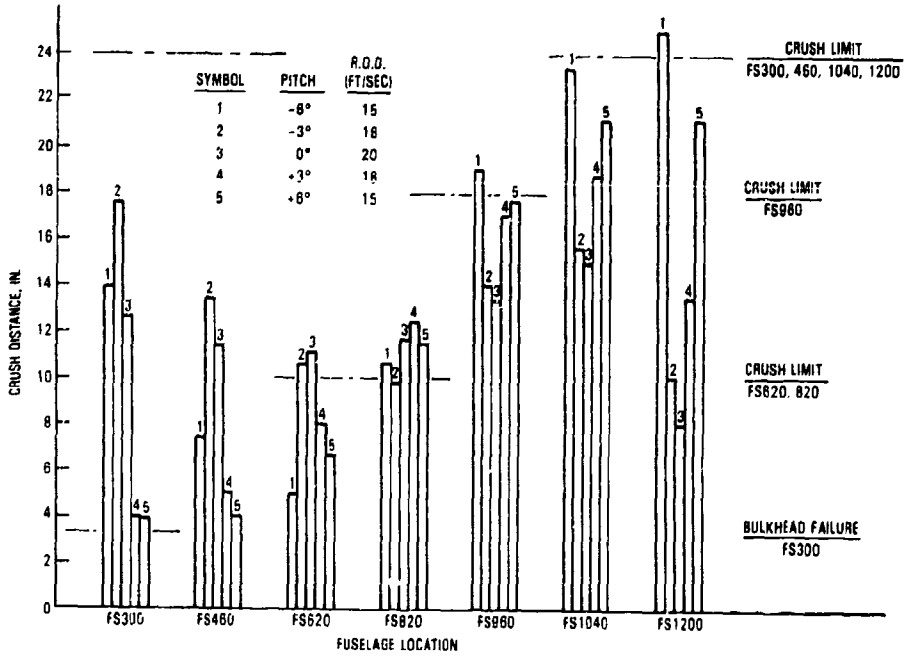

Figure 3-8. Fuselage Crush Distribution

impact conditions at which LIC values exceed 1.0. The respective crush limits are noted in this latter figure. Crush beyond these limits results in an extremely stiff load-deflection curve, which tends to produce correspondingly higher loads. The crush spring at FS300 is unique in that it represents a bulkhead which produces high loads for a small deflection. The load associated with deflections beyond 4.4 inches is extremely small. From figure 3-8 it can be observed that some impact conditions cause crushing of the fuselage which results in the occurrence of restiffening loads. Figures 3-9 and 3-10 show the envelopes of peak acceleration, airplane initial impact velocity and floor velocity change. The latter can be higher than the airplane initial velocity due to (1) rebound and (2) rotational velocity. The peak acceleration (g_p), pulse definition (triangular, base duration) and floor velocity change are the parameters which govern potential seat dynamic test requirements. The data shown in figure 3-9, are for a 0.150-second triangular pulse. It is based on using the highest velocity change pulses from figures 3-6 and 3-7 and adjusting the peak g_p and Δt to produce the same velocity change. The data provided in figures 3-9 and 3-10 indicate that the positive pitch attitudes provide for higher velocity change pulses. It appears that the initial impact on the aft fuselage occurs with more available initial crushing (FS960, 1200) than when impacting on the forward fuselage (FS460, 820), and thus the floor pulses tend to be of longer duration (compare figures 3-6 and 3-7).

3.1.1.2 Refined Analyses

The initial analytical results were obtained prior to the incorporation into the model of a revised nose gear bulkhead crush representation. This model change is described in Sections 3.2.1 and 3.3.1. Subsequent to this revision, several conditions were rerun and the analyses were expanded. Table 3-1 shows a summary of previously presented responses for the -6 degree, 0 degree and +6 degree pitch attitudes investigated. The significant response change in velocity (ΔV), peak acceleration (g_p), equivalent triangular pulses (for equal ΔV) for base durations of 0.150 and 0.200 second, and the associated fuselage crush distances, are presented. Figures 3-11 and 3-12 show the peak vertical accelerations and associated triangular base durations

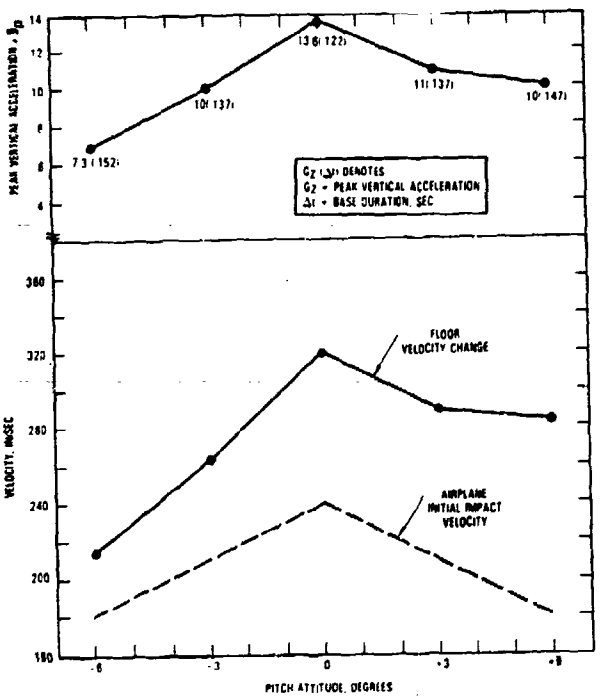

Figure 3-9. Forward Fuselage Floor Dynamic Triangular Pulse Parameters as a Function of Airplane Pitch Attitudes at Impact

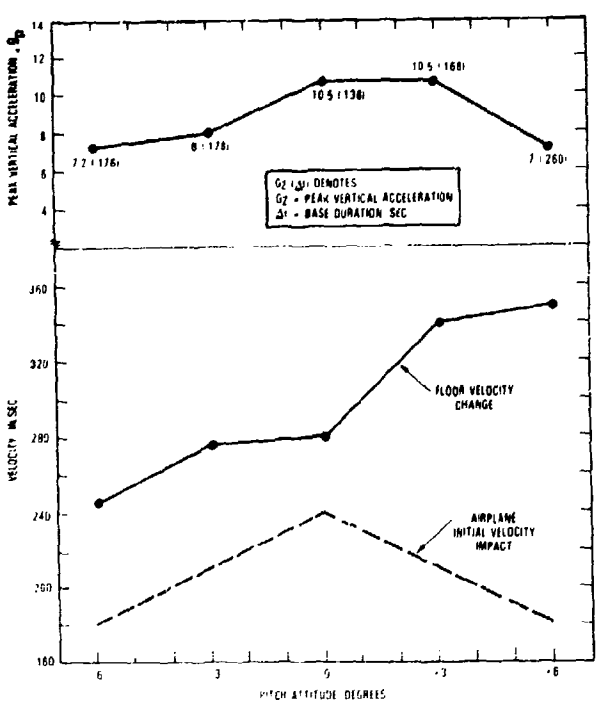

Figure 3-10. Aft Fuselage Floor Dynamic Triangular Pulse Parameters as a Function of Airplane Pitch Attitude at Impact

TABLE 3-1. AIR-TO-GROUND IMPACT ANALYSES RESULTS

IMPACT CONDITION	FUSELAGE STATION	g_{peak}	VELOCITY CHANGE, IN./SEC	PEAK ACCELERATION, g *		CRUSH DISTANCE, INCHES
				Δt = 0.150 SECONDS	Δt = 0.200 SECONDS	
SIX-DEGREE NOSE-DOWN PITCH, 15 FT/SEC SINK SPEED	300	12.0	235	8.1	6.1	12.6
	460	8.5	135	4.7	3.5	7.3
	620	7.2	110	3.7	2.8	4.8
	820	8.3	210	7.2	5.4	10.6
	960	9.0	240	8.2	6.2	19.1
	1040	12.4	190	6.5	4.9	23.3
	1200	12.2	160	5.5	4.1	24.9
ZERO-DEGREE PITCH, 20 FT/SEC SINK SPEED	300	11.2	400	13.8	10.4	12.5
	460	13.6	320	11.0	8.3	11.4
	620	13.0	315	10.9	8.2	11.1
	820	10.7	290	10.0	7.5	11.5
	960	11.4	276	3.6	7.2	13.5
	1040	10.0	272	9.3	7.0	14.5
	1200	10.4	260	8.9	6.7	8.0
SIX-DEGREE NOSE-UP PITCH, 15 FT/SEC SINK SPEED	300	19.3	360	12.4	9.3	3.9
	460	9.9	280	9.7	7.3	4.1
	620	7.9	180	6.3	4.7	6.5
	820	7.5	170	5.9	4.4	11.3
	960	7.3	200	6.9	5.2	17.6
	1040	6.8	290	9.5	7.5	21.1
	1200	6.8	345	11.8	8.9	21.2

* FOR A TRIANGULAR PULSE SHAPE WITH A BASE DURATION (Δt) AND VELOCITY CHANGE AS NOTED

obtained directly from the analyses for the forward fuselage (FS300, 460, 620) and the mid-aft fuselage (FS960, 1040, 1200). Figures 3-11 and 3-12 update the data presented in figures 3-9 and 3-10. The responses shown in figures 3-11 and 3-12 contain pulses which have a Δt range primarily between 0.137 second and 0.178 second, peak vertical acceleration values between 7g and 13g, and velocity changes between 216 in/sec and 400 in/sec. These values are associated with an envelope of impact conditions in which the fuselage shell integrity is considered at the threshold of exceedance. The longitudinal pulse for these conditions is assumed to be proportional to the vertical pulse in magnitude as a function of ground coefficient of friction (i.e., $\mu = 0.5$, $g_x = 0.5g_z$). The data shown in table 3-1 are plotted in figures 3-13 through 3-16. The accelerations, shown in figure 3-13, are presented without regard to time duration. Figures 3-14 and 3-15 present the analyses results on the

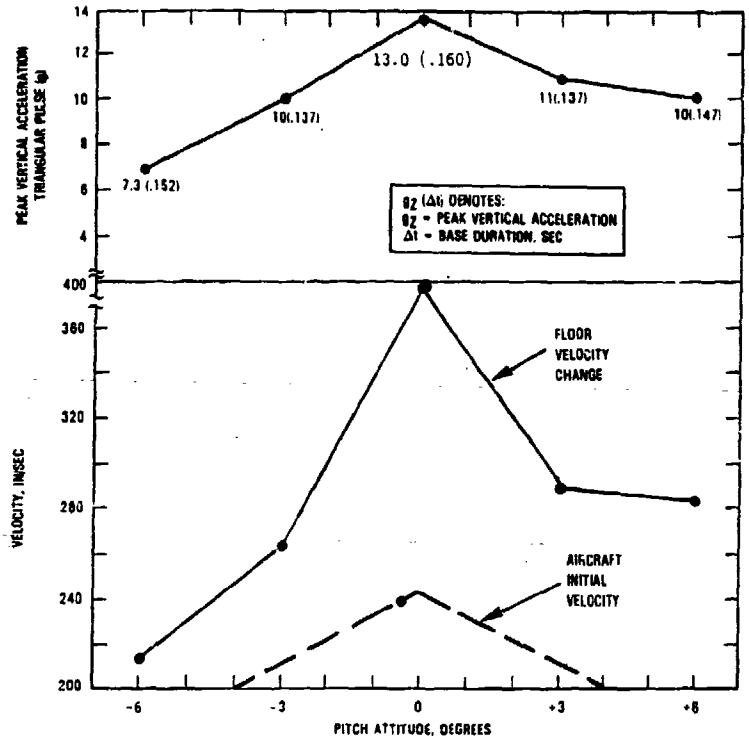

Figure 3-11. Forward Fuselage Floor Dynamic Triangular Pulse Parameters as a Function of Airplane Pitch Attitude at Impact - Revised Analysis

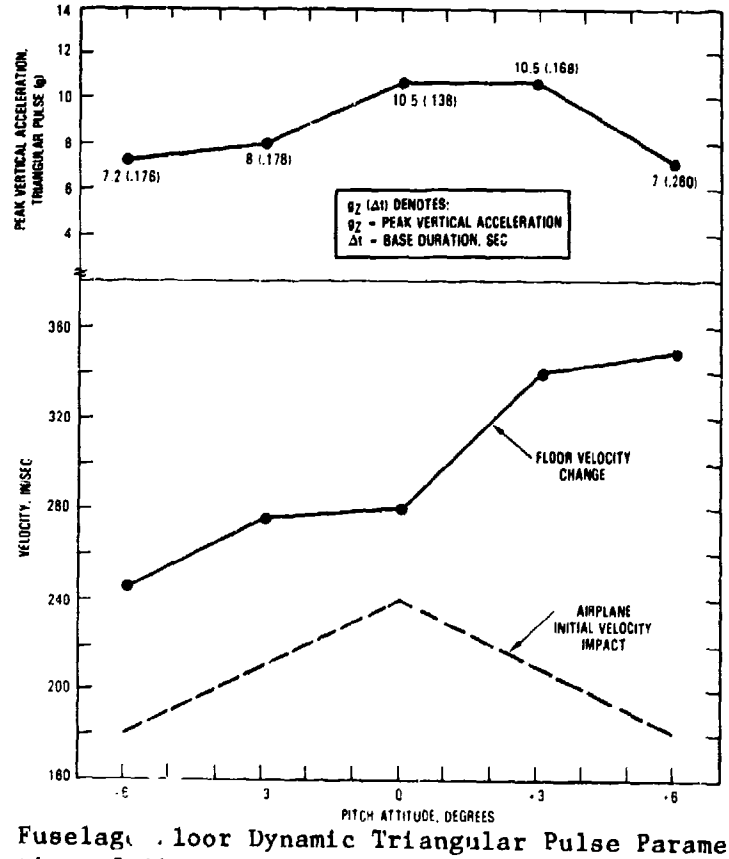

Figure 3-12. Aft Fuselage Floor Dynamic Triangular Pulse Parameters as a Function of Airplane Pitch Attitude at Impact - Revised Analysis

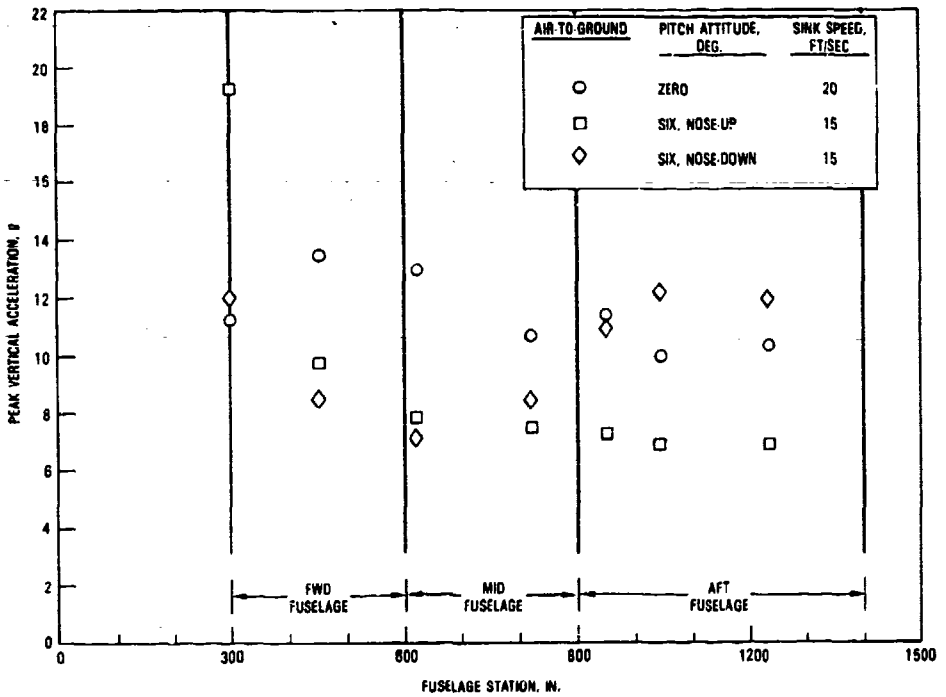

Figure 3-13. Peak Vertical Acceleration Versus Fuselage Station

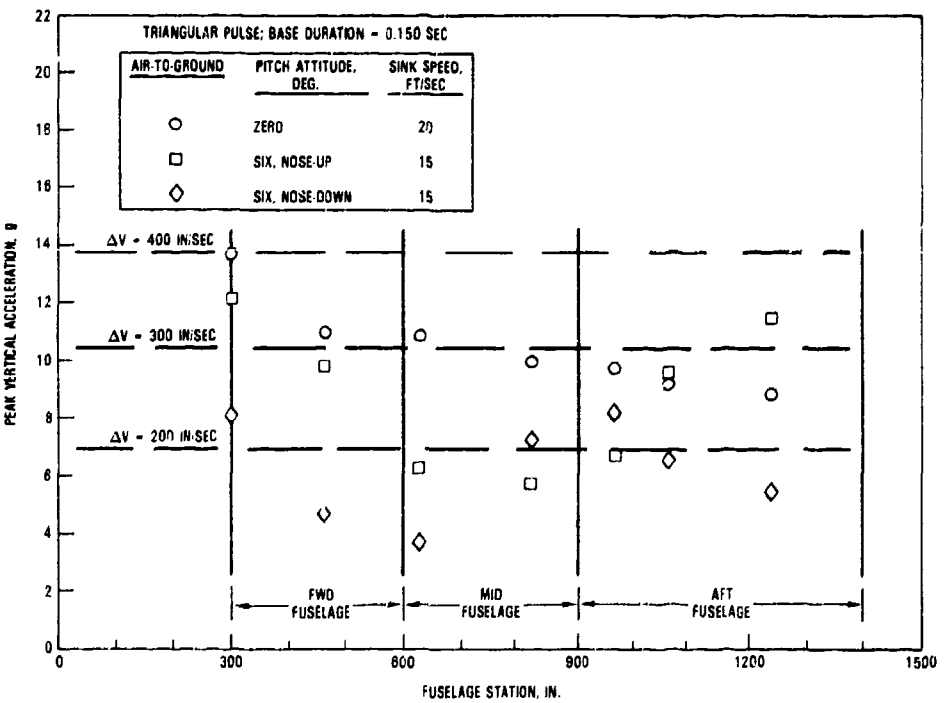

Figure 3-14. Vertical Triangular Pulse Versus Fuselage Station, Base Duration - 0.150 sec.

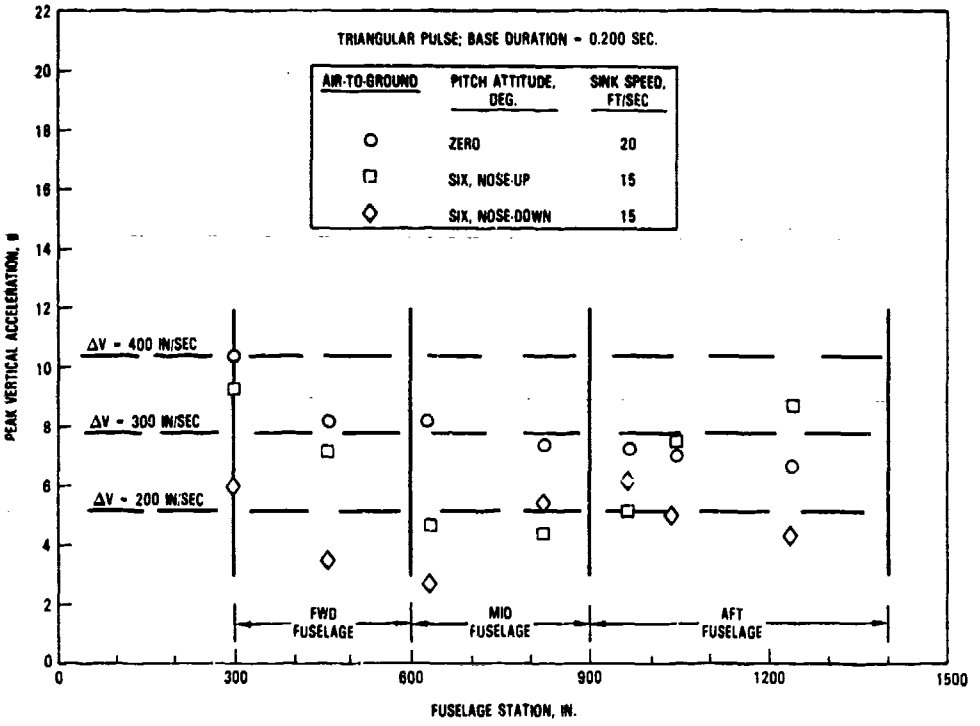

Figure 3-15. Vertical Triangular Acceleration Pulse Versus Fuselage Station, Base Duration - 0.200 sec.

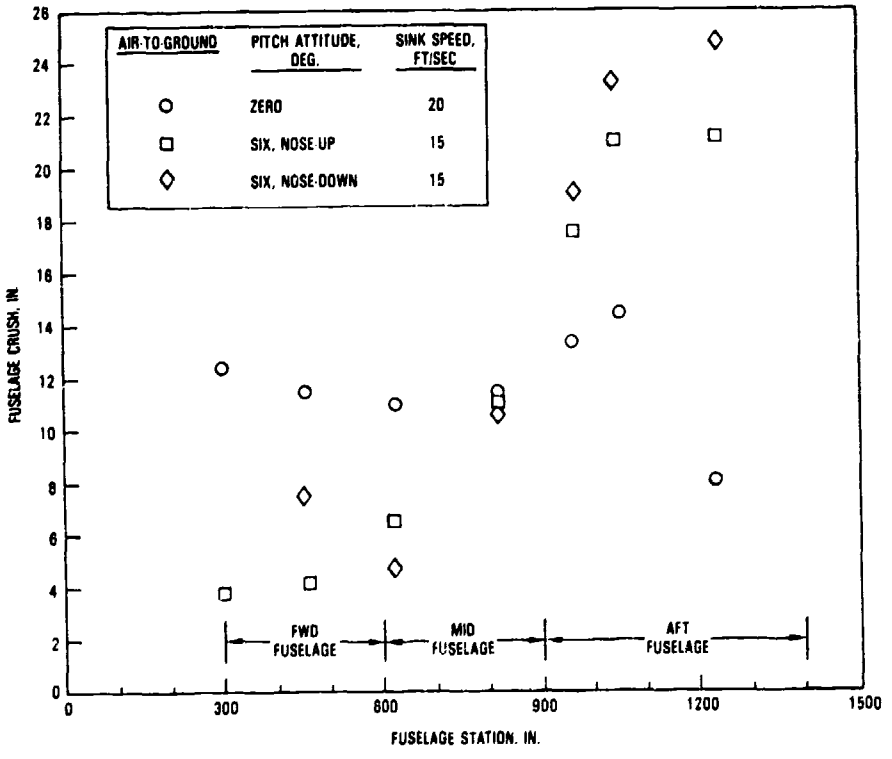

Figure 3-16. Fuselage Crush Distribution

basis of 0.150 second and 0.200 second base duration triangular pulses, respectively. These pulse durations are reasonable approximations for floor dynamic test pulses. Also shown, in figures 3-14 and 3-15, are lines of constant velocity change (ΔV). As can be observed from these two plots, the response for the most part reflects a velocity change approaching 300 in/sec to 400 in/sec in the most forward passenger region (FS300), 300 in/sec in the passenger mid-cabin region and 300 in/sec to 350 in/sec in the passenger aft cabin area. The crushing distribution for the air-to-ground impacts is shown in figure 3-16. Passenger forward cabin and mid-cabin underfloor crushing can reach 10 to 12 inches. Passenger aft cabin underfloor crushing can be more extensive (particularly between the main landing gear aft bulkhead (FS960)) and the fuselage aft pressure bulkhead (FS1400), and reach 20 to 25 inches. The latter crush is within the range of crush obtained during FAA/NASA narrow-body fuselage section testing performed at initial impact velocities of 20 ft/sec to 35 ft/sec. The floor peak accelerations, measured during the FAA/NASA section tests, are approximately 8g to 10g. This compares with the 7g to 10.5g, shown in figure 3-12.

The data shown in figures 3-11 through 3-16 and table 3-1 reflect a tendency for the modeled aircraft to rotate after initial impact. In the case of an initial nose-down impact, the airplane eventually settles on the aft fueslage, which shows substantial crush. The flat (zero-degree pitch) impact shows a relatively evenly distributed peak acceleration and fuselage crush distribution. However, there is an indication that the velocity change is greater at the extreme forward of the fuselage. The initial nose-up impact results in a higher peak acceleration and velocity change at the forward fuselage than at the aft fuselage where the airplane initially hits the ground. It is possible that the analytical simulation allows for more rebound than exists and thus the velocity changes associated with post-impact behavior are more severe than those experienced at initial impact. However, the following data tend to suggest that rotational and rebound effects could be significant: (1) During the CID test when the fuselage first impacts the ground the sink speed is noted to be 14 to 15 ft/sec. The integrated acceleration traces indicate that the changes of velocity for the associated

pulses from the cockpit (forward of the impact location) through to the wing leading edge station (aft of the impact location) vary from 15.2 to 21.0 ft/sec., and (2) the result of NASA light fixed-wing aircraft tests which are reported in numerous documents. Reference 9 reports on light airplane (twin-engine, low-wing) crash tests (gears retracted) at three pitch angles (impact on concrete) and reference 10 data report on low-wing, single-engine crash tests (gears extended) under three different conditions, including 30 degrees nose-down onto concrete terrain. In both reports the data indicated that the subsequent slap down can be significant such that the latter peak accelerations approach the magnitude experienced at the initial impact location. There are, of course, differences in structure and size between light fixed-wing and transport category aircraft. The extended size of the larger aircraft could easily induce higher rotational velocities, particularly if structural failure is localized and the aircraft remains rigid, as it appears to have happened in the full-scale CID crash test.

Subsequent to the reformulation of information that is presented in table 3-1 and figures 3-11 through 3-16, additional analyses were performed to investigate:

- The change in the crush characterization of the nose-gear bulkhead (similar to that used in the ramp impact) to ascertain if the aircraft air-to-ground analyses results are affected.

- The incorporation of wing and engine responses and the monitoring of wing shear and bending moment versus estimated strength allowables. Wing correlation results reported in reference 1 showed reasonable agreement between test and analyses results for wing bending and shear; and thus airframe strength considerations extended to wing, as well as fuselage capability, appear appropriate.

The conditions analyzed are noted in table 3-2. The results for the fuselage responses to these conditions are shown in table 3-3. A sample plot of acceleration responses for Condition No. 7 at mid-fuselage location (FS820) is shown in figure 3-17. The unfiltered acceleration peak is 13.6g (vertical)

and 5.1g (longitudinal). The base duration of this pulse is about 0.108 second and the change in vertical velocity during this time is 315 in/sec. Based on a triangular pulse of equal velocity change and base duration, the peak amplitude is 15.1g which is the value shown in table 3-3.

The acceleration response for several groups of conditions in the form of a triangular pulse is shown in figures 3-18, 3-19 and 3-20. The data is a cross-plot of peak g, Δt, and ΔV. Similarly, figures 3-21, 3-22 and 3-23 show fuselage LIC and underside crush for the same sets of conditions. The data from all these conditions (7 through 12) are plotted slightly different in figure 3-24. This figure contains the same data (g, Δt and ΔV) as figures 3-18, 3-19 and 3-20, but shows envelopes of velocity change. The majority of the response data clusters between ΔV of 22 ft/sec to 27 ft/sec and a Δt between 0.12 second and 0.16 second.

TABLE 3-2. DESCRIPTION OF ANALYSES: AIR-TO-GROUND IMPACT CONDITIONS

CONDITION NO.	AIRPLANE INITIAL SINK SPEED FT/SEC	PITCH ATTITUDE DEGREES	INITIAL LIFT	ENGINE GROUND CONTACT	FORWARD VELOCITY COMPONENT (155 KTS)	REVISED NOSE GEAR BULKHEAD CRUSH
1	22	0	NO	YES	YES	YES
2	22	+1	NO	YES	YES	YES
3	20	+1	NO	YES	YES	YES
4	17.3	+1	NO	YES	YES	YES
5	17.3	+1	YES	YES	YES	YES
6	22	0	NO	NO	NO	YES
7	22	0	NO	NO	YES	YES
8	20	0	NO	NO	YES	NO
9	20	0	NO	NO	YES	YES
10	15	-6	NO	NO	YES	YES
11	15	+6	NO	NO	YES	YES
12	15	-6	NO	NO	YES	NO
13	15	+6	NO	NO	YES	NO

TABLE 3-3. FUSELAGE RESPONSE PARAMETERS FOR DIFFERENT IMPACT CONDITIONS

	Condition No. 1	Condition No. 2	Condition No. 3	Condition No. 4	Condition No. 5	Condition No. 6	Condition No. 7	Condition No. 8	Condition No. 9	Condition No. 10	Condition No. 11	Condition No. 12	Condition No. 13
LIC Ratio @ FS													
350	.71	.82	.57	.59	.57	.50	.57	.87	.52	.97	.65	1.0	.63
450	.71	.95	.59	.60	.68	.57	.64	1.0	.46	.97	.73	1.15	.76
540	.82	.94	.68	.73	.80	.71	.74	1.0	.28	.86	.94	0.99	.93
600/620	.68	.83	.66	.67	.75	.71	.77	.90	.70	.79	.94	.90	.91
960	.60	1.2	.74	.52	.71	.53	.72	.62	67	.98	.83	1.27	.82
990	.77	1.1	.97	.55	.78	.64	.78	.78	.61	1.3	.89	.92	.88
1090	.68	.95	.93	.71	.97	.74	.69	.72	.56	1.17	1.05	.84	.99
1160	.75	1.02	.81	.65	.89	.83	.77	.70	.62	1.03	1.00	.77	.97
1210	.94	.99	.86	.58	.75	1.02	.99	.90	.82	1.03	.89	.82	.86
1320	.92	1.07	.84	.61	.76	.98	.95	.85	.79	1.01	.88	.82	.86
1400	.99	1.08	.9	.68	.83	1.08	1.04	.95	.87	1.07	.93	.87	.9
Crush (inches), @ FS													
300	10.0	9.4	7.7	5.9	5.0	8.8	10.1	12.4	8.7	3.9	4.3	12.6	3.9
450	10.1	9.5	8.2	5.8	4.3	9.4	10.3	11.4	8.8	–	4.4	7.3	4.1
620	10.8	10.5	8.9	7.3	5.1	10.6	11.1	11.2	10.0	3.1	6.6	4.8	6.5
820	11.8	12.4	11.7	10.4	7.3	12.3	12.1	11.5	11.5	11.2	11.4	10.6	11.3
960	13.8	14.9	14.1	12.8	9.8	15.0	15.8	13.5	14.3	19.2	17.8	19.1	17.6
1040	16.3	17.0	14.6	12.9	10.3	16.9	17.7	14.9	15.2	22.9	21.1	23.3	21.1
1240	10.7	11.3	6.4	3.8	2.4	10.8	11.7	8.1	7.4	23.7	21.2	24.9	21.2
Triangular Pulse Data @ FS, (g, Δt) ΔV													
199	(17.2,.145) 484	(28.5,.110) 587	(17.9,.150) 525	(25.2,.095) 468	(26.6,.095) 494	(11.8,.222) 500	(16.8,.144) 467	(20.2,.108) 430	(11.9,.156) 371	(17.8,.066) 230	(27.0,.090) 470	(19.0,.084) 287	(27.8,.084) 450
300	(14.6,.150) 429	(17.5,.135) 483	(17.3,.130) 429	(18.3,.095) 335	(21.0,.090) 365	(14.0,.162) 441	(15.0,.144) 417	(15.0,.126) 364	(10.6,.180) 349	(13.4,.072) 187	(21.0,.090) 362	(9.0,.158) 256	(19.0,.102) 389
460	(18.6,.105) 377	(12.5,.165) 413	(17.4,.100) 350	(11.3,.335) 296	(11.0,.150) 319	(17.7,.108) 370	(18.9,.102) 376	(14.0,.120) 322	(13.0,.126) 316	(5.7,.150) 166	(10.2,.144) 285	(4.7,.168) 155	(9.2,.150) 261
620	(16.6,.110) 355	16.4 (.105) 347	(13.1,.125) 324	(9.1,.150) 264	(8.0,.170) 263	(15.9,.114) 350	(17.8,.102) 351	(14.0,.114) 309	(11.7,.132) 298	(8.0,.138) 205	(6.3,.176) 224	(5.8,.162) 175	(6.4,.148) 178
820	(13.4,.120) 310	12.1 (.135) 314	(10.3,.145) 287	(8.1,.150) 234	(8.7,.140) 236	(14.4,.114) 316	(15.1,.108) 315	(12.9,.144) 286	(10.9,.132) 278	(10.2,.144) 270	(5.1,.180) 153	(6.0, 192) 220	(5.2,.174) 171
960	(12.2,.125) 295	12.5 (.130) 312	(11.0,.135) 285	(7.6,.150) 219	(8.8,.140) 239	(12.8,.120) 296	(12.8,.120) 299	(11.0,.126) 269	(10.4,.132) 266	(11.8,.144) 324	(5.5,.246) 258	(7.0,.196) 295	(5.1,.244) 256
1040	(12.0,.125) 289	13.3 (.125) 320	(11.0,.135) 288	(7.6,.145) 212	(9.2,.130) 250	(12.2,.120) 283	(12.6,.120) 291	(10.4,.132) 265	(10.2,.132) 260	(13.3,.144) 366	(6.1,.246) 290	(8.4,.186) 296	(6.2,.244) 293
1200	(11.0,.125) 262	13.7 (.125) 341	(11.2,.135) 290	(7.1,.175) 238	(10.6,.140) 268	(10.1,.126) 247	(11.6,.120) 269	(9.8,.138) 190*	(9.2,.138) 242	(13.5,.156) 402	(7.2,.252) 350	(10.7,.200) 386	(7.2,.252) 350
1400	(8.6,.200) 335	10.2 (.189) 363	(9.7,.190) 331	(7.6,.190) 277	(10.9,.140) 282	(7.3,.210) 297	(8.1,.210) 334	(8.1,.204) 319	(7.6,.210) 309	(13.6,.19) 500	(8.4,.258) 420	(11.4,.240) 528	(8.2,.252) 396

*Also (6.8,.228) 300

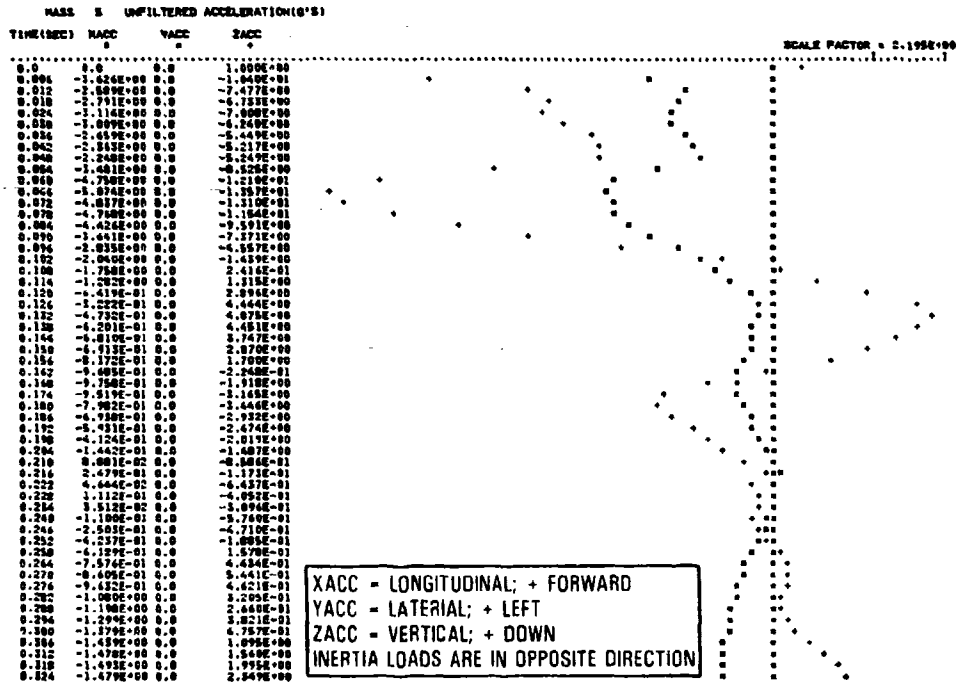

Figure 3-17. Fuselage Mass No. 5 Acceleration Response, Condition No. 7

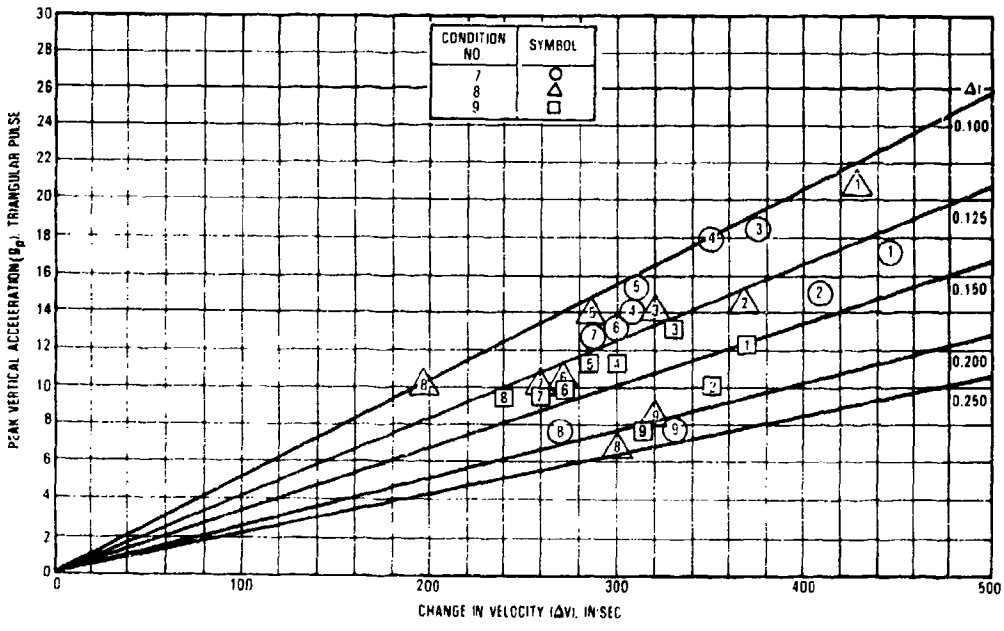

Figure 3-18. Comparison of Pulse Data for Conditions 7, 8, 9

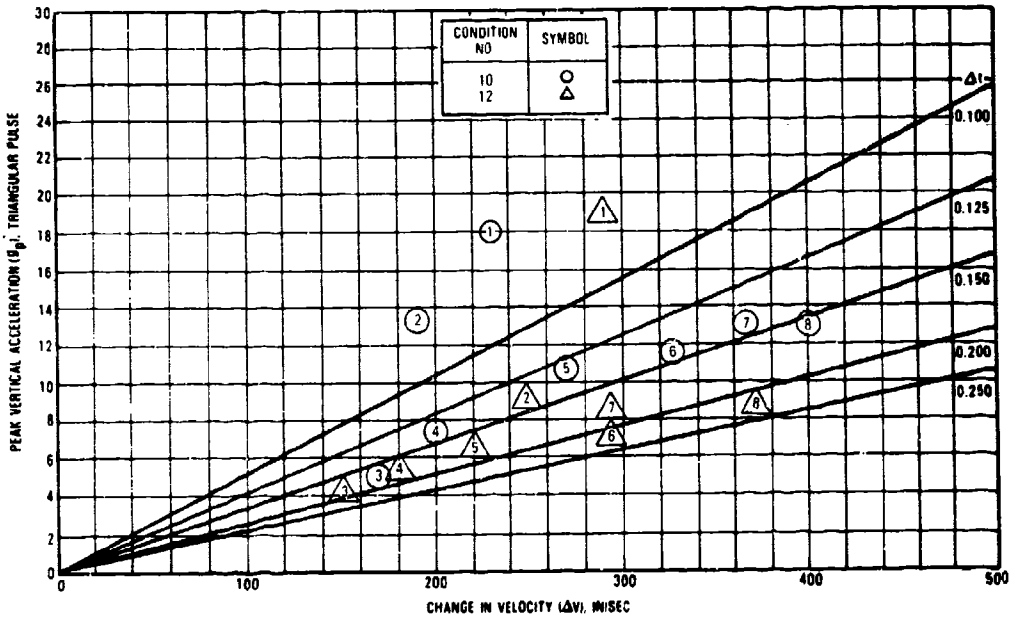

Figure 3-19. Comparison of Pulse Data for Conditons 10, 12

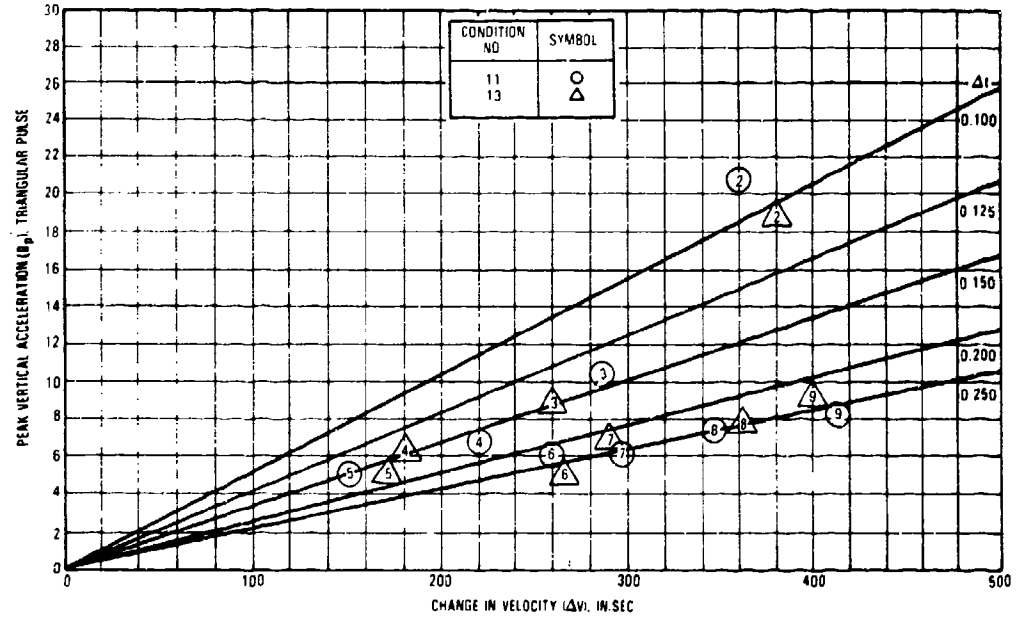

Figure 3-20. Comparisons of Pulse Data For Conditions 11, 13

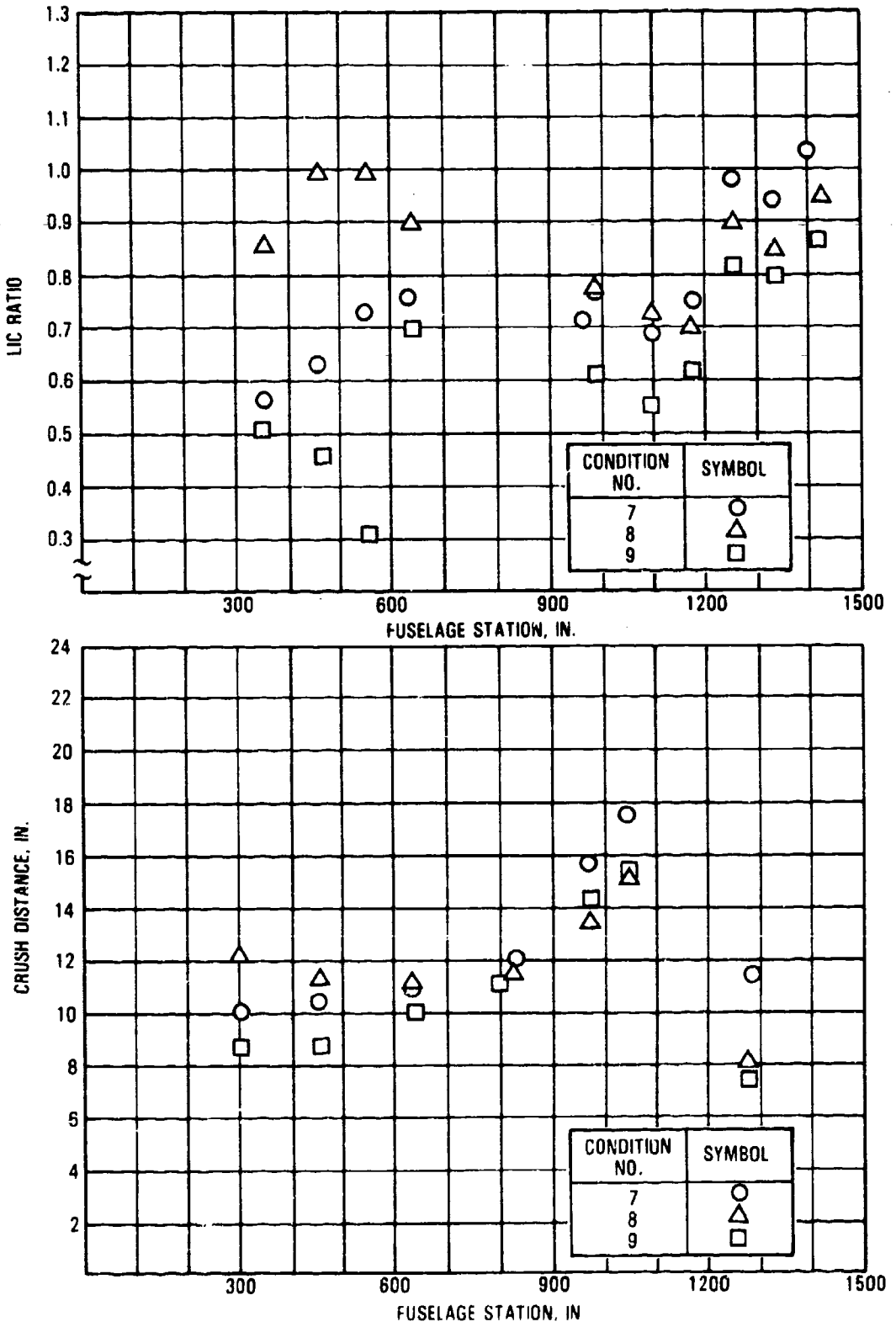

Figure 3-21. Comparison of LIC and Crush Data for Conditions 7, 8, 9

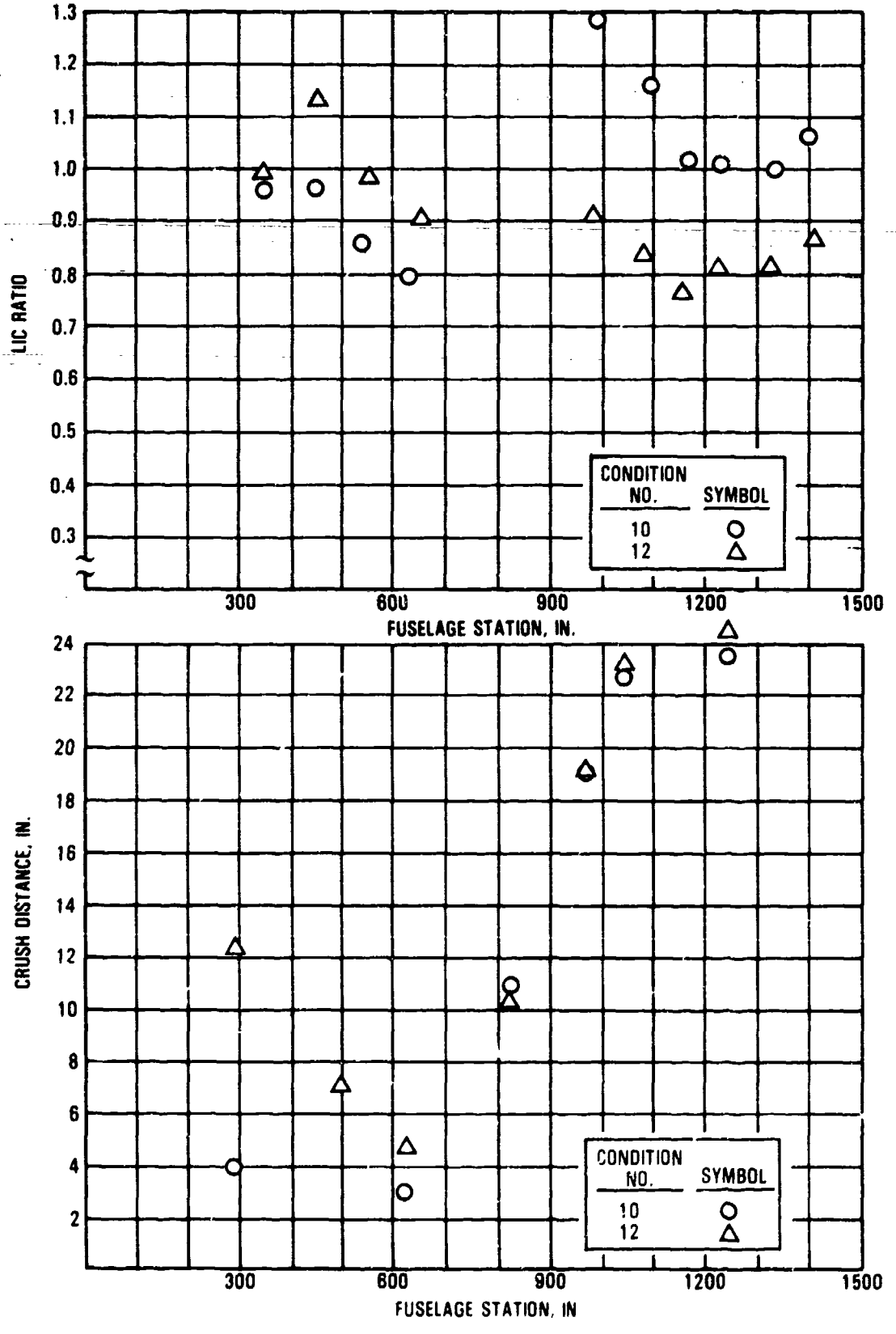

Figure 3-22. Comparison of LIC and Crush Data for Conditions 10, 12

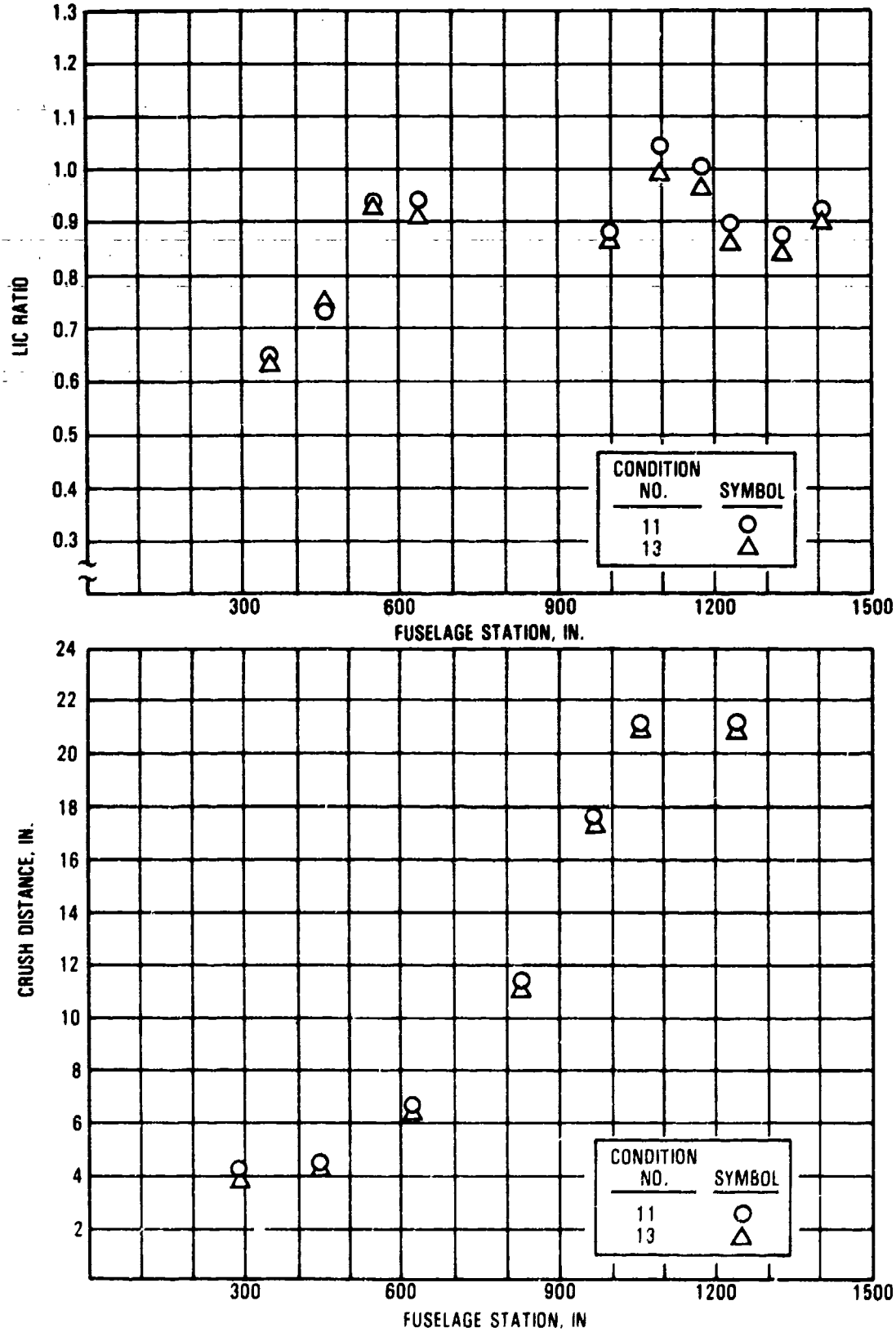

Figure 3-23. Comparison of LIC and Crush Data for Conditions 11, 13

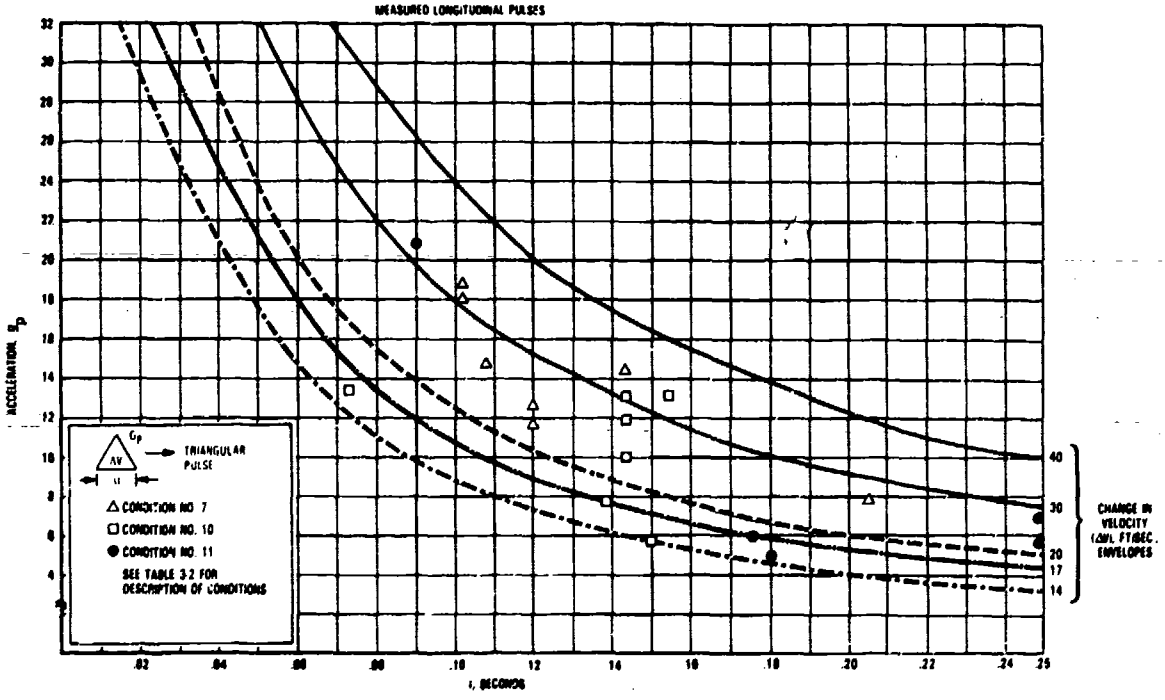

Figure 3-24. Analytically Obtained Vertical Pulses

The wing/engine responses are tabulated in table 3-4. The wing response data for Condition No. 7 (table 3-2), indicates that the bending moments are approaching the estimated bending ultimate strength and the shears are exceeding the estimate ultimate shear capability along the wing span. The peak accelerations are 14.3g vertical and 4.8g longitudinal (fore-aft) at wing inboard mass location No. 11. The analytically obtained wing mass No. 11 pulse data is shown in figure 3-25. The response data indicates an equivalent (same velocity, time period) triangular pulse in the vertical direction of:

peak acceleration (g_p) = 13.5g
change in velocity (ΔV) = 312 in/sec.
base duration (Δt) = 0.120 sec.

In the longitudinal direction, the equivalent triangular pulse can be described as:

peak acceleration (g_p) = 6.2g
change in velocity (ΔV) = 140 in/sec.
base duration (Δt) = 0.120 sec.

TABLE 3-4. WING AND ENGINE RESPONSE ANALYSIS RESULTS

	Condition No. 1	Condition No. 2	Condition No. 3	Condition No. 4	Condition No. 5	Condition No. 6	Condition No. 7	Condition No. 8 (b)	Condition No. 9	Condition No. 10	Condition No. 11	Condition No. 12 (b)	Condition No. 13 (b)
Peak Acceleration @ B.L.													
118.3	14.3	13.3	8.6	7.6	8.6	14.2	14.3		8.4	8.0	7.4		
271.8	13.0	13.2	10.0	7.0	7.7	10.8	10.9		7.4	8.0	4.2		
430.7	16.8	17.4	12.3	9.8	7.3	11.8	12.0		8.0	9.5	5.3		
583.5	15.0	13.9	11.8	7.0	5.1	8.5	10.1		8.6	4.8	6.7		
740.6	34.3	36.6	30.4	13.1	17.1	18.6	19.2		16.2	17.8	11.8		
Peak Engine Acceleration @ B.L.													
321.6	12.1	12.8	11.7	10.0	8.9	13.3	12.8		10.0	9.4	5.1		
551.6	13.8	14.3	11.6	14.8	8.0	8.9	8.6		7.5	8.1	5.8		
Peak Wing Shear (S_z) LB x 10^3 Between B.L.'s													
0-118.3 (a) (250)	262.0	290.0	269.0	203.4	127.8	316.8	332.0		262.0	279.0	263.0		
118.3-271.8 (200)	215.0	228.0	182.0	129.7	72.9	265.0	264.0		209.0	235.0	157.0		
271.8-430.7 (110)	70.0	83.0	67.7	46.8	46.4	91.3	84.0		72.6	80.0	84.0		
430.7-583.5 (40)	54.6	56.0	38.7	38.7	35.8	81.4	79.0		68.0	80.0	71.0		
Peak Wing Bending Moment (M_y) in-lb. x 10^6 @ B.L. (a)													
Root (75)	53.2	57.3	49.5	37.5	19.6	67.6	69.0		57.6	65.8	55.8		
118.3 (50)	37.0	38.4	34.0	26.2	15.7	46.3	46.5		44.8	48.0	48.0		
271.8 (30)	24.3	24.9	16.8	16.2	12.5	31.3	32.0		29.1	29.0	27.0		
430.7 (15)	16.7	17.3	12.5	9.6	7.2	14.9	15.3		14.2	14.4	12.5		
583.5 (10)	9.3	9.9	8.1	3.7	4.1	5.1	5.3		4.5	4.9	3.4		

(a) ( ) – Denotes estimated ultimate strength

(b) Wing data was not obtained for these earlier runs.

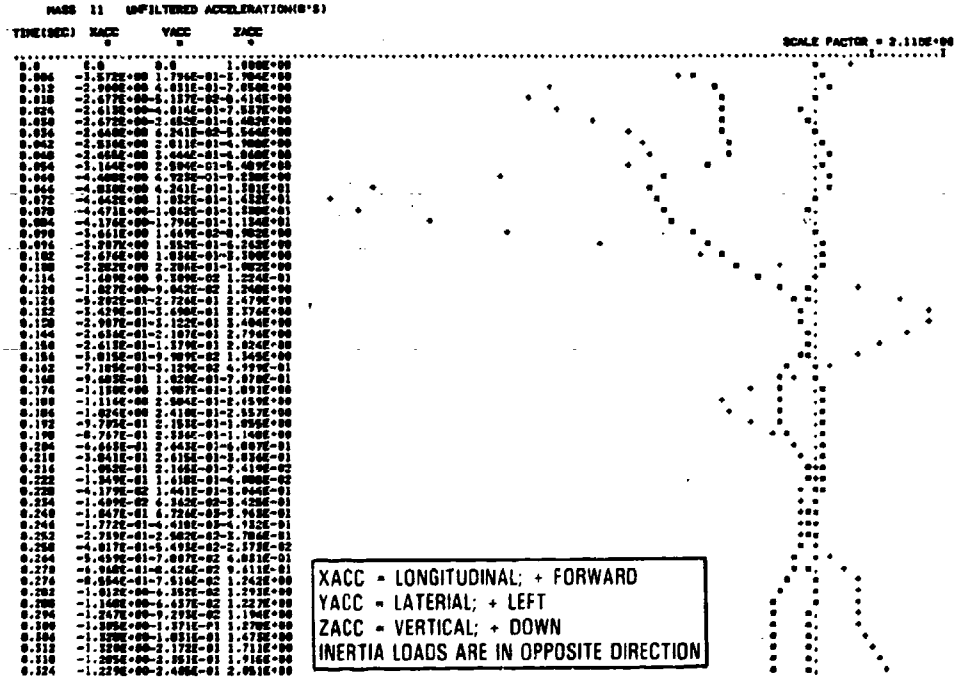

Figure 3-25. Wing Mass No. 11 Acceleration Response, Condition 7

A summary of the variation in acceleration pulse along the wing span is noted in table 3-5. The responses shown for wing masses 14 and 15 occur within 0.250 second after initial fuselage impact with the ground. Subsequent to this time, these masses exhibit large oscillatory motion and associated higher velocity and accelerations. Since the condition analyzed has zero lift, the wing tip (mass 15) shows the potential for ground contact after about 0.250 second, which would alter the responses thereafter. The model does not contain ground contact springs for the outer wing masses, however, so the wing responses noted can be considered associated with the deceleration forces without wing obstacle/ground contact mass No.11. Responses can be taken as representative for such a high sink speed impact, particularly for the wing inboard tanks. Comparisons of wing shear and moments for the level pitch attitude condition at two different sink speeds (Condition Nos. 7 and 9)

TABLE 3-5. VARIATION OF ACCELERATION PULSE ALONG WING SPAN

Location	Direction	Triangular Pulse Parameters		
		$g_{(peak)}$	Δt (sec)	ΔV (in/sec)
Mass 12	Up	10.8	.150	316
	Aft	5.4	.144	142
Mass 13	Up	11.2	.132	368
	Aft	5.5	.220	150
Mass 14	Up	8.2	.078	140
	Aft	6.2	.246	300
Mass 15	Down	21.5	.120	482
	Aft	13.4	.138	371

are shown in figure 3-26. It can be observed that the increase in initial sink speed from 20 ft/sec to 22 ft/sec produced a slightly higher bending moment distribution and a significant increase in shear loads. Figure 3-27 presents comparative wing bending and shear data for the nose-down impact (No. 10) and the nose-up impact (No. 11). The results are similar except for the shear BL inboard of the inboard engine. This aspect of the data appears inconsistent and could relate to engine-wing modeling.

The comparison of results for many of the conditions analyzed is shown in table 3-6.

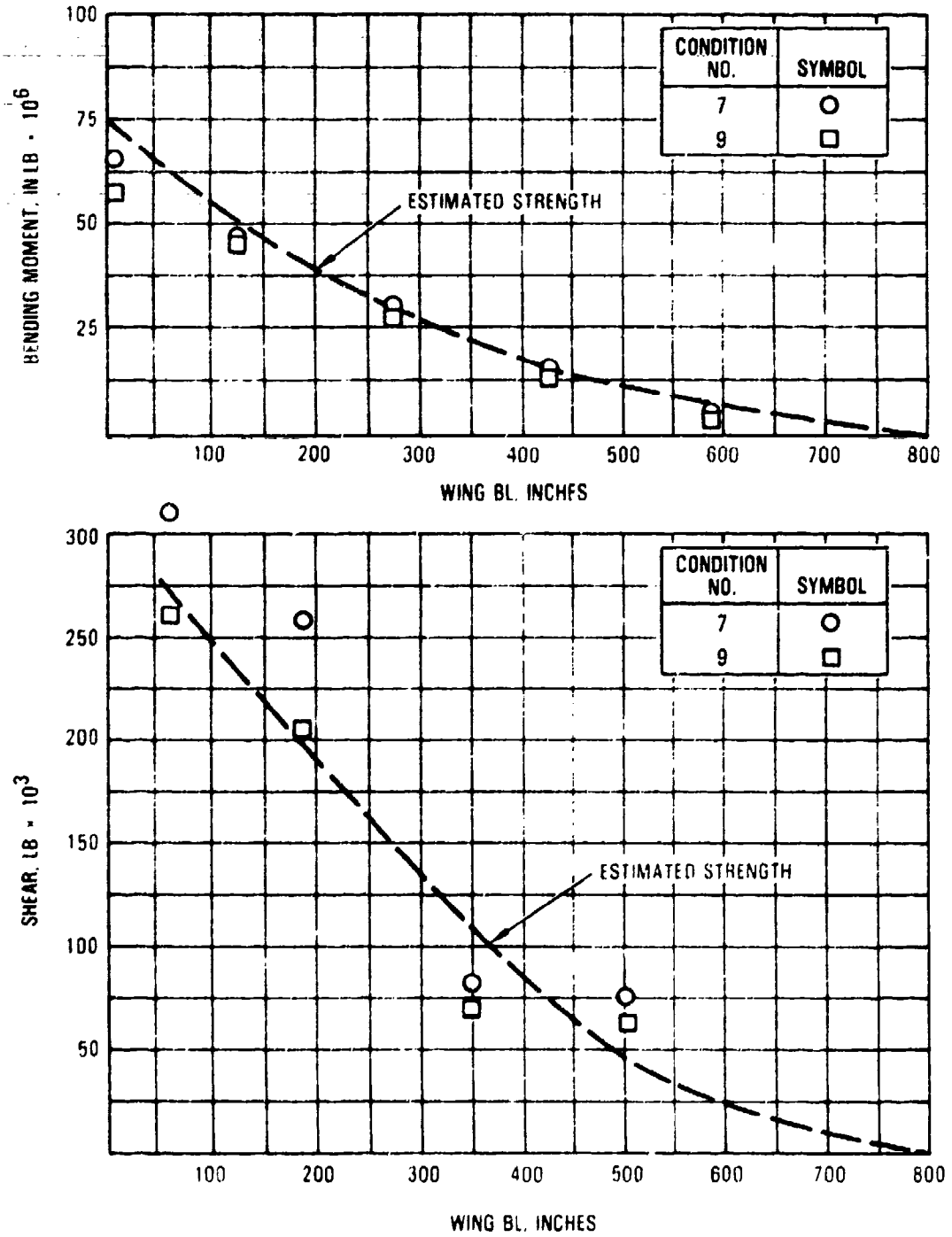

Figure 3-26. Comparison of Wing Shear and Bending, Conditions 7, 9

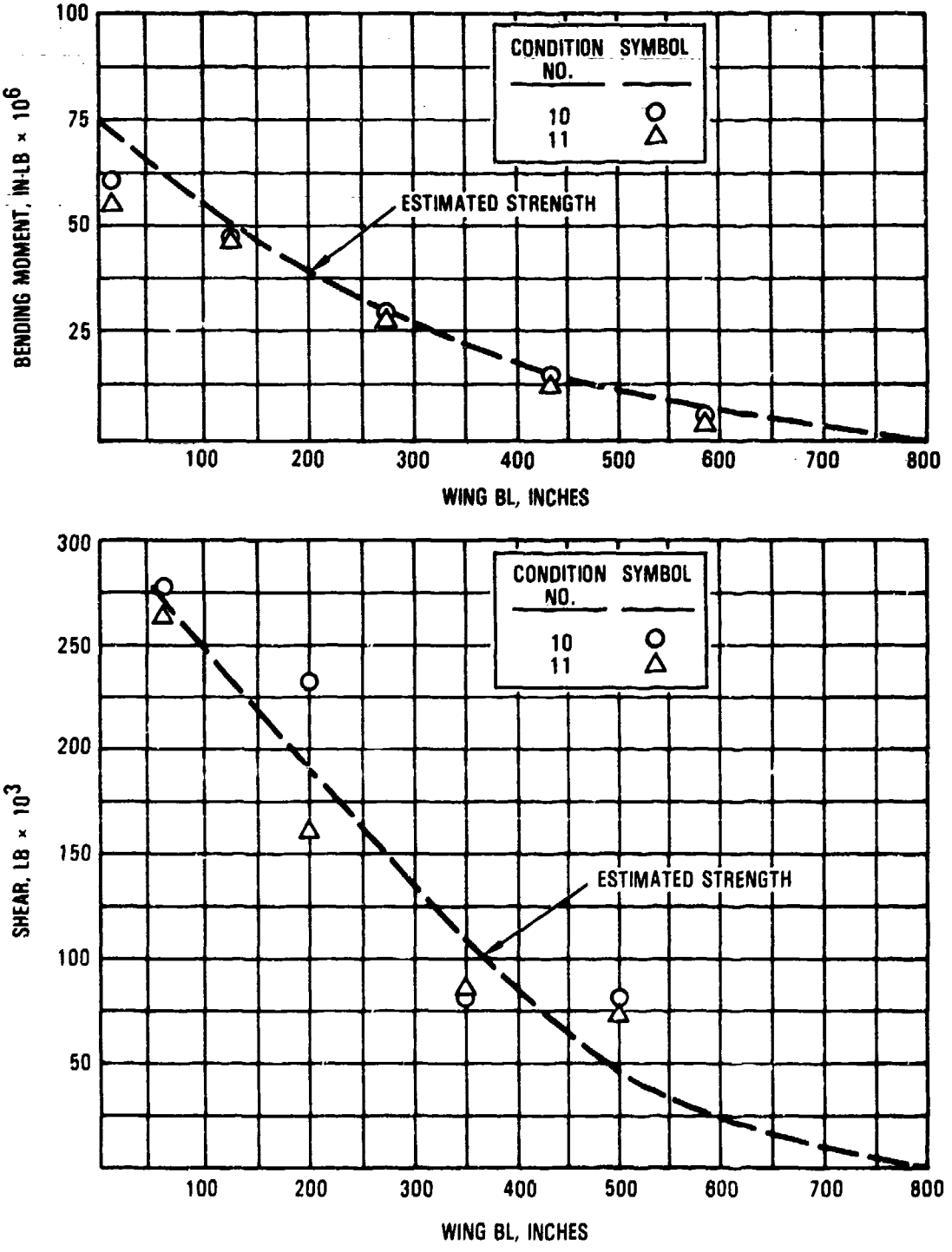

Figure 3-27. Comparison of Wing Shear and Bending, Conditions 10, 11

TABLE 3-6. COMPARISONS OF ANALYSES RESULTS FOR DIFFERENT IMPACT CONDITIONS

Condition A vs. Condition B[a]	Discussion of Results
No. 1 vs. No. 2 Comparison of 0^0 and $+1^0$ pitch, engine contact, equal sink speed (22 ft/sec).	$+1^0$ pitch (No. 2) results in higher LIC's (~ 10-15%), higher ΔV's at extremes, slightly less crush (fwd) and more crush (aft). Both conditions produce high Wing Shears (S_z) and Bending Moment (M_y), particularly inboard of BL 271.8. Condition No. 2 slightly higher S_z and M_y.
No. 2 vs. No. 3 Comparison of 22 and 20 ft/sec sink speed, Same pitch ($+1^0$), engine contact.	Higher sink speed (No. 2) produces LIC $\geqslant$ 1.0, more crush and increased ΔV's (~ 10%). LIC $\geqslant$ 1.0 estimated to occur closer to 21 ft/sec. Wing S_z and M_y at condition No. 3 appear to be within allowables but exceed strengths at condition No. 2.
No. 4 vs. No. 5 Comparison of effect of no lift and initial aerodynamic loading, same pitch ($+1^0$). Same sink speed (17.3 ft/sec) and engine contact.	Initial Lift (No. 5) produces slightly lower LIC, less crush and higher ΔV's (5-10%). Neither condition reaches LIC = 1.0. Neither condition produces wing S_z and M_y near allowables. Impact sequences differ.
No. 6 vs. No. 7 Comparison of no forward velocity and fwd. velocity. Same sink speed (22 ft/sec), pitch (0^0), no lift, no engine contact.	Results are similar. No fwd. velocity condition (No. 6) produces less forward fuselage crush. ΔV's and LIC's within 5-10%. Wing S_z and M_y about the same. Exceed estimated allowables. These conditions produce higher wing responses than similar conditions (No. 1 and No. 2) but with engine ground contact.
No. 1 vs. No. 7 Comparison of engine ground contact versus no engine ground contact for same sink speed (22 ft/sec), pitch (0^0) and no lift.	Results are similar for fuselage responses for condition No. 1. Inboard engine fails shortly after ground contact (further model review is warranted). Outboard engine contacts much later and fails after peak fuselage crush occurs. Wing S_z and M_y substantially higher for condition No. 7.
No. 8 vs. No. 9 Comparison of effect of revising nose gear bulkhead crush spring. No. 9 with revised crush characteristics. No. 8 with 'old' crush charactersitics. Same sink speed (22 ft/sec), pitch (0^0) and no engine contact.	Revised crush characteristics (No. 9) results in less forward fuselage crush, lower LIC's (all $<$ 0.87), lower ΔV's. However, wing S_z and M_y values marginal compared to estimated allowable strength. This could be a limiting factor.
No. 7 vs. No. 8 Comparison of effect of revising nose gear bulkhead crush spring. No. 7 has revised crush, but is run at 22 ft/sec sink speed. No. 8 has 'old' crush and a sink speed (20 ft/sec.). Same pitch (0^0), no lift, no engine contact.	Higher sink speed and revised crush condition (No. 7) equates to condition No. 8 with regard to fuselage LIC's. No. 7 produces higher ΔV's (~ 5 to 15%). However, No. 7 produces substantially higher wing S_z and M_y responses, particularly when compared to the estimated allowables.
No. 10 vs. No. 12 Comparison of effect of revising nose gear bulkhead crush spring. No. 10 has revised crush. Same sink speed (15 ft/sec), pitch (-6^0), no lift, no engine contact.	The revised crush condition (No. 10) produces substantially less forward fuselage crush and slightly less aft crush (~ 5%). Case No. 10 results in aft fuselage LIC's $>$ 1.0 and forward fuselage LIC's nearly = 1.0 while case No. 12 produced LIC $>$ 1. in the forward fuselage and LIC $\leqslant$ .87 in the aft. ΔV's for No. 10 are generally higher throughout. The wing S_z and M_y values are high enough to exceed the allowable strengths for No. 10. No wing responses were plotted for No. 12. The current results for the -6^0 pitch probably suggest lower initial sink speeds (perhaps 14 ft/sec) are appropriate to stay within airframe strength.
No. 11 vs. No. 13 Comparison of effect of revising nose gear bulkhead crush spring. No. 11 has revised crush. Same sink speed (15 ft/sec), pitch ($+6^0$), no lift, no engine contact.	The revised crush condition (No. 11) produces about the results (LIC, crush and pulses) as No. 13. The wing S_z and M_y values are lower than the corresponding -6^0 pitch case (No. 10) and probably just below the allowables. The previously reported $+6^0$ pitch results still appear appropriate.

(a) See Table 3-2 for description of conditions.

3.1.2 Air-to-Ground, Gears Extended

An all-gears-extended configuration was analyzed for the following impact conditions:

	Sink Speed (ft/sec)	Pitch Attitude (degrees)
1.	18	-6
2.	20	0
3.	18	+6

For all three cases the following assumptions apply:

- No lift forces
- Forward velocity = 262 ft/sec
- Ground coefficient (u) = 0.35
- Main gear failure loads;
  - Fz, Vertical Force = 428,000 lb.,
  - Fx, Longitudinal Force = 165,000 lb.
- Nose gear failure loads;
  - Fz = 130,000 lb., Fx = 78,000 lb.

Prior to the analysis of the three no-lift cases, a comparison of lift versus no-lift was performed for 20 ft/sec sink speed, +1 degree pitch attitude. Both of these cases, as well as all subsequent runs were for a period of 0.49 second after impact. With lift forces, the gears withstand the impact load for a longer time. During this period of time the fuselage loads are relatively low, averaging about 3g vertically for approximately 0.35 second. Without lift, the main gear experiences a failure at 0.146 second after impact and subsequently the fuselage experiences significantly higher forces when it impacts the ground. The lift condition, if run at higher initial impact velocities, would also result in main gear failures and subsequent fuselage impact with the ground. Thus, the no-lift analysis allows for evaluating critical fuselage impact loads in a shorter analysis time. In all three no-lift cases, the nose and main gears fail and the fuselage contacts the ground.

Table 3-7 compares the fuselage LIC ratios, crush distances, and vertical acceleration pulses for the -6, -0 and +6-degree impact attitudes. In all three impact conditions, an LIC ratio of 1.0 or greater is reached in the forward, mid, and/or aft fuselage regions. For the -6 degree pitch condition, the fuselage has crushed only in the forward region. During the 0.49 second of analysis, the airplane has not rotated onto the mid or aft fuselage. For the +6 degree pitch condition, the fuselage rotates onto the forward end and slaps down on the nose. The high-short duration primary response pulses include this effect. The triangular pulses associated with all three conditions vary in time duration, acceleration level and change in velocity. These pulses are plotted on a peak g versus Δt curve, figure 3-28. With the exception of the fuselage extremes (i.e., nose location) the change in velocity associated with pulses at limits of fuselage structural integrity are generally 25 ft/sec or less.

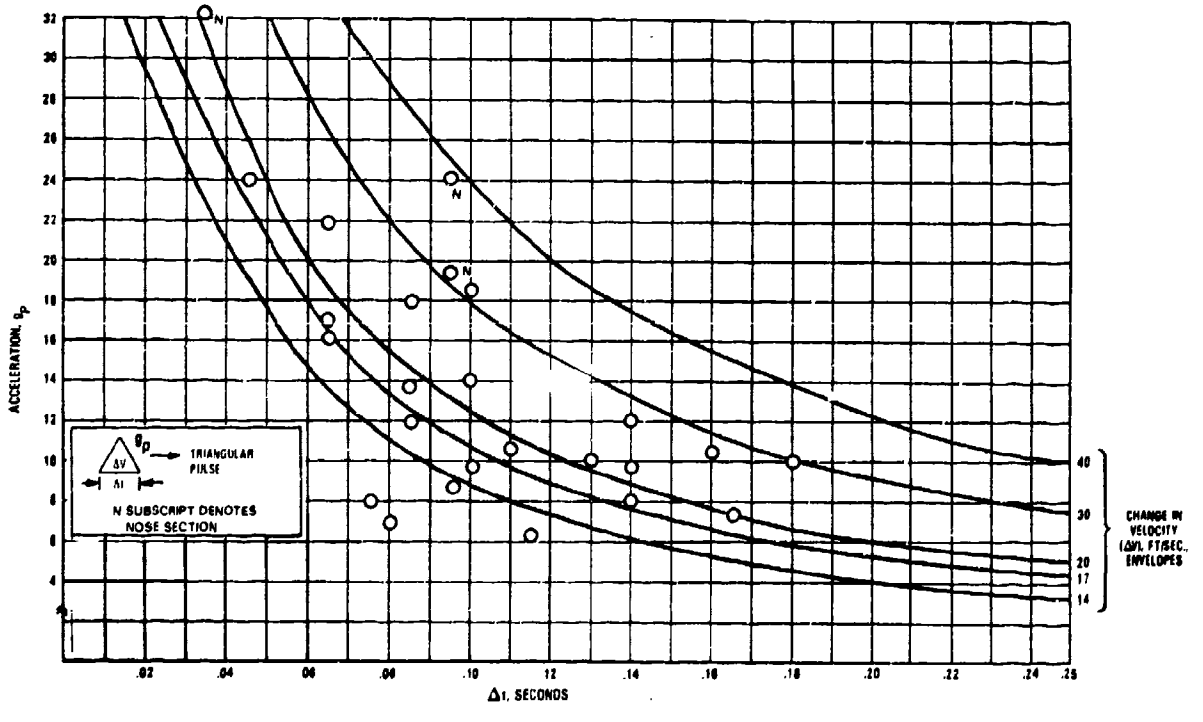

Figure 3-28. Analytically Obtained Vertical Pulses - Gears Extended Condition

TABLE 3-7. COMPARISON OF PEAK LIC RATIO, FUSELAGE CRUSH, AND VERTICAL ACCELERATION FOR ALL GEARS EXTENDED CONDITIONS

	MAXIMUM LIC RATIO			MAXIMUM CRUSH, INCHES			ACCELERATION, TRIANGULAR PULSE g_{peak}, (Δv,Δt)		
F.S. LOCATION	①	②	③	①	②	③	①	②	③
199	-	-		6.0	4.7	+	19.4 (355,.095)	23.6 (440,.095)	38.0 (312,.035)
300	.43	.475	.33	9.7	13.0	8.4+	18.0 (295,.085)	18.6 (370,.100)	24.0 (240,.045) 9.6 (188,.100)
350	.86	.78	.82						
450	.91	.90	.88	3.2	11.7	6.1+	13.8 (226,.085)	10.2 (354,.180)	16.2 (215,.065)
480	1.47	.80	.96						
540	1.47	.84	1.02						
600	1.25	.75	.92						
620	1.12	.87	1.05	-	10.6	6.8+	8.6 (160,.095)	10.6 (330,.160)	6.8 (170,.080)
960/960	.80/.83	1.05/.93	1.01/1.15	-	10.8	12.0	10.4 (90,.065)	7.6 (250,.165)	10.0 (250,.130)
990	.89	1.13	1.53			-			
1090	1.15	.98	1.00	-	9.7	14.9	7.9 (100,.075)	8.2 (230,.140)	9.8 (260,.140)
1160	1.04	.92	1.11			-			
1210	.83	1.06	1.08		.2+	15.8	7.4 (100,.070)	17.2 (220,.065)	22.0 (260,.065) 12.0 (310,.140)
1320	.88	.97	1.03			-			
1400/1400	1.13/1.06	1.1/1.1	1.15/1.18				7.4 (100,.070)	12 (200,.085)	14.0 (300,.100)

① 18 ft/sec sink speed, -6 degree pitch
② 20 ft/sec sink speed, 0 degree pitch
③ 18 ft/sec sink speed, +6 degree pitch

\+ Indicates peak crush value was not reached at time =0.49 second

Table 3-8 shows the wing span-wise bending moment and shear distribution for the three-pitch attitude conditions. The shear and bending moments are highest for the 0 degree condition. The shear values indicate that the strength of the wing is either marginal or exceeded for some of these conditions. The previous analyses predicted high outboard wing shear relative to the estimated strength, which was not confirmed by CID test data. Thus, it is most likely that the wing strength is satisfactory or at worst marginal for the three conditions analyzed.

TABLE 3-8. KRASH WING PEAK BENDING MOMENT AND SHEAR RESPONSES

MASS NO.	BL	BENDING MOMENT, IN.-LB x 10^6			
		①	②	③	ESTIMATED ULTIMATE
5	ROOT	33.	48.	41.	75.
11	-118	27.6	29.	25.	50.
12	-271	8.6	18.	18.	30.
13	-430	5.3	8.1	6.7	15.
14	-583	4.5	4.1	3.4	10.
15	-740	<1.	<1.	<1.	5.
MASS NO. i-j	BL	SHEAR, LB x 10^3			
		①	②	③	ESTIMATED ULTIMATE
11-12	0/-118	269.	277.	179.	250.-300.
11-12	-118/-271	84.	142.	123.	200.
12-13	-271/-430	61.	80.	61.	110.
13-14	-430/-583	32.	54.	48.	40.
14-15	-583/-740	23.	24.	23.	10.

① sink speed = 18 ft/sec, pitch = -6 degrees
② sink speed = 20 ft/sec, pitch = 0 degrees
③ sink speed = 18 ft/sec, pitch = +6 degrees
④ values are not simultaneous

3.1.3 Comparison with Previous Air-to-Ground Analysis

The analysis of a medium size transport aircraft (155,000 lb. gross weight) which is about the size of the L-1649 and about 20,000 lb. lighter than the maximum design landing weight of the CID test article, was reported in reference 4. The dimensions of the aircraft analyzed are shown in figure 3-29. The crushing springs used in the reference 4 model are shown in figure 3-30. The stiffness series No. 1 was the initial crushing data used and the limited deformation distance coupled with excessive force as the structure bottomed producing unrealistic results. Stiffness series Nos. 2, 3 and 4 included refinements based on drop test results. Reference 4 analysis results are presented in table 3-9. A comparison of the results for the 15 ft/sec impact with the aircraft in a 0 degree pitch attitude is shown in table 3-10. The models show peak vertical accelerations within the range of 9 to 10 g's (Reference 4) and 9 to 10.5 g's (CID model). The LIC ratios for both models show that the margins of safety at that impact level are between 0.3 to 0.58 (reference 4) and between 0.32 to 0.52 (CID model). The reference 4 model shows generally more crush than the CID model, particularly at the aft end. Crush is a function of both fuselage contour and fuselage underside crushing characteristics. Figure 3-31 shows how the two airplane contours differ, which partially explains the difference in aft fuselage crush. Figure 3-32 compares the fuselage underside crush springs used for the two models. The CID model appears to provide higher crush energy absorption which would also tend to reduce the crush distance.

TABLE 3-9. A SUMMARY OF TEST CASE COMPUTER RUNS (REFERENCE 4)

Angle[1] (deg)	Velocity[2] (ft/sec)	Stiffness[3]	Mode[4]	Sta. 1[5] (max g)		Sta. 2[5] (max g)		Sta. 5[5] (max g)		Sta. 6[5] (max g)		Sta. 9[5] (max g)	
				+	-	+	-	+	-	+	-	+	-
0	15	3	Flex	20	-11	11	-7	12	-6	8	-7	14	-9
+2	10	4	Flex	31	-22	15	-13	10	-9	16	-11	16	-11
+5	10	3	Flex	33	-24	20	-15	17	-12	19	-11	21	-19
+5	15	3	Rigid	8	-2	7	-2	5	—	4	-2	5	-4
+5	15	3	Flex	35	-24	27	-17	-17	-21	22	-12	24	-21
+5	20	3	Flex	35	-23	16	-14	14	-16	14	-18	22	-22
-5	15	4	Flex	35	-20	17	-10	9	-10	10	-10	14	-20
-7.5	15	3	Flex	19	-17	17	-17	16	-13	13	-13	22	-26
5° Ramp		3	Flex	34	-22	17	-15	16	-11	12	-8	15	-16

Maximum Displacement (Structure Crushed), Inches

				Sta. 1 (in.)	Sta. 2 (in.)	Sta. 3 (in.)	Sta. 4 (in.)	Sta. 5 (in.)	Sta. 6 (in.)	Sta. 7 (in.)	Sta. 8 (in.)	Sta. 9 (in.)
0	15	3	Flex	0	10	10	11	11	16	15	34	32
2	10	4	Flex	1	9	7	6	6	6	11	17	16
5	10	3	Flex	2	[illegible]	4	2	3	20	39	40†	40†
5	15	3	Rigid	13	18	14	12	12	23	36	40†	40†
5	15	3	Flex	2	11	13	5	5	22	40†	40†	40†
5	20	3	Flex	16	23	20	17	18	40†	40†	40†	40†
-5	15	4	Flex	1	6	18	21	24	30	34	38	35
-7.5	15	3	Flex	0	15	25	37	40†	40†	40†	40†	40†
5° Ramp		3	Flex	0	2	10	17	25	40†	40†	40†	40†

Angle[1] (deg)	Velocity[2] (ft/sec)	Stiffness[3]	Mode[4]	Maximum Plus Moment (Compression Top) (in.-kips) Sta. 2[5]	Sta. 3[5]	Sta. 4[5]	Sta. 5[5]	Sta. 6[5]	Sta. 7[5]	Sta. 8[5]	Sta. 9[5]
0	15	3	Flex	6,116	9,846	11,516	10,187	16,679	8,532	8,845	8,358
2	10	4	Flex	12,585	23,327‡	32,442‡	37,173‡	58,116‡	35,784‡	28,710‡	24,024‡
5	10	3	Flex	13,538	19,995	26,804	32,316‡	51,816‡	36,785‡	29,047‡	23,832‡
5	15	3	Rigid	16,555	29,722‡	39,976‡	45,495‡	51,081‡	37,932‡	24,930‡	12,835‡
5	15	3	Flex	17,215‡	25,083‡	32,734‡	42,451‡	56,212‡	58,092‡	45,738‡	44,674‡
5	20	3	Flex	14,277	22,427	26,855	33,524‡	66,815‡	45,189‡	41,449‡	31,891‡
-5	15	4	Flex	10,842	15,029	16,282	13,790	43,077‡	21,160	13,469	11,074‡
-7.5	15	3	Flex	9,839	12,611	24,954	29,935‡	41,837‡	35,043‡	36,700‡	28,483‡
5° Ramp		3	Flex	17,807‡	25,460‡	30,657‡	34,596‡	51,195‡	29,215‡	25,760‡	17,595‡
Calculated Allowable M				16,800	22,800	27,200	29,800	34,000	29,000	19,400	10,100

Maximum Minus Moment (Tension Top)

0	15	3	Flex	-12,307	-20,130	-24,831	-30,547	-32,088	-26,537	-20,012	-17,749
2	10	4	Flex	-13,926	-24,448	-34,534	-40,690	-66,274	-62,451‡	-42,881	-25,845
5	10	3	Flex	-11,474	-15,618	-25,675	-31,830	-35,327	-36,515	-24,926	-17,160
5	15	3	Rigid	-3,688	-10,561	-21,175	-33,711	-49,053	-42,750	-24,005	-12,904
5	15	3	Flex	-16,617	-24,633	-34,611	-39,530	-73,565	-54,590	-38,856	-36,071
5	20	3	Flex	-15,990	-25,197	-29,493	-43,764	-59,279	-47,235	-39,206	-23,503
-5	15	4	Flex	-9,866	-16,217	-28,690	-33,034	-38,257	-25,261	-19,382	-22,075
-7.5	15	3	Flex	-10,403	-19,833	-31,972	-38,854	-28,810	-37,343	-20,276	-13,320
5° Ramp		3	Flex	-4,709	-7,542	-11,984	-12,156	-19,196	-28,093	-19,397	-12,479
Calculated Allowable M				-16,800	-30,000	-38,000	-45,000	-80,000	-62,000	-45,000	-30,000

Notes: 1. + impact angle is nose down.
2. Velocity component normal to fuselage.
3. Stiffness series per Figure 4 (lower fuselage crushing).
4. Flexible mode is 6 modes with dampening.
5. Reference Figure 1 for station locations.

† Beyond Floor Level
‡ Allowable Moment Exceeded

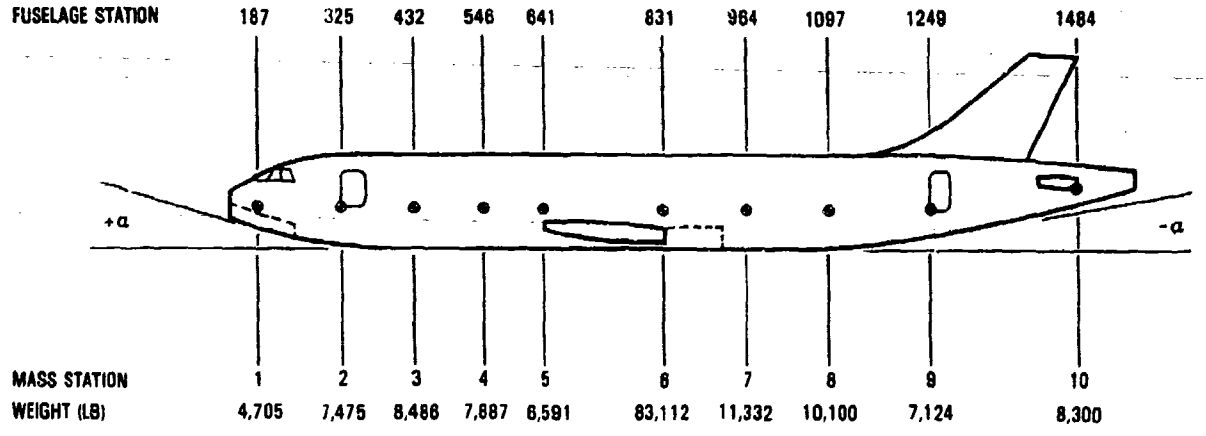

(a) REFERENCE 4 AIRPLANE CONFIGURATION

Figure 3-29. Analytical Study, Test Case Model (Reference 4)

TABLE 3-10. COMPARISON OF ANALYSIS RESULTS, SINK SPEED = 15 FT/SEC, 0 DEGREE PITCH

FUSELAGE STATION			PEAK VERTICAL ACCELERATION, g		LIC RATIOS		CRUSH DISTANCE, IN.	
REFERENCE 2		CID	REFERENCE 4	CID	REFERENCE 4	CID	REFERENCE 4	CID
325		300/350	10	9.0	0.70	0.55	10	7.6
432		450	–	–	0.67	0.55	10	6.4
546		540	–	–	0.65	0.52	11	6.3
641	*	620 (a)	10	10.5	0.67	0.48 (a)	11	6.3
631	*	820 (a)	–	–	0.42	0.57 (a)	16	6.7
964	*	960	–	–	0.45	0.56	15	9.3 (c)
1097		1040/1090	8	8.9	0.46	0.68	34	9.7 (c)
1249		1210/1240	–	–	0.60	0.49	32	1.4 (c)

(a) BULKHEAD CRUSHING

(b) AVERAGE OF TWO VALUES

(c) MAXIMUM VALUE AT END OF ANALYSIS

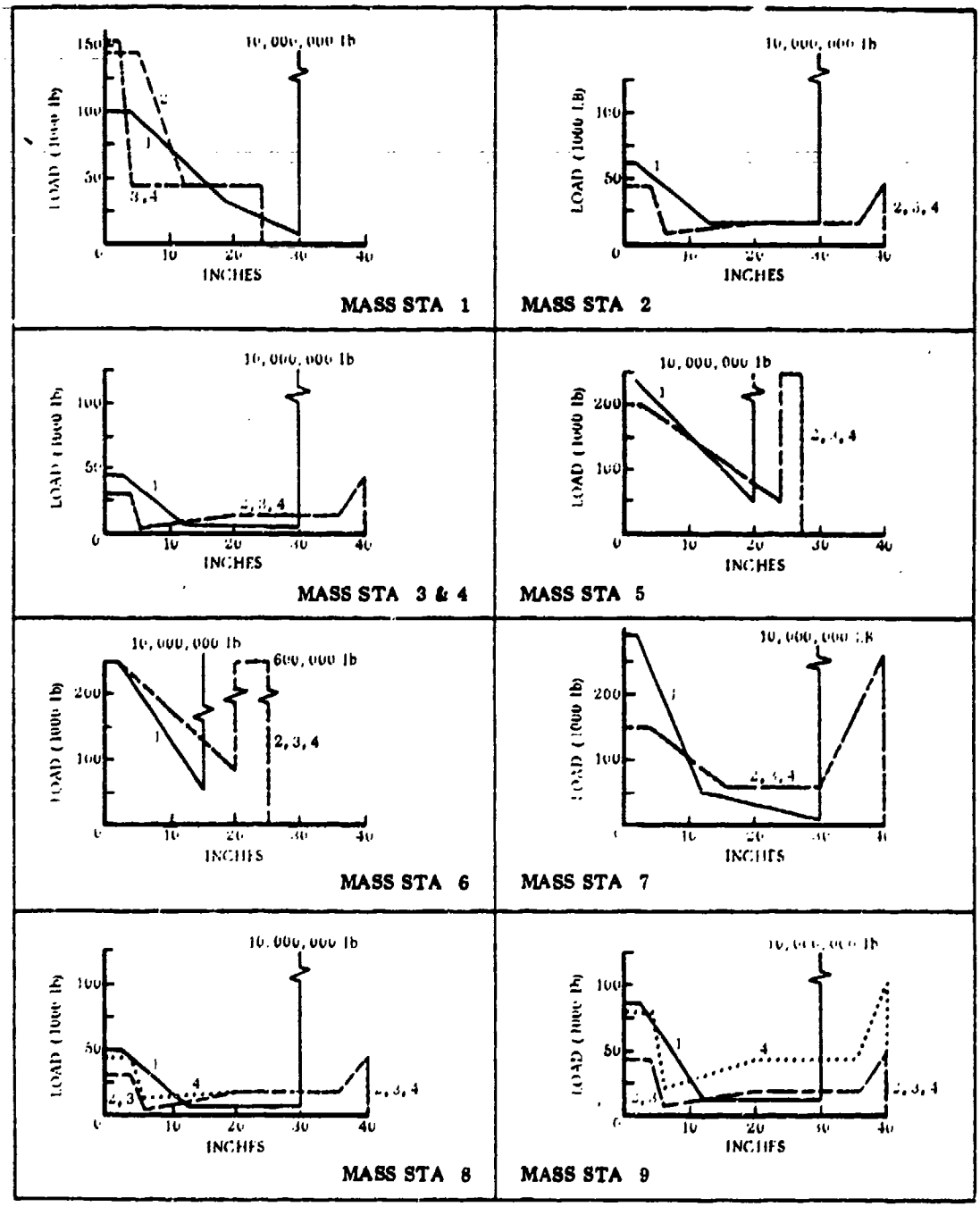

Figure 3-30. Lower Fuselage Spring Data - Test Cases (Reference 4)

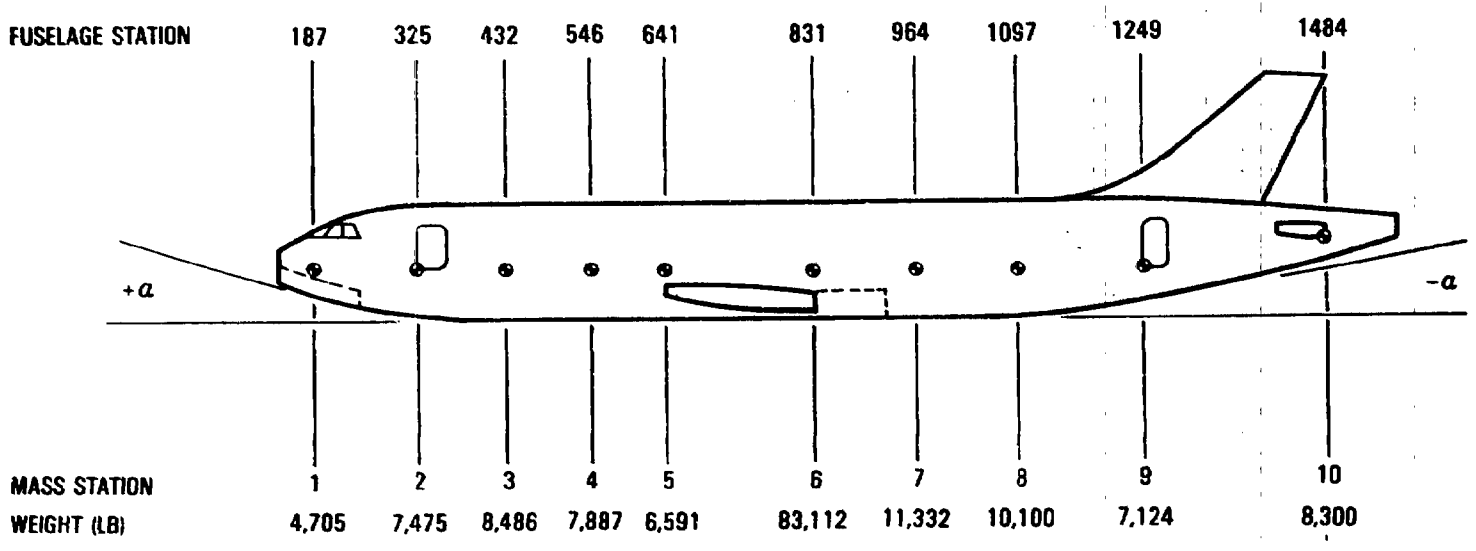

(a) REFERENCE 4 AIRPLANE CONFIGURATION

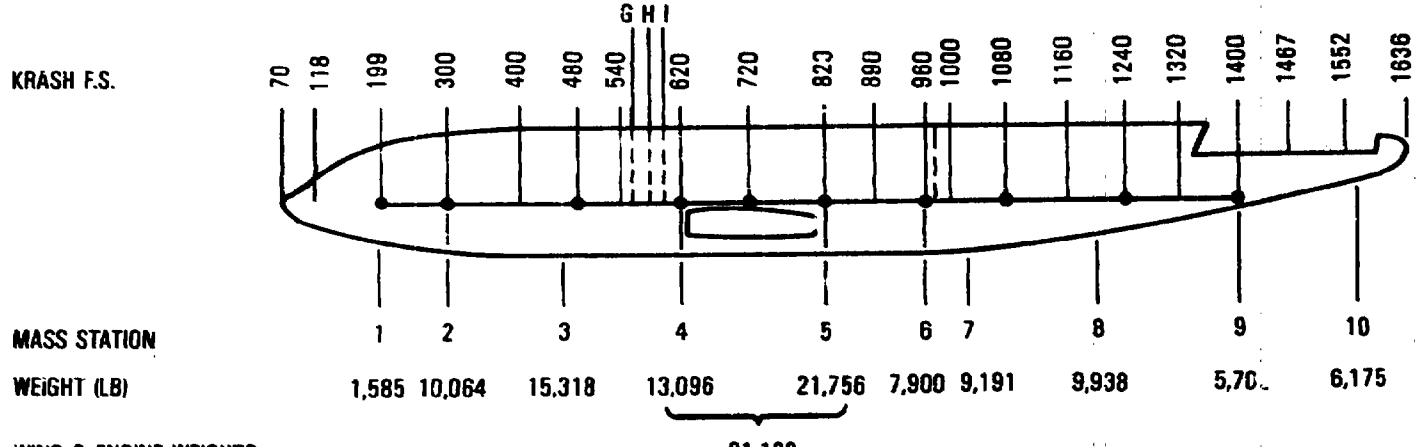

(b) CID AIRPLANE CONFIGURATION

Figure 3-31. Comparison of Airplane Configurations

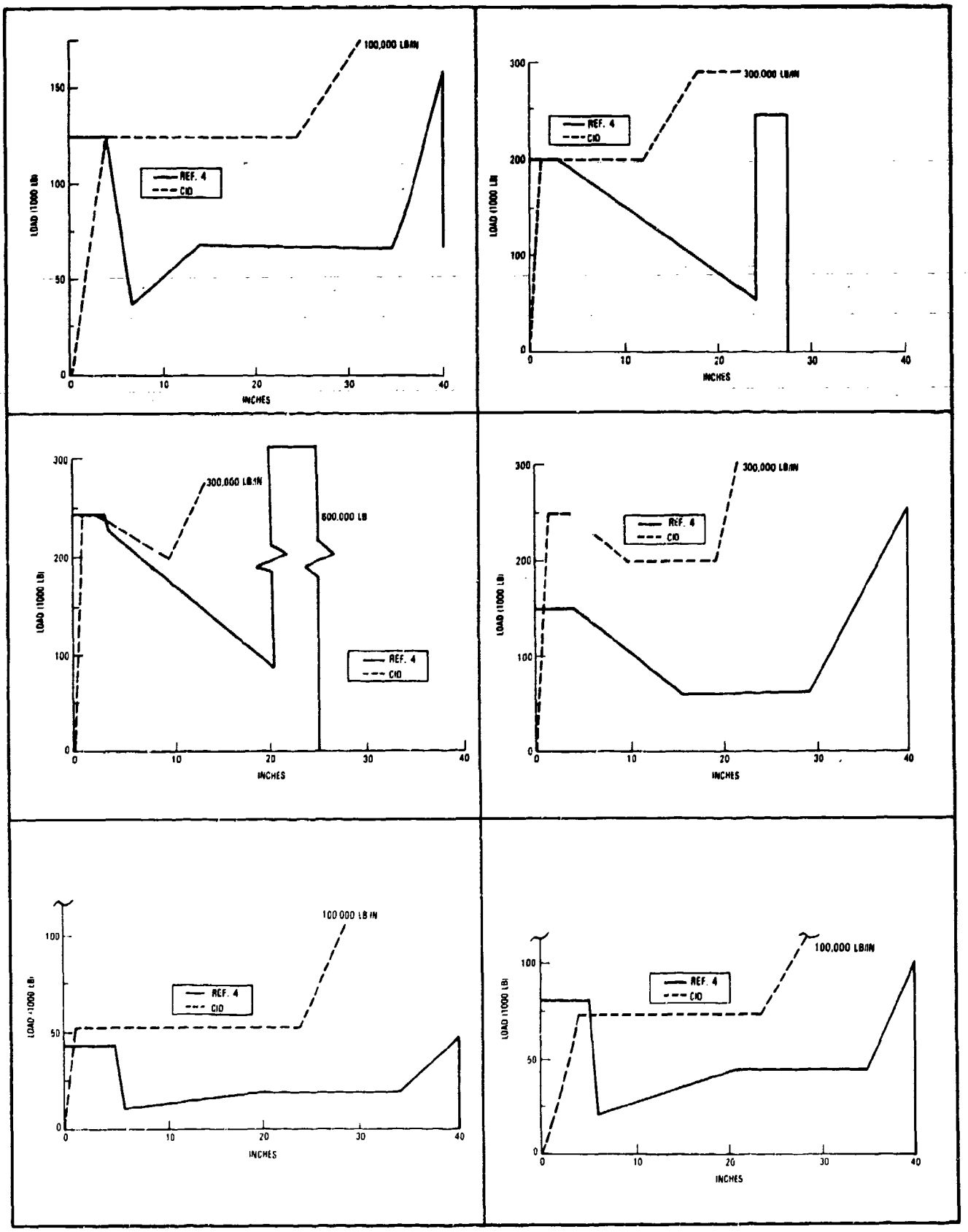

Figure 3-32. Comparison of Lower Fuselage Spring Data

The comparisons for the nose-up and nose-down impact simulations show similar trends with regard to each model, although the differences are more widespread. For example, a comparison of peak accelerations at the same three locations shown in table 3-10 indicates the differences in the peak acceleration values as shown in table 3-11. The fundamental bending frequency of the airplane described in reference 4 is 3.25 Hz, which is close to the fundamental bending frequency of the CID test airplane (3.37 Hz). However, from analytically obtained sample acceleration time histories (figure 3-33) that are presented in reference 4, it appears that the reference 4 model exhibits higher frequency responses which account for higher peak values. Similarly, the comparison for crush and LIC ratios at the two pitch attitudes shows differences in magnitude, but similar trends. The LIC ratios, shown in table 3-11, are based on bending allowables which produce tension at the top of the fuselage shell. The data from table 3-8 indicate that the reference 4 study used lower compression bending allowables; thus, exceedance of strength was usually due to the compression loads. The CID analysis assumes equal bending strength in compression and tension. However, it does base failure on combined moment and shear. From the LIC ratios, shown in table 3-11, it is noted that the nose-down impact is in good agreement except for the fuselage extremes and at the mid-fuselage (FS820). FS820 values for the CID were not available, thus FS620 values were used in the analysis. In reality, FS820 strength is greater than the strength at either FS620 or FS960 as shown in table 3-12. With the proper strength values the LIC ratio at FS820 shown in table 3-11 would be reduced to less than 1.0 and show good agreement with the reference 4 results. For the nose-up impact, the CID LIC ratios are generally higher. Table 3-12 shows the bending allowables used in the two analyses, as well as the allowable for the smaller airplane if scaled to the strength of the larger airplane. The scale factor used is the ratio of the fuselage shell radius cubed. Typical fuselage diameters are 140 inches and 170 inches, respectively for the two airplanes analyzed. Both the suggested scale factor and fuselage size were obtained from the mass and size scaling trend study described in reference 5. It is only a guideline and may represent an upper limit. However, by using such a factor it can be seen that the CID allowables

TABLE 3-11. COMPARISON OF ANALYSIS RESULTS

FUSELAGE STATION LOCATION		NOSE-DOWN (a)						NOS-UP (b)					
		PEAK VERTICAL ACCELERATION (g)		CRUSH DISTANCE (inches)		LIC RATIO		PEAK VERTICAL ACCELERATION (g)		CRUSH DISTANCE (inches)		LIC RATIO	
	CID	REF. 4	CID	REF. 4	CID	REF. 4	CID	REF. 4	CID	REF. 4	CID	REF. 4	CID
325	300/350	27	12.0	15	0.4	1.00	0.63	17	19	11	13.8	0.63	1.00
432	460	–	–	25	4.1	0.75	0.76	–	–	13	7.3	0.67	1.15
546	540	–	–	37	5.2	0.90	0.93	–	–	5	6.0	0.84	0.99
641	620	17	7.0	40 (c)	6.5	0.91	0.91	16	8	5	4.8	0.89	0.81
831	820	–	–	40 (c)	11.1	0.91	1.37(d)	–	–	22	10.6	0.36	1.13(d)
964	960	–	–	40 (c)	17.7	0.90	0.81(d)	–	–	40 (c)	19.1	0.60	0.99(d)
1097	1040/1090	22	12.4	40 (c)	21.0	0.89	0.99	13	7	40 (c)	23.3	0.45	0.84
1249	1210/1240	–	–	40 (c)	21.1	1.2	0.86	–	–	40 (c)	24.9	0.42	0.83

(a) 5 DEGREES FOR REF. 4; 6 DEGREES FOR CID

(b) 7.5 DEGREES FOR REF. 4; 6 DEGREES FOR CID

(c) BEYOND FLOOR LEVEL

(d) AVERAGE OF TWO VALUES

TABLE 3-12. COMPARISON OF ULTIMATE BENDING MOMENTS

F.S. LOCATION		REFERENCE 4 ULTIMATE (in-Kips)		CID ULTIMATE (in-Kips)	REFERENCE 4 DATA SCALED (a)	
		COMPRESSION	TENSION	TENSION = COMPRESSION	COMPRESSION	TENSION
325	350	16800	16800	39000	29000	29000
432	450	22800	30000	45000	39398	51840
546	540	27200	38000	50000	47000	65664
641	620	29800	45000	62500	51494	77760
831	820	34000	80000	(b)	58752	138000
964	960	29000	62000	96000	50112	107000
1097	1090	19400	45000	75000	33523	77760
1249	1210	10100	30000	50000	17280	51840

(a) SCALED FACTOR = 1.728, $\sigma = Mc/I \propto M/\gamma^3$ (b) USED FS620 VALUE, SHOULD BE $\geq$ FS860 VALUE

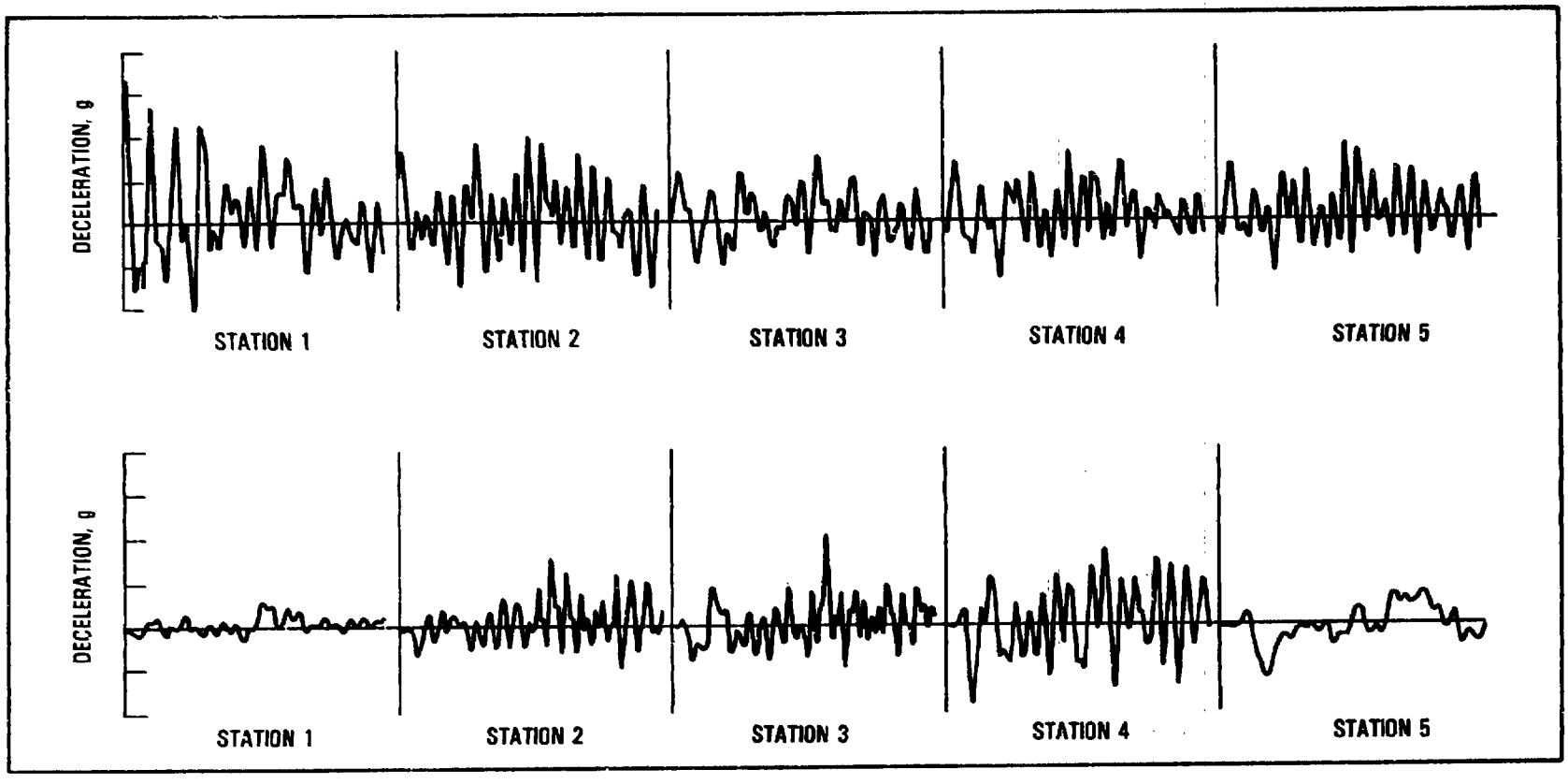

Figure 3-33. Deceleration - Fuselage Crash Impact Study - Flexible Body - 5 Degree Impact Angle - 10 Ft/Sec Normal Velocity - Stiffness 4 (Reference 4)

are reasonable, although somewhat high, except at FS820 for the reasons stated earlier.

Figure 3-34 shows a comparison of initial impact velocity versus pitch attitude at the limit of airplane airframe integrity generated from the two analyses. Despite some differences between the two approaches (i.e., computer programs, airplane configurations, crush characteristics) the curves still show a similar assessment.

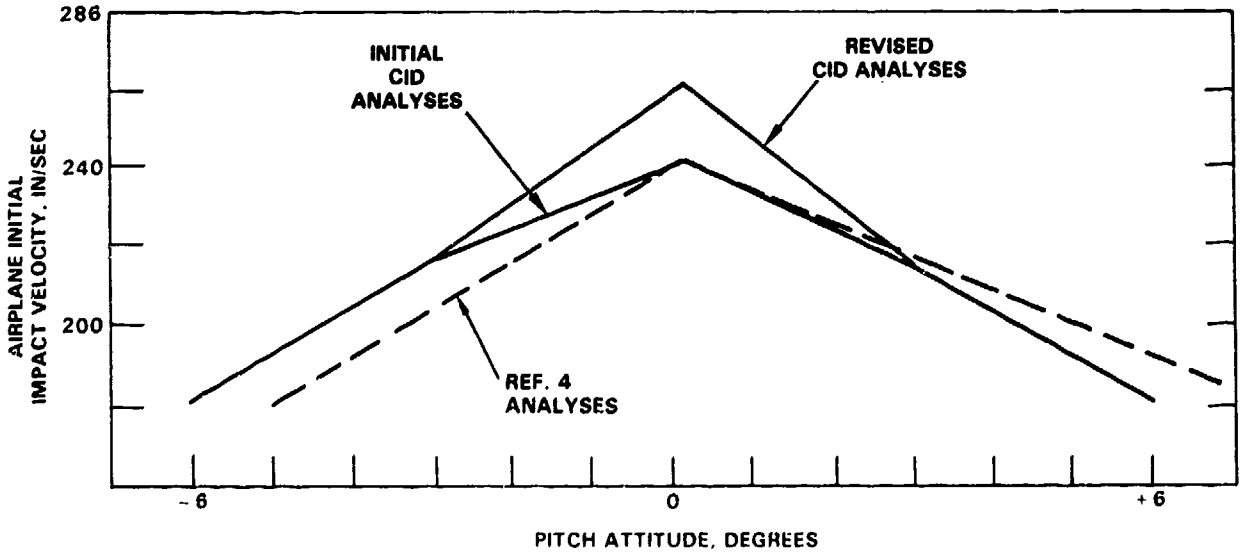

Figure 3-34. Airplane Impact Velocity Versus Pitch Attitude, Air-to-Ground Scenario

3.2 COMBINED LONGITUDINAL-VERTICAL PULSE

For the air-to-ground conditions analyzed in this study, the magnitude of the floor longitudinal pulses are relatively low in relation to the vertical pulse. This is due primarily to the fact that the impact attitude is shallow ($\leq$ 6 degrees) and thus the longitudinal acceleration is approximately equal to the coefficient of friction times the peak vertical acceleration. As the impact angle increases, the relative magnitudes of the longitudinal and

vertical pulses become closer. The L-1649 test (reference 6) results, which were obtained for 6-degree and 20-degree slope impacts, illustrate this point. As the impact angle increases, the longitudinal pulse would dominate (i.e., 90-degree slope or wall). This trend is illustrated in figure 3-35. However, the magnitude of the longitudinal pulse does not necessarily increase as the effective longitudinal velocity change (ΔV) increases, as was observed from the L-1649 crash test results, shown in figure 3-36.

In the L-1649 test there were two distinct ground impacts: a 6-degree impact by the airplane moving at a forward velocity of 172 ft/sec (ENV* = 18.4 ft/sec); and a 20-degree slope impact by the airplane moving at a forward velocity of 110 ft/sec (ENV = 37.6 ft/sec). In the latter impact, the airframe's structural integrity was exceeded, as noted by failure of the fuselage shell at two locations: aft of the cockpit and aft of the wing trailing edge (figure 3-37). From figure 3-36 it can be noted that the peak acceleration at an airplane cockpit location, FS195, is approximately 20g for both the 6- and 20-degree slope impacts, despite the fact that the effective longitudinal velocity resulting from the latter impact is approximately 30 percent higher than the effective velocity change (ΔV) associated with the impact onto the shallower slope. At the mid-fuselage station (FS685), the response shapes are similar and magnitudes are nearly equal, despite the latter having a longer duration and, consequently, a higher effective longitudinal ΔV. The ramp impact represents a ground-to-ground impact condition which provides both vertical and longitudinal pulses of substantial levels.

3.2.1 Ground-to-Ground Analysis

Several preliminary computer simulation runs were made to investigate responses for a ramp impact. The stick model, three views of which are shown in figure 3-38, was used. The ramp angle (4.4 degrees) and forward speed (3140 in/sec) were constant for these initial runs, so that the ENV is approximately 20 ft/sec for all cases. Nine cases are tabulated in table 3-13. For this type of impact, it was found that the treatment of the

*ENV = Effective Normal Velocity = product of forward velocity and sine of ramp angle

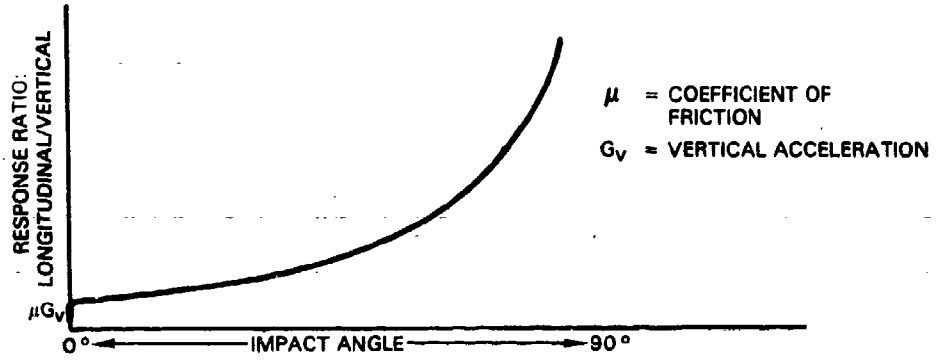

Figure 3-35. Trend of Relative Responses Versus Impact Angle

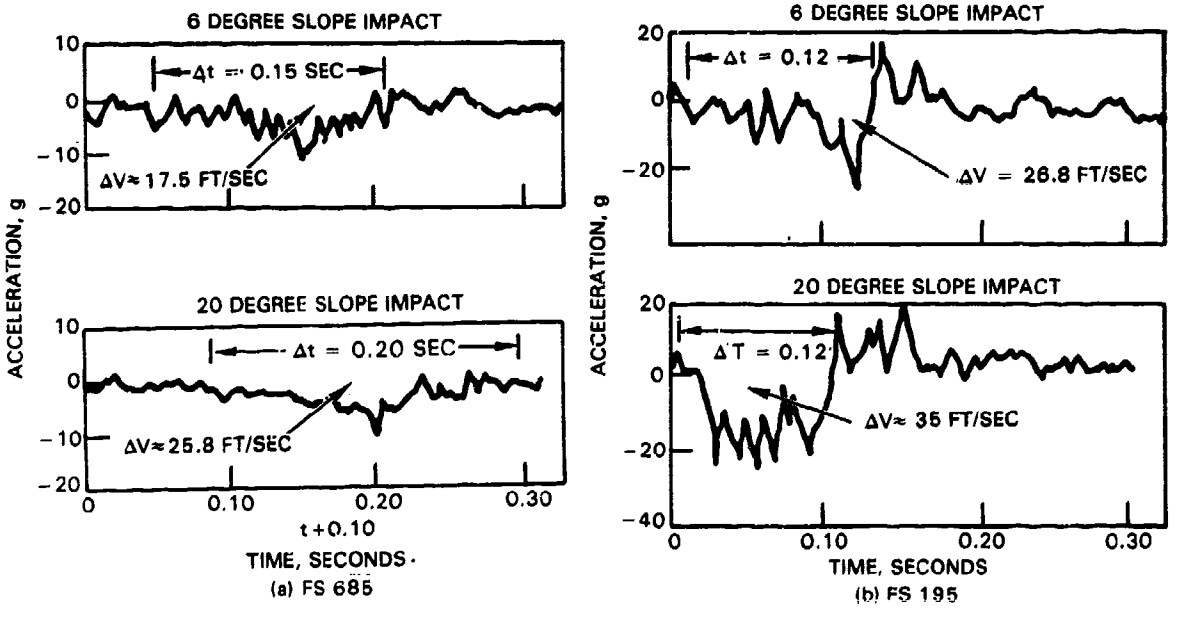

Figure 3-36. L-1649 Measured Longitudinal Pulses at Two Locations and for Two Impact Conditions

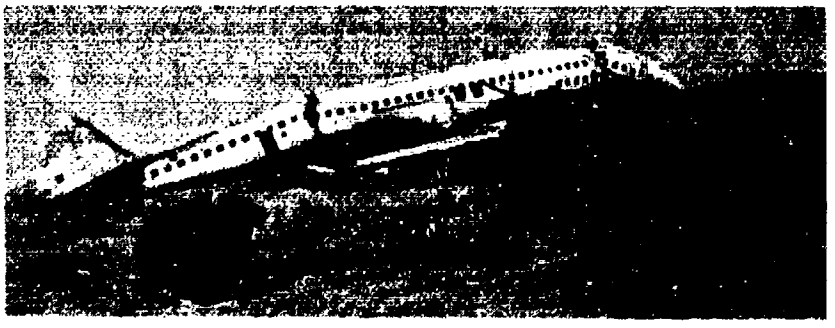

Figure 3-37. L-1649 Wreckage Shows Two Fuselage Breaks

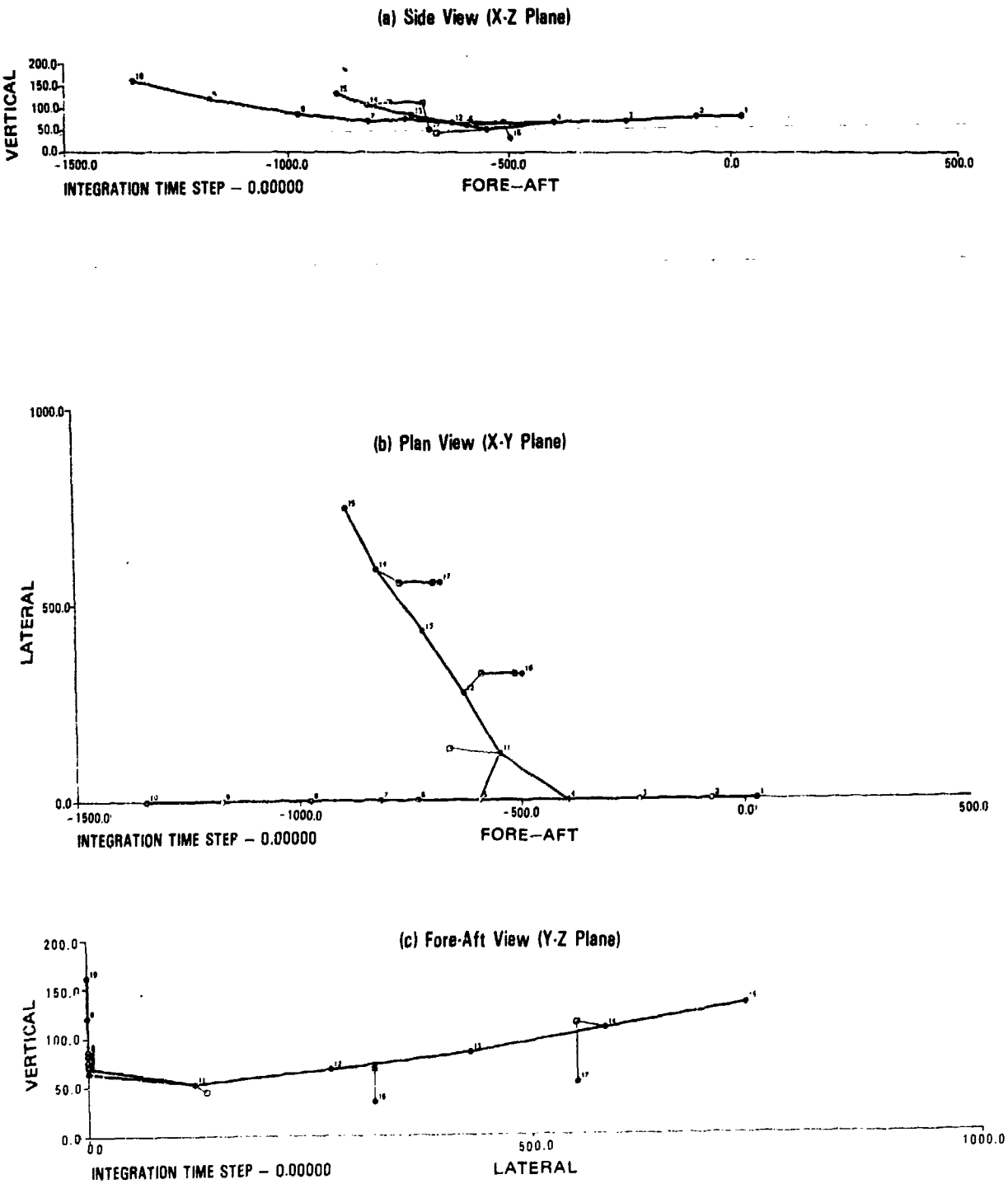

Figure 3-38. Baseline Stick Model

TABLE 3-13. PRELIMINARY RAMP IMPACT CASES

CASE NO.	NOSE SPRINGS (FS 300) LOAD DEFLECTION CURVE (FIG 3-39) C	D	K_D	GROUND FLEXIBILITY	GROUND COEFF. FRICTION (μ)
1	20	24	50,000	RIGID	1.0
2	10	24	50,000	RIGID	1.0
3	20	24	50,000	1×10^{-5} IN/LB	1.0
4	20	24	50,000	4×10^{-5} IN/LB	1.0
5	4.4	30	100,000	RIGID	1.0
6	10	18	50,000	RIGID	1.0
7	4.4	18	100,000	RIGID	1.0
8	4.4	18	100,000	RIGID (b)	1.0
9	4.4	18	100,000	RIGID (b)	0.5

(a) SLOPE ANGLE = 4.4°
FWD. VELOCITY = 3140 IN/SEC
ENV = 3140 (SIN 4.4°) ≈ 20 FT/SEC

(b) FOR CRUSH SPRING AT FS 199, "D" = 10

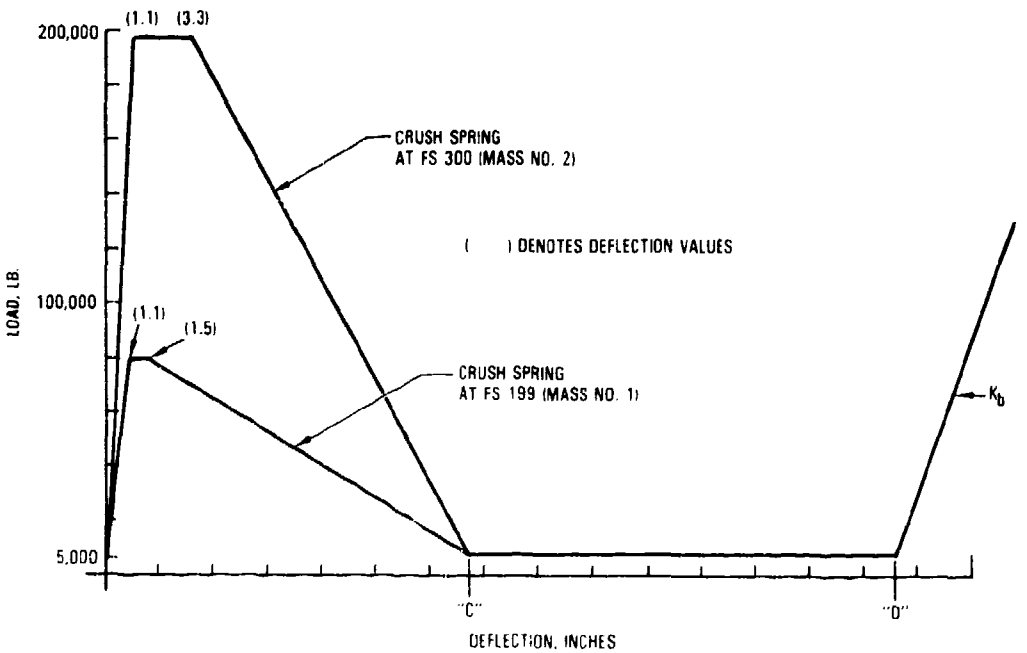

Figure 3-39. Nose Gear Bulkhead Crush Spring Characteristics

nose gear bulkhead crush springs can significantly influence the results. Figure 3-39 shows the characteristic crush springs used for the nose gear bulkhead representation. The nose gear crush characteristics for cases 8 and 9, in table 3-13, were used for the previously reported air-to-ground impacts. For those conditions, deflections at masses 1 and 2 were not high enough to cause spring, K_c to bottom. However, for the ramp impact, the influence of impacting the nose section and deflecting the spring sufficiently to bottom it out (particularly at FS199) produced loads which exceeded the airfame capability (LIC > 1.0) by substantial margins. Based on the L-1649 ramp impact test results (reference 6), the deflections at the forward region appeared excessive. Based on the test results, reported in reference 4, the KRASH model representation of the nose gear bulkhead region crush did not appear to provide adequate energy absorption. The test and analysis results are reported in reference 4 and were discussed in more detail earlier in this section. The nose gear bulkhead is assumed to fail after the initial peak loads of 100,000 lb. and 200,000 lb. at FS199 and FS300, respectively, are reached. Thereafter, the load-carrying capability is considered to be significantly reduced. Because of the possibility that the load-carrying capability was reduced too drastically, variations in these two crush (FS199 and FS300) characteristics were investigated along with the effect of flexible ground. The latter is realistic since the L-1649 impacted on an earthern slope. Case Nos. 1 and 4 are considered to be more realistic representations than the initial runs (cases 7, 8, 9). The LIC ratio, fuselage crush and peak acceleration data obtained from these two conditions, along with case No. 8 results, are shown in table 3-14. The acceleration values shown in table 3-14 do not necessarily occur simultaneously and the base duration of triangular pulses are generally less than 0.150 second, particularly for the higher peak values. Case No. 1 values appear to provide a closer match to the L-1649 test results. Case No. 4 values appear to be low and may reflect too much ground displacement. When the ground flexibility is stiffened (case No. 3, table 3-13), the acceleration peaks values increase approximately 30 percent and 20 percent for the vertical and longitudinal directions, respectively. However, the LIC ratios generally reflect the same overall magnitudes, although there are individual changes.

Acceleration time plots for case No. 1, table 3-14, for the vertical and longitudinal directions are shown in figures 3-40 and 3-41, respectively. Case No. 1 shows LIC values greater than 1.0 at two locations (FS1090, FS1160). Both results are considered to be on the high side. Figure 3-42 shows the analysis results versus the LIC curve used in the analysis, as well as the correct curve which is appropriate for FS1080. The LIC value (1.08) would reduce 10 pe[illegible] with the corrected curve. Furthermore, the results are sensitive to the slope of the LIC curve in the region shown. If, for example, My and Sz values of 75,000 in-lbs and 250,000 lb were extended and no interaction line used, the LIC ratio would be closer to 0.75. Similarily, figure 3-43 shows the LIC curve at FS1160. As shown, the margin is -.02. Projecting the My and Sz values without the interaction, as was done for figure 3-42, results in a 0.80 LIC ratio.

A review of LIC curves at other fuselage stations indicated that even if the curves were revised as noted to decrease the LIC ratios to 0.75 or 0.80 at these two locations, the most critical location would be at the forward fuselage FS540. The margin there would be +0.09 instead of +0.06 (LIC =0.94) as noted in table 3-14. Thus, the case No. 1 results (LIC = 0.91) are interpreted as marginal with regard to fuselage strength. Subsequent ramp impact analysis, described later in this section, are run at a higher ENV to account for the LIC curves possibly resulting in somewhat higher ratios in some locations. If the LIC data is changed in the model the comparison with earlier air-to-ground results would be distorted.

Figure 3-44 is a cross-plot of the associated velocity changes in the vertical (ΔV_z) and longitudinal (ΔV_x) directions. The velocity change values are obtained for an approximate 200 msec duration and can be taken at several periods in each run for different combinations of ΔV_x and ΔV_z. The ramp analysis results are superimposed on the air-to-ground analysis results in figures 3-45 and 3-46 for acceleration and crush, respectively.

Subsequent to the preliminary ramp impact runs described, additional analyses were performed to investigate various ramp impact conditions. Three

TABLE 3-14. PRELIMINARY RAMP IMPACT ANALYTICAL RESULTS

	CASE NO.		
	1	4	8
LIC RATION F.S.			
300	0.47	0.44	2.20
350	0.92	0.98	1.05
450	0.89	0.88	1.24
480	0.90	0.99	1.19
540	0.94	1.05	1.22
600	0.82	0.91	1.12
620	0.76	0.73	1.02
960/960	0.7/0.79	0.71/0.8	0.8/0.82
990	0.86	0.87	1.0
1090	1.08	1.01	1.08
1160	1.02	0.98	1.03
1210	0.89	0.93	0.9
1320	0.88	0.94	0.88
1400/1400	0.93/0.77	0.74/0.97	0.95/0.82
CRUSH (IN) @ FS		(INCLUDES GROUND CRUSH DISTANCE)	
199	9.0	10.0 (4)	14.3
300	14.0	15.2 (8)	17.0
460	8.4	10.6 (5)	9.7
620	5.8	9.0 (8)	6.1
820	7.5	12.2 (10.4)	6.3
960	13.8	18.6 (10.4)	11.1
1040	16.3	21.5 (2.3)	13.1
1200	13.5	18.4 (3.0)	4.6
1400	–		
(a) PEAK ACCEL. @ F.S.			
199 (1)	20.5/11.2	12.0/5.3	30.7/1.8
300 (2)	10.8/9.3	8.6/5.3	21.5/9.4
460 (3)	7.4/5.5	5.2/5.1	11.3/6.5
620 (4)	5.4/5.8	3.6/4.9	12.3*/4.8
820 (5)	5.1/5.4	4.0/4.8	8./5.3
960 (6)	9.1*/6.8	4.4/4.7	6.6/5.8
1040 (7)	10.3*/6.8	4.4/4.5	8.3*/6.4*
1200 (8)	9.1*/6.7	6.2/4.5	11.1*/6.0
1400 (9)	13./6.5	10.6/4.3	11.1/5.9

(a) DENOTES MASS NUMBER UNFILTERED DATA, VERTICAL/LONGITUDINAL
* SHARP .010 DURATION PEAK

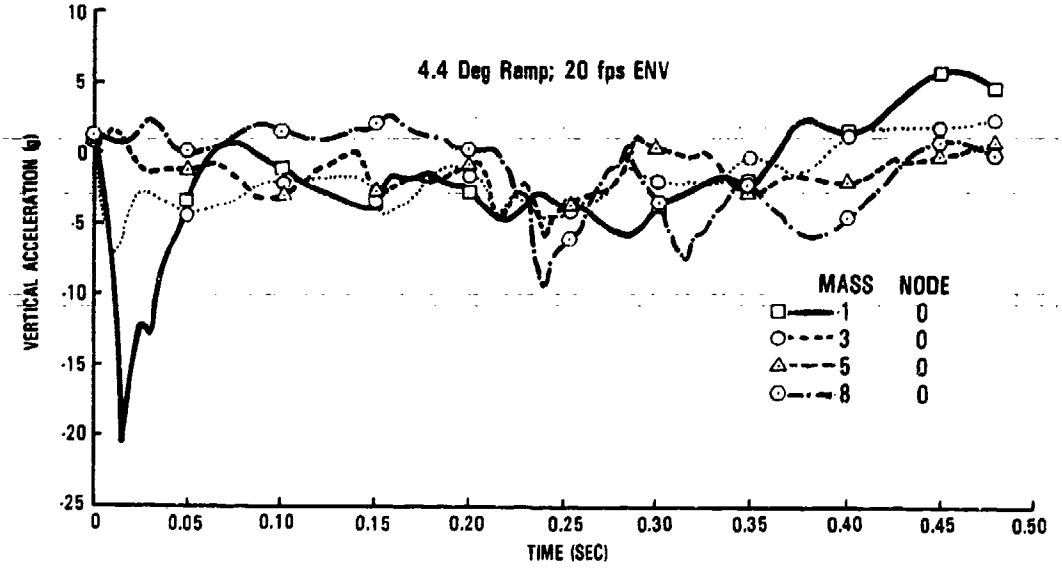

Figure 3-40. Baseline Stick Model - Vertical Pulses

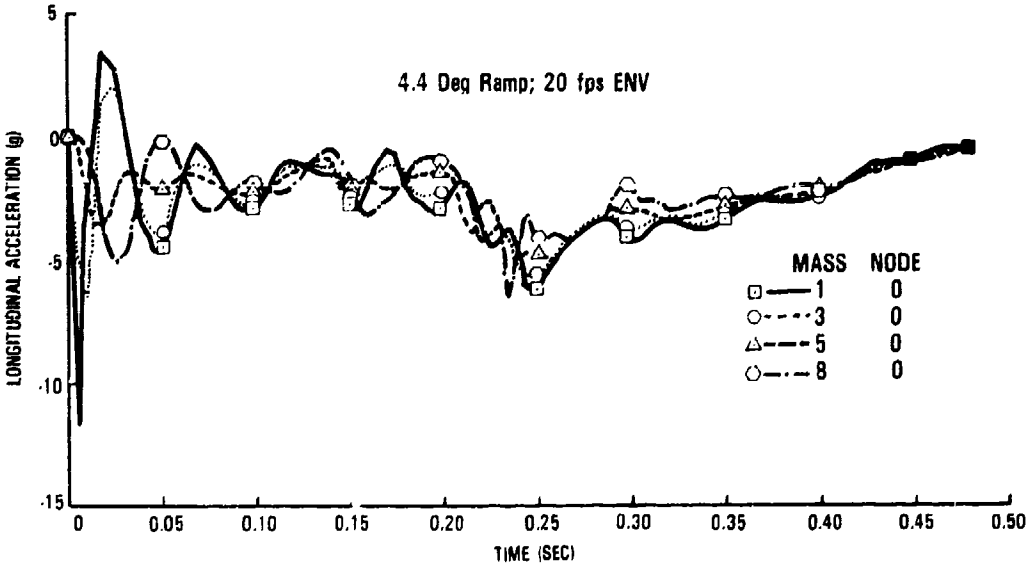

Figure 3-41. Baseline Stick Model - Longitudinal Pulses

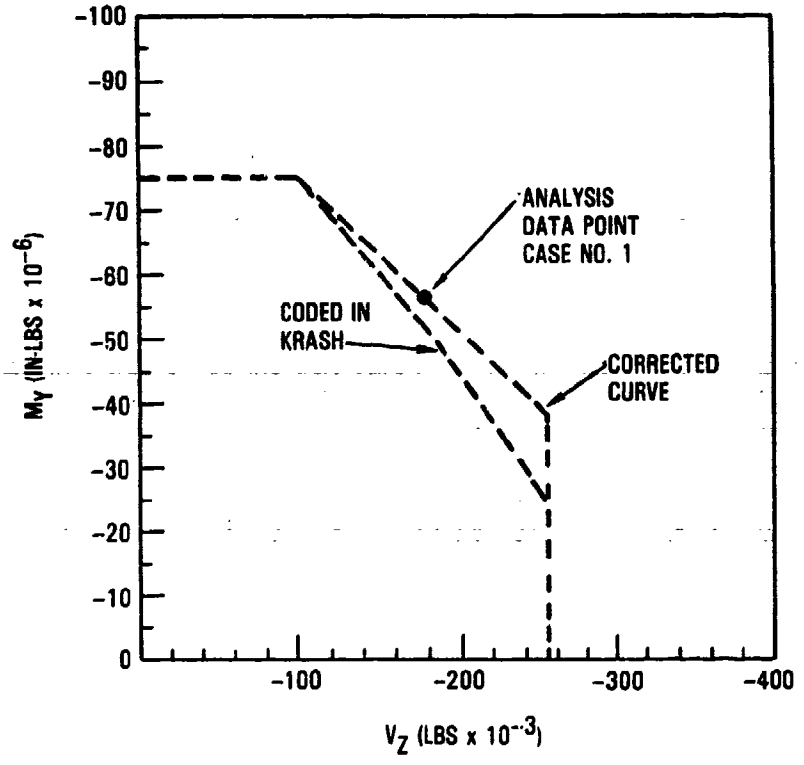

Figure 3-42. Maximum Allowable Moment and Shear Envelope - Negative Bending - Body Station 1120 (FS1080)

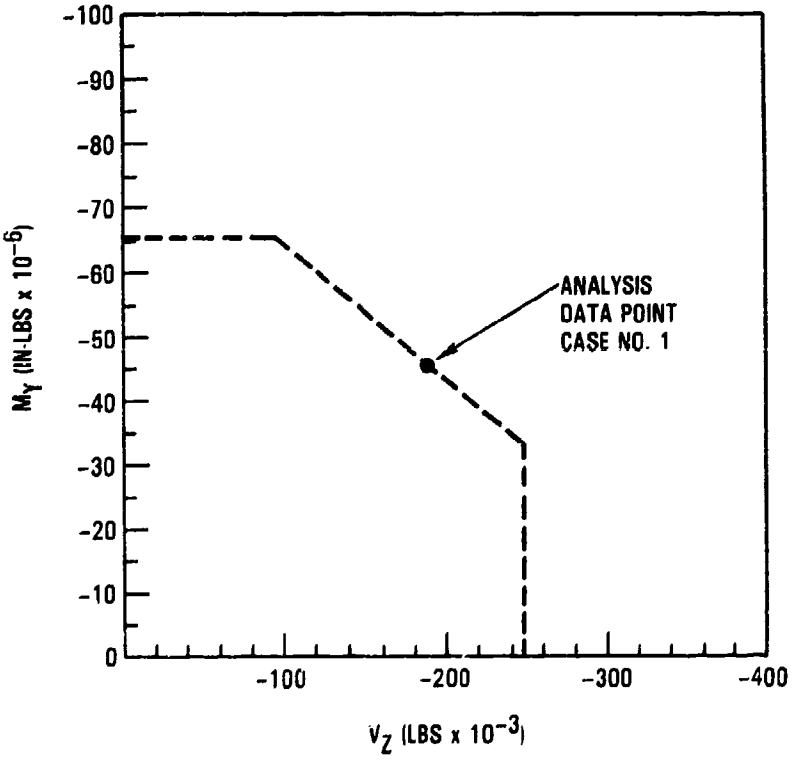

Figure 3-43. Maximum Allowable Moment and Shear Envelope - Negative Bending - Station 1200 (FS1160)

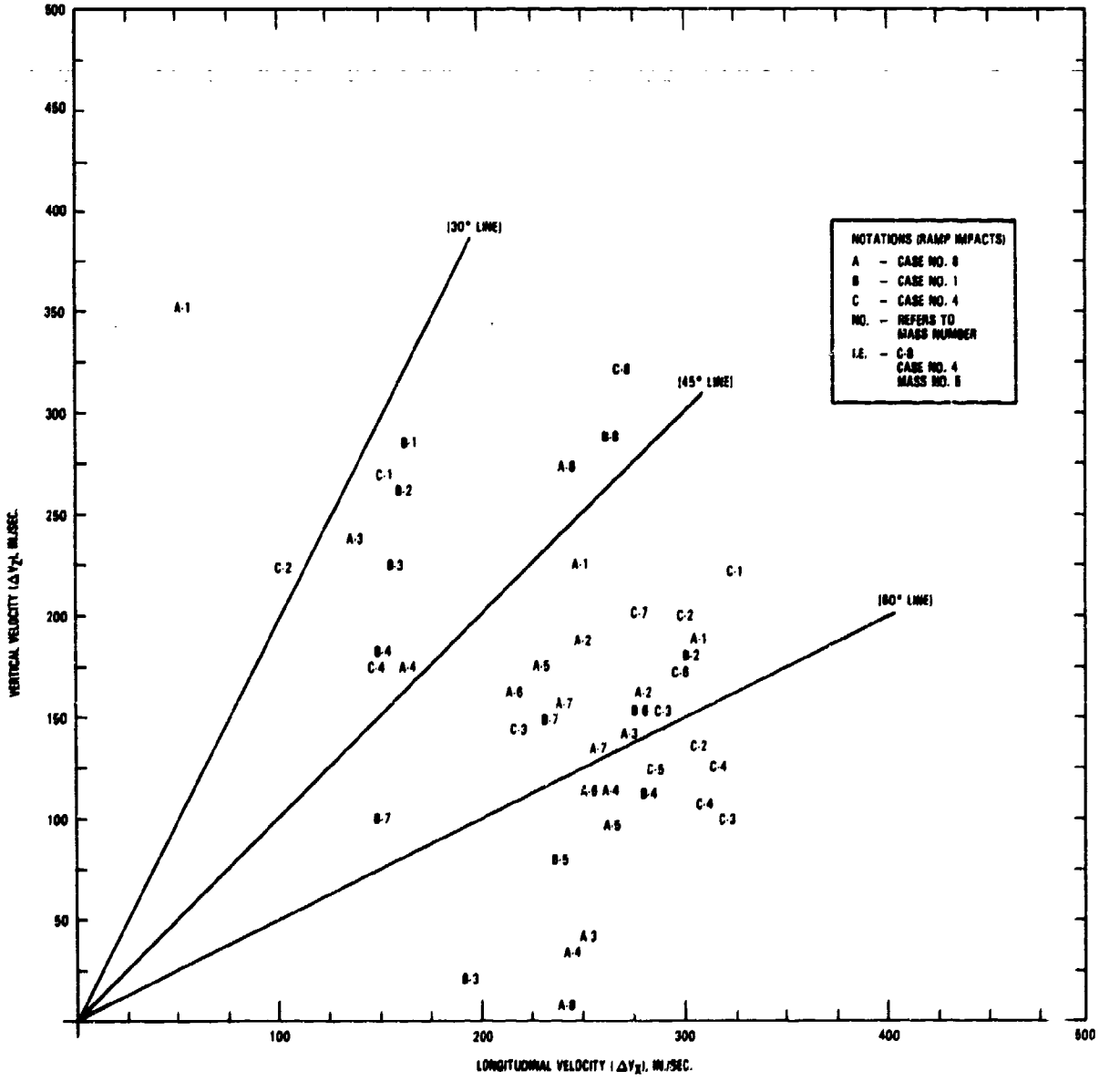

Figure 3-44. Vertical Velocity Versus Longitudinal Velocity Data Points; Slope Impact

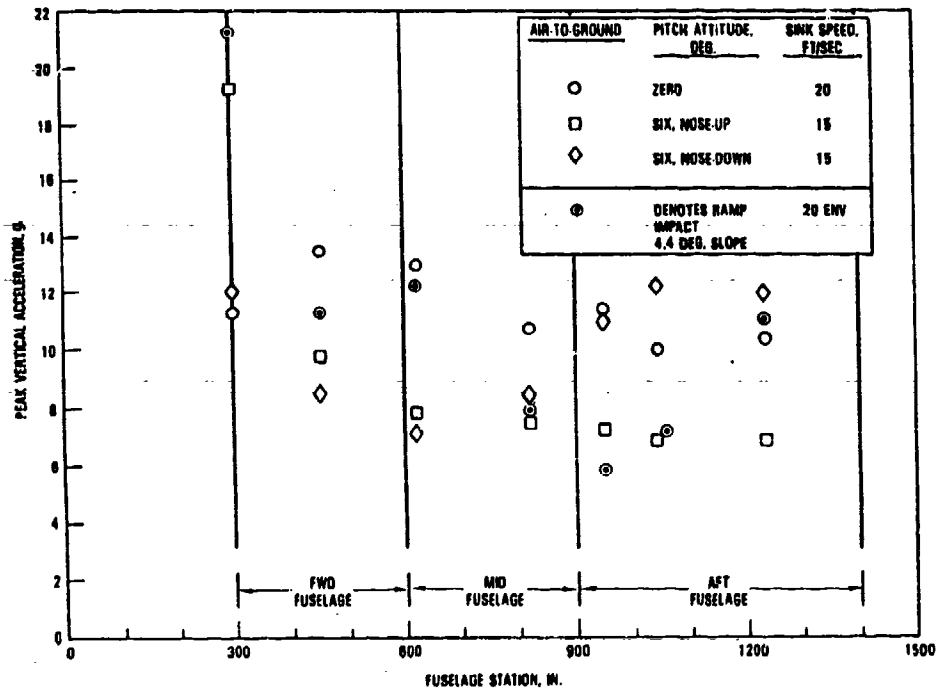

Figure 3-45. Peak Vertical Acceleration Versus Fuselage Station

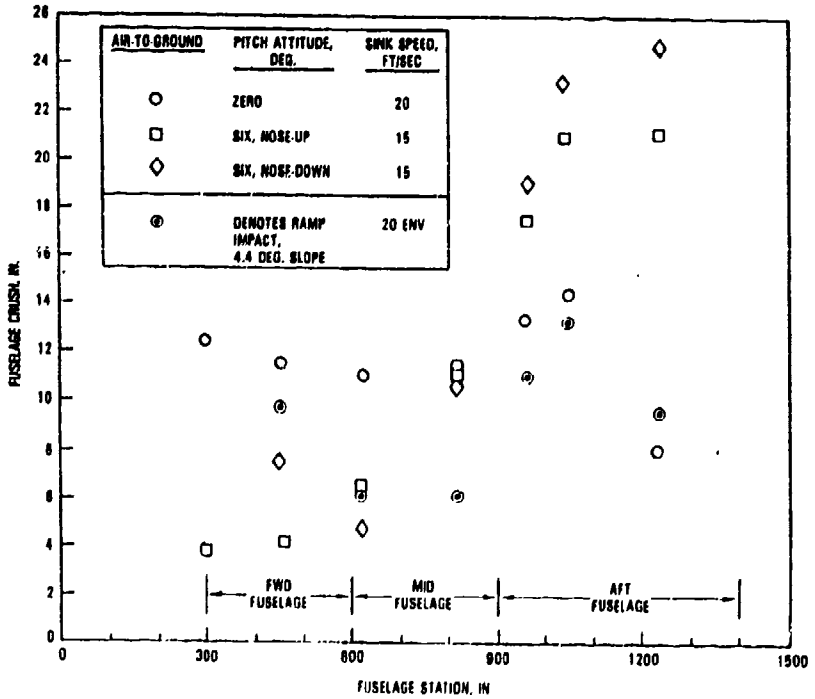

Figure 3-46. Fuselage Crush Distribution

ramp angles were considered: 20, 8.8 and 4.4 degrees. The cases considered are tabulated in table 3-15. In all cases the forward speed of the vehicle was allowed to vary in order that the ENV could be maintained at 25 ft/sec.The forward speeds of the vehicle are 73.1, 163.4 and 325.9 ft/sec for ramp angles of 20, 8.8 and 4.4 degrees, respectively.

Typically, the analytically determined vertical response of the airplane to a ramp impact is an initial acceleration peak immediately after impact with the ramp and then a secondary peak 0.10 to 0.20 second following the initial ramp impact. This second peak occurs when a crush spring "bottoms." In some cases, a third acceleration peak is evidenced within the time period investigated as the vehicle rotates and the aft section impacts the ground. Vertical acceleration response histories of forward, mid, and aft fuselage section masses are shown in figure 3-47. The amplitude of the initial peak of the forward section mass varies as the forward speed of the vehicle; 7.9g for the 20 degree ramp case compared to 19.8g for the 4.4 degree ramp case. The second response peak of the forward section mass appears to be a function of the ENV since the amplitude remains relatively constant for the three cases, 26.8g, 22.3g, and 22.7g for ramp angles of 20, 8.8, and 4.4 degrees, respectively.

The longitudinal response characteristics of the vehicle are not as well defined as the vertical response characteristics, see figure 3-48. Only in the 4.4 degree ramp impact case are the longitudinal characteristics similar to those of the vertical response, i.e., an initial response peak followed by a second peak 0.15 second later. Neither of the other two cases predict an initial impact peak and only the 20 degree case predicts the large second peak.

Maximum vertical and longitudinal response peaks for the 20, the 8.8 and the 4.4 degree ramp cases are summarized in table 3-16, columns 1, 3, and 6, respectively. The peak values shown occur at different times in the runs and not simultaneously. The base duration of the peak amplitudes are generally less than 0.10 second.

TABLE 3-15. RAMP IMPACT CASES

RAMP ANGLE (DEG)	FWD VEL (FT/SEC)	ENV* (FT/SEC)	GROUND FLEX (IN/LB)	REMARKS
20.0	73.1	25.0	–	BASELINE MODEL
20.0	110.0	37.6	–	BASELINE MODEL
8.8	163.4	25.0	–	BASELINE MODEL
8.0	235.0	32.7	–	BASELINE MODEL
6.0	177.0	18.5	–	BASELINE MODEL
4.4	325.9	25.0	–	BASELINE MODEL
20.0	73.1	25.0	–	ROTATE MASS 1 – 20 DEG. NOSE UP
8.8	163.4	25.0	–	ROTATE MASS 1 – 8.8 DEG NOSE UP
4.4	325.9	25.0	–	ROTATE MASS 1 – 4.4 DEG NOSE UP
20.0	73.1	25.0	–	BASELINE MODEL WITH PLOW FORCE = 1×10^5 (LB) AT VERTICAL SPRINGS 1 AND 2 FOR FIRST 0.1 SECONDS OF RUN.
20.0	73.1	25.0	–	MASS NODE 1 ADDED WITH HORIZONTAL SPRING. K1 SPRING SET.
20.0	73.1	25.0	–	MASS NODE 1 ADDED WITH HORIZONTAL SPRING. K2 SPRING SET.
20.0	73.1	25.0	–	MASS NODE 1 ADDED WITH HORIZONTAL SPRING. K3 SPRING SET.
20.0	73.1	25.0	–	MASS NODE 1 ADDED WITH HORIZONTAL SPRING. K4 SPRING SET.
20.0	73.1	25.0	$4\ 16 \times 10^{-5}$	BASELINE MODEL WITH MASS 1 ROTATED 20 DEG. NOSE UP
20.0	73.1	25.0	$4\ 16 \times 10^{-5}$	MASS 1 NODE ADDED WITH HORIZONTAL SPRING. K1 SPRING SET.

*EFFECTIVE NORMAL VELOCITY

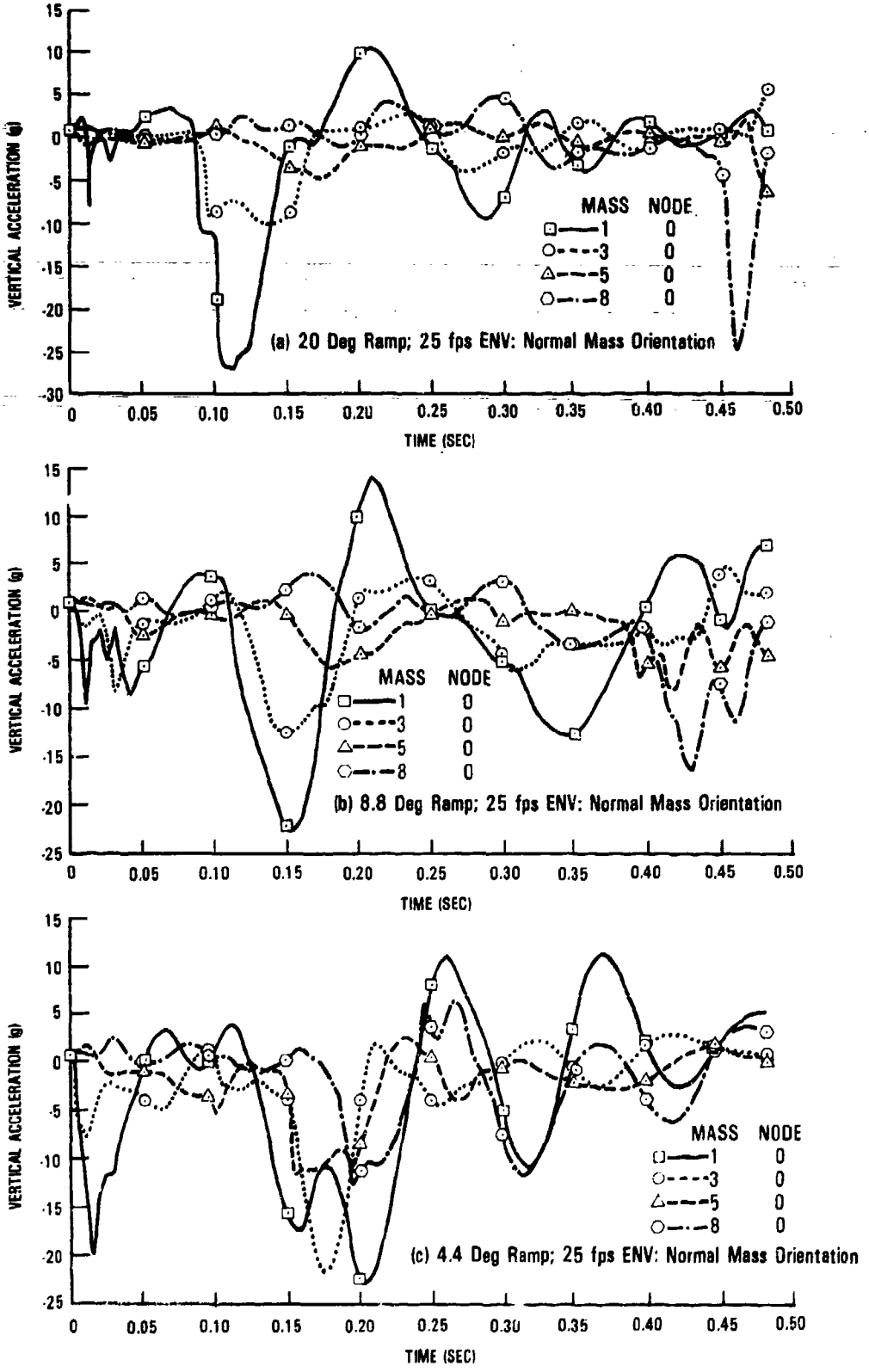

Figure 3-47. Stick Model Vertical Acceleration Histories

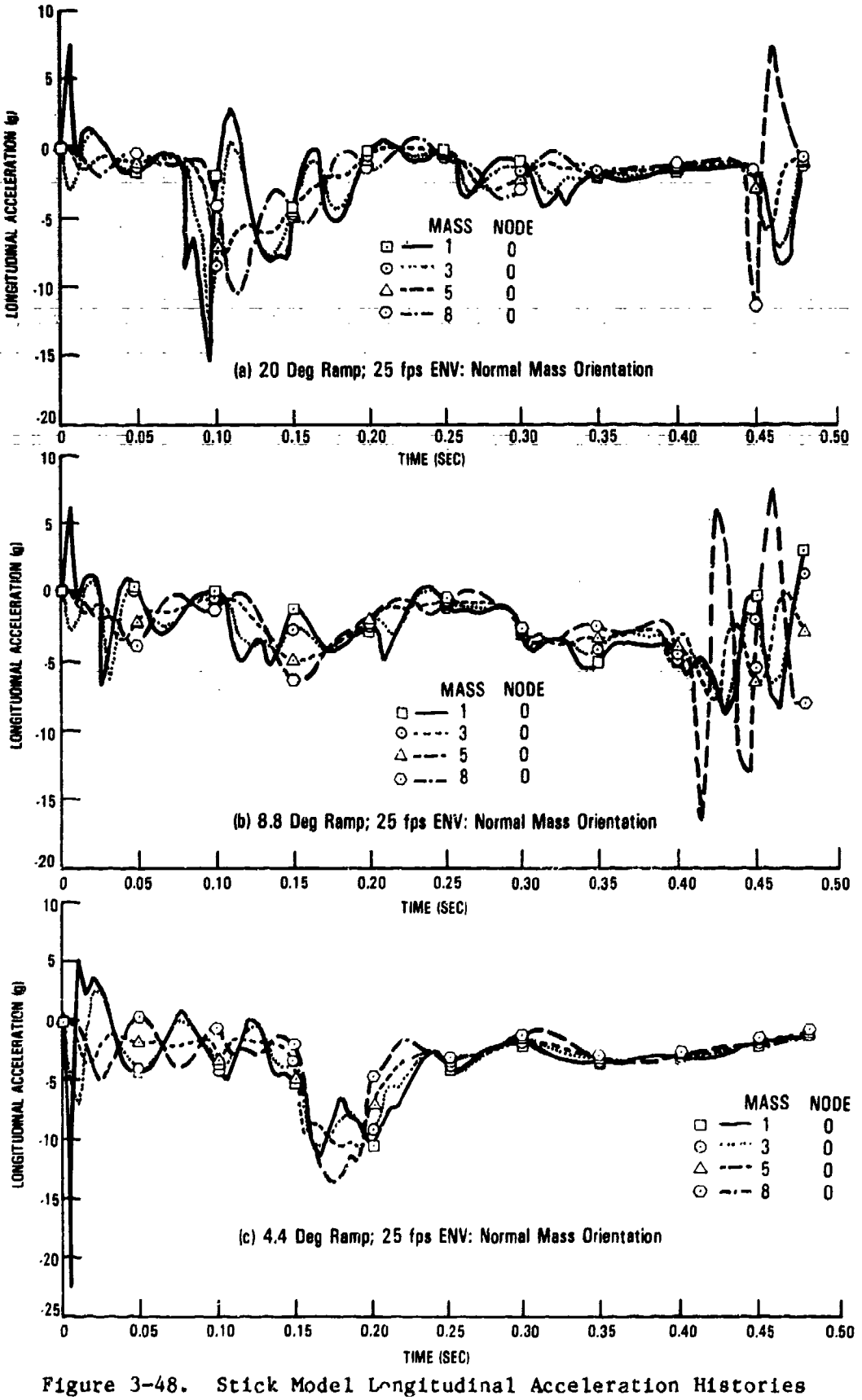

Figure 3-48. Stick Model Longitudinal Acceleration Histories

TABLE 3-16. MAXIMUM ACCELERATION

COLUMN	1	2	3	4	5	6	7	8
	BASELINE MODEL						MASS 1 ROTATED	
SPRING SET	K1	K1	K1	K1	K1	K1	K1	K1
ENV (FT/SEC)	25	37.6	25	32.7	18.5	25	25	25
FWD VEL (FT/SEC)	73.1	110	163.4	235	177	325.8	73.1	163.4
RAMP ANGLE (DEG)	20	20	8.8	8	6	4.4	20	8.8
FUSELAGE STATION								
199	-10.4/-26.8	-20.6/--60.0	-5.2/-12.4	-15.5/-38.8	-7.0/-14.2	-22.6/-22.7	-8.6/-22.4	-12.9/-20.0
300	-13.2/-18.5	+24.5/--40.6	-8.6/-18.2	-15.2/-28.0	-7.1/-8.6	-6.4/-17.5	-13.8/-16.3	-12.2/-17.1
460	-12.5/-10.1	-18.2/--15.0	-6.5/-12.6	-13.5/-16.7	-6.2/-8.8	-10.4/-21.5	-8.0/-11.3	-7.8/-12.3
620	-7.9/-8.0	-15.6/+12.6	-7.8/-7.5	-12.6/-12.0	-5.5/-5.2	-9.4/-15.9	-6.8/-7.6	-7.2/-7.5
820	-7.8/-4.6	-14.3/+8.7	-7.4/-7.5	-11.9/-18.4	-5.5/-7.1	-10.5/-11.4	-7.3/-3.5	-7.8/-8.2
960	-8.5/-3.9	+20.1/--13.7	-9.1/-9.7	-13.4/-19.2	-5.5/-13.3	-13.1/-8.0	-8.4/-3.5	-8.5/-11.5
1043.5	-9.4/-11.2	+28.8/--20.1	-9.6/-12.6	-15.9/-25.6	-5.5/-16.2	-12.1/-13.7	-8.8/-11.9	-10.5/-12.9
1201.1	-10.5/-14.9	+42.1/--27.6	-16.5/-16.1	+25.6/-30.3	-7.8/-14.3	-13.4/-12.4	-2.6/-23.1	-14.1/-15.8
1400	-10.0/-24.4	+72.5/--81.7	-18.4/-20.1	+40.4/-59.6	-9.2/-13.3	-15.3/-8.6	-9.5/-34.9	-19.2/-22.9

COLUMN	9	10	11	12	13	14	15	16
		PLOW FORCE	MASS 1 NODE ADDED				GROUND FLEXIBILITY	
SPRING SET	K1	K1	K1	K2	K3	K4	K1	K1
ENV (FT/SEC)	25	25	25	25	25	25	25	25
FWD VEL (FT/SEC)	325.9	73.1	73.1	73.1	73.1	73.1	73.1	73.1
RAMP ANGLE (DEG)	4.4	20	20	20	20	20	20	20
FUSELAGE STATION								
199	-24.0/-23.7	-12.0/-16.4	-8.1/-31.7	-26.1/-28.3	-22.9/-20.8	-10.9/-27.5	-4.3/-12.9	-5.3/-8.6
300	-10.1/-17.4	-14.8/-15.5	-15.9/-22.7	-10.2/-20.1	-12.3/-17.1	-9.7/-21.1	-4.6/-8.7	-5.0/+5.4
460	-10.4/-21.3	-10.8/-13.2	-11.6/-9.5	-7.9/-8.8	-9.9/+7.7	-8.2/-9.5	-4.2/-5.6	-4.3/-4.1
620	-10.1/-15.9	-7.5/-9.0	-7.0/-8.5	-5.9/-7.8	-6.3/+6.1	-6.0/-7.9	-4.1/-3.8	-3.4/-3.4
820	-10.7/-11.2	-7.1/-4.8	-6.9/-4.6	-6.1/-4.4	-6.2/-3.6	-6.2/-4.5	-4.3/-3.0	-3.3/-2.3
960	-13.3/-9.5	-8.1/+3.2	-6.7/-5.7	-6.0/-2.5	-6.4/-7.2	-6.4/-2.5	-4.5/-2.3	-3.7/-2.6
1043.5	-12.0/-13.7	-9.9/+3.0	-6.9/-7.9	-6.3/-2.3	-6.7/-11.1	-6.8/-2.2	-4.6/-3.6	-3.8/-3.4
1201.1	-13.3/-11.3	-7.6/-21.1	-7.1/-10.9	-6.3/+4.2	+10.8/-14.7	-6.9/+4.2	-4.7/-5.9	-4.3/-5.4
1400	-15.1/-8.6	-8.7/-36.1	+9.3/-17.1	-7.5/+6.5	+17.7/-28.3	-7.9/+6.5	-4.8/-10.5	-5.0/-8.4

TABLE 3-17. MAXIMUM L1C RATIOS

COLUMN	1	2	3	4	5	6	7	8
	BASELINE MODEL						MASS 1 ROTATED	
SPRING SET	K1	K1	K1	K1	K1	K1	K1	K1
ENV (FT/SEC)	25	37.6	25	32.7	18.5	25	25	25
FWD VEL (FT/SEC)	73.1	110	163.4	235	177	325.9	73.1	163.4
RAMP ANGLE (DEG)	20	20	8.8	8	6	4.4	20	8.8
FUSELAGE STATION								
300	1.75	3.25	1.61	1.97	.50	.43	1.72	1.59
350	1.62	1.79	1.38	1.95	.90	.92	1.65	1.32
450	1.69	1.82	1.45	1.93	.87	1.06	1.73	1.42
480	1.14	1.45	1.32	1.33	.76	1.07	1.15	1.32
540	1.15	1.55	1.41	1.43	.78	1.10	1.17	1.42
600	1.07	1.35	1.26	1.27	.71	1.00	1.08	1.26
620	.89	1.07	.89	1.99	.75	2.19	.89	.88
820	1.12	1.49	1.22	1.68	.74	1.73	1.13	1.21
820	1.25	1.74	1.34	1.55	.82	.91	1.26	1.33
960	.68	.91	.73	.93	.56	.83	.68	.73
960	.63	.90	.64	.92	.57	.75	.64	.63
990	.68	1.08	.70	1.07	.67	.88	.68	.69
1090	.79	1.08	.75	1.46	.71	.95	.79	.74
1160	.75	1.03	.73	1.38	.72	.94	.75	.72
1210	.58	1.12	.64	1.10	.79	1.02	.57	.62
1320	.59	1.37	.64	1.44	.78	1.01	.57	.63
1400	.66	1.91	.82	1.96	.83	1.08	.62	.81
1400	.71	1.32	.70	1.59	.68	1.09	.72	.81

COLUMN	9	10	11	12	13	14	15	16
	PLOW FORCE		MASS 1 NODE ADDED				GROUND FLEXIBILITY	
SPRING SET	K1	K1	K1	K2	K3	K4	K1	K1
ENV (FT/SEC)	25	25	25	25	25	25	25	25
FWD VEL (FT/SEC)	325.9	73.1	73.1	73.1	73.1	73.1	73.1	73.1
RAMP ANGLE (DEG)	4.4	20	20	20	20	20	20	20
FUSELAGE STATION								
300	.40	1.45	1.68	1.64	1.66	1.66	1.18	1.15
350	.91	1.57	1.04	1.05	1.02	1.05	1.12	1.16
450	1.05	1.57	1.22	1.23	1.17	1.22	1.24	1.33
480	1.09	1.12	1.00	1.02	.98	1.02	1.11	1.07
540	1.11	1.12	1.04	1.05	1 04	1.05	1.10	1.07
600	1.02	1.05	.93	.95	.92	.95	1.04	1.00
620	2.21	.90	.83	.84	.81	.84	.86	.86
820	1.73	1.14	1 00	1.01	.94	1.02	1.10	1.04
820	.91	1.28	1.12	1.13	1.10	1.14	1.23	1.16
960	.83	.70	.57	.57	.59	.56	.59	.59
960	.76	.65	.50	.49	.57	.48	.47	.50
990	.88	.70	.54	.52	.88	.52	.60	.88
1090	.96	.81	.60	.62	.66	.62	.48	.52
1160	.95	.76	.57	.58	.62	.58	.48	.49
1210	1.01	.59	.50	.57	.51	.56	.48	.44
1320	1.01	.59	.48	.56	.60	.56	.46	.45
1400	1.08	.64	.64	.59	.72	.59	.50	.46
1400	1.08	.53	.59	.48	44	.48	.43	.37

The LIC ratios for the 20 and 8.8 degree ramp impact cases (see table 3-17, columns 1 and 3) indicate a general failure (LIC > 1) in the forward sections of the airplane. In the 4.4 degree impact case (table 3-17, column 6), the analysis indicates that a major failure of the mid-section at FS620 (LIC > 2) occurs and also marginal failures of the nose and aft sections (LIC ratios between 0.9 and 1.1). The high load at FS620 is produced when the crushing deflection at that station exceeds 10 inches. At this deflection the spring bottoms and becomes very stiff, thus producing very high loads for small increases in deflection. The LIC ratios for the 4.4 degree ramp are higher from FS620 to FS1400 when compared to the 8.8 degree and 20 degree ramp results. This trend at first impression would appear inconsistent. However, for the same ENV, the airplane forward velocity is almost 2 to 5 times faster. For the shallower (4.4 degree) ramp angle condition, the mid-fuselage contacts the slope (masses at FS300 and 460-960 do make ground contact at t = 0.0) at about .080 second after initial airplane contact with the ground. The FS620 spring forces continue to act for about 0.150 second thereafter, during which time the vertical velocity change at that location is noted to be 250 in/sec (~21 ft/sec). For the shallow ramp condition, the aircraft is completely on the ramp at the conclusion of the analysis (t = 0.48 seconds). Conversely, for the steep (20-degree) ramp condition only a portion of the airplane (FS199-460) has traversed the ramp during this same time period. For this condition the mid-fuselage stations (FS620 - FS960) along with the nose section (FS199) make initial ground contact. The FS620 spring barely stays in contact with the ground and does not contact the sloped portion of the ground. During the time the spring at FS620 is in ground contact, the normal velocity change is minimal. The analysis results, if representative of the actual condition, would suggest that for a specified ENV the location of the critical LIC ratio could vary as a function of ramp angle as is depicted in figure 3-49. The LIC's in the KRASH model are related to vertical shears and bending moments. Thus, at a 90 degree ramp angle the forces should be primarily axial and the vertical loads are expected to reduce, hence the projection of low LIC's at 90 degrees. Similarly, for a zero degree ramp the vertical forces theoretically would be small as the airplane slides, and thus there would also be no significant vertical shear or bending moments (LIC's = 0).

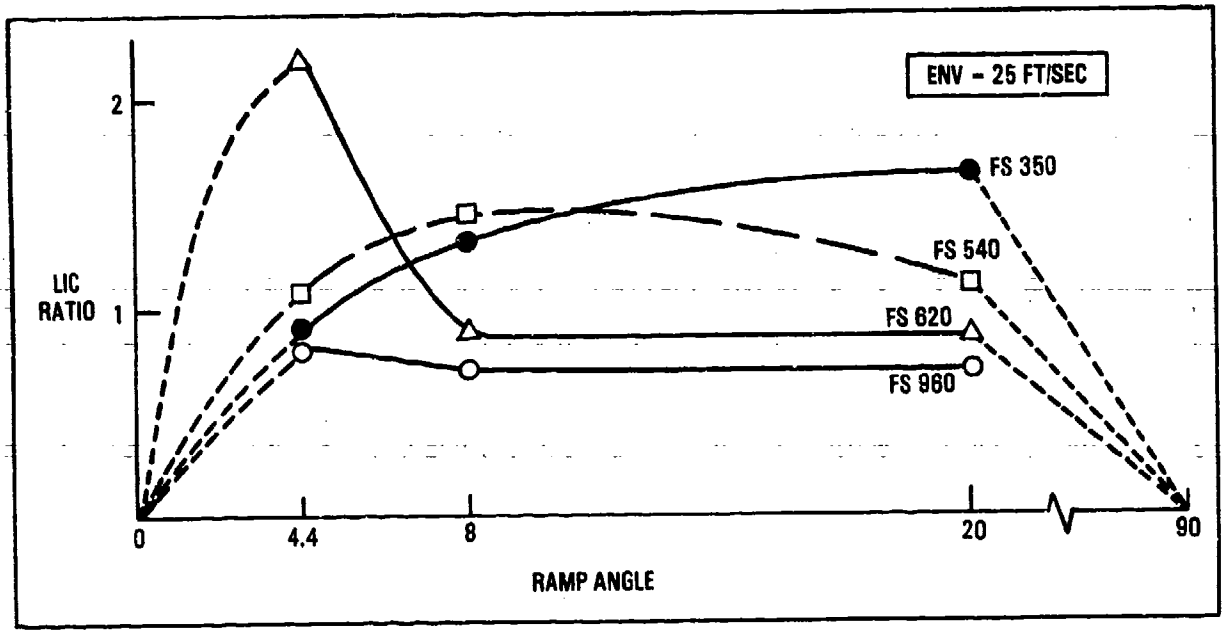

Figure 3-49. LIC Ratio Versus Ramp Angle, ENV = 25 ft/sec

On the other hand, the analysis could be predicting this trend as a result of modeling the contact regions too rigidly. The air-to-ground ± 6 degree pitch attitude impacts also showed significant airplane rigid body rotation after initial impact. The relative positions of the aircraft at t = 0.48 seconds for the three slope impacts are shown in figure 3-50. Maximum crushing deflections are summarized in columns 1, 3, and 6 of table 3-18 for the three ramp cases. Note that the crushing deflection is fairly uniform over the length of the fuselage in the 4.4 degree ramp case. In the 20 degree ramp case, however, the major crush takes place in the forward and aft sections of the fuselage as the vehicle rides up the ramp and rotates thus causing the aft section to impact the ground. The KRASH model representation of the fuselage underside crush could be too stiff and therefore causing too much rotation for the higher ramp angle impacts.

The energy distribution at the end of each of the three cases is summarized at the top of page 3-62.

Ramp Angle Degrees	Percent of Total System Energy			
	Strain	Damping	Crushing	Friction
20	1.00	0.59	2.22	52.32
8.8	0.38	0.14	1.11	36.98
4.4	0.17	0.06	0.34	24.38

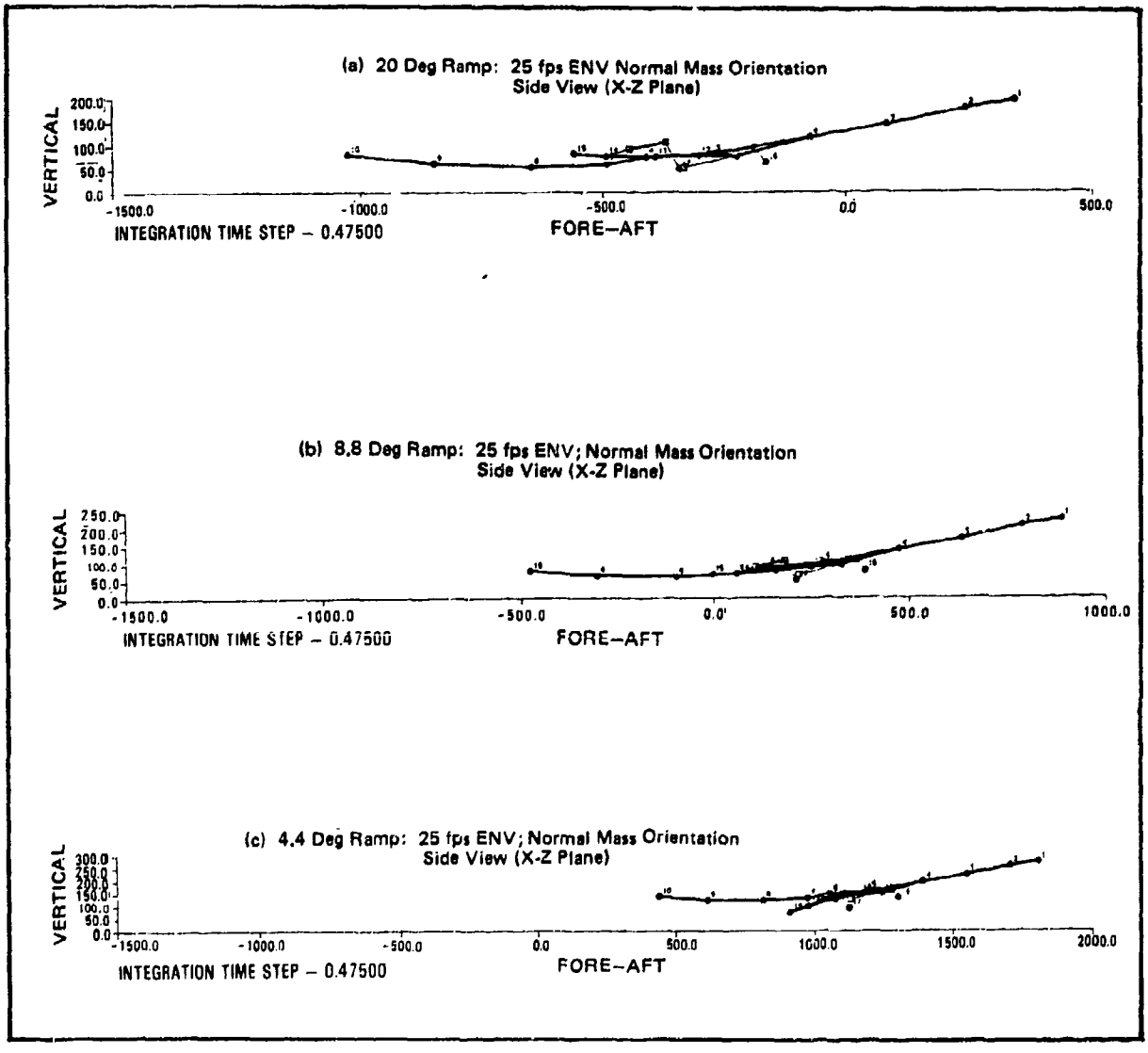

Figure 3-50. Stick Model Mass Position Plot

TABLE 3-18. MAXIMUM CRUSHING SPRING DEFLECTIONS

COLUMN		1	2	3	4	5	6	7	8
		BASELINE MODEL						MASS ROTATED	
SPRING SET		K1	K1	K1	K1	K1	K1	K1	K1
ENV (FT/SEC)		25	37.6	25	32.7	18.5	25	25	25
FWD VEL (FT/SEC)		73-1	110	163.4	235	177	325.9	73.1	163.4
RAMP ANGLE (DEG)		20	20	8.8	8	6	4.4	20	8.8
FS	SPRING AXIS								
199	1	16.1	23.5	--	--	--	--	--	--
199	3	33.7	36.7	30.9	32.7	10.5	24.7	33.9	30.6
300	3	7.9	21.7*	27.2	30.1	13.3	28.5	6.0	26.8
460	3	--	8.4*	12.8	16.5	5.5	20.3	--	12.9
620	3	0.2	0.2	6.1	12.1	2.7	13.0	0.1	5.9
820	3	0.3	0.4	7.1*	10.8	4.2	6.3	0.4	6.8*
960	3	1.1	1.0	8.4*	13.5	9.2*	10.9	1.1	8.2*
1043.5	3	10.5	10.5	7.5*	15.1*	10.9*	14.3*	10.4*	7.2*
1201.1	3	19.2	20.9	13.6	13.0*	10.6	13.6*	19.0*	13.6
1400	3	1.1*	4.1	--	--	--	--	--	--

* END OF RUN VALUE

COLUMN		9	10	11	12	13	14	15	16
		MASS ROTATED	PLOW FORCE	MASS 1 NODE ADDED				GROUND FLEXIBILITY	
SPRING SET		K1	K1	K1	K2	K3	K4	K1	K1
ENV (FT/SEC)		25	25	25	25	25	25	25	25
FWD VEL (FT/SEC)		325.9	73.1	73.1	73.1	73.1	73.1	73.1	73.1
RAMP ANGLE (DEG)		4.4	20	20	20	20	20	20	20
FS	SPRING AXIS								
199	1	--	--	23.7	22.6	43.4	22.8	--	22.3
199	3	24.6	32.2	18.2	18.0	22.1	17.9	30.1	22.7
300	3	28.4	4.2	0.8	1.0	3.5	1.2	10.6	0.8
460	3	20.2	--	--	--	--	--	0.1	--
620	3	13.0	0.8	0.2	0.2	0.2	0.2	0.2	0.1
820	3	6.4	0.5	0.6	0.6	0.4	0.6	0.3	0.2
960	3	10.9	1.0	0.8	0.8	0.8	0.8	0.5	0.5
1043.5	3	14.3*	10.4*	9.7	9.2	10.1	9.1	12.0*	11.8
1201.1	3	13.6*	18.9*	18.4	17.3*	18.5	17.1	18.8*	19.4*
1400	3	--	0.8	0.1	--	0.4	--	0.8*	1.3*

* END OF RUN

In each of the three baseline cases, the dominant energy dissipation mechanism is the friction between the crushing springs and the ground, ranging from 24 percent to over 50 percent of the total energy of the system.

Comparing the baseline results with available data measured on the L-1649 revealed that the relatively large longitudinal acceleration response pulse present in the forward section of the L-1649 (particularly at the 20-degree slope impact) was not obtained in the baseline analyses (see figure 3-36).

Modifications were made to the B720 stick model in an attempt to duplicate the large initial longitudinal acceleration pulse observed in the L-1649 data. The model changes investigated are listed below. The results of runs made with each of the modifications are tabulated in the referenced columns of tables 3-16, 3-17 and 3-18.

(1) Mass 1, and therefore the spring attached to mass 1, was rotated nose-up an angle equal to the ramp angle. Thus, the vertical (direction 3) crushing spring is initially oriented normal to the ramp. Results for ramp angles of 20, 8.8 and 4.4 degrees are tabulated in columns 7 through 9.

(2) Mass 1 was rotated and a plowing force of 100,000 pounds was applied to mass 1 and mass 2 crushing springs. Results for a ramp angle of 20 degrees are tabulated in column 10.

(3) A massless node was added to mass 1. The horizontal crushing spring (direction 1) previously attached to mass 1 was moved and attached to the new node. The node was located such that at the time of impact, both the horizontal spring attached to mass 1, node 1 and the vertical spring attached to mass 1 were in contact with the ramp. Results for a ramp angle of 20 degrees are tabulated in column 11.

(4) The load deflection curves for the crushing springs attached to mass 1; mass 1, node 1; and mass 2 of the modification (3) model were altered. The baseline load deflection curves, see figures 3-51 and 3-52, are referred to as the K1 spring set, while the three modifications investigated are called the K2, the K3 and the K4 spring sets (see figures 3-53 through 3-55). The results for three modified spring sets and a ramp angle of 20 degrees are tabulated in columns 12 through 14.

(5) A flexible ground (flexibility = 0.0000416 inch/pound) was added to the modification (1) and the modification (3) models. The results for a ramp angle of 20 degrees are tabulated in columns 15 and 16. This representation tends to result in lower response amplitude since the ground as well as the structure deforms.

Although a broad range of modifications were applied to the baseline model, the large initial longitudinal acceleration response pulse at the extreme (nose) forward section of the fuselage apparent in the L-1649 data could not be simulated. However, the longitudinal pulse magnitudes throughout the remainder of the aircraft show agreement between analysis and measured responses during the length of analysis time investigated.

The overall response characteristics of the B-720 stick model for various ramp impact conditions were determined. Except as noted, the characteristics determined were, in general, consistent with those observed in the L-1649 data. The stick model representation, however, may not have been of sufficient local detail to adequately predict the initial forward section longitudinal response pulse as seen in the L-1649 response data. Equivalent triangular pulse response levels were determined from the longitudinal and vertical response histories of the various stick models considered in this study. Response levels for model masses 1, 3, 5 and 8 are shown in figures 3-56 and 3-57.

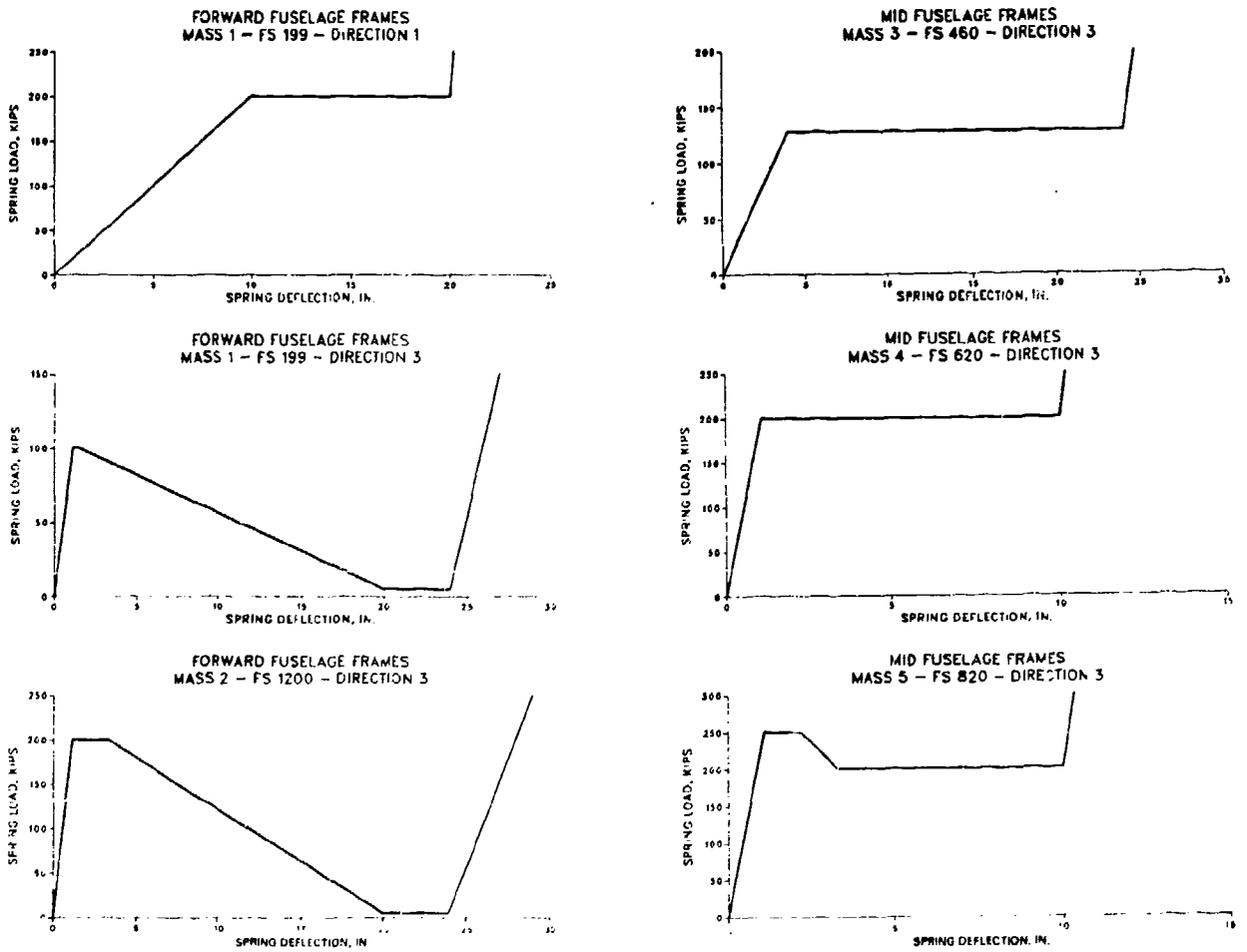

Figure 3-51. Load-Deflection Curves for Baseline Model (Masses 1-5)

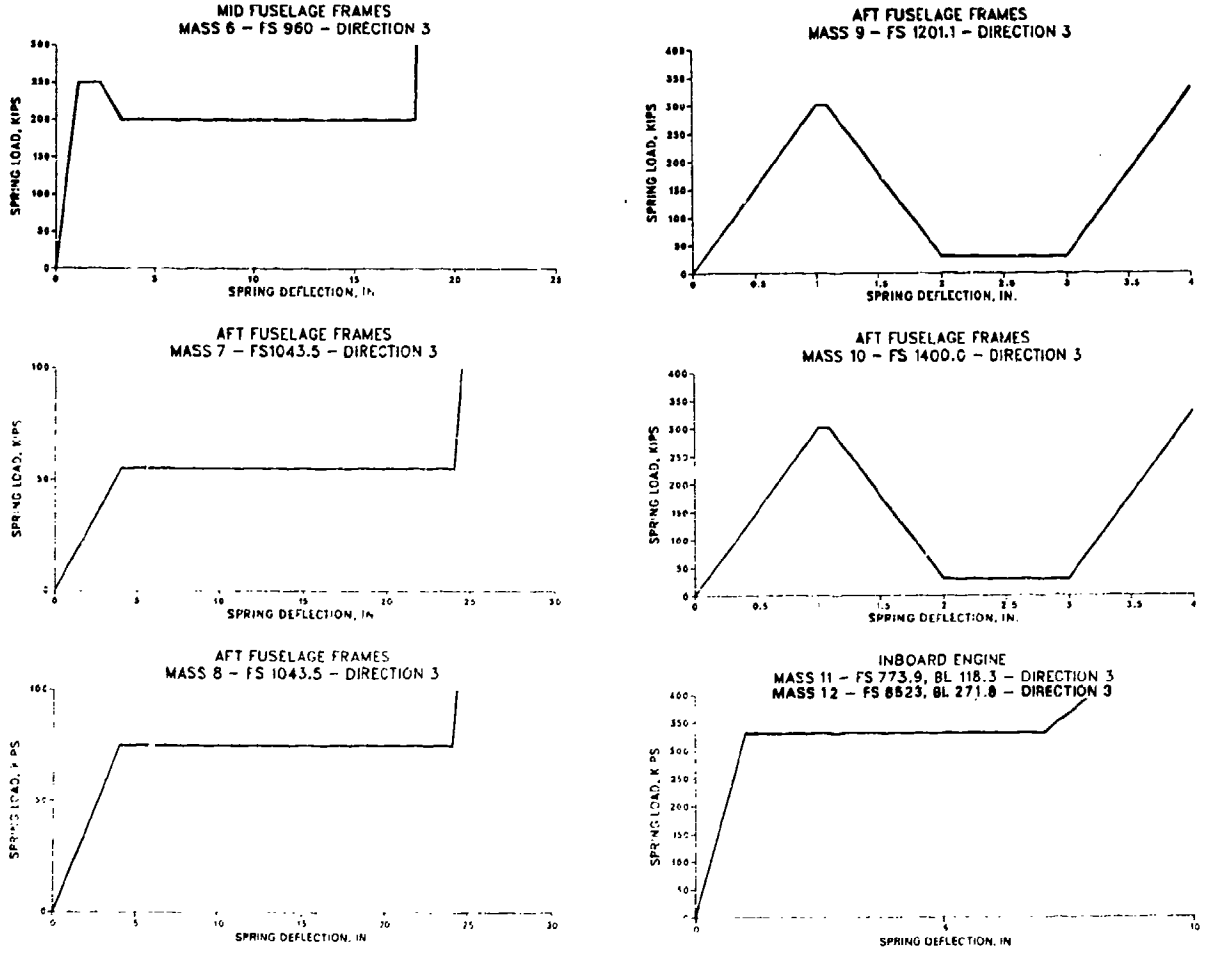

Figure 3-52. Load-Deflection Curves for Baseline Model (Masses 6-12)

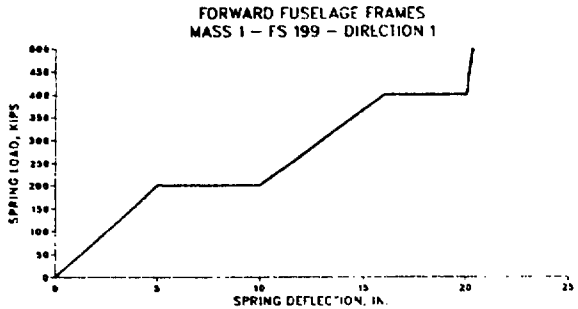

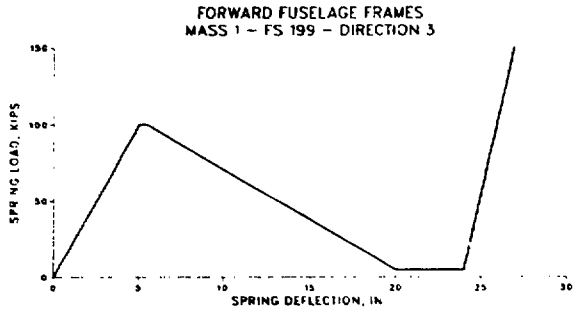

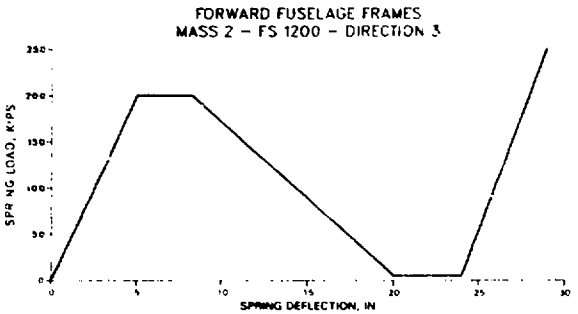

Figure 3-53. Load-Deflection Curves - Set K2

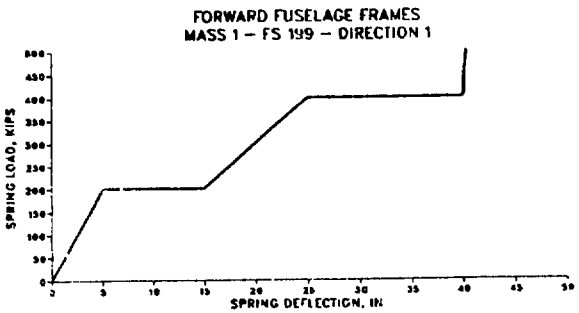

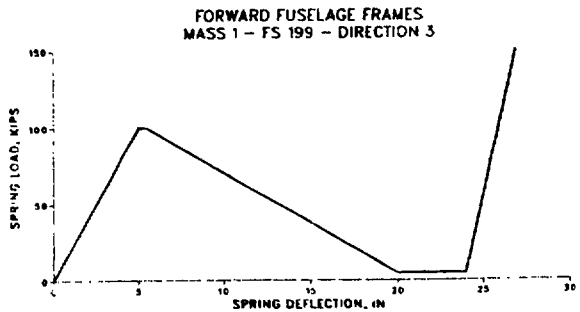

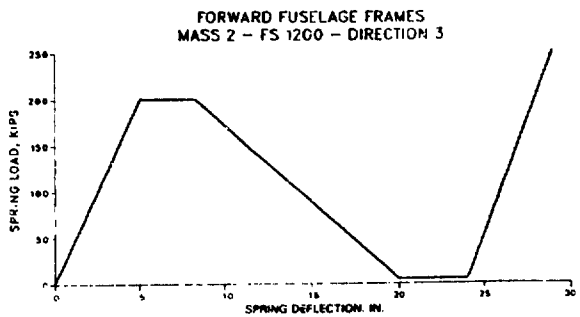

Figure 3-54. Load-Deflection Curves - Set K3

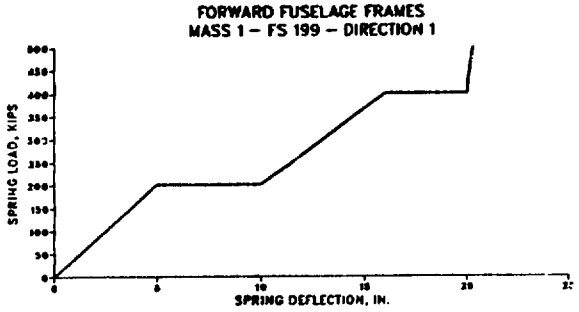

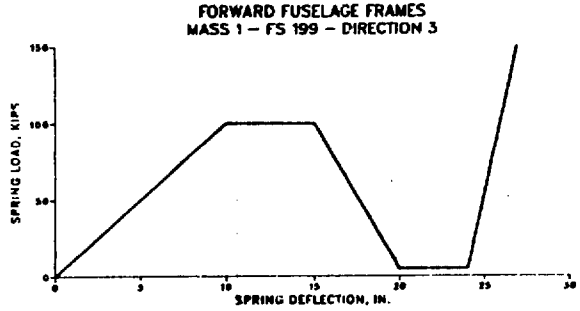

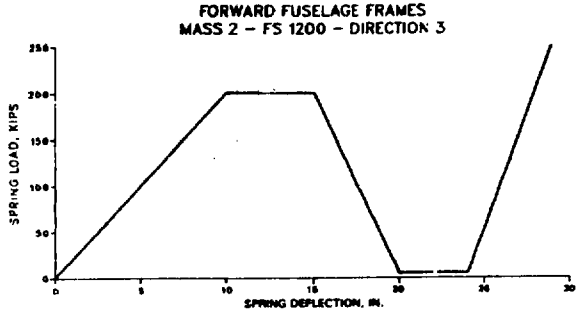

Figure 3-55. Load-Deflection Curves - Set K4

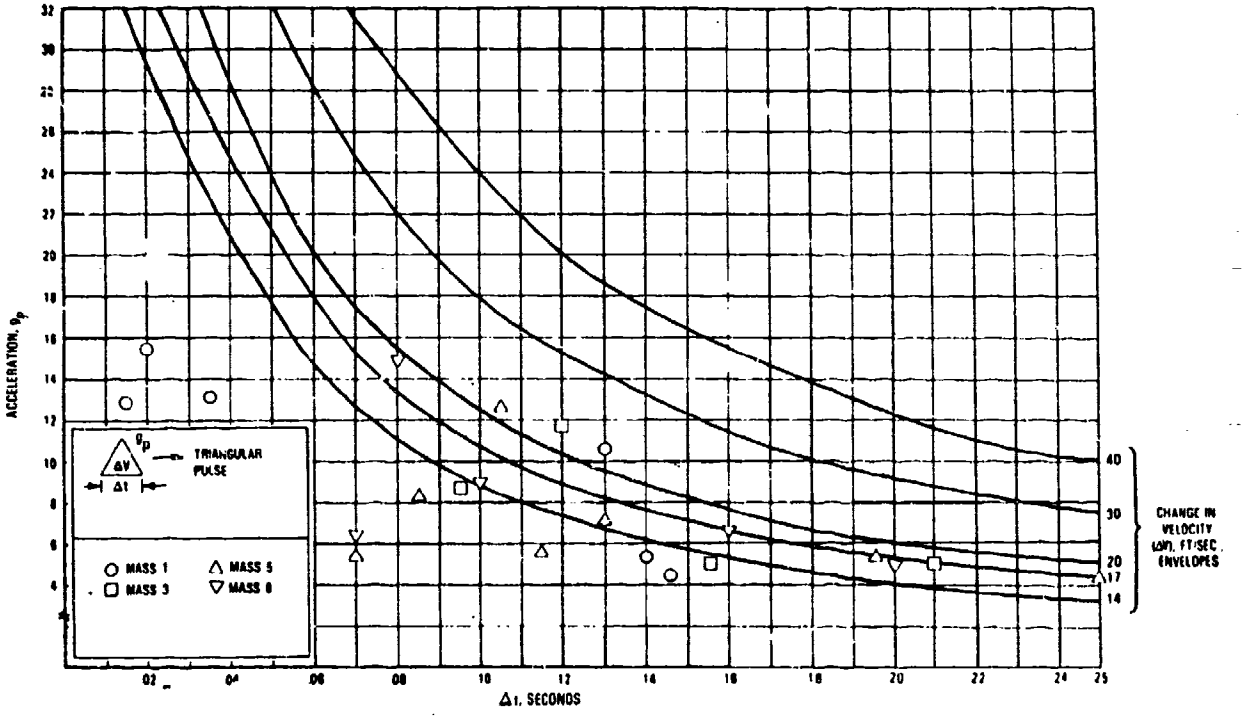

Figure 3-56. Longitudinal Pulses Obtained from Ramp Impacts

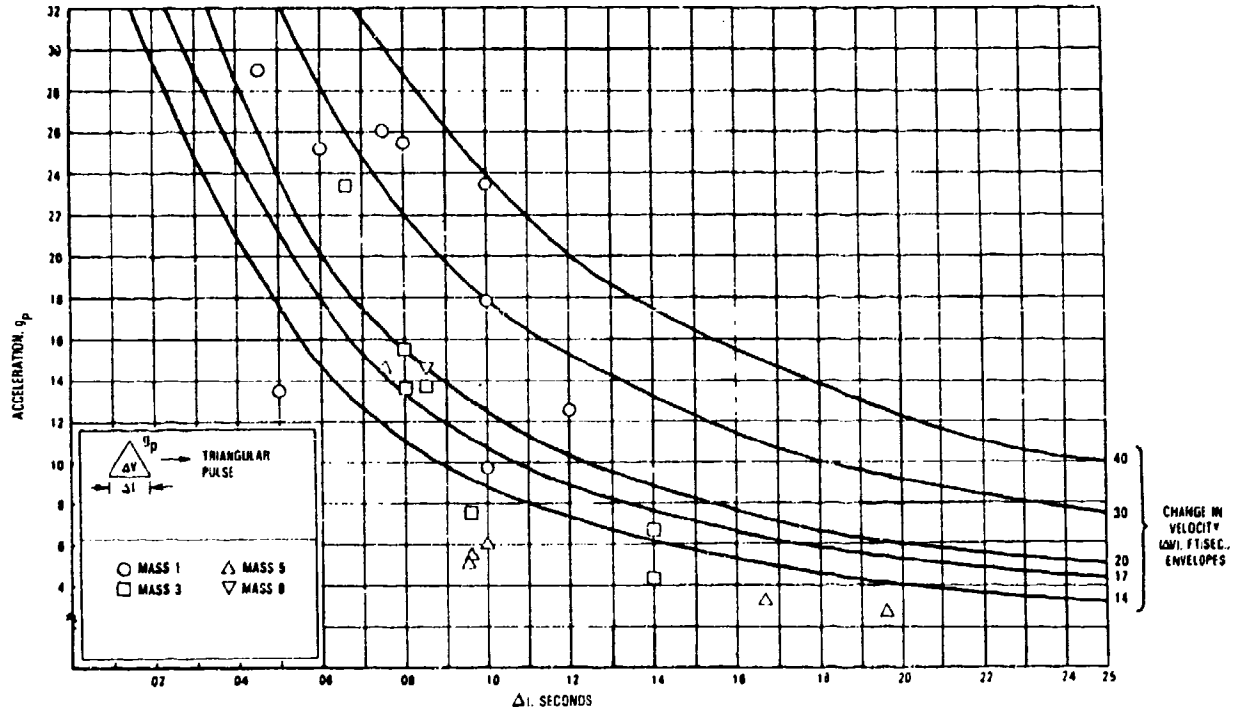

Figure 3-57. Vertical Pulses Obtained from Ramp Impacts

Tables 3-15 through 3-18 also contain analytical results for three additional impact conditions:

1. 6-degree ramp, ENV = 18.5 ft/sec, forward velocity = 177 ft/sec
2. 20-degree ramp, ENV = 37.6 ft/sec, forward velocity = 110 ft/sec
3. 8-degree ramp, ENV = 32.7 ft/sec, forward velocity = 235 ft/sec

The first two conditions are associated with the initial and second slope impacts for the L-1649 crash test (Reference 6). The latter condition is the impact associated with the DC-7 crash test (reference 7). Note that both the KRASH analysis and the L-1649 test results for the 6-degree slope impact indicate that no fuselage failure would have occurred. The analysis results indicate strength margins of at least +0.10. The 20-degree and the 8-degree slope impact conditions noted above did result in forward fuselage and subsequent rear fuselage failures during the respective crash tests. The analysis for both impacts show the likelihood of substantial failure occurring in both locations, as can be noted by the high LIC ratios. Acceleration history plots for these conditions are noted in figures 3-58 and 3-59 for the vertical and longitudinal directions, respectively. Figures 3-60 and 3-61 show the acceleration, Δt, ΔV relationships for the aforementioned additional three cases.

3.2.2 Full-Scale Test Data

The full-scale crash tests of the L-1649 (reference 6), in particular, and the DC-7 (reference 7), to a limited extent, provide the most meaningful combined vertical-longitudinal floor pulse data for medium sized transport airplanes. The CID (reference 8) being an air-to-ground impact resulted primarily in vertical pulses significantly higher than the corresponding longitudinal pulses. The magnitude of the longitudinal direction pulses was predictably related to the magnitude of the vertical pulses by the ground coefficient of friction. The floor accelerations obtained from the CID test were integrated. The change in vertical velocity associated with the accelerations pulses measured along the floor varied from 9 ft/sec to 21 ft/sec at initial fuselage impact. Two typical pulses, a cockpit floor

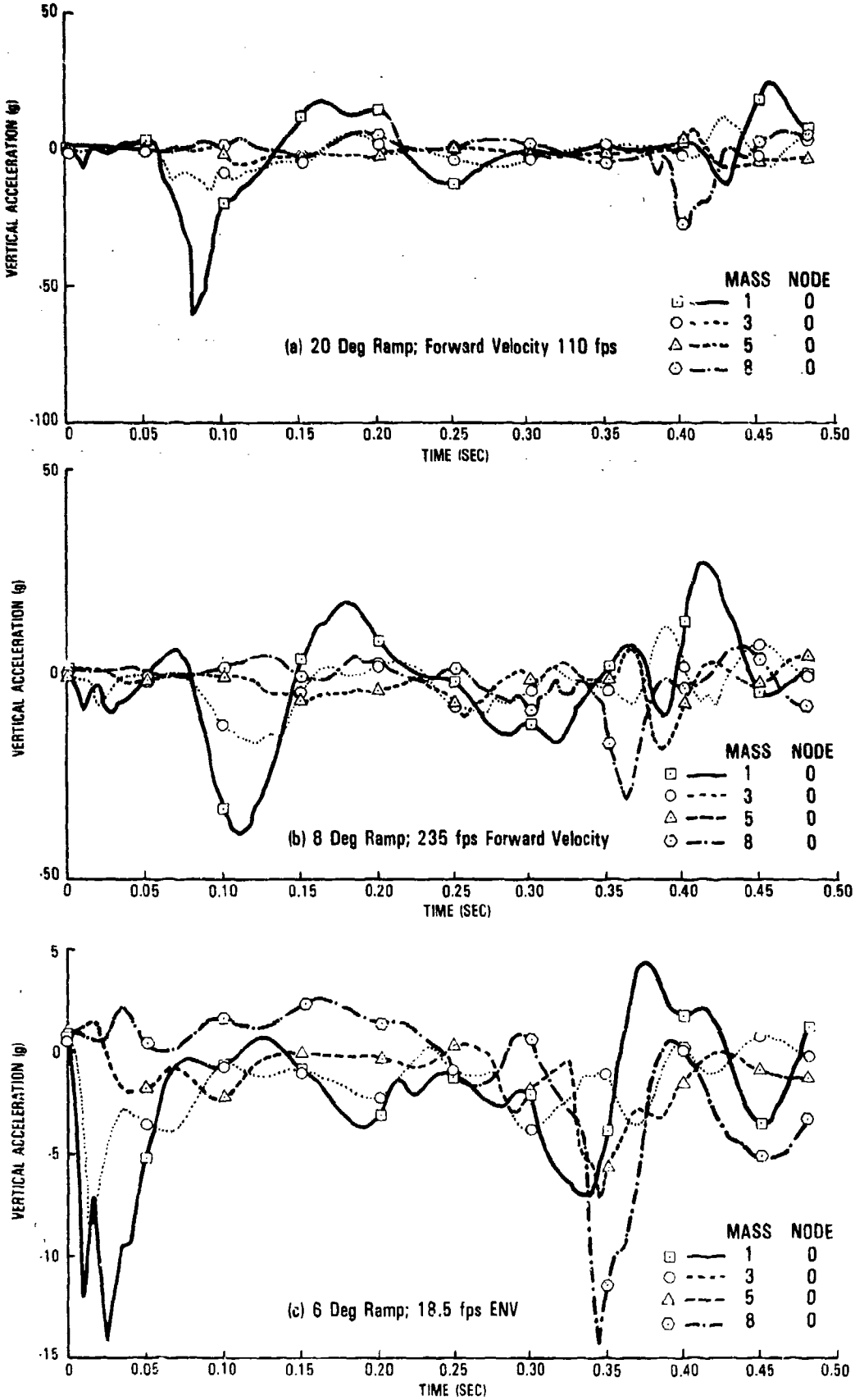

Figure 3-58. Baseline Stick Model Vertical Acceleration Histories

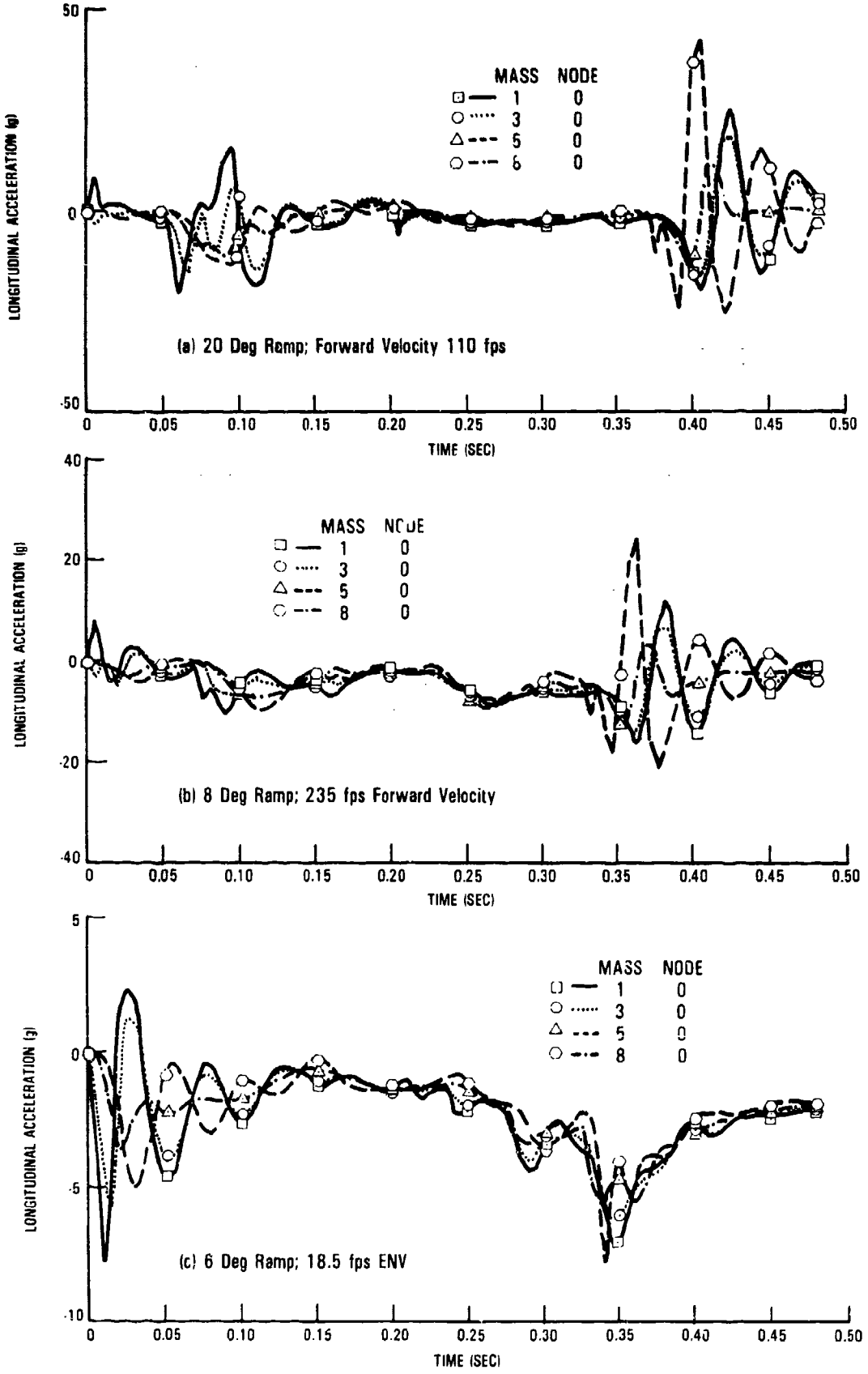

Figure 3-59. Baseline Stick Model Longitudinal Acceleration Histories

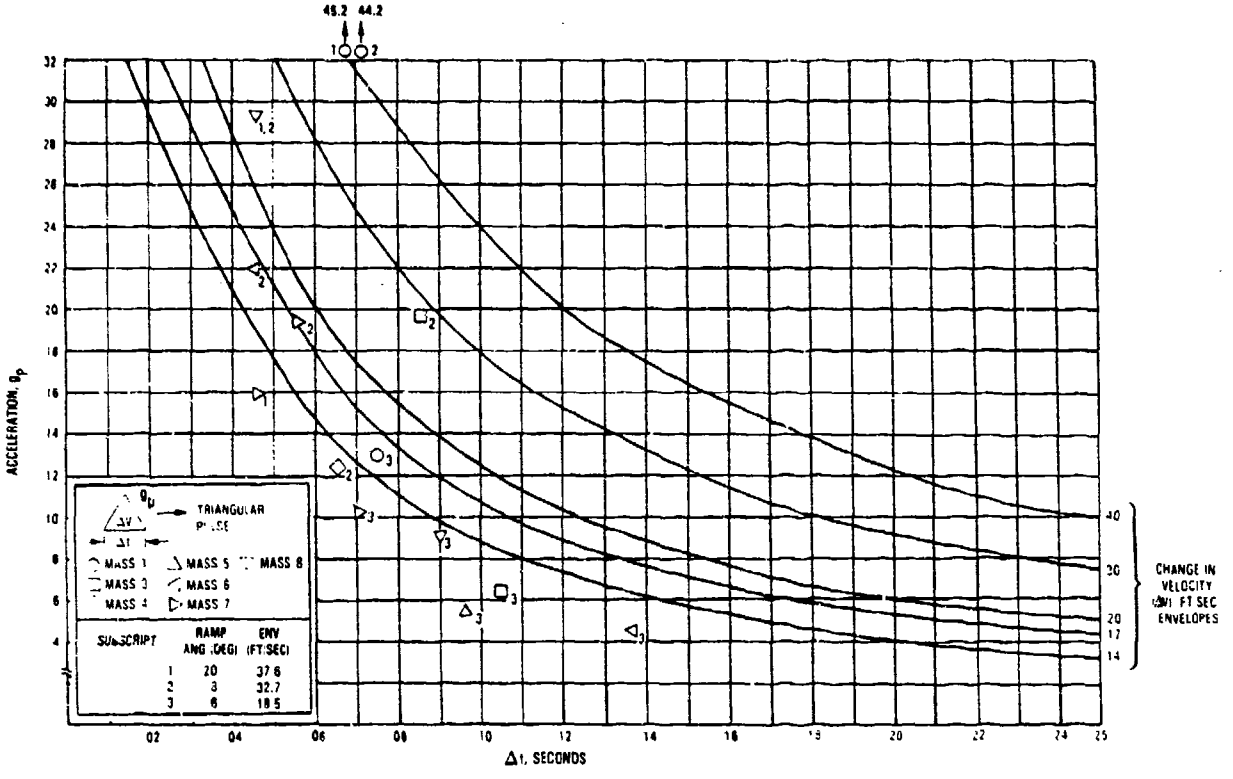

Figure 3-60. Vertical Pulses Obtained from Ramp Impact

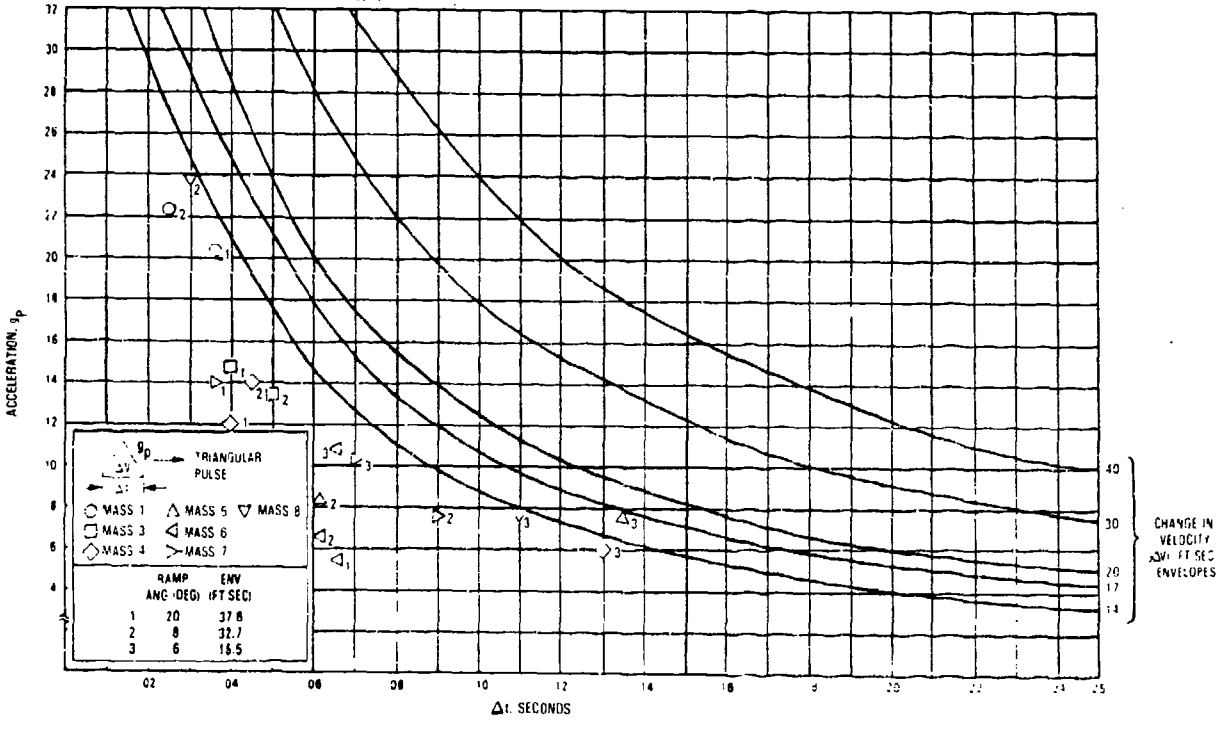

Figure 3-61. Longitudinal Pulses Obtained from Ramp Impact

location (BS228) and a forward fuselage floor location (BS540), are shown in figure 3-62, along with the calculated change in velocity, ΔV. The L-1649 floor pulses were obtained by integrating the acceleration time histories for both a 6-degree and 20-degree slope impact by the inch. The change in longitudinal velocity for the 6-degree slope impact varied from 14.2 ft/sec to 28.7 ft/sec in the passenger region and was 26.8 ft/sec in the cockpit. The corresponding change in vertical velocity for this same impact conditions varied from 14.5 ft/sec to 22.7 ft/sec in the passenger region and reached 31.2 ft/sec in the cockpit. The L-1649 impact floor pulses and velocity changes for the 6 degree slope are shown in figure 3-63. For the 20-degree slope impact, the L-1649 floor longitudinal pulses show a change in velocity from 15 ft/sec to 26.6 ft/sec in the passenger region and approximately 35 ft/sec in the cockpit. The corresponding vertical velocity change was 15 ft/sec in the passenger region and 39.5 ft/sec in the cockpit. Two major fuselage breaks occurred during the 20-degree slope impact. The 20-degree slope floor pulse data and associated calculated velocity changes are shown in figures 3-64a and 3-64b. Corresponding floor pulse data for the DC-7 test are only available from the cockpit for the 8-degree slope impact. These data are shown in figure 3-65. A summary of velocity change data obtained from both the L-1649 and DC-7 tests are shown in table 3-19. Composites of the vertical and longitudinal triangular shaped pulses from all three (L-1649, DC-7, CID) full-scale crash tests are shown in figures 3-66 and 3-67, respectively. Figure 3-66 also contains measured pulses from fuselage section vertical drop tests.

3.3 LONGITUDINAL PULSE

The air-to-ground impacts onto a rigid surface provide predominately vertical pulses. The longitudinal forces that will be developed for this type of condition, particularly within a pitch range of ± 6 degrees, will normally be related to the ground coefficient of friction (μ). For metal-to-concrete contact, a coefficient of friction of 0.3 to 0.5 is generally used. In order to develop substantial longitudinal forces, the impact will have to be to a sloped mound or the terrain will have to be extremely soft such that the μ can increase to 1.0 or more. The extreme case with regard to a pure longitudinal force, would result from a head-on collision with an obstacle, such as a

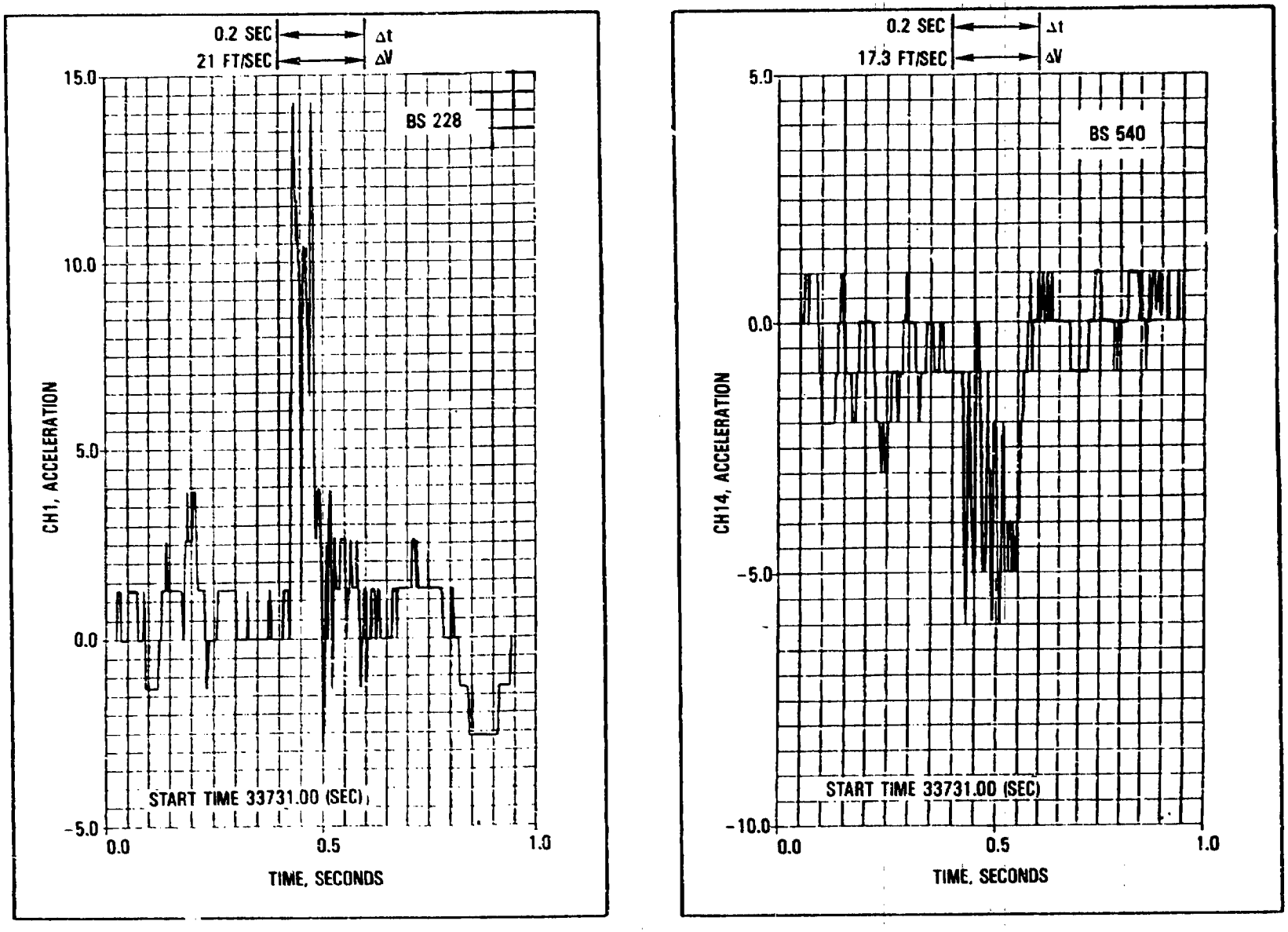

Figure 3-62. CID Test Normal (Vertical) Direction Floor Accelerations - BS228 - BS540

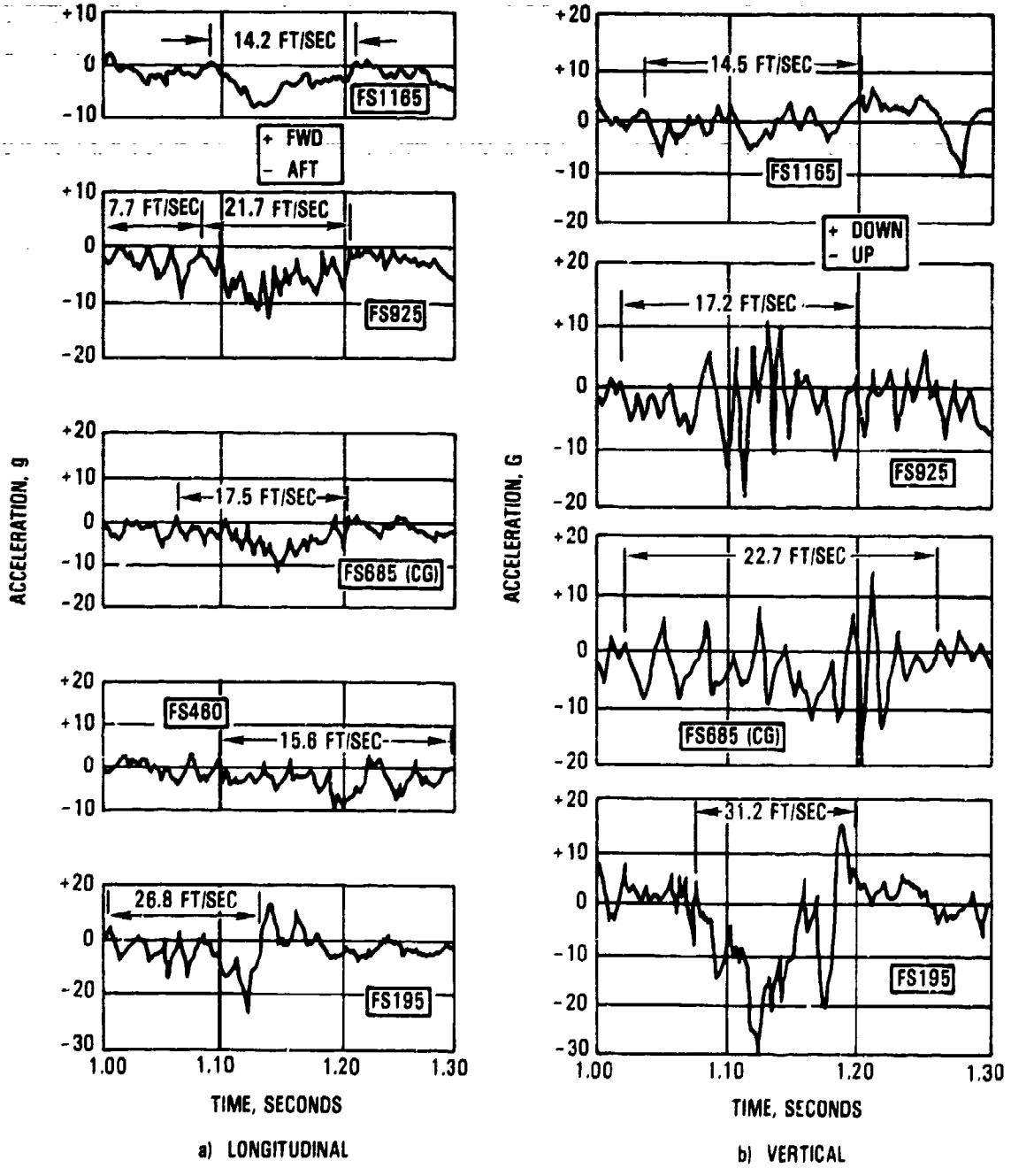

Figure 3-63. Floor Accelerations, L-1649 Test, 6 Degree Slope Impact

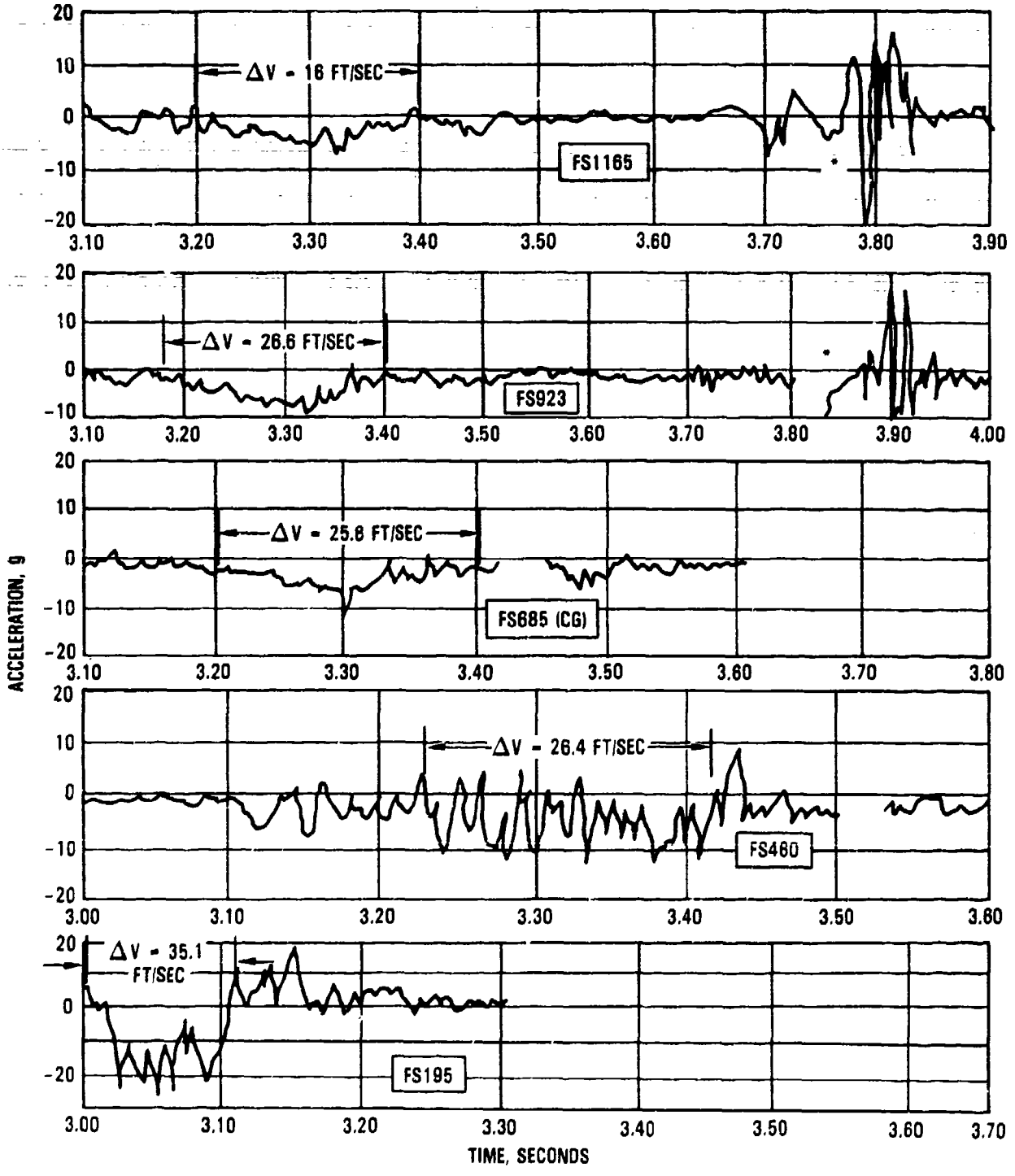

a) LONGITUDINAL

Figure 3-64a. Floor Acceleration, L-1649 Test, 20 Degree Slope Impact

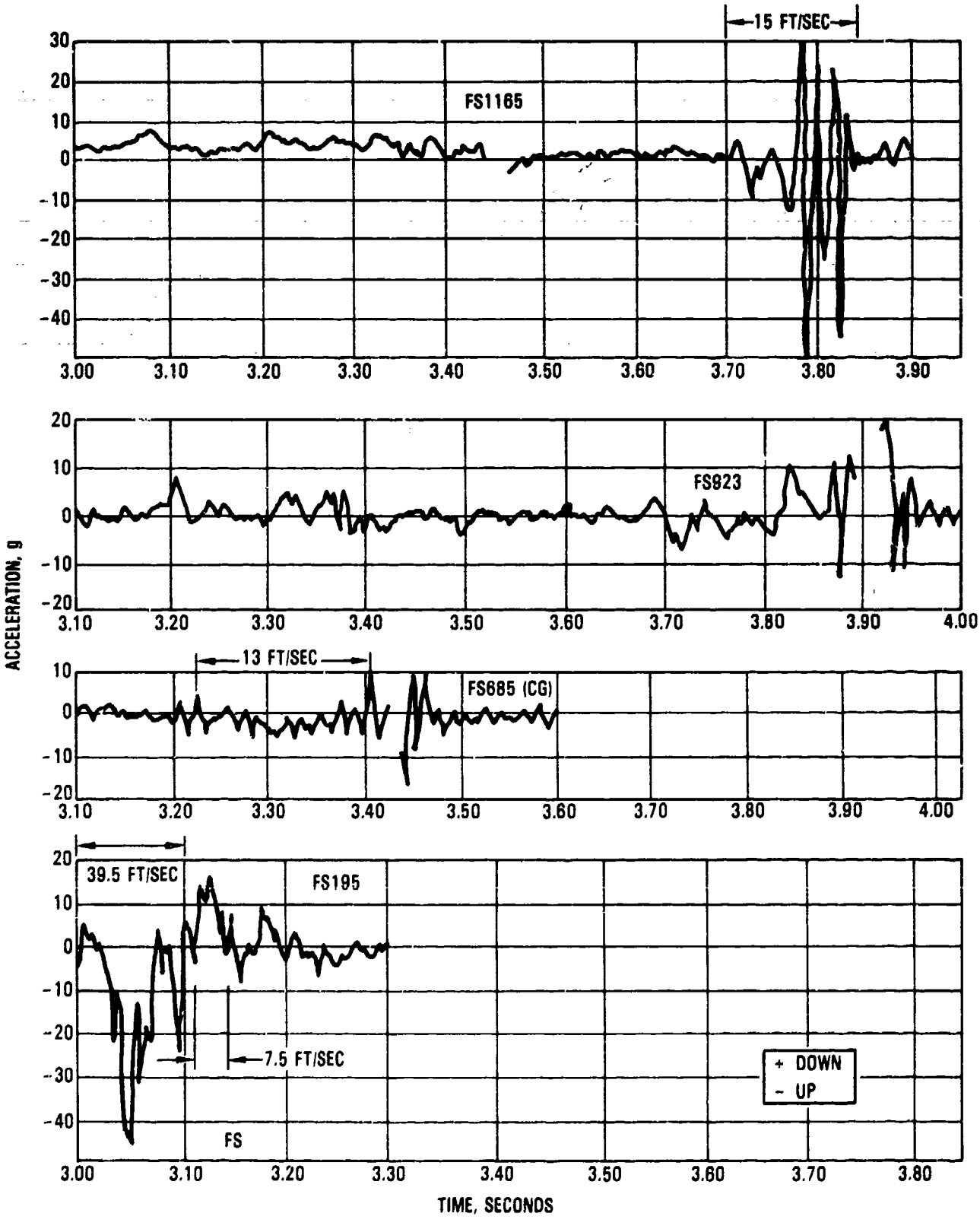

b) VERTICAL

Figure 3-64b. Floor Deceleration, L1649 Test, 20 Degree Slope Impact

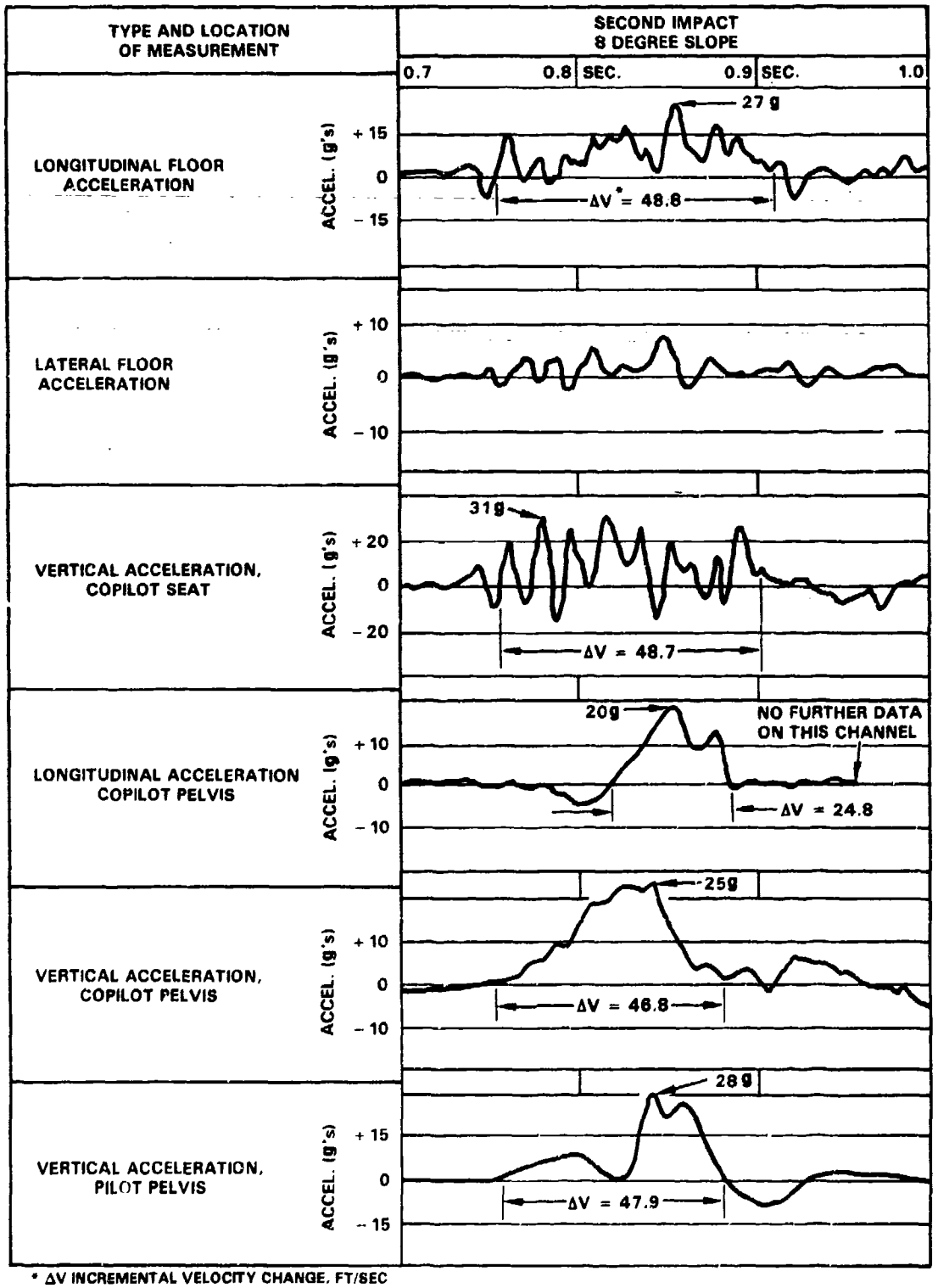

Figure 3-65. DC-7 Test, Measured Acceleration, Eight-Degree Slope Impact

TABLE 3-19. FLOOR PULSE VELOCITY CHANGES OBTAINED FROM THE L-1649 AND DC-7 TESTS

L1649 TEST

SIX-DEGREE SLOPE IMPACT – NO FUSELAGE FAILURE	
COCKPIT (NOSE) RESPONSE	MID-FUSELAGE CABIN RESPONSE
ΔV_Z = 31.2 FT/SEC ΔV_X = 26.8 FT/SEC	ΔV_Z = 14.5–22.7 FT/SEC ΔV_X = 14–28.7 FT/SEC
TWENTY-DEGREE SLOPE IMPACT – FUSELAGE FAILURE (RUPTURE)	
COCKPIT (NOSE) RESPONSE	MID-FUSELAGE CABIN RESPONSE
ΔV_Z 39.5 FT/SEC ΔV_X = 35 FT/SEC	ΔV_Z = 13–15 FT/SEC ΔV_X = 16–26.6 FT/SEC

DC-7 TEST

EIGHT DEGREE SLOPE IMPACT – FUSELAGE FAILURE (RUPTURE)	
COCKPIT (NOSE) RESPONSE	MID-FUSELAGE CABIN RESPONSE
ΔV_Z = 40.8 FT/SEC ΔV_X = 24.8–48.8 FT/SEC	NONE AVAILABLE

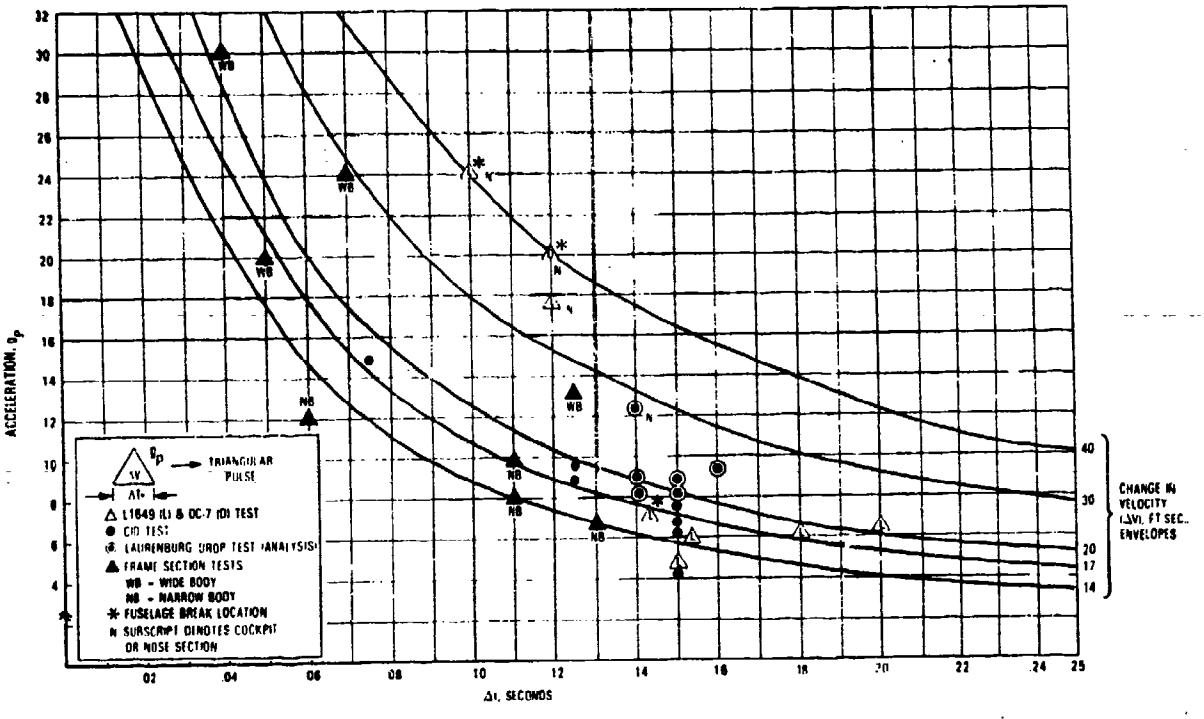

Figure 3-66. Measured Vertical Pulses

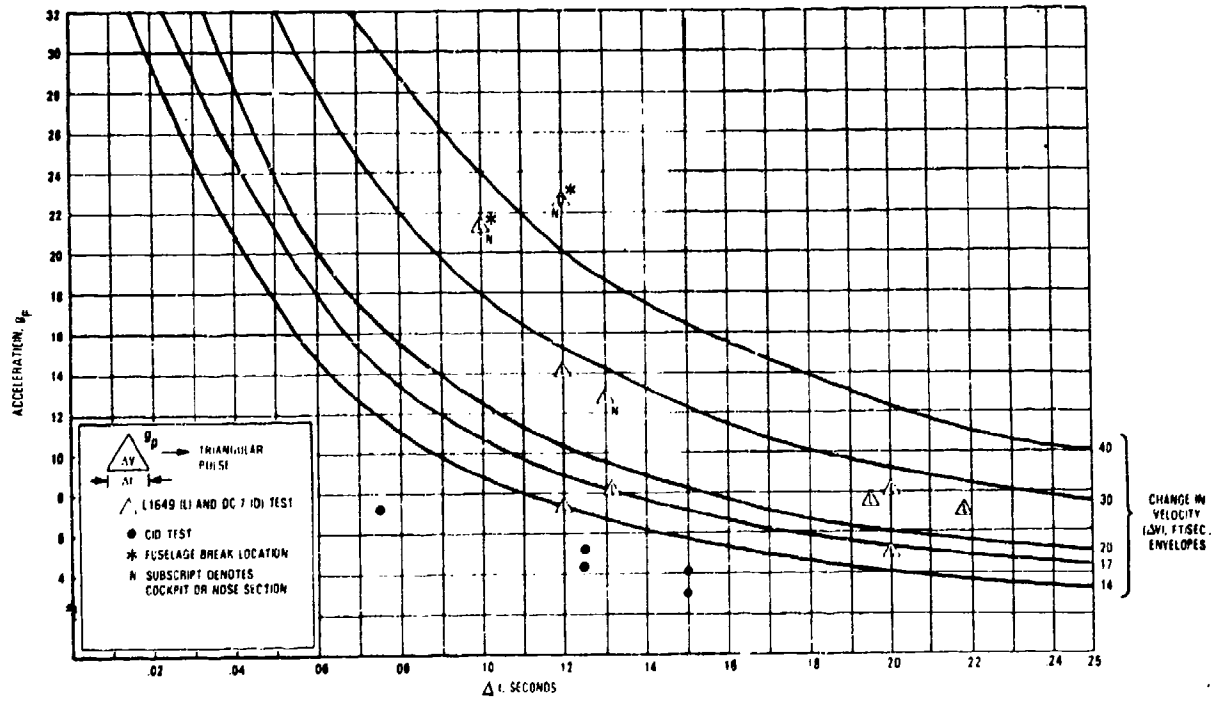

Figure 3-67. Measured Longitudinal Pulses

mountainside. Thus, if the axial crushing characteristics of transport airplane sections were available, an estimate of the responses in the longitudinal direction could be made.

3.3.1 Specimen Test Data

Cylinder axial crush tests were performed and the results are reported in reference 4. A summation of the tests are as follows: three types of specimens were drop-tested, cylindrical sections were tested to represent fuselage axial collapse and crushing, partial cylinders were tested to represent vertical collapse of fuselage structure below the passenger floor, and a structurally complete nose section (except for the nose landing gear) of a jet transport was tested to determine the vertical collapse characteristics of the structure. The axial cylinder structural configurations are shown in figure 3-68. The test results are shown in table 3-20. The collapse characteristics of three types of axial cylinder construction was similar in that accordian collapse was typical. Stringers required higher loads to collapse while the hat section stringer, close spaced frame cylinder provided the most effective configuration. The maximum energy absorbed was only 92,500 ft-lb per foot crushed (Cylinder No. 3).

One type of failure that could seriously affect crashworthiness occured on the zee-stiffened cylinder. A longitudinal skin splice was opened during two separate drops. A failure of this type can open up a large gap in the fuselage which could then allow an excellent path for ingestion of foreign material.

The tear resistance of typical built-up, plate-stringer lower fuselage shell sturcture is affected by the skin material and the longitudinal stiffener, or stringer spacing to a great extent. Stringer material is of lesser consequence. Thick, ductile skin with closely spaced stringers appears to be the best combination. The thick skins resist puncture and the stringers act as crack stoppers if tearing does occur in the skin. Widely spaced stringers allow long tears which result in "plows" and "scoops," that can cause significant damage to the passenger floor and floor support structure as foreign objects are forced inside the shell.

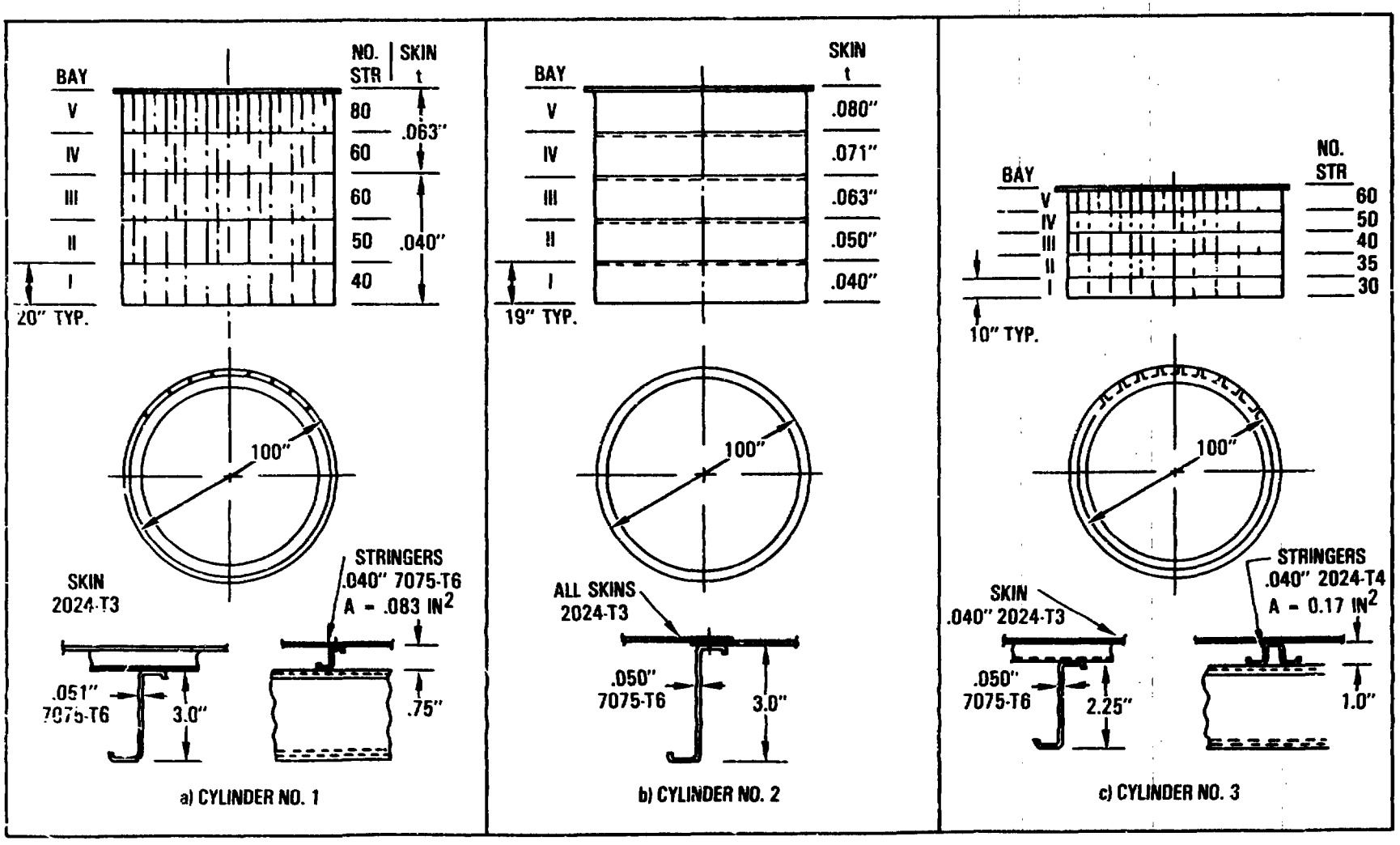

Figure 3-68. Structural Configurations, Axial Test Cylinders (Reference 4)

TABLE 3-20. DROP TEST RESULTS AXIAL CYLINDER (REFERENCE 4)

SPECIMEN	TYPE	DROP NO.	HEIGHT (FT)	WEIGHT (LB)	VELOCITY (FT/SEC)	PEAK (G)	PEAK LOAD (LB)	IMPACT
1	AXIAL CYLINDER	1	2	3,500	11	55	193,000	NEGLIGIBLE.
1	AXIAL CYLINDER	2	4	3,500	16	62	220,000	LOCAL CRUSHING AT IMPACT END.
1	AXIAL CYLINDER	3	8	3,500	23	45	157,000	SEVERE BUCKLES IN BAY I, SKIN SEAM SPLIT.
1	AXIAL CYLINDER	4	10	3,500	25	29	102,000	COMPLETE COLLAPSE OF BAY I, BUCKLES IN BAY II.
1	AXIAL CYLINDER	5	4	9,700	16	27	262,000	REMAINING BAY II CRUSHED, BUCKLES IN BAY III.
1	AXIAL CYLINDER	6	8	9,700	23	17	165,000	BAY CRUSHED, BUCKLES IN BAY IV.
1	AXIAL CYLINDER	7	12	9,700	28	27.5	267,000	BAY IV CRUSHED, SKIN SEAM OPENED IN BAY V. TOTAL ENERGY = 315,800 FT-LB DEFORMATION = 5.6 FT
2	AXIAL CYLINDER	1	2	9,600	11	11	106,000	COMPLETE ACCORDIAN COLLAPSE OF BAYS I AND II.
2	AXIAL CYLINDER	2	4	9,600	16	16.5	158,000	COMPLETE ACCORDIAN COLLAPSE OF BAY III.
2	AXIAL CYLINDER	3	6	9,600	20	12.5	192,000	COMPLETE ACCORDIAN COLLAPSE OF BAY IV. TOTAL ENERGY = 115,200 FT-LB DEFORMATION = 5.4 FT
3	AXIAL CYLINDER	1	8	9,600	23	25.6	246,000	BAY I COMPLETELY CRUSHED.
3	AXIAL CYLINDER	2	15	9,600	31	33.8	325,000	BAYS II, III, AND IV CRUSHED, BAY V BUCKLED. TOTAL ENERGY = 220,800 FT-LB DEFORMATION = 2.32 FT

A general increase in strength of the lower shell axial material is not the most efficient way to improve the crashworthy characteristics of a fuselage. In order to significantly improve the energy absorbing capacity by strengthening, a severe weight penalty is generally incurred and the decelerations levels produced as the structure is crushed would increase. An increase in longitudinal deceleration levels may produce axial failures in the occupied areas or cause early failures in the occupant tie-down chain (seats, seat attachment, seat belt, etc.). Gradually increasing axial strength towards the wing, particularly of the lower shell is generally required by the existing fuselage bending requirements. This configuration affords increased crashworthiness since it delays failure near the wing-to-fuselage joint.

Review of the test results, provided in Table 3-20, in the following manner provides some points of interest:

- The average force acting = $\frac{\text{Energy (ft-lb.)}}{\text{Deformation (ft)}}$ = lb.

- The average acceleration = $\frac{\text{Avg. Force (lb.)}}{\text{Weight (lb.)}}$ = g

- The pulse duration (Δt) (based on momentum considerations) = $\frac{\text{Weight} \cdot \text{Velocity}}{g \cdot \text{Force}_{Avg}}$ = sec

Summarizing these terms for the three test speciments the following information is obtained:

Specimen	Avg. Force (lb)	Avg. Accel. (g)	Constant Force Pulse Duration (sec)
No. 1	56571	5.8	.149
No. 2	21333	2.2	.279
No. 3	95172	9.9	.097

If, instead of a constant force, a triangular pulse is considered, then the combination of force and incremental time would have to be revised to provide the same area under the curve.

Considering specimen No. 1 to be more typical of current aircraft design, then the upper limit for a pure longitudinal pulse, triangular in nature, would be more like $\leq$12g peak, approximately 0.15 second base duration and a velocity change of $\leq$ 30 ft/sec. The axial cylinder No. 1 section test results, provided in reference 4, are representative of an airplane with a gross weight of 50,000 lb. The analysis described in reference 4 indicated that, under the assumptions of (1) uniform compression on the cross-section, and (2) instantaneous and constant load, a cylinder of the cross-section noted would absorb only 1-1/2 percent of the kinetic energy per foot of structure that is crushed for a 50,000 lb. aircraft moving forward at a velocity of 100 mph. Using average test-allowable energies, the energy dissipated by structural crushing is reduced to only 0.33 percent of the aircraft's kinetic energy (16,800,000 ft-lb) per foot crushed. Both of these assumptions require 100 percent efficiency in energy absorption which is not the case. Therefore, the energy dissipated by structural crushing is closer to 0.2 percent. Larger aircraft, while weighing more, also have additional material cross-sectional area, and thus, the results of the axial cylinder tests are most likely applicable to them as well.

Reference 4 also describes the results of a drop test of a jet transport fuselage nose section. The section was structurally complete, except for the nose landing gear, and included the entire forward pressure bulkhead, nose landing gear box and pilot's cockpit wind screen (figure 3-69). Steel floor beams and floor panels were added to the section to increase the mass and provide the required center-of-gravity. The specimen was drop tested in an approximately 10 degree nose-down attitude to simulate the effects of vertical descent velocity. Impact was made on steel flooring covered with 1/2-inch plywood. The total weight of the specimen was 10,700 lb.

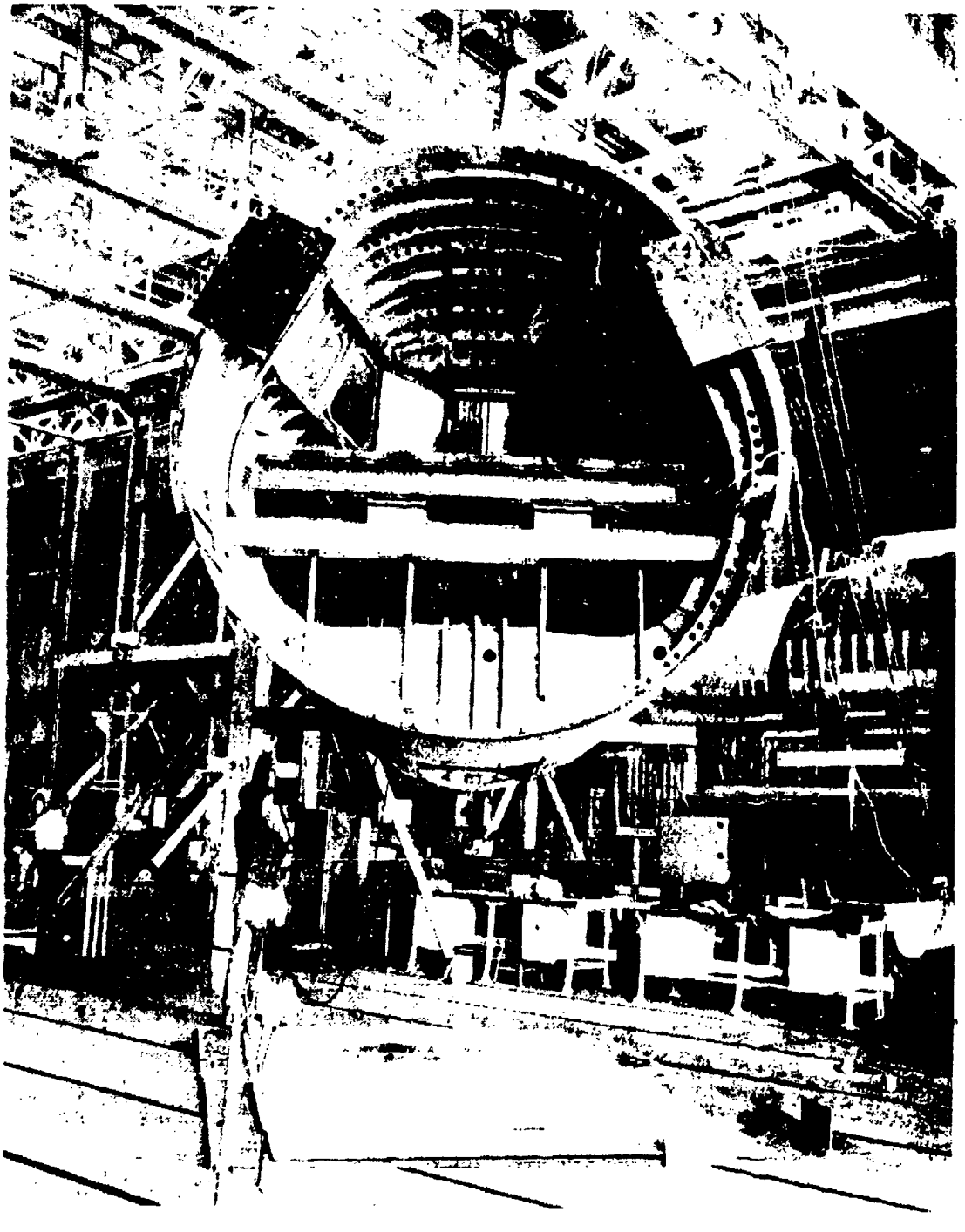

Figure 3-69. Fuselage Nose Section Prior to Drop (Reference 4)

The first drop, from 6 feet, simulated a 20 ft/sec vertical impact velocity. The forward pressure bulkhead was crushed and the aft bulkhead and intermediate frames failed. The total vertical collapse was approximately 6 inches as the nose landing gear beams moved up and, for all practical purposes, remained intact.

The final drop was made from 8 feet, or approximately 23 ft/sec sink speed. The forward bulkhead, aft bulkhead and intermediate frames continued to collapse, allowing the nose gear beams to continue upward until they contacted the floor structure. The fuselage floor beams were crushed by the box structure and the maximum deceleration occurred as the box structure contacted the steel floor structure. The average deceleration prior to this final impact was approximately 6g with an increase to 18g at final impact.

The tests of this structure indicate that the nose landing gear beam support structure failure sequence is the primary concern rather than the actual energy absorbing capability. The structure withstood an impact velocity of approximately 20 ft/sec without catastrophic damage to the crew area. The failures produced by the initial impact, however, included a complete tension rupture on the aft bulkhead. This rupture allowed sufficient vertical translation of the comparatively intact nose landing gear beams during the second test to crush the crew floor support structure. The maximum loads developed by the structure would produce excessive bending moments along the fuselage, particularly in the wing attachment area. The fuselage nose test results are shown in table 3-21.

TABLE 3-21. DROP TEST RESULTS FUSELAGE NOSE (REFERENCE 4)

SPECIMEN	TYPE	DROP NO.	HEIGHT (FT)	WEIGHT (LB)	VELOCITY (FT/SEC)	PEAK (G)	PEAK LOAD (LB)	IMPACT DAMAGE
	FUSELAGE NOSE	1	6	10,700	20	35.5[2]	380,000	AFT BULKHEAD FAILED IN TENSION, NOSE BULKHEAD CRUSHED.
	FUSELAGE NOSE	2	8	10,700	23	26	278,000	NOSE LANDING GEAR BEAMS RAISED AND CRUSHED FLOOR. DROP 1 ENERGY - 64,000 FT-LB DEFORMATION - 0.50 FT

NOTES: 1. CRUSHED PORTION (BAY I AND 9 INCHES OF BAY II) CUTOFF.
2. AVERAGE IS 15g.

A comparison of the energy absorption capability between the KRASH model crush parameters at the nose gear bulkhead location (mass 1, FS199 and mass 2, FS300) and the reference 4 crush parameters at similar locations (mass 1, FS187 and mass 2, FS325) are as follows:

ENERGY ABSORPTION CAPABILITY (IN-LB)

KRASH Models		Reference 4 (Fig. 3-27)	
Original for air-to-ground analysis	Revised for ramp impact Case No.1	Curve 2	Curve 3
900,000*	3,100,000	2,300,000	2,100,000

* Restiffens at 10 inches of crush. All others are based on 24 inches of crush available before restiffening.

From the above tabulated data, it can be seen that the original nose gear bulkhead crush model did not provide for significant energy absorption. The revised model parameters are higher than the data used in the reference 2 analysis. However, when scaled by the ratio of airplane weight (1.26), the reference 4 numbers would be 2,900,000 and 2,600,000, respectively.

3.3.2 Analyses Data

The KRASH stick model used in the previous air-to-ground and ramp impact studies, was adapted for a longitudinal pulse study. The airplane is assumed to be moving forward in a level attitude when it hits a frontal 90-degree rigid wall. The cockpit of the fuselage (FS199) is represented by a nonlinear crush spring. The forward fuselage structure (FS199-620) is represented by nonlinear axial beams. The aircraft representation and properties are shown in figure 3-70 and table 3-22, respectively. The study was performed parametrically for:

- Forward impact velocity range (20 to 50 ft/sec)
- Three fuselage crush springs (figure 3-71)
- Three nonlinear beam characteristics (figure 3-72)

The fuselage crush variation represents an approximate spring rate between 26,700 lb/in and 40,000 lb/in. The lower rate approximates the data from tests reported in reference 4. The nonlinear beam variation allows for uniform deformation of 5, 10 and 20 inches of compression before failure. The lower spring rate (26,700 lb/in) and 20 inches uniform crush represent a design of highly crushable structure. Conversely, the higher spring rates and less uniform beam deformation is representative of a stiff, less yielding structure. The fuselage crush condition, K2, and beam nonlinear condition, N1, are considered the nominal representation for the narrowbody airplane being studied.

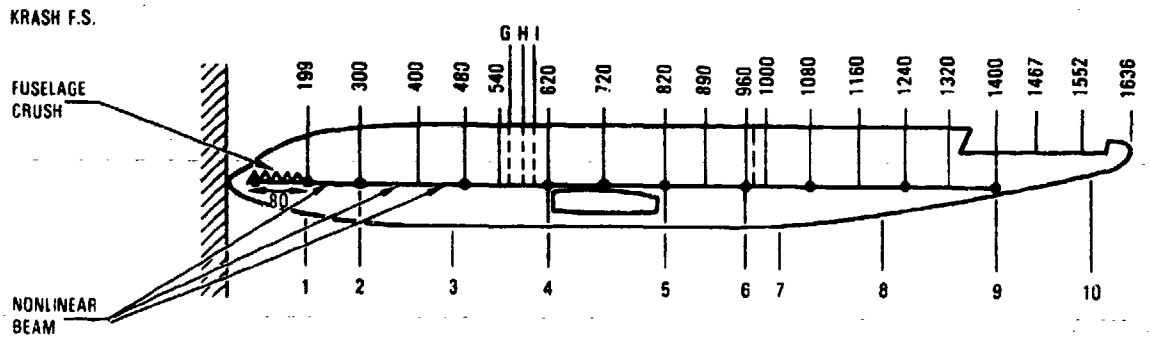

Figure 3-70. KRASH Model for Forward Impact Into a 90 Degree Wall

TABLE 3-22. MODEL PROPERTIES

MASSES			BEAMS					
NO.	F.S.	W.L.	NO.	I-J	LENGTH IN	AXIAL STIFF. X 10^6 LB./IN	COMPRESSIVE FAILURE LOAD LB X 10^6	DEFLECTION @ FAILURE IN
1	199	219.	1	1-2	101.	3.17	1.088	.343
2	300	217.9	2	2-3	160.3	2.25	1.224	.545
3	460	208.3	3	3-4	160.	2.25	1.224	.544
4	520	205.8	4	4-5	200.	2.95	2.006	.080
5	820	200.	5	5-6	140.5	4.2	2.006	.478
6	960	211.9	6	6-7	83.7	6.81	1.938	.285
7	1043	206.6	7	7-8	158.4	3.03	1.632	.538
8	1201	222.4	8	8-9	201.7	1.83	1.258	.685
9	1400	255.8	9	9-10	175.	1.43	.850	.595
10	1570	297.0						

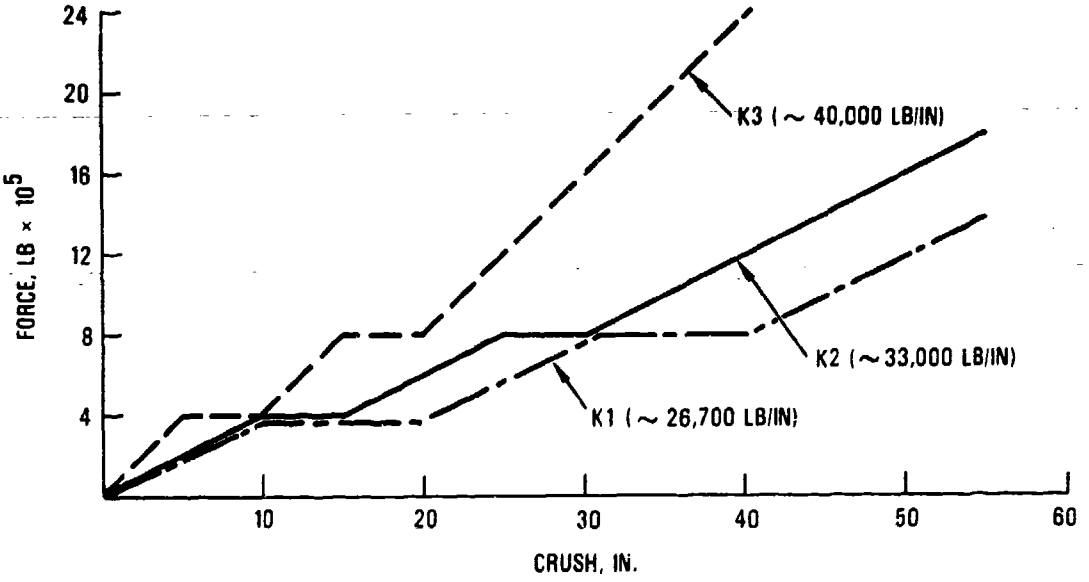

Figure 3-71. Axial Crush Spring Load-Deflection Characteristics

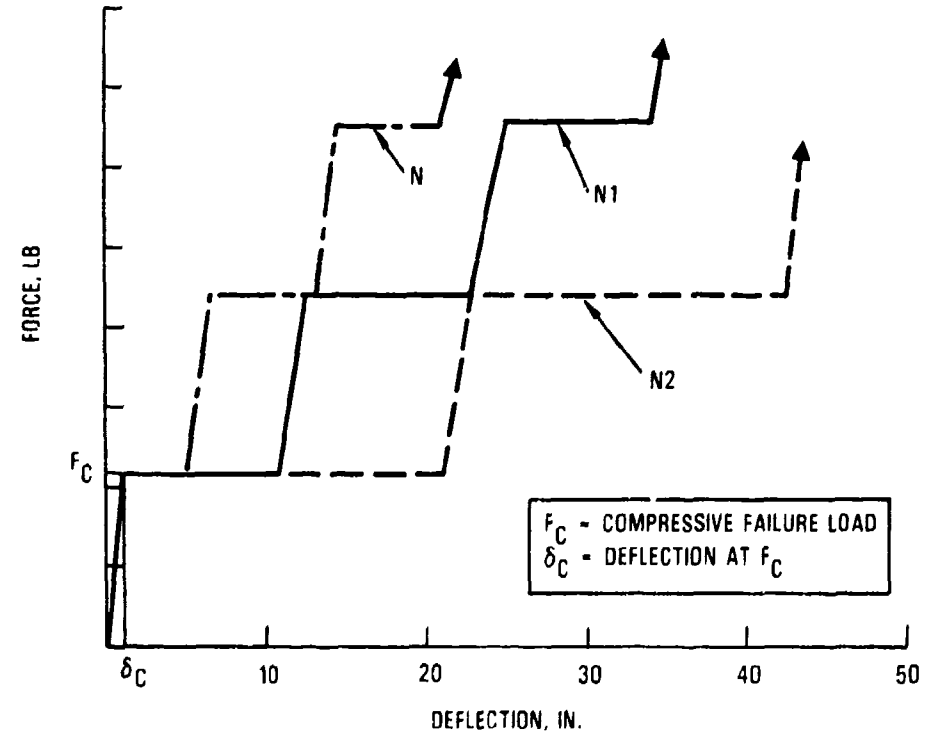

Figure 3-72. Beam Axial Non-Linear Load-Deflection Behavior

The results of this phase of the parametric sensitivity study are summarized in tables 3-23 to 3-25 and figures 3-73 to 3-76. The energy distribution, Table 3-23, shows:

- Increase in strain energy percent as the crush spring stiffens, impact velocity increases and internal beam stiffness lessens.

- The forward velocity is arrested in approximately 0.190 to 0.250 second, the lower incremental time value is associated with the stiffer structure (i.e., K3, N1).

The relationship between average acceleration and structural deformation for the nominal conditions (K2, N1), shown in table 3-24, indicates:

- Increased failure, average acceleration and total crush distance as the impact velocity increases.

The variation in average acceleration and deformation as a function of velocity, K variation and N variation is shown in table 3-25.

- Average acceleration increases as impact velocity, fuselage stiffness, K, and internal beam stiffness, N, decrease.

- Total crush distance increases as impact velocity increases and internal beam stiffness, N, decreases.

- Total crush distance decreases as fuselage stiffness, K, increases.

Figure 3-73 depicts the results noted in tables 3-24 and 3-25. Figure 3-74 shows the peak acceleration distribution along the fuselage as a function of impact velocities (30 ft/sec and 40 ft/sec) and the three forward fuselage spring rates. Figure 3-75 depicts the variation in average acceleration and total crush as a function of impact velocity for the nominal condition (K2, N1). Figure 3-76 attempts to relate the extent of airframe

TABLE 3-23. ENERGY DISTRIBUTION AS FUNCTION OF IMPACT VELOCITY AND NONLINEAR DEFORMATION CHARACTERISTICS

VELOCITY	N1			N2			NX
	K1	K2	K3	K1	K2	K3	K1
20 FT/SEC	(KE = 14.3 X 10^6 IN-LB)						
CE SE KE_{MIN}		89.3 9.4 (T = .21)					
30 FT/SEC	(KE = 32.3 X 10^6 IN-LB)						
CE SE KE_{MIN}	92.0 7.3 (T = .24)	64.8 34.3 (T = .22)	52.3 45.0 (T = .19)	92.0 7.3 (T = .24)	64.8 34.3 (T = .22)	41.8 56.8 (T = .20)	72.3 26.2 (T = .22)
40 FT/SEC	(KE = 57.44 X 10^6 IN-LB)						
CE SE KE_{MIN}	67.2 30.7 (T = .25)	55.2 41.8 (T = .23)	28.3 66.4 (T = .20)	55.2 43.2 (T = .25)	53.9 44.6 (T = .24)	22.5 75.1 (T = .23)	
50 FT/SEC	(KE = 89.75 X 10^6 IN-LB)						
CE SE KE_{MIN}		44.0 49.9 (T = 0.24)					

CE, SE = CRUSH AND STRAIN ENERGY PERCENT OF TOTAL, AT TIME WHEN KE IS A MINIMUM. DAMPING AND POTENTIAL ENERGY ACCOUNT FOR THE BALANCE.

(T = .xx) = TIME AT WHICH KE IS A MINIMUM

TABLE 3-24. IMPACT VELOCITY VARIATION

Δ V FT/SEC	G AVG	DEFORMATION, INCHES					
		FORWARD FUSELAGE FS70-199	BEAM NO. 1 FS 199 - 300	BEAM NO. 2 FS 300 - 460	BEAM NO. 3 FS 460 - 620	BEAM NOS. 4 - 9 FA620-1400	TOTAL
20	3.	28.*	10.25	.34	.31	.22	39.1
30	4.5	39.3*	8.0*	.50	.46	.34	48.6
40	6.	49.*	10.5*	10.8*	.56*	.40	71.3
50	7.5	54.*	10.8*	11.1*	11.4*	.70	88.0

* BEAM EXCEEDS COMPRESSIVE FAILURE LOAD

TABLE 3-25. FUSELAGE AXIAL CRUSH SPRING AND BEAM NONLINEARITY VARIATIONS

CRUSH SPRING	G AVG	DEFORMATION, INCHES					
		FORWARD FUSELAGE FS70-199	BEAM NO. 1 FS199-300	BEAM NO. 2 FA300-460	BEAM NO. 3 FS460-620	BEAM NOS. 4 - 9 FS62-1400	TOTAL
30 FT/SEC IMPACT VELOCITY; N1							
K1	4.0	49.6*	.37 *	.50	.46	.40	51.3
K2	4.5	39.3*	8.0*	.50	.46	.34	48.6
K3	4.5	26.7*	10.5*	.56*	.53	.40	38.7
30 FT/SEC IMPACT VELOCITY; N2							
K1	4.0	49.6*	.37 *	0.5	.45	.40	51.3
K2	4.5	39.3*	8.0*	0.5	.46	.34	48.6
K3	5.0	25.4*	14.3*	4.8*	.45	.36	45.3
40 FT/SEC IMPACT VELOCITY; N1							
K1	5.6	57.5*	10.5*	2.65*(b)	.56*	.41	71.6(b)
K2	6.0	49.0*	10.55*	10.8*	.56*	.40	71.3
K3	6.0(b)	32.3*	10.65*	10.7*	6.8*	.44	60.9
40 FT/SEC IMPACT VELOCITY; N2							
K1	4.5	51.5*	20.5*	5.5*	.50	.35	78.4
K2	5.0	45.6*	20.5*	.63*	.55*	.50	67.6
K3	5.8	30.9*	20.6*	13.1*	.56*	.35	65.5

* DENOTES COMPRESSIVE FAILURE LOAD EXCEEDED.

(a) FWD. BEAM MASSES (1 AND 2) SHOW SUBSTANTIALLY HIGHER LEVELS

(b) INCREASES AT FINAL TIME

failure as a function of the velocity impact level. At 30 ft/sec, it can be anticipated that the forward passenger occupiable region will experience failures. These failures will progress as the impact velocity level increases.

The results of this phase of the study suggest that:

- At 20 ft/sec, no airframe failure in the passenger region (FS460-aft) is expected.

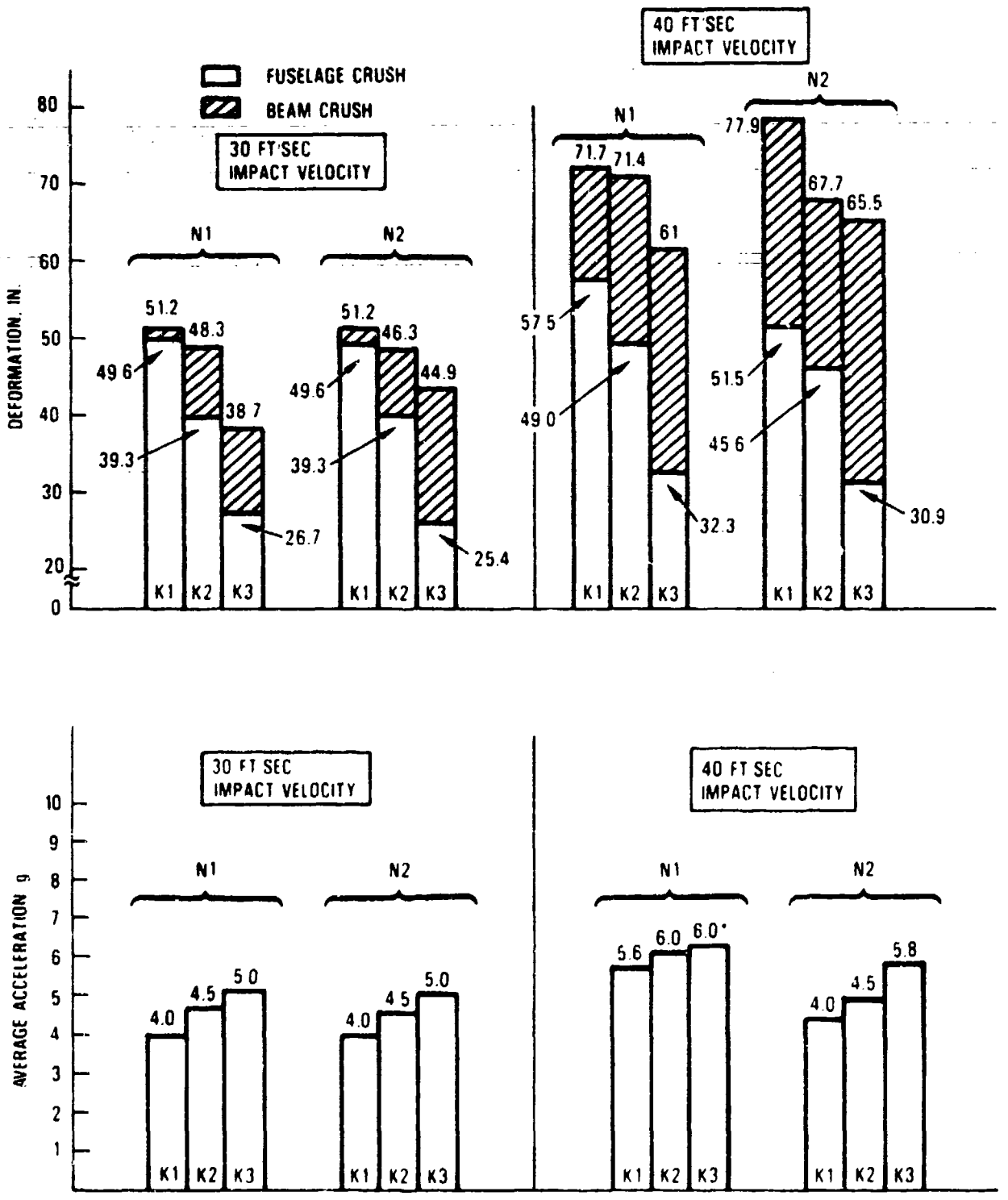

Figure 3-73. Deformed Distance and Average Acceleration Results

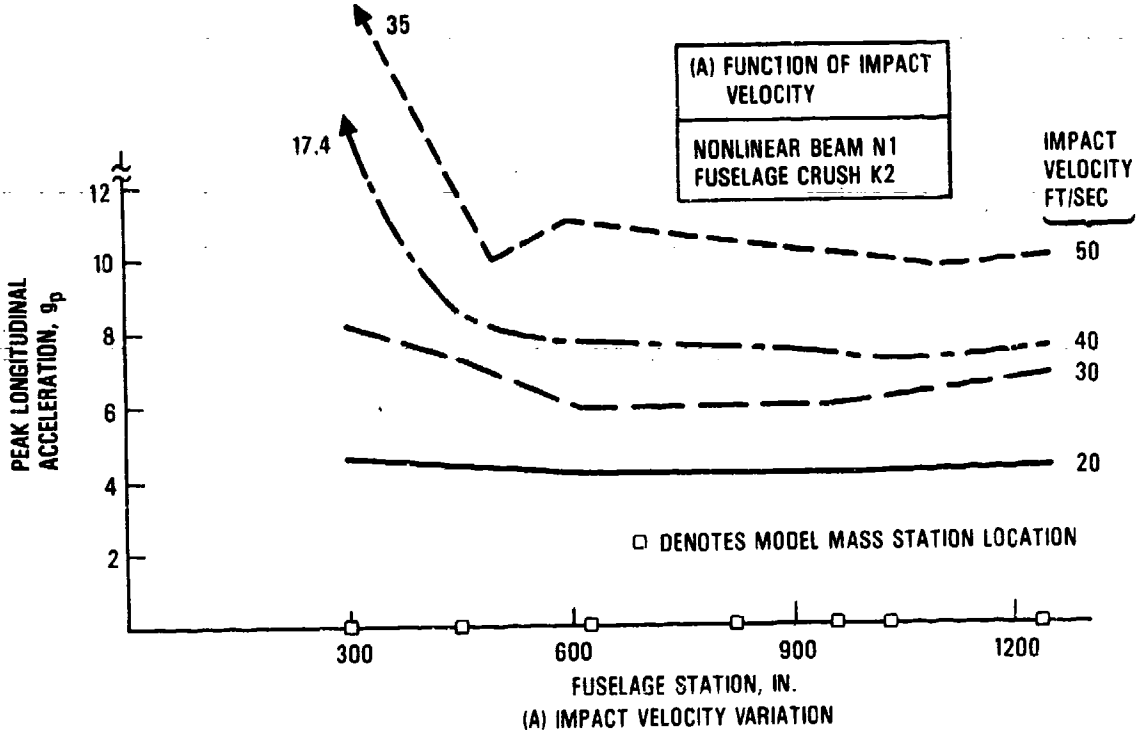

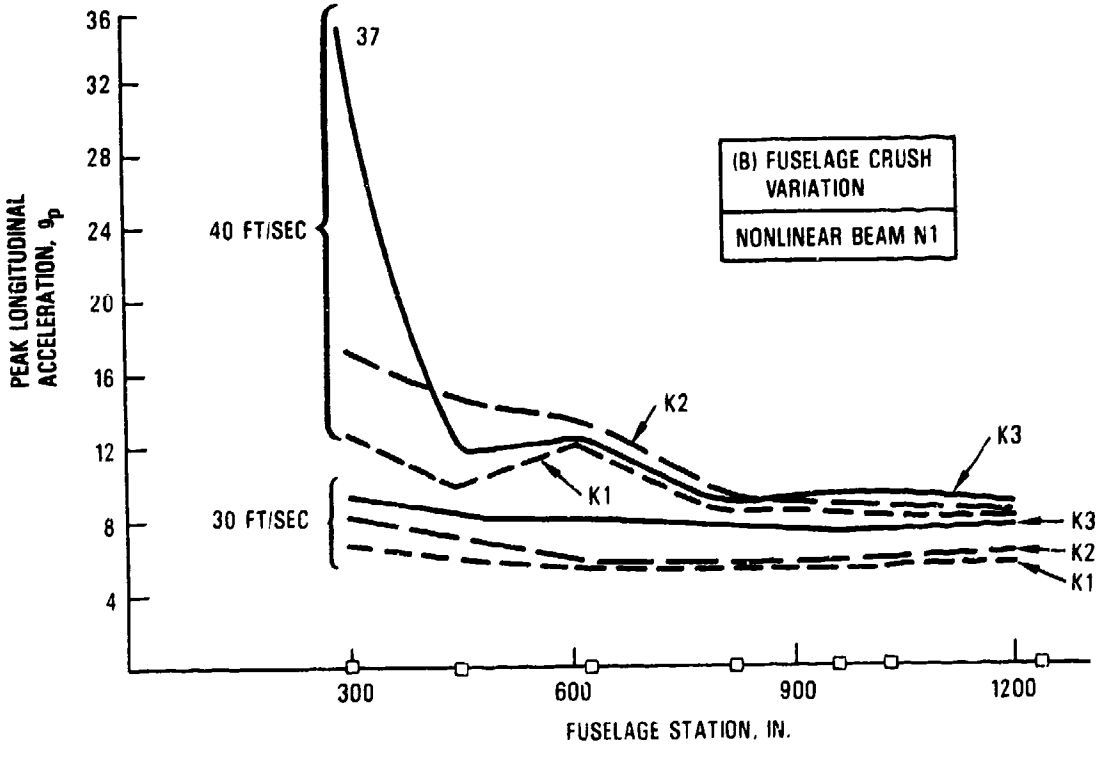

Figure 3-74. Peak Acceleration Distribution

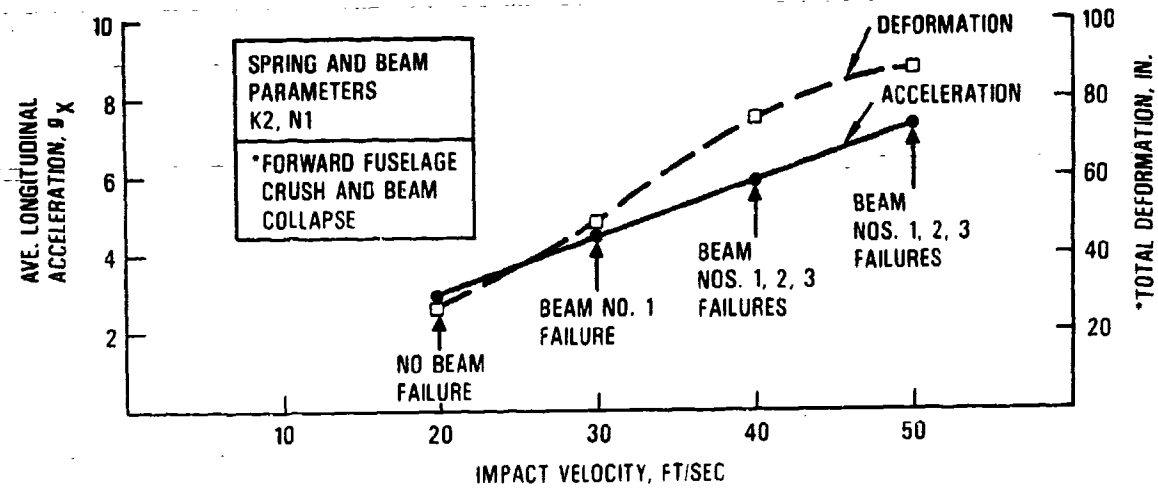

Figure 3-75. Acceleration Versus Impact Velocity

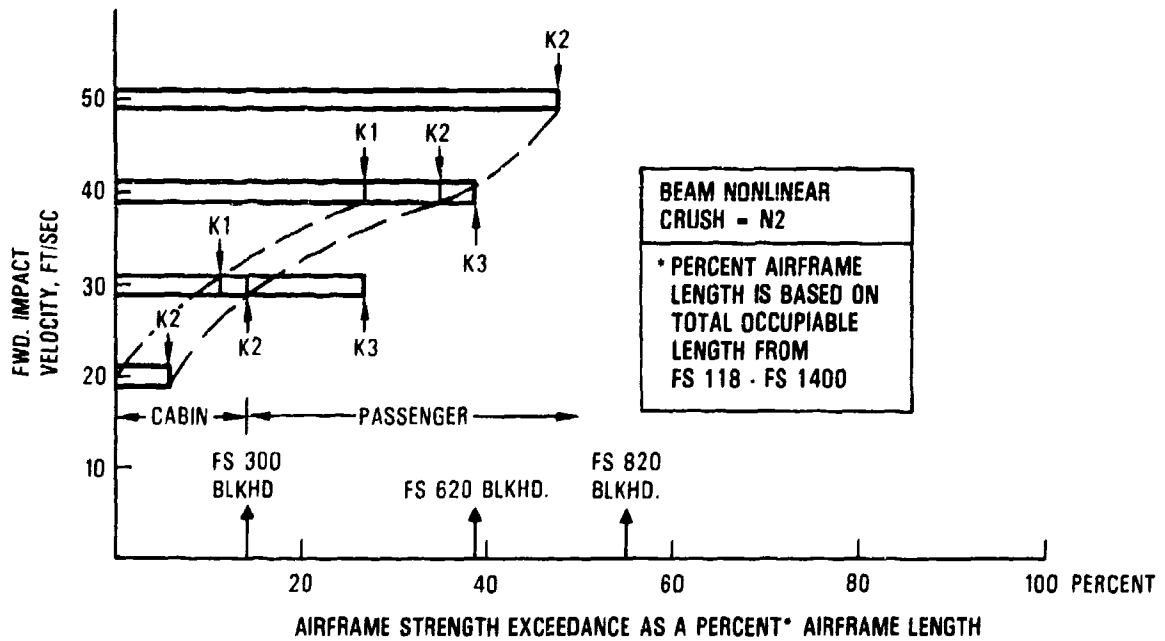

Figure 3-76. Airframe Strength Exceedance as a Function of Impact Velocity

- At 30 ft/sec, 3 feet to 4 feet of crush is anticipated. The average acceleration is between 4g and 5g (7.5g experienced at condition K3, N1), beam failure extends to FS460 (mid-forward fuselage).

- At 40 ft/sec, 5 feet to 6.5 feet of crush is anticipated, the average acceleration is 4.5g to 6g, beam failure extends to FS620 (wing leading edge bulkhead).

- It is inconsistent to anticipate high g's, extreme crush and extended time duration to occur simultaneous. The less crush (stiffer structure, i.e., K3, N1) will produce high acceleration in a smaller time span and, consequently, with loads which will produce airframe failures and at lower velocity changes. Conversely, increased crush (i.e., K1, N2) will produce lower accelerations over an extended time. For a given K, N parameter set, failure loads will be associated with a higher velocity.

- The wing responses (masses 11-15 in the KRASH model) for the longitudinal impact show peak accelerations of between 5.7g and 9.5g. The triangular pulse characteristic of this impact obtained from an average of several 30 ft/sec forward velocity impacts is:

$$\text{peak acceleration, } g_p = 9g$$

$$\text{change in velocity, } \Delta V, = 390 \text{ in/sec}$$

$$\text{base duration, } \Delta t, = 0.225 \text{ sec}$$

3.4 EFFECT OF BULKHEAD CRUSHING VARIATION

In the previous analyses, the bottoming of the bulkhead crush springs in the simulation appears to have the most significant effect on producing failures. The FS620, 820 and 960 bulkhead springs used are shown in figure 3-77. To investigate how the results would be altered, the vertical-only symmetrical impact condition with zero pitch attitude and no aerodynamic loading was analyzed with revised crush characteristics as denoted in figure 3-77.

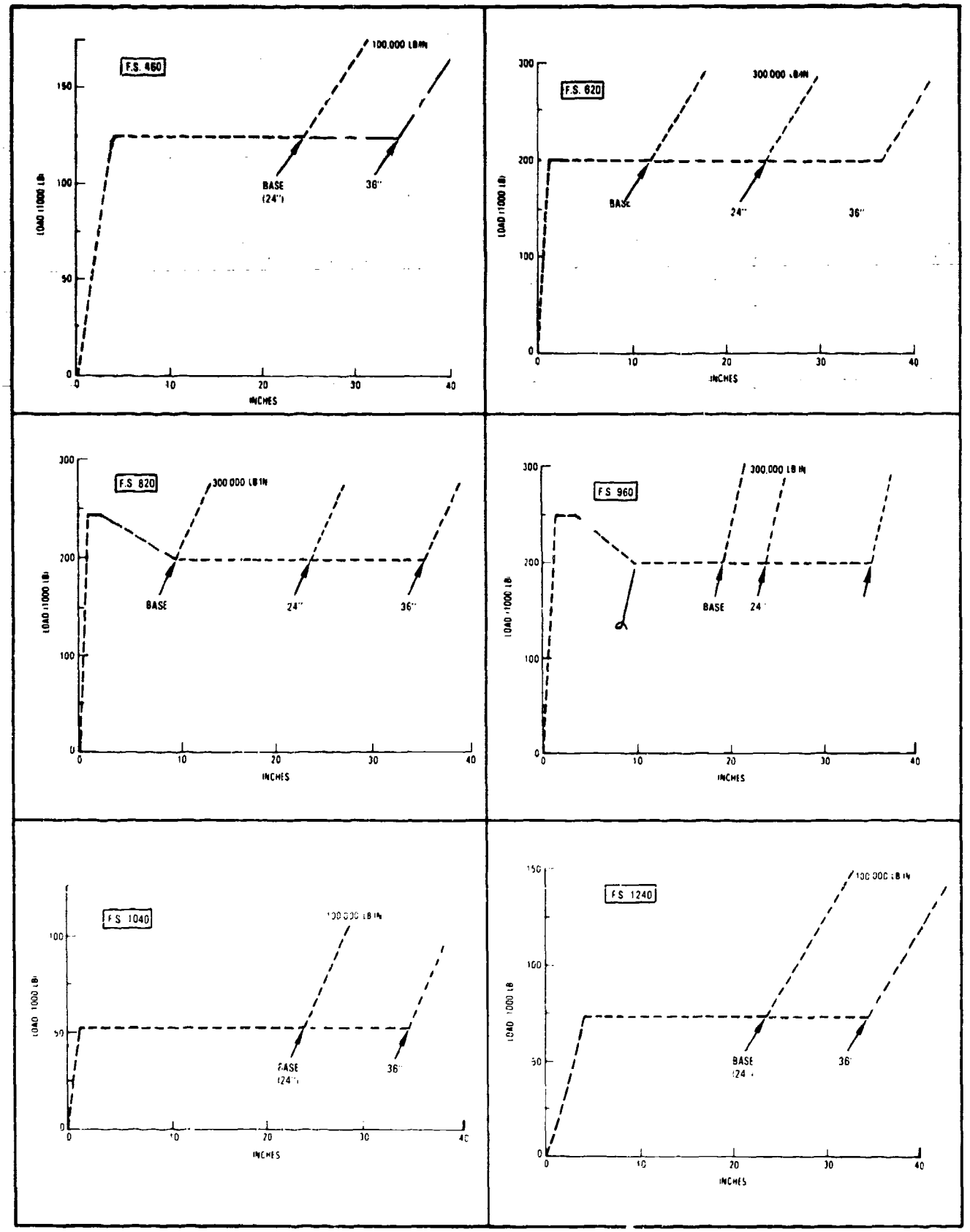

Figure 3-77. Variation of Lower Fuselage Spring Data

The results are tabulated in tables 3-26 to 3-30. The increase in uniform crush (to 24 inches) reduces the loads (LIC ratios decrease), increases the overall crush and reduces the vertical acceleration values for the same 22 ft/sec impact velocity. This allows the airplane to impact at a higher initial sink speed before realizing LICs greater than 1.0 (an indication of airframe failure). The increased crush (case 2) at a 22 ft/sec impact velocity produces lower acceleration, longer duration pulses with less change overall in velocity, ΔV, due to less rebounding and rotation. Increasing the impact velocity to 25 ft/sec with the increased crush (case 3) increases the acceleration levels but reduces the pulse duration and results in a higher velocity change, ΔV, in the mid-to-aft fuselage. The acceleration levels in the forward fuselage do not change significantly, although the pulse durations and ΔV's are somewhat higher. Cases 1, 2 and 3 results for the fuselage are shown in table 3-26. The wing responses for the comparative cases are shown in table 3-27. The immediate effect of additional fuselage crush at a corresponding initial sink speed (22 ft/sec) is to reduce the wing shear and bending moments to less than allowable values (cases 1 and 2). The increase in sink speed to 25 ft/sec with additional crush (case 3) raises the wing shear and moments to levels which are generally lower but comparable to the initial results (case 1). Compatibility between fuselage and wing strengths is closer for the case 3 results. Of interest, the wing and engine peak accelerations are lower for case 3 versus case 1.

The results of the analysis in which the uniform crush is allowed to reach 36 inches is represented by cases 4 and 5. At a 25 ft/sec initial impact velocity (case 4), the fuselage aft pressure bulkhead barely makes contact with the ground. At a 27.5 ft/sec initial impact velocity, the aft bulkhead produces significant loads as it is an extremely stiff structure. The summary of fuselage and wing responses for the 36-inch cases, as well as the comparisons with the original baseline case, are shown in tables 3-28 and 3-29, respectively.

TABLE 3-26. COMPARISON OF FLOOR RESPONSE RESULTS - INCREASE TO 24 INCH CRUSH

FUSELAGE STATION	LIC RATIOS			FUSELAGE CRUSH, IN			ACCELERATION RESPONSE					
							PEAK g			EQUIVALENT TRIANGULAR PULSE g (Δt) ΔV*		
	(1)	(2)	(3)	(1)	(2)	(3)	(1)	(2)	(3)	(1)	(2)	(3)
300/500	0.48	0.37	0.37	8.8	8.8	10.8	12.0	12.0	17.0	14.1(0.162)441	13.3(0.144)371	13.3(0.150)390
450	0.55	0.35	0.35	9.4	9.5	12.2	14.7	11.8	11.3	17.7(0.108)370	11.0(0.156)328	12.0(0.150)347
480/540	0.70	0.41	0.41									
600/620	0.75	0.71	0.83	10.6	11.9	15.6	15.6	10.5	10.5	15.9(0.114)350	9.4(0.162)293	10.4(0.174)352
820	0.76	1.05	1.68	12.3	16.8	21.2	13.6	10.7	10.6	14.4(0.114)316	6.7(0.222)286	10.4(0.174)347
960	0.52	0.79	1.54	15.0	21.9	25.1	11.8	7.5	12.3	12.8(0.120)296	5.4(0.264)276	10.2(0.174)342
990	0.64	0.59	0.89	16.9	24.2	26.1	11.7	7.9	14.6	12.1(0.120)283	5.4(0.264)272	10.2(0.174)338
1090	0.75	0.41	0.82									
1160	0.84	0.37	0.89									
1210	1.04	0.43	1.01	10.8	19.2	20.2	13.0	6.0	16.6	10.1(0.126)247	5.2(0.270)269	9.3(0.174)315
1320	0.99	0.44	1.02									
1400	1.10	0.45	1.07				8.3	4.9	12.0	9.2(0.150)265	5.6(0.240)272	8.6(0.216)385

NOTE: FOR ALL CASES; NO ENGINE GROUND CONTACT, FWD, VELOCITY, OR AERODYNAMIC LIFT; 24" UNIFORM CRUSH UNLESS SPECIFIED OTHERWISE.

(1) 22 FT/SEC SINK SPEED, UNIFORM CRUSH DISTANCE AT FS 620, 820, 960 = 10", 10", 18".

(2) 22 FT/SEC SINK SPEED, UNIFORM CRUSH DISTANCE AT FS 620, 820, 960, = 24", 24", 24".

(3) 25 FT/SEC SINK SPEED, SAME AS (2) CRUSH DISTANCE.

* Δt IN SECONDS, ΔV IN INCHES/SECONDS.

TABLE 3-27. COMPARISON OF WING RESPONSE RESULTS - INCREASE TO 24 INCH CRUSH

SHEAR (S_Z) LOADS X 10^3 LB				
B. L. LOCATION	ALLOWABLE	(1)	(2)	(3)
0 – 118	250	326.	216.	282.
118 – 271	200	265.	169.	210.
271 – 430	110	91.	79.	93.
430 – 583	40	81.	75.	92.6
583 – 743	10	29.	21.7	32.0
BENDING (M_Y) MOMENTS X 10^6 IN-LB				
B. L. LOCATION	ALLOWABLE	(1)	(2)	(3)
ROOT	75	67.6	47.2	58.3
BL 118	50	46.3	49.	54.
BL 271	30	31.3	28.7	33.
BL 430	15	14.9	14.4	17.7
BL 583	10	5.1	3.8	5.7
PEAK VERTICAL ACCELERATIONS				
B. L. LOCATION		(1)	(2)	(3)
118		14.2	8.1	8.5
271		10.8	5.8	7.3
430		11.8	4.9	7.2
583		8.5	6.8	9.3
743		18.6	13.5	20.4
INBOARD ENGINE		13.3	9.2	9.7
OUTBOARD ENGINE		8.9	6.8	9.0

NOTE: FOR ALL CASES; NO ENGINE GROUND CONTACT, FWD. VELOCITY, OR AERODYNAMIC LIFT; 24" UNIFORM CRUSH UNLESS SPECIFIED OTHERWISE.

(1) 22 FT/SEC SINK SPEED, UNIFORM CRUSH DISTANCE AT FS 620, 820, 960 = 10", 10", 18"

(2) 22 FT/SEC SINK SPEED, UNIFORM CRUSH DISTANCE AT FS 620, 820, 960 = 24", 24", 24"

(3) 25 FT/SEC SINK SPEED, SAME AS (2) CRUSH DISTANCE.

TABLE 3-28. COMPARISON OF FLOOR RESPONSE RESULTS - INCREASE TO 36 INCH CRUSH

FUSELAGE STATION	LIC RATIOS			FUSELAGE CRUSH, IN			ACCELERATION RESPONSE					
							PEAK g			EQUIVALENT TRIANGULAR PULSE g (Δt) ΔV*		
	(1)	(2)	(3)	(1)	(2)	(3)	(1)	(2)	(3)	(1)	(2)	(3)
300/350	0.48	0.37	0.45	8.8	10.8	12.2	12.0	17.1	16.6	14.1(0.162)441	20.0(0.090)349	19.6(0.096)362
450	0.55	0.33	0.50	9.4	12.2	14.6	14.7	11.3	11.6	17.7(0.108)370	11.5(0.162)358	12.5(0.174)420
480/540	0.70	0.40	0.51									
600/620	0.75	0.75	0.98	10.6	15.5	18.9	15.6	10.5	10.5	15.9(0.114)350	10.2(0.162)320	11.9(0.174)396
820	0.76	1.07	1.27	12.3	22.2	24.9	13.6	10.6	10.6	14.4(0.114)316	7.8(0.204)308	10.8(0.174)361
960	0.52	0.80	1.10	15.0	28.8	32.2	11.8	9.4	12.5	12.8(0.120)296	7.2(0.198)274	10.2(0.174)342
990	0.64	0.59	0.81	16.9	32.4	35.4	11.7	7.8	13.1	12.1(0.120)283	6.5(0.198)252 5.2(0.294)300	9.4(0.180)330
1090	0.75	0.43	0.73									
1160	0.84	0.41	0.87									
1210	1.04	0.48	1.01	10.8	29.4	32.3	13.0	6.7	13.4	10.1(0.126)247	5.2(0.294)300	9.0(0.198)287 6.2(0.300)367
1320	0.99	0.49	.99									
1400	1.10	0.50	1.07				8.3	5.1	16.7	9.2(0.150)265	5.3(0.300)300	9.0(0.198)346

NOTE: FOR ALL CASES; NO ENGINE GROUND CONTACT, FWD, VELOCITY, OR AERODYNAMIC LIFT; 24" UNIFORM CRUSH UNLESS SPECIFIED OTHERWISE.

(1) 22 FT/SEC SINK SPEED, UNIFORM CRUSH DISTANCE AT FS 620, 820, 960 = 10", 10", 18".

(4) 25 FT/SEC SINK SPEED, UNIFORM CRUSH DISTANCE AT ALL LOCATIONS = 36", EXCEPT AT AFT BULKHEADS (FS1400).

(5) 27.5 FT/SEC SINK SPEED, SAME AS (2) CRUSH DISTANCE.

* Δt IN SECONDS, ΔV IN INCHES/SECONDS.

TABLE 3-29. COMPARISON OF WING RESPONSE RESULTS - INCREASE TO 36 INCH CRUSH

	SHEAR (S_Z) LOADS X 10^3 LB			
B. L. LOCATION	ALLOWABLE	(1)	(2)	(3)
0 – 118	250	326.	229.	233.
118 – 271	200	265.	182.	258.
271 – 430	110	91.	86.5	99.7
430 – 583	40	81.	79.5	89.
583 – 743	10	29.	24.4	31.1
	BENDING (M_Y) MOMENTS X 10^6 IN-LB			
B. L. LOCATION	ALLOWABLE	(1)	(2)	(3)
ROOT	75	67.6	49.	51.5
BL 118	50	46.3	54.	59.
BL 271	30	31.3	30.	32.
BL 430	15	14.9	15.3	16.4
BL 583	10	5.1	5.4	6.0
	PEAK VERTICAL ACCELERATIONS			
B. L. LOCATION		(1)	(2)	(3)
118		14.2	8.2	12.3
271		10.8	5.6	9.6
430		11.8	5.7	9.5
583		8.5	6.0	9.9
743		18.6	15.0	19.6
INBOARD ENGINE		13.3	9.7	11.5
OUTBOARD ENGINE		8.9	7.4	9.2

NOTE: FOR ALL CASES; NO ENGINE GROUND CONTACT, FWD. VELOCITY, OR AERODYNAMIC LIFT; 24" UNIFORM CRUSH UNLESS SPECIFIED OTHERWISE.

(1) 22 FT/SEC SINK SPEED, UNIFORM CRUSH DISTANCE AT FS 620, 820, 960, 10", 10", 18"

(2) 25 FT/SEC SINK SPEED, UNIFORM CRUSH DISTANCE AT ALL LOCATIONS = 36", EXCEPT AT AFT FUSELAGE BULKHEAD (FS1400).

(3) 27.5 FT/SEC SINK SPEED, SAME AS (2) CRUSH DISTANCE.

TABLE 3-30. OVERALL SUMMARY OF RESULTS

CONDITION	INITIAL SINK VELOCITY FT/SEC	FLOOR ΔV RANGE FT/SEC			TYPICAL TRIANGULAR PULSES			
		MAXIMUM @ FS 300 BLKHD. & FS1400 BLKHD.	PASSENGER REGION		FS 460–820		FS 960–1200	
			FS460–820	FS960–1240	g_p	Δt SEC	g_p	Δt SEC
ORIGINAL CRUSH (CASE1)	22	36.7	26.3–30.8	20.6–24.7	14.4–17.7	0.120–0.114	10.1–12.8	0.126–0.120
24 INCH CRUSH (CASE 2)	22	31.0	23.8–27.3	22.4–23.	6.7–11.0	0.222–0.156	5.2–6.4	0.270–0.264
24 INCH CRUSH (CASE 3)	25	32.5	28.9–29.3	26.3–28.5	10.4–12.0	0.174–0.150	9.3–10.2	0.174
36 INCH CRUSH* (CASE 4)	25	29.0**	25.7–30.0	23.–25.	7.8–11.5	0.204–0.162	5.2–7.2	0.294–0.198
36 INCH CRUSH* (CASE 5)	27.5	30.1**	30–35	27.5–30.6	10.2–12.5	0.174	9–9.4	0.198–0.180

*AFT FUSELAGE BULKHEAD AT FS1400 IMPACTS AT 25 FT/SEC SINK SPEED AND EXCEEDS FAILURE LOAD AT 27.5 FT/SEC CONDITION.

**PRIMARY PULSE Δt .100 SECONDS, HIGHER ΔV's BUT LOWER g, LONGER Δt

An overall comparison of the fuselage pulse data for five cases is provided in table 3-30. As with previous KRASH analyses results, the trends indicate that the more available crush, the lower the accelerations (g), the longer the pulse duration (Δt), and the relatively same or slightly higher velocity change (ΔV) occur at the threshold of airframe structural integrity.

The vertical acceleration pulse data presented in tables 3-26 through 3-30 are shown in figure 3-78, where the triangular pulse peak magnitude, g_p, base time duration, Δt, and change in velocity, ΔV, parameters are depicted. Also shown in figure 3-78 are measured responses from a vertical drop test of an FAA-conducted narrow-body fuselage section (CID type) with an impact velocity of 35 ft/sec. The fuselage crushed between 24 and 30 inches in this test.

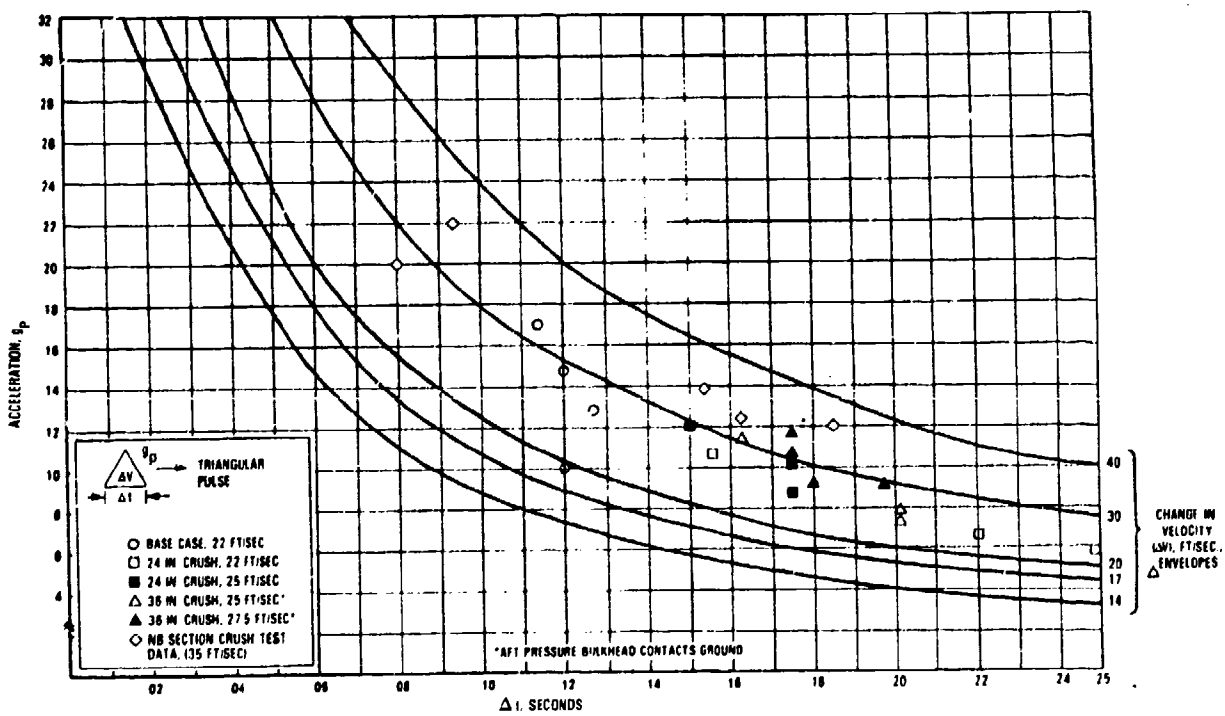

Figure 3-78. Analytically Obtained Vertical Pulses, Air-to-Ground Impact-Crush Variation

FINAL SECTION 3

SECTION 4

4.0 CRASH DESIGN VELOCITY ENVELOPE

The results of the parametric analyses and supporting test data have been presented in Section 3. The full-scale and section drop test triangular pulse data are summarized in figures 4-1 and 4-2 for the vertical and longitudinal directions, respectively. The test data in figure 4-1 show that typically high accelerations are associated with short durations and that the trend is for a decrease in amplitude as the duration of the pulse increases. The test data also show that while the pulses in the passenger cabin region of a transport airplane can vary substantially, they are generally associated with a change of velocity at or below 30 ft/sec, without the fuselage strength (shell bending, shear) being exceeded. Typically the vertical response can be characterized as a triangular pulse with a velocity change of 25 ft/sec, base duration of 0.15 second, and a peak amplitude of 10g. The aircraft impact velocities associated with full-scale test data show no fuselage breaks occurred for an impact with a sink speed of 18.5 ft/sec or less, and a break occurs during an impact with a sink speed of 35 ft/sec. The full-scale crash test data are void between these two impact magnitudes. The test data in figure 4-2 show the same peak acceleration versus pulse duration trends for the longitudinal pulse as depicted for the vertical pulses in figure 4-1. The number of test data points is much less for the longitudinal direction than is available for the vertical direction. The characteristics of a longitudinal triangular pulse is a velocity change of 26 ft/sec, a base of duration of 0.200 second, and a peak amplitude of 8g. The data presented in figures 4-1 and 4-2, as well as subsequent figures 4-3 through 4-6 is in the form of a triangular pulse with the following parameters: velocity change, ΔV, peak amplitude, g, and pulse rise time, t_r. The relationship between acceleration, velocity change and base duration for a triangular pulse is:

$$\Delta V = 1/2(g)\ (32.2)\ \Delta t \quad \text{(units in feet/second)}$$

The pulse rise time, t_r, which is normally referred to in dynamic test requirements, is approximately equal to 1/2 the pulse base duration, Δt.

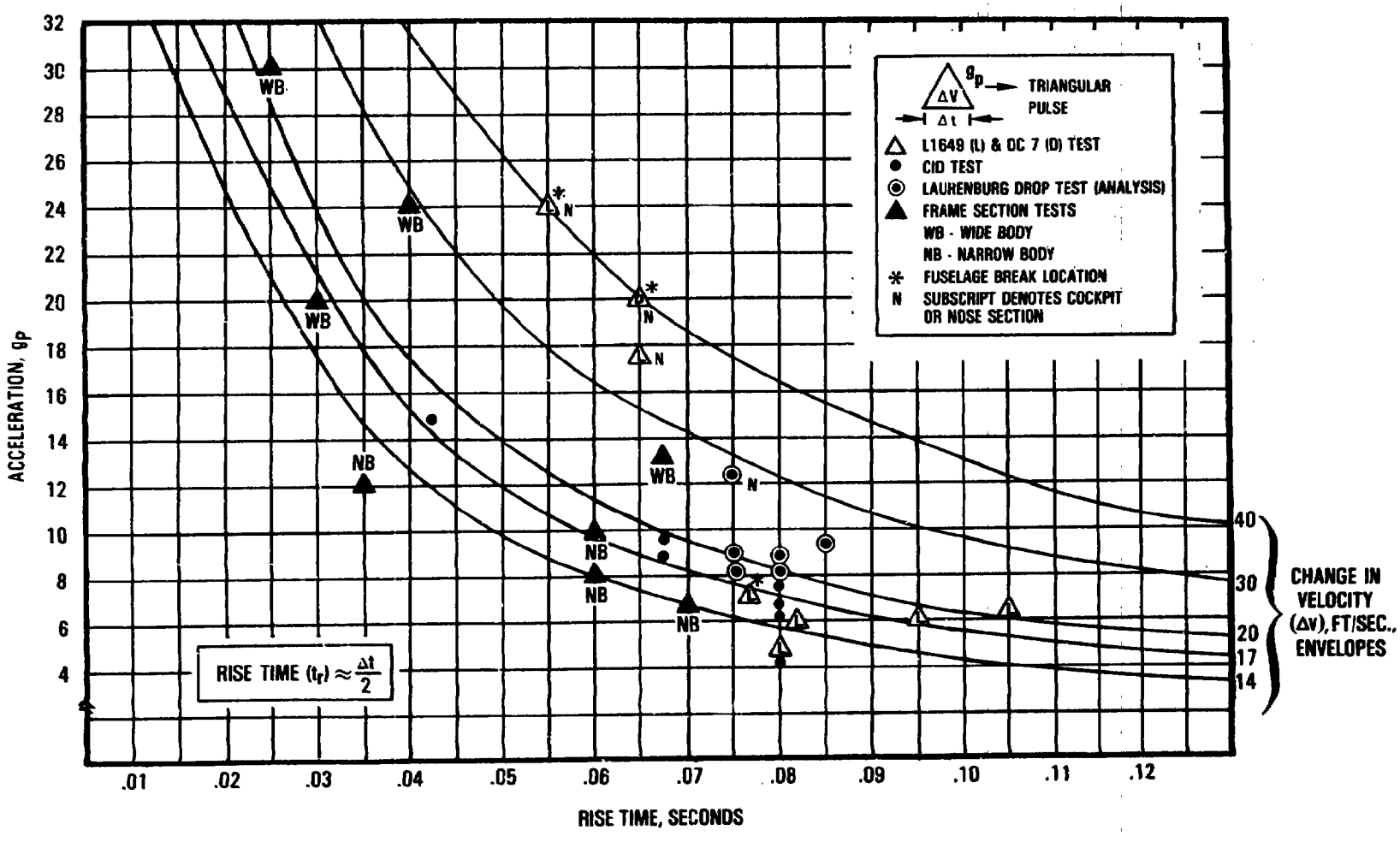

Figure 4-1. Summary of Measured Vertical Pulses

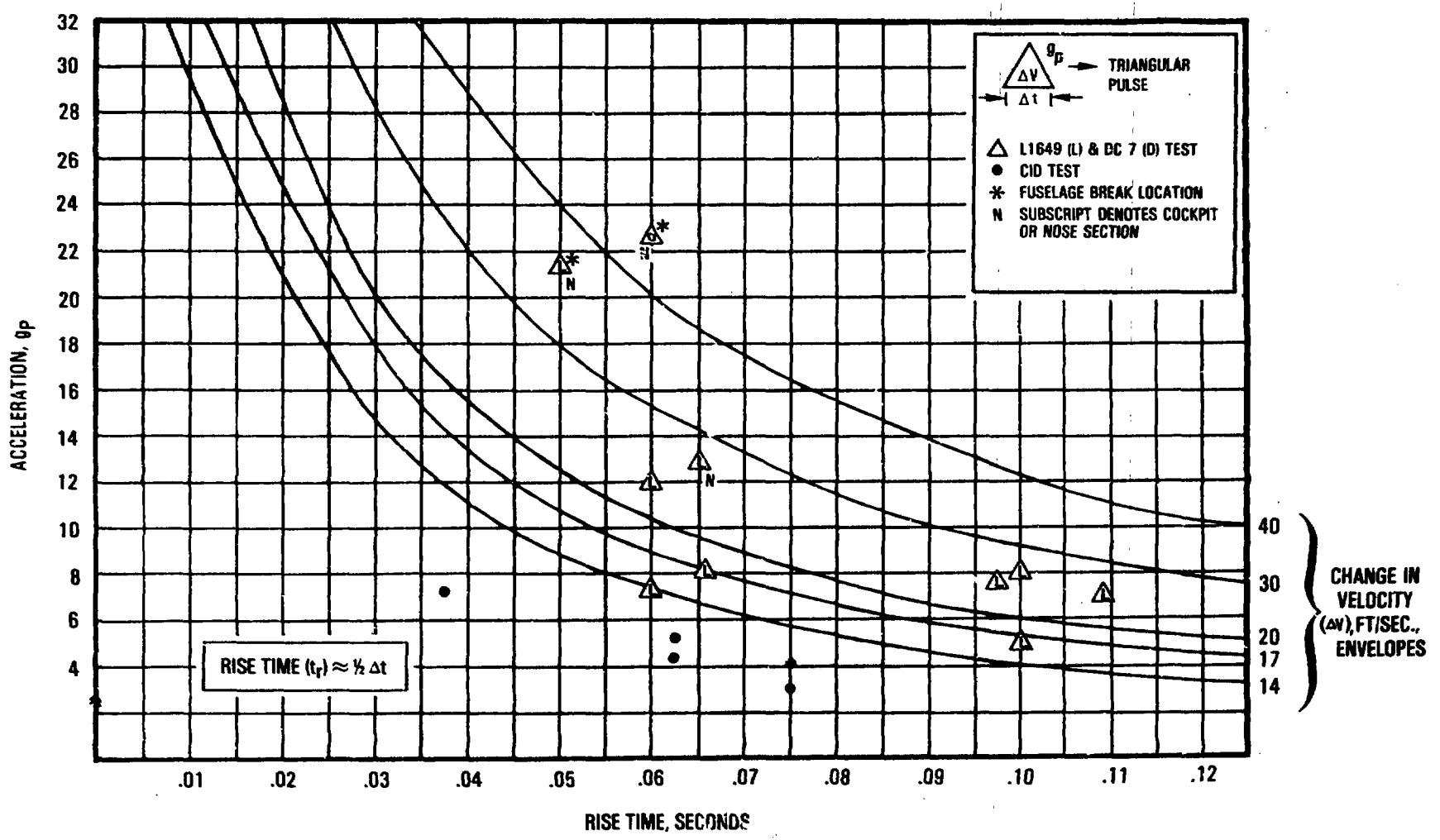

Figure 4-2. Summary of Measured Longitudinal Pulses

The analytically obtained vertical response data are summarized in figures 4-3 and 4-4. Air-to-ground gears retracted and extended cases are shown in figure 4-3. The vertical pulses for the air-to-ground analyses with fuselage crush variations are shown in figure 4-4. The air-to-ground analyses results presented in figure 4-3 suggest the characteristic triangular pulse in the vertical direction is a change of velocity in the range of 20 ft/sec to 25 ft/sec, a base duration of between 0.11 and 0.16 second and a peak amplitude range of 8g to 12g. As is noted, the sink speed condition for the airframe which produces this pulse does not exceed 22 ft/sec (0-degree pitch) with gears retracted and maintains fuselage structural integrity. Figure 4-4 provides analytical vertical response data obtained from the investigation into fuselage crush variation (Section 3.4). A triangular pulse of the nature of a change of velocity of 25 to 30 ft/sec, a base duration of between 0.15 second to 0.20 second and a peak amplitude of 8g to 12g would be a reasonable extrapolation of this data. For the data presented in figures 4-3 and 4-4, the amplitude versus pulse duration trend observed in the test data is evident. For air-to-ground impacts the longitudinal pulse can be approximated as having the same triangular pulse characteristics as the vertical pulse, but with an amplitude of between 0.4 and 0.5 times that of the peak vertical g, depending on ground coefficient of friction.

The ramp impact analyses results are shown in figures 4-5 and 4-6 for the longitudinal and vertical pulses, respectively. Both the longitudinal and vertical pulses obtained from this set of analyses indicate relatively shorter duration pulses (less than 0.14 second base duration). While these pulses appear of shorter duration when compared to L1649 test data, the trend of higher peak accelerations at short pulse durations and lower peak accelerations at the longer durations prevails. Other than high vertical responses at the nose section for the 8 and 20 degree ramp impacts the velocity change throughout the fuselage is less than 30 ft/sec. The L-1649 ramp impact test data (reference 6) showed similar trends.

The data presented in figures 4-1 through 4-6 are summarized in table 4-1. Included are full-scale and section test results as well as KRASH analyses of various impact scenarios. While it is difficult to make direct

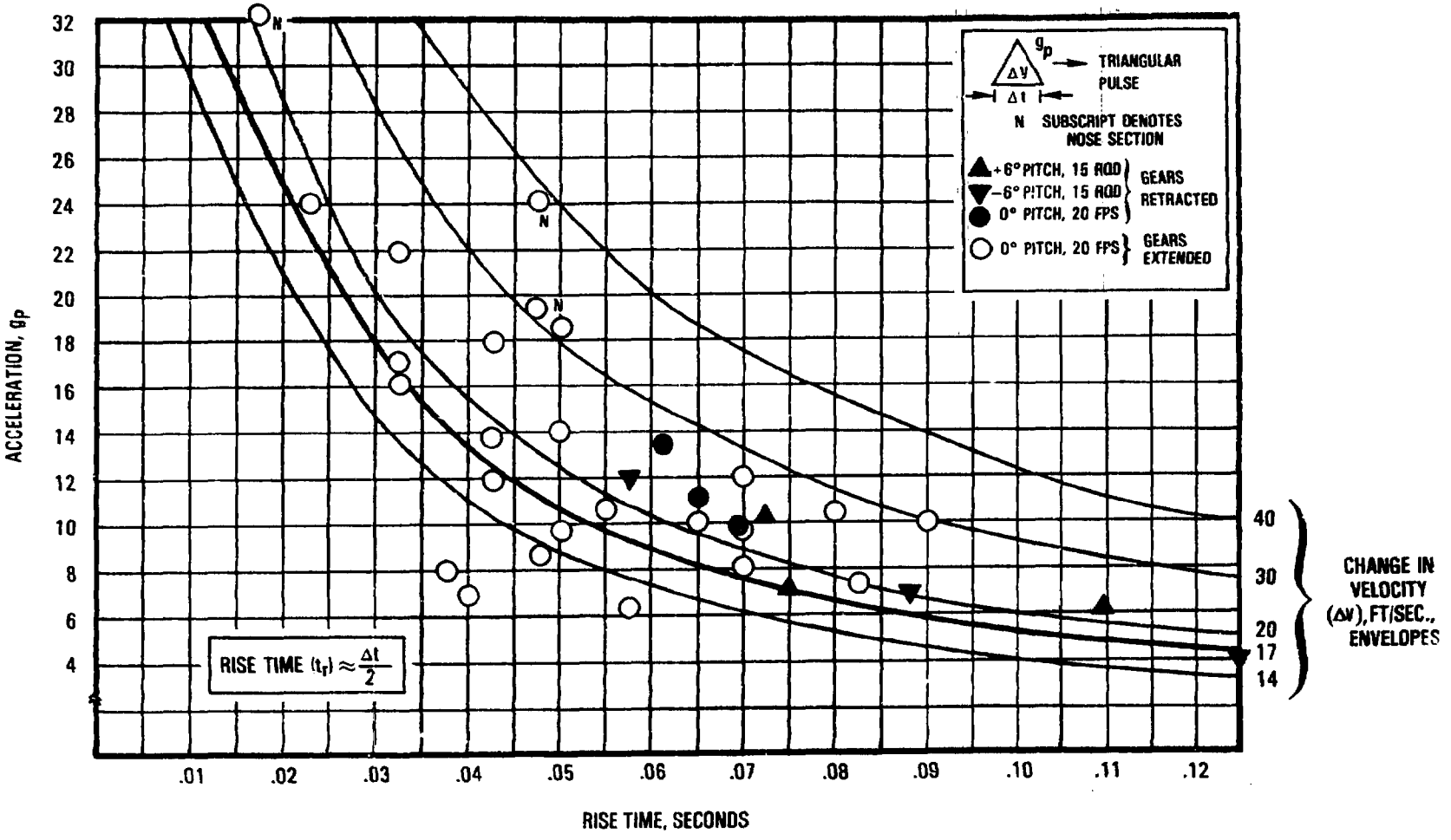

Figure 4-3. Analytically Obtained Vertical Pulses - Air-to-Ground, Gears Extended and Retracted

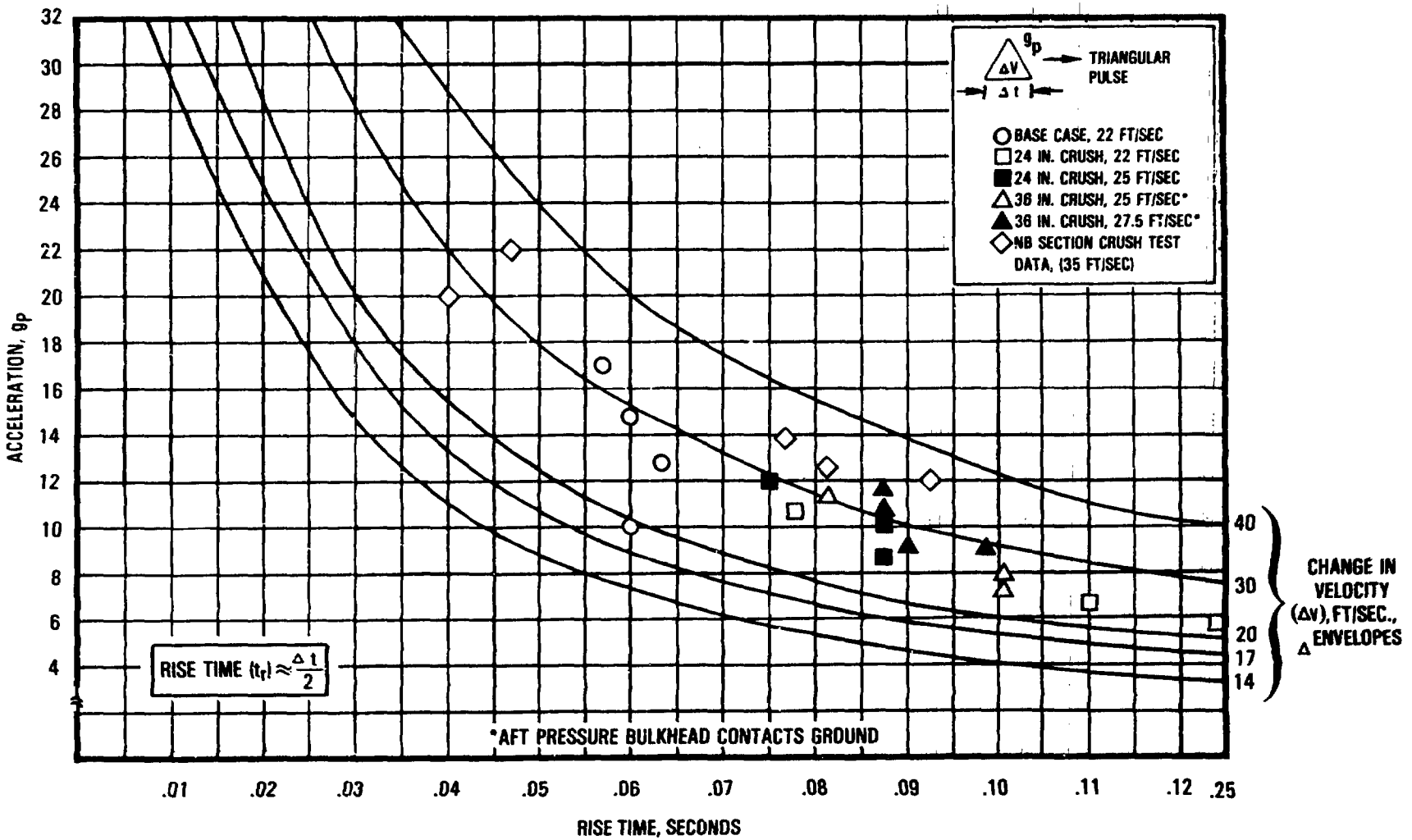

Figure 4-4. Analyticlly Obtained Vertical Pulses, Air-to-Ground Impact-Crush Variation

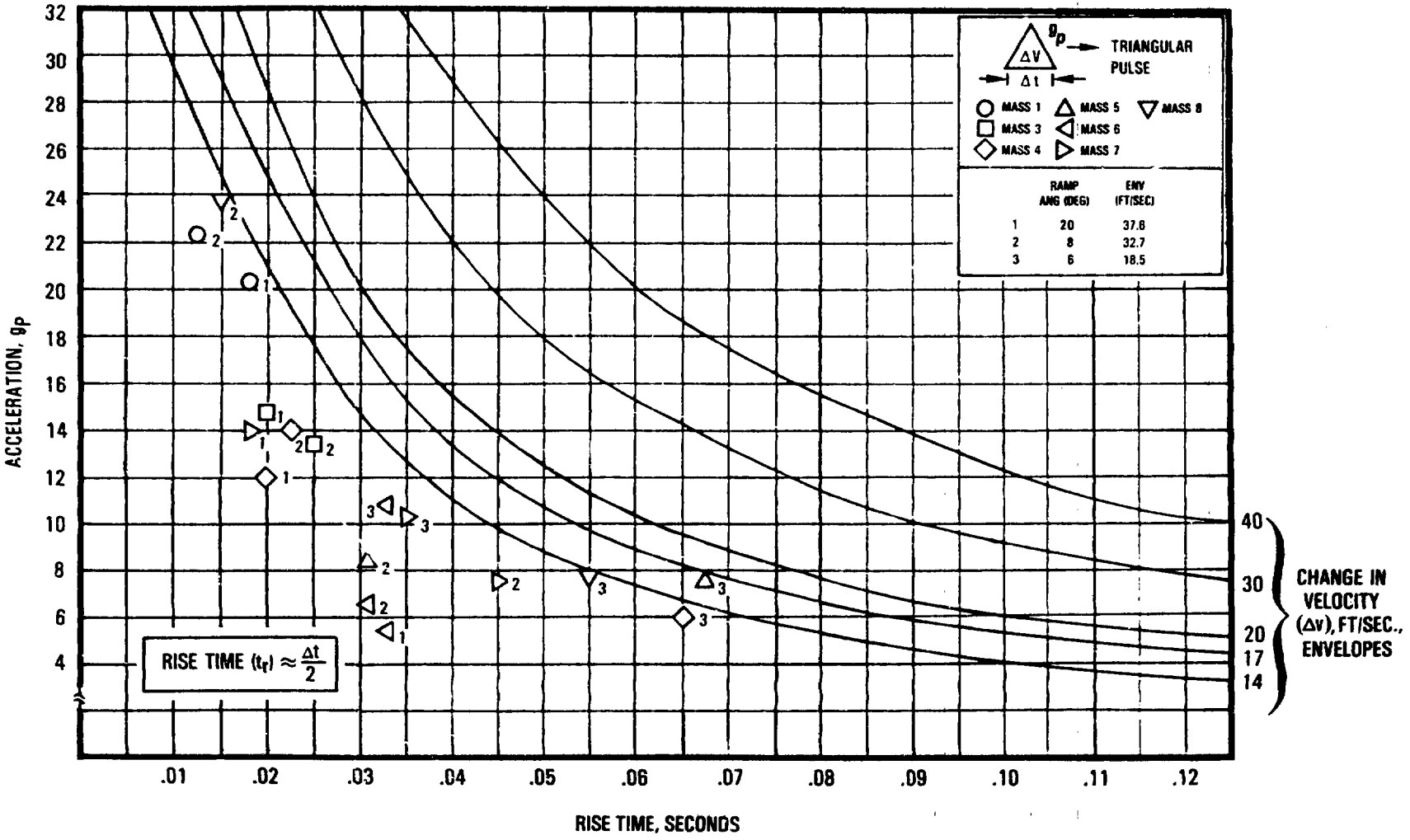

Figure 4-5. Longitudinal Pulses Obtained from Ramp Impacts

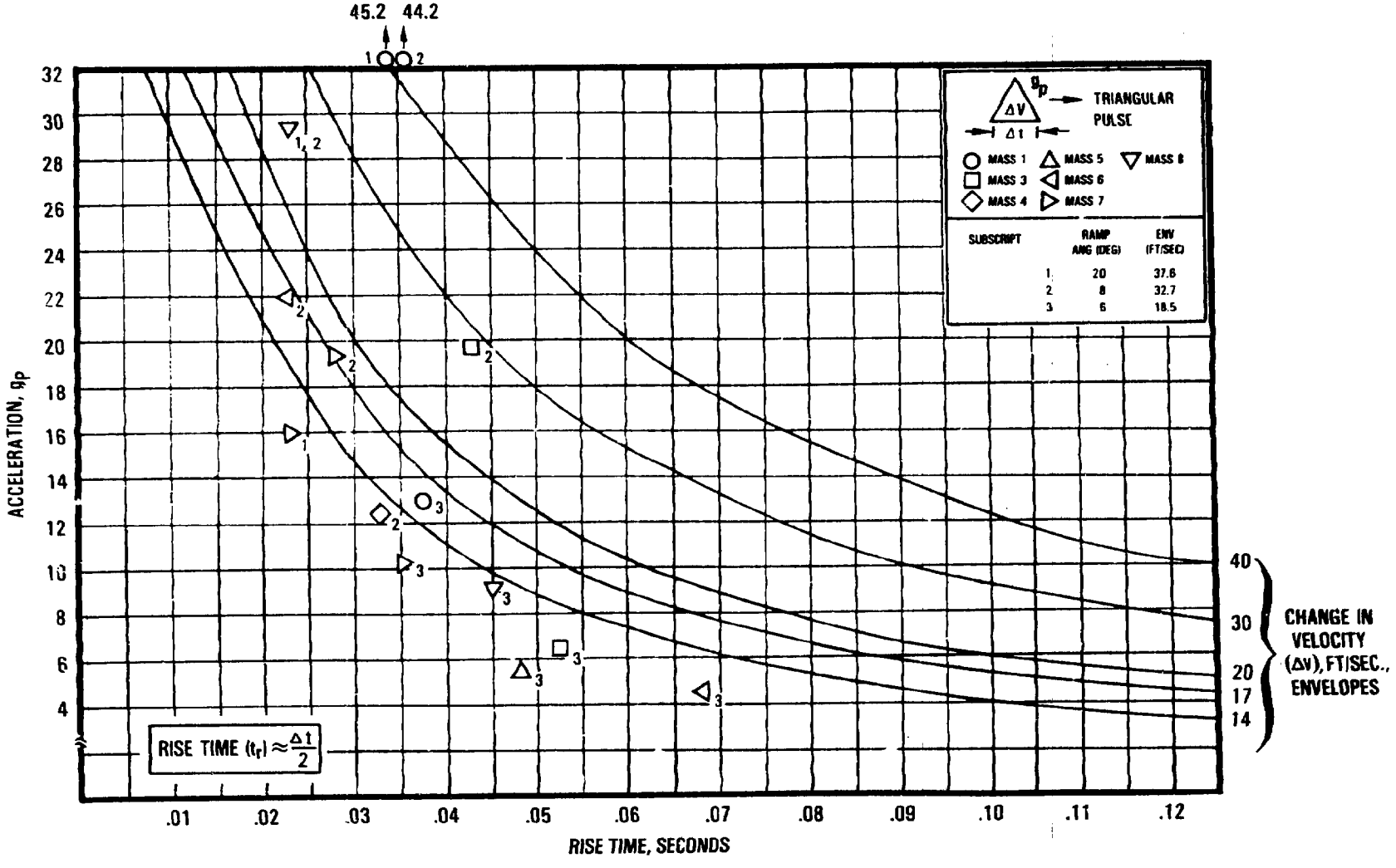

Figure 4-6. Vertical Pulses Obtained from Ramp Impacts

TABLE 4-1. SUMMARY OF FLOOR RESPONSE PULSES

Condition No.	Data	A/P (Section) Initial Impact at Sink Speed, Ft/Sec	Triangular Pulse Range						Compare With Condition No.	Ref.
			Longitudinal			Vertical				
			Ampl. g	Δt sec	ΔV ft/sec	Ampl. g	Δt sec	ΔV ft/sec		
	o TEST Full-Scale Airplane									
1	L-1649 [6° slope]	18.5	8-10	.12-.20	14-29	5-10	.15-.20	15-23	12	6
2	L-1649 [20° slope]	37.6 (2) (3)	5-10	.20-.22	16-27	5-10	.15-.20	15-25	14, 15	6
3	CID [Air-to-Ground, -2° pitch]	14-15 (1)	—	—	—	6-8	.13-.20	14-21	8	12
	Sections									
4	Narrow-body section-vertical drop, 18" crush	20	—	—	—	8-10	.11-.13	17-20	8, 9, 10	11,13
5	Wide-body section-vertical drop, 18" crush	20	—	—	—	13	.13	20	—	14
6	Narrow-body section-drop, 24"-30" crush	35	—	—	—	12-14	.15-.18	33-38	11	15
7	Axial Cylinder-longitudinal	—	12	.15	30	—	—	--	16	4
	o AIRPLANE ANALYSES									
8	Laurinburg (+1° pitch)	17	—	—	—	8-10	.14-.16	17-20	3, 4	2,6
9	Air-to-Ground (gears retracted, 0° pitch, 18" crush)	22 (2)	—	—	—	10-13	.13-.14	22-26	4	*
10	Air-to-Ground (gears extended, 0° pitch, 18" crush)	20 (2)	—	—	—	8-11	.14-.18	20-30	4	*
11	Air-to-ground (gears retracted, 0° pitch, 24"-36" crush)	25-27.5 (2)	—	—	—	8-12	.15-.20	25-30	6	*
12	Ground-to-ground (6° slope)	18.5	8	.11-.14	14-17	6-9	.08-.11	10-15	1	*
13	Ground-to-ground (20° slope)	25.0 (2)	5-8	.16-.21	17-26	6-8	.11-.16	14-20	—	*
14	Ground-to-ground (20° slope)	37.6 (2) (4)	8	.11-.14	14-17	14	.10	22	2	*
15	Ground-to-ground (8° slope)	32.7 (2) (4)	8-14	.05-.06	10-14	20	.09	30	2	*
16	90° wall-longitudinal	—	9-10	.20-.24	30	—	—	--	7	*

(1) Fuselage impact

(2) Fuselage break or strength exceedance

(3) Nose section triangular pulse responses; vertical ΔV = 39.5 ft/sec, Δt = .10 sec, amplitude = 24g
longitudinal ΔV = 35.1 ft/sec, Δt = .12 sec, amplitude = 18g

(4) Nose section responses; vertical ΔV = 44-45 ft/sec, Δt = .07-.08 sec, amplitude = 34g

* Section 3 of this report

comparisons for each test condition, an attempt is made to relate analyses which are reasonably close to test conditions. For example, conditions 1 and 12 are comparable because both involve a full airplane impact onto a 6-degree slope with the same ENV. Condition 2 compares with conditions 14 and 15 because the ENVs are reasonably close, even though the ramp angles differ. The fuselage impact with the ground during the CID test (condition 3) is compared with the Laurinburg analysis (condition 8) only because both are relatively flat, symmetrical impacts in the sink speed range of 15.5 $\pm$1.5 ft/sec. Narrow-body section drop test data (condition 4) are compared to conditions 8, 9, and 10 because the sink speed, attitude and crush distance experienced are reasonably close. The high sink speed test condition (No. 6) is compared to the parameter analysis in which extensive crush is allowed (condition 11). The longitudinal cylinder test and wall impact analyses conditions (Nos. 7 and 16) are also compared.

The composite of the analyses and test data is presented in figure 4-7 as vertical velocity change versus longitudinal velocity change. The data are representative of a triangular pulse with a base duration of between 0.15 and 0.20 second. The amplitude associated with the pulse can be obtained from the following relationship:

$$g = \frac{\Delta V}{16.1 \Delta t} \qquad \begin{array}{l} \Delta t = \text{sec.} \\ \Delta V = \text{ft/sec.} \end{array}$$

Also shown in figure 4-7 is the envelope of the data in an attempt to indicate the estimated region of structural integrity. On the basis of the analyses and test results, two potential velocity change envelopes evolve: airframe integrity and seat dynamic pulse definition. These envelopes are shown in figure 4-8. The seat dynamic pulse is higher than the structural integrity envelope and accounts for rotational and rebound effects.

The velocity envelopes shown in figures 4-7 and 4-8 suggest the following test conditions for seat dynamic triangular pulses.

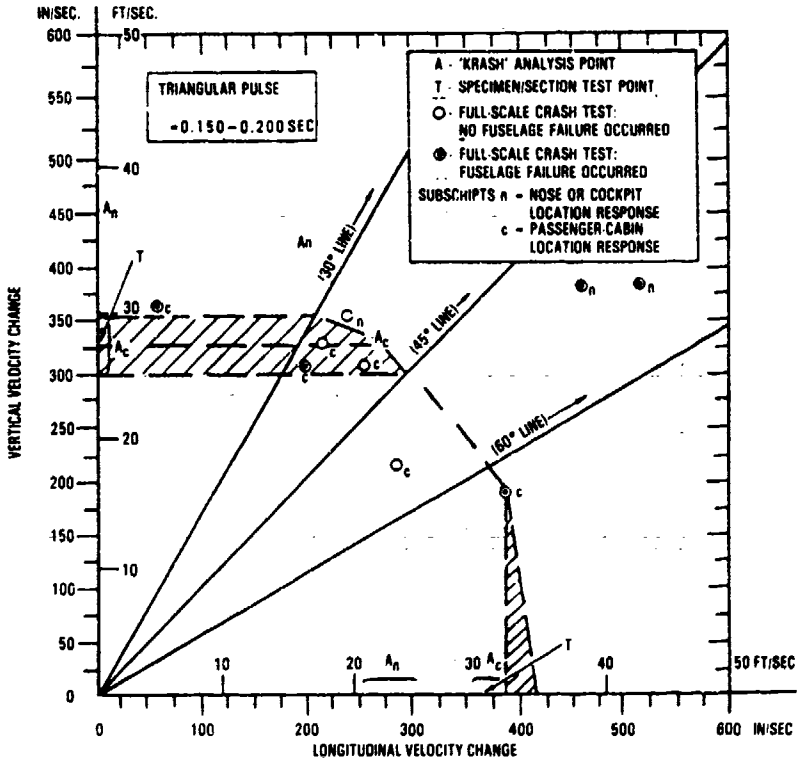

Figure 4-7. Velocity Envelope for Transport Category Airplane Seat Dynamic Pulses

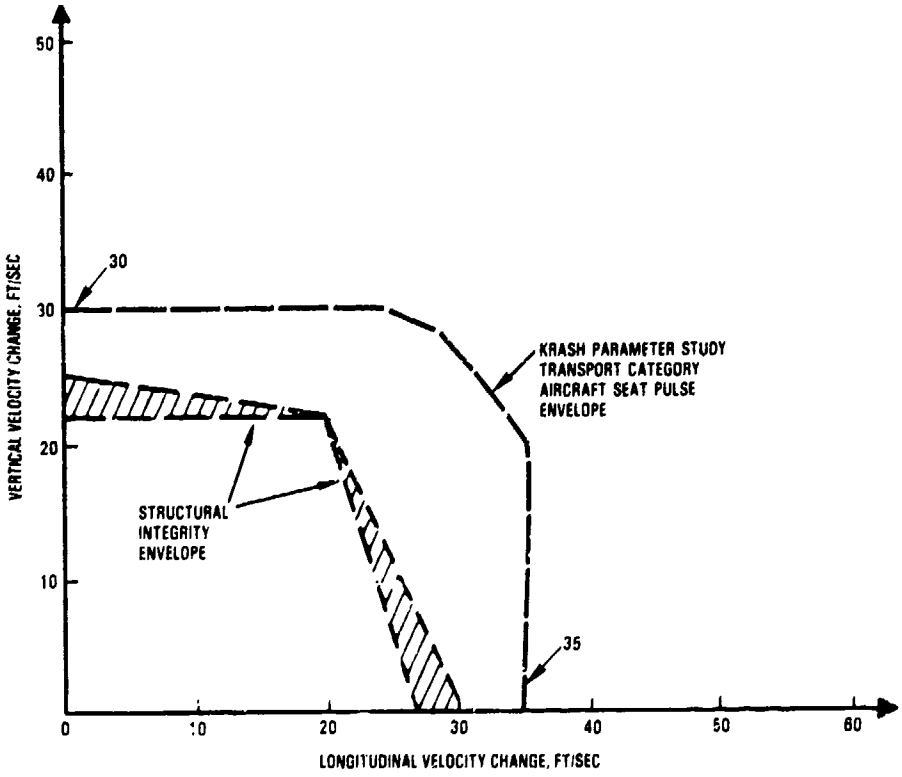

Figure 4-8. Structure and Seat Test Velocity Change Envelopes

1. Combined Vertical-Longitudinal with the following resultant parameters:

$\Delta V \cong 33.5$ ft/sec;

$\Delta t \cong 0.150$ second

$G_{peak} \cong 13.8$

With a seat orientated 30 degrees from the vertical, the respective vertical and longitudinal components will be:

Vertical

$G_p \cong 12g$

$\Delta V \cong 29$ ft/sec

Longitudinal

$G_p \cong 6.9g$

$\Delta V \cong 16.8$ ft/sec

2. Longitudinal-only

$\Delta V \cong 35$ ft/sec

$\Delta t \cong 0.200$ second

$G_{peak} \cong 11.0g$

The first condition represents a high sink speed impact in which the longitudinal forces are related to the vertical forces approximately by a high ($\mu \geq .5$) coefficient of friction. The second condition is an extreme case in which the only significant pulse would be longitudinal. Both conditions would appear to provide margins (1) above a realistic crash environment, and (2) above the structural integrity of the airframe.

END SECTION IV

SECTION 5

SUMMARY OF RESULTS

The effort described herein included parametric sensitivity analyses which incorporated:

- pre-CID test fuselage section test data
- post-CID test correlation results
- previous available full-scale crash test data (L1649, DC-7)
- previous available section test data and analytical modeling data (reference 4)

For the air-to-ground analyses the following assumptions were adhered to:

- Impact directly on fuselage, no engine crush involved
- Symmetrical impact, no roll or yaw
- No initial external loading, i.e., aerodynamic forces
- No rupture of beams
- Load interaction curve (LIC) > 1.0 indicates limit of airframe integrity
- Maximum crush before restiffening occurs is:

  10-inch wing center section, FS620-820
  18-inch wing MLG aft bulkhead, FS960
  24-inch fuselage frame sections, FS300, 460, 1040, 1240

Analysis results were initially obtained prior to the incorporation into the model of a revised nose-gear bulkhead crush representation which was obtained from reference 4 data and is described in Sections 3.2.1 and 3.3.1. Subsequent to the initial runs analyses were performed to incorporate:

- revised nose-gear bulkhead crush characteristics
- wing and engine response to allow monitoring of wing shear and bending moment versus estimated strength allowables

A summary of conditions analyzed for this type of impact condition is presented in table 3-2. The results of these analyses are presented in Section 3.1.1.

The parametric study fuselage crush results for the revised nose gear bulkhead representation (Cases 7, 10, 11 in Table 3-2) are compared to the test data results in Figure 5-1. From Figure 5-1 it can be observed that parametric analyses results indicate that the underside crush throughout the entire fuselage length can be greater than that experienced during either the "Laurinburg" or "CID" full-scale tests. The analyses are performed at the threshold of airframe structural integrity which is more severe than either of the test conditions.

For the air-to-ground, gear extended analyses the following three conditions were determined to be approximately the level at which fuselage structural integrity would be exceeded:

	Sink Speed (ft/sec)	Pitch Attitude (deg.)
1.	18	-6
2.	20	0
3.	18	+6

For all cases of this type of impact the following assumptions applied:

- No lift forces
- Forward velocity = 262 ft/sec
- Ground coefficient (μ) = 0.35
- Main gear failure loads;

  Fz, Vertical Force = 428,000 lb.,
  Fx, Longitudinal Force = 165,000 lb.

- Nose gear failure loads;

  Fz = 130,000 lb., Fx = 78,000 lb.

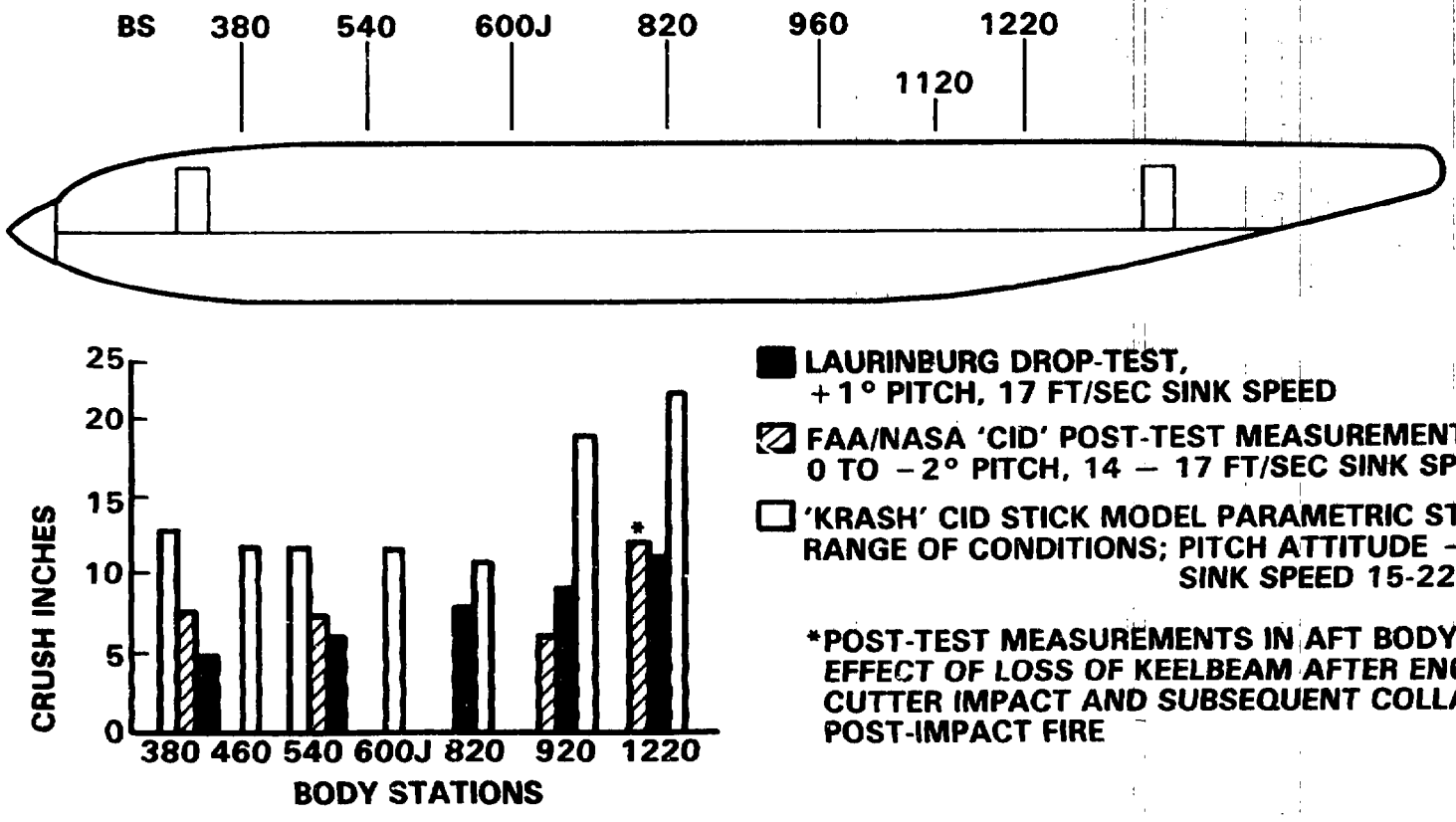

Figure 5-1. Fuselage Crush Comparison; "Laurinburg", "CID", and Parametric Analyses

The no lift analysis allows for evaluating critical fuselage impact loads in a shorter analysis than otherwise would be accomplished with lift forces acting. The results of these analyses are presented in section 3.1.2.

KRASH analyses results were also compared to previous air-to-ground impact analyses of a medium sized transport category airplane reported in reference 4. The two configurations (reference 4 and CID models) are compared in figure 3-31. Differences that exist between the LIC, crush and accelerations values of the two models are described and explained. For example, the reference 4 peak accelerations are higher because the analysis contains very high frequency (short duration) responses which are normally filtered in current test practices when compared to analytical models. The reference 4 results also show higher fuselage crush which are easily explained by the load-deflection curves used in that model. Overall the model results are similar when one compares the airplane initial impact velocity versus pitch attitude curves as presented in figure 3-34. The results of those analyses are presented in section 3.1.3.

For the air-to-ground impact conditions the magnitude of longitudinal pulses are relatively low in relation to the magnitude of the vertical pulses. To obtain combined longitudinal-vertical pulses such as those described in reference 6, ground-to-ground (ramp) impacts were performed. Included in these analyses were the following:

1. 6-degree ramp, ENV = 18.5 ft/sec, forward velocity = 177 ft/sec
2. 20-degree ramp, ENV = 37.6 ft/sec, forward velocity = 110 ft/sec
3. 8-degree ramp, ENV = 32.7 ft/sec, forward velocity = 235 ft/sec

These cases are representative of the reference 6 and 7 test conditions. The assessment of the fuselage failure modes experienced during the tests versus that obtained by analysis via LIC curves showed good agreement. The results of these analyses are described in section 3.2.1.

The measured acceleration obtained pulses from the L1649 (reference 6) and DC-7 (reference 7) full-scale ramp impact tests were integrated to obtain velocity changes as noted in figures 3-63 to 3-65 and table 3-19. The acceleration pulses and subsequent velocity calculations obtained from the L1649 test are of particular interest for the following reasons:

- The gross takeoff weight (GTOW) for the L-1649 is approximately 159,000 pounds which represents a mid-sized transport category aircraft.
- The aircraft fuselage experienced two significant structural breaks during a ground slope impact.
- The floor acceleration data illustrates a response trend which is considered to be characteristic of the larger FAR 25 transport airplanes.

Briefly, this test incorporated two sequential impacts of the aircraft onto an earthen mound. Prior to the initial impact onto a 6-degree slope with the airplane moving with a forward velocity of 172 ft/sec (ENV = 18.5 ft/sec), the nose and main gears were failed, and the wing fuel tanks were ruptured as part of the crash scenario. Subsequent to the 6-degree slope impact, in which no airframe failures were experienced, the aircraft impacted a 20-degree slope while moving with a forward velocity of 110 ft/sec (ENV = 37.6 ft/sec) and two fuselage breaks occurred, as can be observed in figure 3-37. The longitudinal accelerations at two floor locations are shown in figure 3-36. From figure 3-36 it can be noted that the peak g acceleration at the aircraft cockpit location (FS195) is approximately 20g for both the 6- and 20-degree slope impacts, despite the fact that the effective longitudinal velocity change resulting from the latter impact is approximately 30 percent higher than the effective longitudinal velocity change, ΔV, associated with the impact onto the shallower slope. At the mid-fuselage station (FS685), the response shapes are similar and the magnitudes are nearly equal (despite the longer duration and, consequently, a higher effective longitudinal ΔV). The vertical responses obtained during this test were not as clearly defined from the data. The distribution of the longitudinal floor pulses for the two slope impacts show that the cockpit floor response is substantially higher than the

responses throughout the passenger floor region. While the oscillatory nature of the response from FS685 to FS1165 suggests short duration peaks of 15g to 20g exist, the longer duration pulse that normally applied to seat testing, is more nearly < 10g peak. These data are provided in section 3.2.2.

Specimen test data obtained from reference 4 was utilized to refine the KRASH model. In particular fuselage nose gear bulkhead load-deflection behavior obtained from the reference 4 report showed that the earlier KRASH models underestimated the energy absorption capability in that region as noted below:

ENERGY ABSORPTION CAPABILITY (IN-LB)

KRASH Models		Reference 4 (Fig. 3-27)	
Original for air-to-ground analysis	Revised for ramp impact Case No. 1	Curve 2	Curve 3
900,000*	3,100,000	2,300,000 2,900,000**	2,100,000 2,600,000**

* Restiffens at 10 inches of crush. All others are based on 24 inches of crush available before restiffening.
** When scaled by the ratio of the airplane weights (1.26)

In addition, cylinder axial crush test data was reviewed to obtain the following parameters.

- The average force acting = $\frac{\text{Energy (ft-lb)}}{\text{Deformation (ft)}}$ = lb.
- The average acceleration = $\frac{\text{Avg. Force (lb.)}}{\text{Weight (lb.)}}$ = g
- The pulse duration (Δt) (based on momentum considerations°) = $\frac{\text{Weight.Velocity}}{\text{g.Force}_{\text{Avg}}}$ = sec

Summarizing these terms for the three test specimens the following information is obtained:

Specimen	Avg. Force (1b)	Avg. Accel. (g)	Constant Force Pulse Duration (sec)
No. 1*	56571	5.8	.149
No. 2	21333	2.2	.279
No. 3	95172	9.9	.097
* More Typical of Airplane Construction			

Using the reference 4 data and the model shown in figure 3-70 analyses were performed to obtain longitudinal pulses for a straight-on collision into a rigid vertical obstruction. The fuselage cockpit was represented by crush springs and the fuselage aft of the cockpit by nonlinear beams. The study was performed parametrically for variations in

- forward impact velocity
- crush spring characteristics
- nonlinear beam characteristics

The results of this sensitivity study suggest that:

- at 20 ft/sec impact velocity, no airframe failure in the passenger region (FS460 and aft) would be anticipated
- at 30 ft/sec impact velocity 3 to 4 ft. of crush could occur and the average acceleration would be between 4g to 5g
- at 40 ft/sec, 5 to 6.5 ft. of crush could occur with an average acceleration of 4.5 g to 6g.
- a Δt of $\approx$.200 seconds is required for the KE to be absorbed in the 20 to 50 ft/sec impact range.

The results of these analyses are described in section 3.3.2.

Since the analysis results are tied to the model assumptions an additional parameter sensitivity analysis was performed to ascertain the affect of extended crush distance in critical bulkhead regions. The results show that the additional crush distance allows the airplane to impact at a higher initial sink speed before realizing a fuselage break (LIC > 1.0). However, the increased crush tends to produce lower accelerations and longer duration pulses. At some point the physical constraints of the location of the bulkheads limit the amount of crush before a "hard point" is encountered. The analyses showed that for the CID configuration, the aft bulkhead (FS1400) impacts the ground for a sink speed of 25 ft/sec and exceeds its failure load at a sink speed of 27.5 ft/sec, even with allowing 36 inches of crush throughout the rest of the structure. Table 3-30 illustrates the trend of pulse velocity, g_p, Δt versus allowable crush. These analyses results are provided in section 3.4.

The available experimental data and analytical data developed during the effort described in this report have been combined to develop a crash design velocity envelope based on current transport fuselage strength. The analytical data are presented in the form of triangular pulse parameters: velocity change, ΔV, peak amplitude, g, and pulse rise time t_r (pulse base duration, $\Delta t \approx 2\ t_r$). Samples of these data are provided in figures 4-1 through 4-6, and a summary of these results is shown in table 4-1. It is difficult to make direct comparisons because for each condition there are many factors to consider such as: number, location and type of responses (strength, crush, acceleration), time histories, sequence of events, initial impact conditions. For some test and analyses conditions, extensive documentation of results has been previously presented; e.g., Reference 2 describes all the pre-CID analysis and testing, including the Laurinburg and section drop test data, while reference 3 describes in detail the CID correlation, a brief portion of which is presented in section 2 of this report. Therefore, table 4-1 does not make a direct comparison between section drop test nor full-scale crash test and analyses, but instead, only

shows how the analyses performed during the current study relate to the available test data. The purpose of making such a comparison is to allow the total available data (analyses and tests) to be used to develop crash design velocity envelopes, which are shown in figures 4-7 and 4-8.

The parametric sensitivity analyses combines data which evolved over a series of FAA sponsored R&D programs. Table 5-1 summarizes the achievements as well as notes the limitations that can be associated with both the test and analysis efforts. Despite the progress noted, there is still a need to acquire additional dynamic response data for transport airplanes. Such added data will enhance confidence in the use of analytical representations to determine aircraft structural responses for impact conditions which may produce significant longitudinal pulses as well as to investigate different design configurations. The analytical procedures could then be expanded to establish rational crash design and seat dynamic testing requirements for the wide range of FAR25 airplane configurations.

The full-scale crash tests, the airplane section tests, and the subsequent modeling do not provide answers to the following pertinent questions:

- What is airframe failure? This is a critical question since it affects the definition of a survivable envelope. The analysis presented in this study use current airframe strength exceedance as the limit of a survivable crash environment.
- Can analysis confidently predict the limits of airframe structural integrity for an envelope of impact conditions and the range of design configurations covered in FAR25? The available test data does not address many impact conditions. The analysis treats only one narrow-body transport airplane configuration.
- What magnitude and duration of floor impact pulse are associated with the critical seat/occupant longitudinal load? The ramp impact produces a severe longitudinal pulse, but only in the nose section of the airplane.

TABLE 5-1. ASSESSMENT OF FAA SPONSORED TEST AND ANALYSES PROGRAMS

ACHIEVEMENTS	LIMITATIONS
• PRE-CID FULL SCALE AIRPLANE, SECTION TESTS, SUPPORTING ANALYSIS HAS PROVIDED DATA WITH REGARDS TO: – THE INITIAL APPLICATION OF MODELING TRANSPORT AIRCRAFT STRUCTURAL DYNAMIC RESPONSES WHICH SHOWED SATISFACTORY AGREEMENT WITH THE L-1649 MID-FUSELAGE RESPONSES AND THAT THE LONGITUDINAL DYNAMIC PULSE WAS ADEQUATELY COVERED BY EXISTING 9g STATIC REQUIREMENTS (REFERENCE 5). – THE CID FUSELAGE IMPACT LEVELS WHICH WERE SUBSTANTIALLY BELOW THE LIMITS OF THE AIRFRAME'S STRUCTURAL INTEGRITY. – REPRESENTATIVE FUSELAGE UNDERSIDE CRUSH CHARACTERISTICS OF TYPICAL NARROW-BODY AIRPLANE SOFT FRAME STRUCTURE AND FLOOR VERTICAL ACCELERATION RESPONSE FOR DIFFERENCE SINK SPEEDS FROM TESTS AND COLLABORATED WITH MODELING ANALYSIS. – THE PRE-CID TEST ANALYSIS INDICATED THAT THE AIRFRAME RESPONSE AND, CONSEQUENTLY, THE IMPACT LEVELS AT WHICH AIRFRAME STRUCTURAL INTEGRITY LEVELS ARE EXCEEDED ARE STRONGLY INFLUENCED BY "HARD POINTS" AND THE DEFLECTION AT WHICH STRUCTURE RE-STIFFENING OCCURS. – THE LAURINBURG TEST WHICH SHOWED THAT "HARD POINTS" EXHIBIT SIGNIFICANTLY MORE CRUSH THAN WAS OBSERVED IN THE LANDING GEAR WHEEL WELL SECTION TEST, WHICH WAS CONDUCTED WITHOUT THE WING STRUCTURE OR ITS EFFECTS. THE LAURINBURG TEST WHICH ALSO PROVIDED DATA RELATED TO FUSELAGE STRENGTH, FUSELAGE UNDERSIDE CRUSH DISTRIBUTIOIN AND IMPROVED THE CID MODELING. – THE PRE-CID AND CID CORRELATION EFFORTS WHICH INDICATED THAT MODELING CAPABILITY COULD BE ENHANCED WITH A WIDER RANGE OF SUPPORTING TEST DATA AND ADDED ANALYTICAL FEATURES, I.E., COMBINED FAILURE LOADS CRITERIA, PLASTIC HINGE REPRESENTATIONS, INITIAL CONDITION LOADINGS.	• WITH REGARD TO TEST DATA: – ONE AIRCRAFT SIZE TESTED – *ONE AIRCRAFT CONFIGURATION TESTED* – THE FUSELAGE SECTION DROP TESTS DO NOT PROVIDE THE LOAD-DEFLECTION OF "HARD POINTS." – THE AMOUNT OF CRUSH EXPERIENCED BY THE SOFT SECTIONS AT THE HIGHER SINK SPEEDS (35 FT/SEC) IS MOST LIKELY NOT REALIZABLE IN A CRASH SCENARIO. SUBSEQUENT PARAMETER STUDIES HAVE SHOWN THAT "HARD POINT" INTERFERENCE WILL OCCUR BEFORE THE FULL CRUSH OF THE SOFT SECTION IS DEVELOPED. – THE LAURINBURG TEST DID NOT (a) PRODUCE FLOOR ACCELERATION MEASUREMENTS, (b) EXHAUST THE CRUSH CAPABILITY OF THE "HARD POINT" STRUCTURE (FLOOR FAILURE DID OCCUR), NOR (c) ADDRESS MORE SEVERE PITCH-UP AND PITCH-DOWN IMPACTS. – THE DATA, WITH THE EXCEPTION OF A WIDE-BODY FUSELAGE SECTION DROP TEST, ARE APPLICABLE TO ONE NARROW-BODY AIRCRAFT CONFIGURATION. – NO TEST DATA AVAILABLE FOR IMPACT AT HIGH PITCH-UP ATTITUDE.
• CID CORRELATION AND POST-CID ANALYSIS HAVE PROVIDED DATA WITH REGARD TO: – AIRFRAME RESPONSE AS A FUNCTION OF SINK SPEED AND PITCH ATTITUDE, – FUSELAGE BENDING AND SHEAR STRUCTURAL INTEGRITY AS A FUNCTION OF IMPACT CONDITION, – THE DEFINITION OF A POTENTIAL FLOOR PULSE LONGITUDINAL VERSUS VERTICAL CHANGE IN VELOCITY ENVELOPE WHICH IS RELATED TO AIRFRAME STRENGTH. – THE CHANGE IN FLOOR PULSE AMPLITUDE, DURATION AND VELOCITY AS A FUNCTION OF THE FUSELAGE CRUSH CHARACTERISTICS. – THE BENDING MOMENT RESPONSES OBTAINED FROM THE CID DATA EXHIBITS LOW FREQUENCY FUSELAGE BENDING MODES. THUS, THE USE OF STICK MODELS TO RELATE TO OVERALL FUSELAGE BENDING LOADS IS APPROPRIATE. – *DIRECT COMPARISON OF FUSELAGE AND WING PEAK RESPONSES AND LENGTHWISE/SPANWISE DISTRIBUTION BETWEEN TEST AND ANALYSES.*	• WITH REGARD TO ANALYSES: – THE MODELING IS PERFORMED FOR ONE AIRPLANE CONFIGURATION. – THE REPONSES FOR PITCH-UP AND PITCH-DOWN CONDITIONS (+6 DEGREES) HAVE NOT BEEN CONFIRMED SINCE AIR-TO-GROUND IMPACT DATA HAS BEEN LIMITED TO LESS THAN 2 DEGREES. – THE ANALYSES DO NOT PRODUCE SUBSTANTIAL LONGITUDINAL PULSES DURING THE GROUND-TO-GROUND IMPACT CONDITION. THE ONLY EVIDENCE OF A RELATIVELY SEVERE LONGITUDINAL PULSE HAS BEEN THE MEASURED NOSE CABIN RESPONSE WHICH OCCURRED WHILE THE FUSELAGE EXPERIENCES A BREAK (e.g., L-1649 IMPACT ONTO A 20-DEGREE SLOPE). – *THE ANALYSES RESULTS ARE STRONGLY DEPENDENT ON THE AVAILABLE CRUSH DISTRIBUTION ALONG THE FUSELAGE UNDERSIDE. HARD POINTS" WHICH ARE LOCATED AT THE NOSE, MAIN GEAR, AFT PRESSURE BULKHEAD AND THE CENTER WING SECTION WILL PRODUCE* LOADS WHICH EXCEED AIRFRAME STRENGTH WHEN "BOTTOMING OUT" OCCURS. LITTLE TEST DATA IS AVAILABLE TO CONFIRM THE CRUSH CAPABILITY OF THESE CRITICAL STRUCTURES.

SECTION 6

CONCLUSIONS

1. Parameter sensitivity study results appear reasonable when compared to available analysis results and test data.

2. Airframe and seat dynamic test crash design velocity change envelopes have been developed which are based on data from full-scale crash test, section impact tests, and KRASH parameter variation analyses.

REFERENCES

1. "Full-Scale Transport Controlled Impact Demonstation Program", FAA Report No. DOT/FAA/CT-82/151, FAA Technical Center, Atlantic City, N.J., January 1984.

2. Wittlin, G., LaBarge, W.L., "KRASH Dynamics Analysis Modeling Transport Airplane Controlled Impact Demonstration Test," FAA Report No. DOT/FAA/CT-85/9, dated May 1986.

3. Wittlin, G., "KRASH Analysis Correlation - Transport Airplane Demonstration Test," FAA Report No. DOT/FAA/CT-86/13, October 1986.

4. Greer, D.L., et al., "Design Study and Model Structures Test Program to Improve Fuselage Crashworthiness," FAA Technical Report DS-67-20, October 1967.

5. Wittlin, G., Lackey, D., "Analytical Modeling of Transport Aircraft Crash Scenarios to Obtain Floor Pulses," FAA Report No. DOT/FAA/CT-83-23, NASA CR 166089, April 1983.

6. Reed, W.H., et al., "Full-Scale Crash Test of a Lockheed Constellation Model L-1649 Aircraft," FAA Technical Report ADS-38, October 1965.

7. Reed, W.H., et al., Full-Scale Crash Test of a Douglas Model DC-7 Aircraft," FAA Technical Report ADS-37, October 1965.

8. NASA Publication 2395, "Full-Scale Transport Controlled Impact Demonstration," April 10, 1985.

9. Vaughan, V.L., et al., "Light Airplane Crash Tests at Three Pitch Angles", NASA Technical Paper 1481, November 1979.

10. Castle, C.B., Alfaro-Bou, E., "Crash Tests of Three Identical Low-Wing Single-Engine Airplanes," NASA Technical Paper 2190, September 1983.

11. Hayduk, R., Williams, S., "Vertical Drop Test of Transport Fuselage Section Located Forward of the Wing," NASA TM85679, August 1983.

12. Williams, S., Hayduk, R., "Vertical Drop Test of a Transport Fuselage Center Section Including the Wheel Wells," NASA TM85706, October 1983.

13. Pugliese, S.M., "707 Fuselage Drop Test Report," Report No. 7252-1, Arvin/Calspan report prepared for the FAA Technical Center, Atlantic City N.J., March 1984.

14. "DC-10 Fuselage Drop Test Report," Report No. 7251-2, Arvin Calscan report prepared for the FAA Technical Center, Atlantic City, N.J., September 1984.

15. "Vertical Drop Test of a Transport Aircraft Section" - DOT/FAA/CT-TN86/34, October 1986.

16. Johnson, D., Gorodz, L., "Crashworthiness Experiment Summary, Full-Scale Transport Controlled Impact Demonstration Program," FAA Report No. DOT/FAA/CT-85/20, June 1986.

17. Nissley, P.M., Heid, T.C., "Structural Design for Fuel Containment Under Survivable Crash Conditions," FAA-TR-ADS-19, August 1964.

APPENDIX

DISTRIBUTION LIST

Civil Aviation Authority (5)
Aviation House
129 Kingsway
London WC2B 6NN England

DOT-FAA AEU-500 (4)
American Embassy
APO New York, NY 09667

Embassy of Australia (1)
Civil Air Attache
1601 Mass. Ave. NW
Washington, DC 20036

University of California (1)
Service Dept Institute of
Transportation Standard Lib
412 McLaughlin Hall
Berkely, CA 94720

Scientific & Tech. Info FAC (1)
ATTN: NASA Rep.
P.O. Box 8757 BWI Airport
Baltimore, MD 21240

British Embassy (1)
Civil Air Attache ATS
3100 Mass Ave. NW
Washington, DC 20008

Northwestern University (1)
Trisnet Repository
Transportation Center Library
Evanston, ILL 60201

Director DuCentre Exp DE LA (1)
Navigation Aerineene
941 Orly, France

ANE-40	(2)	ACT-61A	(2)	ASW-53B	(2)
ASO-52C4	(2)	AAL-400	(2)	AAC-64D	(2)
APM-13 Nigro	(2)	M-493.2 Bldg. 10A	(5)	ACE-66	(2)
AEA-61	(3)	APM-1	(1)	ADL-1	(1)
ADL-32 North	(1)	APA-300	(1)	ALG-300	(1)
AES-3	(1)	AGL-60	(2)	ACT-5	(1)
ANM-60	(2)				

FAA, Chief, Civil Aviation Assistance Group (1)
Madrid, Spain
c/o American Embassy
APO-New York 09285-0001

Al Astorga (1)
Federal Aviation
Administration (CAAG)
American Embassy, Box 38
APO-New York 09285-0001

Dick Tobiason (1)
ATA of America
1709 New York Avenue, NW
Washington, DC 20006

Burton Chesterfield, DMA-603 (1)
DOT Transportation Safety Inst.
6500 South McArthur Blvd.
Oklahoma City, OK 73125

FAA Anchorage ACO
701 C Street, Box 14
Anchorage, Alaska 99513

FAA Fort Worth ACO
P.O. Box 1689
Fort Worth, TX 76101

FAA Atlanta ACO
1075 Inner Loop Road
College Park, Georgia 30337

FAA Long Beach ACO
4344 Donald Douglas Drive
Long Beach, CA 90808

FAA Boston ACO
12 New England Executive PArk
Burlington, Mass. 01803

FAA Los Angeles ACO
P.O. Box 92007, Worldway Postal Center
Hawthorne, CA 90009

FAA Brussels ACO
% American Embassy, APO,
New York, NY 09667

FAA New York ACO
181 So. Frankline Ave., Room 202
Valley Stream, NY 11581

FAA Chicago ACO
2300 E. Devon, Room.232
Des Plains, Illinois 6008

FAA Seattle ACO
17900 Pacific Highway South, C-68966
Seattle, Washington 98168

FAA Denver
10455 East 25th Ave., Suite 307
Aurora, Colorado 98168

FAA Wichita ACO
Mid Continent Airport, Room 100 FAA Bldg.
1891 Airport Road
Wichita, KA 67209

Frank Taylor
3542 Church Road
Ellicott City, MD 21043

Dr. Hans A. Krakauer
Deputy Chairman, International Airline
Pilots Association Group
Apartado 97
8200 Albufeira, Portugal

Mr. Gale Braden (FAA)
5928 Queenston St.
Springfield, VA 22152

Geoffrey Lipman
Executive Director, President du Conseil
International Foundation of Airline
Passenger Associations
Case Postale 462, 1215 Geneve
15 Aeroport, Suisse, Geneva

Richard E. Livingston, Jr.
Director, Aerotech Operations for
the IAPA Group
1805 Crystal Drive, Suite 1112 South
Arlington, VA 22202

Government Activities

FAA, Washington, DC 20591
(Attn: Harold W. Becker, ASF-300;
Thomas McSweeny, AWS-100) (2)

FAA, 4344 Donald Douglas Drive,
Long Beach, CA 90808
(Attn: Stephen Soltis, ANW-102M) (1)

FAA, Central Region Headquarters,
601 East 12th Street, Federal Building,
Kansas City, Missouri, 64106
(Attn: Earsa Tunkesley, ACE-100) (1)

FAA, Southwest Region Headquarters,
4400 Blue Mound Road,
P.O. Box 1689
Fort Worth, Texas 76101
(Attn:: John Shapley, ASW-110) (1)

FAA, Northwest Mountain Region
Headquarters,
17900 Pacific Highway South, C-68966,
Seattle, Washington 98168
(Attn: Steven Wallace, ANW-110) (1)

FAA, Mike Monroney Aeronautical Center,
P.O. Box 25082,
Oaklonoma City, OK 73125
(Attn: Richard Chandler, AAM-119) (1)

NASA, Langley Research Center,
Hampton, VA 23365
(Attn: Emilio Alfaro-Bou, MA-495;
Huey Cardin, MS-495) (2)

U.S. Army Aviation Applies Technology
Directorate, USAARTA, (AVSCOM),
Fort Eustis, VA 23604
(Attn: Roy Burrows, Code SAVRT-TY-ASV) (2)

U.S. Navy Naval Air Development Center,
Warminister, PA 18974
(Attn: Leon Domzalski, Code 60322) (1)

NTSB, 800 Independence Ave. S.E.,
Washington, DC 20594
(Attn: John C. Clark, TE 60) (1)

Non-Government Activities

Beech Aircraft Corp.,
P.O. Box 85,
Wichita, KS 67201
(Attn: Dayton L. Hartley;
James E. Terry; William Schultz) (3)

Bell Helicopter Co.,
P.O. Box 482,
Fort Worth, TX 76101
(Attn: James Cronkite, Dept. 81,
MS 11; Roy G. Fox) (2)

Boeing Airplane Co.,
P.O. Box 3707,
Seattle, WA 98124
(Attn: Edward Widmayer, MC-9W-22) (1)

Boeing Co., Vertol Division,
P.O. Box 16858,
Philadelphia, PA 91942
(Attn: Denise Vassilakos, MS P30-27) (1)

Cessna Aircraft Co.,
P.O. Box 7704,
Wichita, KS 67277
(Attn: John Berwick; Robert Held;
Richard Soloski) (3)

Fairchild Aircraft Corp.,
P.O. Box 3246,
San Antonio, TX 78284
(Attn: Walt Dwyer) (1)

General Dynamics/Convair,
P.O. Box 80847,
San Diego, CA 92138
(Attn: L. Mastay, MA 80-6030) (1)

Grumman Aerospace Corp.,
So. Oyster Bay Road,, Bethpage,
L.I., NY 11714
(Attn: Robert Winter, A08-35;
Allan B. Difko, A08-35) (2)

Gulfstream Aerospace Corp.,
P.O. Box 2206,
Savannah, GA 31402
(Attn: George Westphal) (1)

Non-Government Activities (Continued)

Gulfstream Aerospace Corp.,
P.O. Box 22500,
Oklhoma City, OK 73123
(Attn: Richard Southard) (1)

Lockheed-California Co.,
Burbank, CA 91503
(Attn: Gil Wittlin, D 76-12,
B 63G, PLT A-1) (1)

McDonnell Douglas Corp.,
3855 Lakewood Drive,
Long Beach, CA 90846
(Attn: J. Webster;
John L. Galligher) (2)

McDonnell Douglas Helicopter,
4645 S. Ash Ave.,
Tempe, AZ 85182
(Attn: Lyndon Landborne;
J.K. Sen) (2)

Piper Aircraft Corp.,
2925 Piper Drive,
Vero Beach, FL 32960
(Attn: Marion Dees) (1)

Sikorsky Aircraft,
North Maint Street,
Stratford, CT 06601
(Attn: Brain Cornell, MS 5207A;
Pramonik Mukunda, MS 5207A) (2)

☆ U.S. GOVERNMENT PRINTING OFFICE: 1988—505-068/60251